

# **Advanced Thin Film Composite and Nanocomposite Polyamide Membrane for Water Treatment**

by  
**Behnam Khorshidi Mianae**

A thesis submitted in partial fulfillment of the requirements for the degree of  
**Doctor of Philosophy**

Department of Mechanical Engineering  
University of Alberta

©Behnam Khorshidi, 2017

# Abstract

Membrane technology is currently widely used for separation of ions, colloids, organic matter and macromolecules. Among various membrane processes, nanofiltration (NF) and reverse osmosis (RO) with thin film nanocomposite (TFC) polyamide (PA) membrane at the heart of the separation process is being increasingly employed for sea and brackish water treatment and wastewater reclamation. Over the past decade, the increasing need to implement highly cost and energy efficient membranes processes has accelerated the research effort to fabricate advanced composite membranes with enhanced permeation, thermomechanical, and antifouling properties. In the present research, systematic studies were conducted to fabricate high performance composite PA membrane with improved thermal stability and antifouling propensity. First, the effects of synthesis conditions and chemical additives were studied on the permeation properties of the TFC PA membranes. The composite membranes were prepared by interfacial polymerization (IP) reaction between meta-phenylene diamine (MPD)-aqueous and trimesoyl chloride (TMC)-organic solvents (such as heptane, hexane and cyclohexane) at the surface of polyethersulfone (PES) microporous support. Several influential factors including the concentration of the reacting monomers, reaction time and temperature, thermal curing temperature, and the concentration of chemical additive such as surfactant, pH regulator, co-solvents in the water-based monomer solution was investigated using design of experiment (DOE) methodology. The results revealed that the final permselectivity of a TFC PA membrane is remarkably dependent of its surface physicochemical properties, structural characteristics and the complex internal free volumes which can all be influenced by synthesis conditions. The findings of the first stage of this research provided valuable insight and useful guidelines for the development of TFC PA membranes with wide range of water permeation and salt rejection. These findings were used in the second stage of the research where robust and high performance nanocomposite membranes were prepared by incorporation of metal oxide nanoparticles (NPs) to the membrane structure. Initially, nanocomposite microporous membranes were prepared by integration of indium tin oxide (ITO) NPs to the PES matrix via phase inversion process. The resulting PES-ITO membranes demonstrated higher thermal stability and antifouling porosity compared to pristine PES membranes when tested with industrially produced

water. Finally, titanium dioxide ( $\text{TiO}_2$ ) NPs were effectively incorporated to the PA active layer using a combination of biphasic solvothermal (BST) reaction and IP reaction. The resulting thin film nanocomposite (TFN) PA- $\text{TiO}_2$  membranes showed an enhanced thermal stability and anti-biofouling characteristics compared to base TFC PA membranes.

**Keywords:** Membrane filtration, nanofiltration, reverse osmosis, thin film composite, thin film nanocomposite, polyamide, interfacial polymerization, metal oxide nanoparticle, thermal stable, antifouling.

# Preface

This thesis is the original work by Behnam Khorshidi. The majority of the context in chapter 3, 4, and 5 are published in the following journals:

1. B. Khorshidi, I. Biswas, T. Thundat, M. Sadrzadeh, A novel approach for the fabrication of thin film polyamide-TiO<sub>2</sub> nanocomposite membranes with enhanced thermal stability and anti-biofouling propensity, *Scientific Reports* (under review).
2. B. Khorshidi, T. Thundat, D. Pernitsky, M. Sadrzadeh, A parametric study on the synergistic impacts of chemical additives on permeation properties of thin film composite polyamide membrane, *J. Memb. Sci.* 535 (2017) 248–257. doi:10.1016/j.memsci.2017.04.052.
3. B. Khorshidi, B. Soltannia, T. Thundat, M. Sadrzadeh, Synthesis of thin film composite polyamide membranes: Effect of monohydric and polyhydric alcohol additives in aqueous solution, *J. Memb. Sci.* 523 (2017) 336–345. doi:10.1016/j.memsci.2016.09.062.
4. B. Khorshidi, T. Thundat, B.A. Fleck, M. Sadrzadeh, A novel approach toward fabrication of high performance thin film composite polyamide membranes, *Sci. Rep.* 6 (2016) 22069. doi:10.1038/srep22069.
5. B. Khorshidi, A. Bhinder, T. Thundat, D. Pernitsky, M. Sadrzadeh, Developing high throughput thin film composite polyamide membranes for forward osmosis treatment of SAGD produced water, *J. Memb. Sci.* 511 (2016) 29–39. doi:10.1016/j.memsci.2016.03.052.
6. B. Khorshidi, J. Hajinasiri, G. Ma, S. Bhattacharjee, M. Sadrzadeh, Thermally resistant and electrically conductive PES/ITO nanocomposite membrane, *J. Memb. Sci.* 500 (2016) 151–160. doi:10.1016/j.memsci.2015.11.015.
7. B. Khorshidi, T. Thundat, B.A. Fleck, M. Sadrzadeh, Thin film composite polyamide membranes: Parametric study on the influence of synthesis conditions, *RSC Adv.* 5 (2015) 54985–54997. doi:10.1039/C5RA08317F.

*Dedicated to my parents,  
Maryam and Mohammadtaghi  
And my wife, Fahimeh  
for their endless love and inspiring support.  
Love you*

# Acknowledgement

It was a unique experience for me to finish my PhD studies in University of Alberta and it was not possible without the help and support of a number of incredible people whom I have to express my great appreciation to them. First of all, I would like to particularly thank my main supervisor, Dr. Mohtada Sadrzadeh. You have been more than a supervisor for me and I'd like to thank you so much for whatever I learned from you in my personal and professional life. I would also like to express my gratitude to my second supervisor, Dr. Thomas Thundat. I feel proud to have the opportunity of working with you. Your motivation, enthusiasm and your philosophies in academic life have always inspired me to go forward during my PhD. I am thankful to my committee member, Dr. Brian Fleck for his continuous support and guidance. I would like take the opportunity and give my special thanks to Dr. Subir Bhattacharjee, for being my supervisor in an academic year of 2013-2014. I am very grateful to you for teaching me to become an expert learner in my academic life. In addition, I am very grateful to Josie Nebo and Ni Yang for their continuous support and lab assistance.

I am really fortunate that I have really good colleagues and friends in the Advanced Water Research Laboratory (AWRL) and University of Alberta. Special thanks to Hadi Nazariipoor for the numerous productive discussions that we had in his office. I really appreciate the help and support of my other friends: Behnam Sadri, Babak Vajdi, Ishita Biswas, Mohammad Nojumi, Amir hossein Mahdavi, Ali Mohammadtabar, Simin Shabani, Amin Karkooti, Babak Soltania, Farshad Mohammadtabar, Zayed Almansoori, Ayda Razi, Laleh Shmaei, Debanik Bhattacharjee, Asad Asad, Rouholluh Shokri, Mica Yousuf, Jannat Fatema, Ehsan Shahidi, Soundararajan Desikachari; thank you all.

Above all, I'd like to give my deepest appreciation and gratitude to my family, Mohammadtaghi, Maryam, Farzaneh, Behrooz, Afsaneh, Hamidreza, Mahdi, Atrina and my wife, Fahimeh, for their endless love, patience and support. I can't say enough to thank you for being my strength and inspiration of my life.

Finally, I appreciate the financial support from the following agencies that helped me to finish my PhD research: Natural Sciences and Engineering Research Council of Canada (NSERC), Alberta innovates technology futures (AITF), Canada's Oil Sands Innovation Alliance (COSIA), Suncor Energy Company, ConocoPhillips Corporation, and Devon Energy Company.

# Contents

<b>1</b>	<b>Introduction</b>	<b>1</b>
1.1	Water demand	2
1.2	Overview of SAGD operation	2
1.3	Membrane technology for water treatment	4
1.4	Synthesis techniques of porous and dense membranes	5
1.5	Transport mechanism through NF/RO membranes	8
1.6	Literature review	10
1.7	Research objectives	11
1.8	Thesis structure	12
1.9	Thesis contribution	13
	Reference	14
<b>2</b>	<b>Materials and methods</b>	<b>14</b>
2.1	Materials	15
2.2	Synthesis of ITO NPs	16
2.3	Synthesis of TiO <sub>2</sub> NPs	17
2.4	Synthesis of PES support layer	18
2.5	Synthesis of PES-ITO nanocomposite membrane	18
2.6	Synthesis of TFC membranes	19
2.7	Characterization of synthesized NPs and membranes	20
2.7.1	Analysis of the surface and cross-sectional morphology	20
2.7.2	Evaluation of the chemical composition	20
2.7.3	Analysis of surface topography	21
2.7.4	Evaluation of the membrane surface wettability	21
2.7.5	Measurement of the degree of cross-linking of the PA film	22
2.7.6	Measurement of total organic carbon	22
2.7.7	Evaluation of crystalline structure and size of the solid NPs	23
2.7.8	Measurement of size and stability of NPs in solution	23
2.7.9	Evaluation of the thermal stability of the membranes	23

2.7.10	Measurement of the surface potential of the membranes	23
2.7.11	Measurement of the electrical conductivity of the membranes	24
2.7.12	Evaluation of the leaching of NPs from nanocomposite membrane	24
2.7.13	Evaluation of the water flux and salt rejection of the membranes in RO operation	24
2.7.14	Evaluation of the fouling propensity of the membrane in RO operation	26
2.7.15	Evaluation of the permeation performance of the composite membranes in FO process	26
2.7.16	Determination of the FO membrane structural parameter	28
2.8	Design of experiment (DOE) using Taguchi method	29
2.9	Analysis of Variance (ANOVA)	29
2.10	Performance prediction using Taguchi method	31
<b>3</b>	<b>Effect of synthesis conditions and chemical additives on the properties of TFC PA membranes</b>	<b>32</b>
3.1	Systematic study on the influence of monomer concentration, reaction time and curing temperature on the properties of the TFC PA membranes	33
3.1.1	Introduction	33
3.1.2	Materials and methods	35
3.1.3	Results and discussion	36
3.1.3.1	Chemical composition of the TFC membranes	36
3.1.3.2	Water flux and salt rejection	37
3.1.3.3	Influence of control factors on the properties of the resulting TFC membranes	39
3.1.3.3.1	Effect of MPD and TMC concentration	39
3.1.3.3.2	Effect of curing temperature	45
3.1.3.3.3	Effect of reaction time	45
3.1.3.4	Interaction between MPD and TMC concentration	46
3.1.3.5	ANOVA analysis	49
3.2	Systematic study on the influence of chemical additives on the properties of the TFC PA membranes	51



3.2.1	Introduction	51
3.2.2	Materials and methods	51
3.2.3	Results and discussion	52
3.2.3.1	Trend of influence of additives based on Taguchi marginal mean graphs	52
3.2.3.2	ANOVA analysis	56
3.2.3.3	Prediction of permeation properties of TFC membranes	57
3.2.3.4	Characterization of structural and physicochemical properties of TFC membranes	58
3.3	Investigation of the influence of monohydric and polyhydric alcohol additives on the properties of the TFC PA membranes	66
3.3.1	Introduction	66
3.3.2	Materials and methods	68
3.3.3	Results and discussion	68
3.3.3.1	Surface morphology of synthesized TFC membranes	68
3.3.3.2	Chemical composition of the PA active layer	73
3.3.3.3	Surface wettability and roughness of the synthesized membranes	76
3.3.3.4	Water flux and salt rejection of TFC membranes	79
3.4	Conclusion	81
<b>4</b>	<b>Thermally modulated IP reaction for fabrication of high throughput TFC PA membrane for FO application</b>	<b>83</b>
4.1	Introduction	84
4.2	Materials and methods	86
4.3	Results and discussion	88
4.3.1	Membrane morphology	88
4.3.2	Chemical composition and elemental analysis	91
4.3.3	Surface roughness and wettability of TFC membranes	94
4.3.4	RO permeation performance of the membranes	94
4.3.5	FO separation performance	99
4.3.6	FO separation performance with BFW	104
4.4	Conclusion	106

<b>5</b>	<b>Fabrication of thermally stable and antifouling nanocomposite membranes</b>	<b>107</b>
5.1	Background	108
5.2	Thermally resistant and electrically conductive PES/ITO nanocomposite membrane	109
5.2.1	Introduction	109
5.2.2	Synthesis of PES-ITO	110
5.2.3	Results and discussion	110
5.2.3.1	Size of solid ITO NPs	110
5.2.3.2	Surface and internal structure of PES/ITO membrane	111
5.2.3.3	Leaching of ITO NPs from PES substrate	112
5.2.3.4	Thermal stability of PES/ITO membranes	113
5.2.3.5	Electrical conductivity of PES/ITO membrane	115
5.2.3.6	Separation performance and fouling characteristics	115
5.3	Fabrication of TFN PA-TiO <sub>2</sub> with enhanced thermal stability and anti-biofouling propensity	121
5.3.1	Introduction	121
5.3.2	Synthesis of TFN PA-TiO <sub>2</sub> membranes	122
5.3.3	Results and discussion	123
5.3.3.1	Characterization of TiO <sub>2</sub> NPs	123
5.3.3.2	Characterization of PA-TiO <sub>2</sub> TFN membranes	124
5.3.3.3	Water flux and salt rejection of TFN membranes	128
5.3.3.4	Antibacterial activity of TFN membranes	130
5.4	Conclusion	132
<b>6</b>	<b>Conclusion and future work</b>	<b>133</b>
6.1	Conclusions	134
6.2	Future work	136
6.3	List of contributions	138
6.3.1	Journal Papers	138
6.3.2	Conference presentations	139
	<b>Reference</b>	<b>140</b>
	<b>Appendix: Copyrights and permissions</b>	<b>163</b>

# List of Tables

2.1	Properties of WLS inlet water	16
2.2	Properties of conventionally-treated SAGD BFW	16
3.1	Overview of experimental studies regarding the effects of synthesis conditions on performance of TFC membranes	34
3.2	Control factors (synthesis parameters) and their corresponding levels in Taguchi L <sub>9</sub> design	36
3.3	Synthesis conditions and permeation performance of the confirmation experiments	41
3.4	Atomic concentration of C, O and N in PA layer of C1 and C3 membranes obtained by XPS analysis	43
3.5	Analysis of variance based on water permeation data	50
3.6	The list of control factors and their corresponding levels of variation in the designed experimental trials	52
3.7	ANOVA based on water permeation results. F-table for $\alpha = 0.05$ is 4.26	57
3.8	Predicted water flux and salt rejection of confirmation membranes using Taguchi model	58
3.9	Table 3.9: Degree of cross-linking, surface roughness and contact angle data of the synthesized TFC membranes. All the membranes were prepared using 2.0 wt.% MPD in water and 0.15 wt.% TMC in hexane. The concentrations of additives for the synthesis of the modified TFC membranes were presented in Table 3.6 and Table 3.8	62
3.10	List of the synthesized TFC membranes with corresponding monomer and alcohol concentration in MPD-water solution	68
3.11	Values of group contributions for solubility parameter component for some structural groups	72
3.12	Solubility parameter components of water, hexane and water-alcohol mixtures	73
3.13	Elemental compositions, chemical bonding peak area of the synthesized TFC	76

	membranes	
3.14	Contact angle and surface roughness of the synthesized TFC membranes	77
4.1	Synthesized TFC membranes, organic solution used for dissolving TMC monomer, temperature of the organic solution during the IP reaction. The IP reaction was allowed to proceed for 30 secs and after that, the membranes were thermally treated at 70 °C for 5 min	87
4.2	Selected properties of the organic solvents used for making TFC membranes	87
4.3	Elemental compositions, O/N ratio, chemical bonding peak area and degree of cross-linking of the TFC1 to TFC4 membranes	93
4.4	Contact angle and surface roughness of synthesized TFC membranes	94
4.5	Permeation properties of the commercial RO membranes compared with the lab-made TFC membranes. Test conditions: feed solutions: pure water and 2000 ppm NaCl solution, pressure: 1.52 MPa (220 psi), temperature: 25 °C	96
4.6	Permeation performance of TFC PA flat-sheet membranes in AL-FS orientation	102
5.1	Surface potential and contact angle of nanocomposite and pristine PES membranes	120
5.2	Concentration of MPD, TMC and TiO <sub>2</sub> NPs for the fabrication of TFC and TFN membranes. The invariant synthesis conditions were: 0.2 wt.% SDS, 1 wt.% CSA, 1 wt.% TEA in MPD-water solution, 30 sec IP reaction, 4 minutes heat curing at 60 °C	123

# List of Figures

1.1	Process flow diagram of a SAGD process	3
1.2	Fabrication techniques for preparation of the polymeric membranes	6
1.3	Schematic view of a TFC PA membrane along with the surface and cross-sectional images of the top PA and bottom PES layers	7
1.4	Schematic diagram of the CP layer	9
2.1	Schematic route for synthesis of ITO NPs	17
2.2	Schematic synthesis route for making TiO <sub>2</sub> NPs	18
2.3	Schematic representation of the IP reaction between MPD and TMC at the surface of the microporous PES support	20
2.4	Chemical structure of polyamide film. m and n represents the cross-linked and the linear parts, respectively (m+n=1)	22
2.5	Schematic view of the cross-flow RO filtration setup	25
2.6	Schematic view of the FO setup. All the TFC membranes were tested in active layer toward feed side (AL-FS) orientation	28
3.1	ATR-FTIR spectra of TFC membranes and base PES support	37
3.2	Water flux and salt rejection of all synthesized membranes. The performance measurements were carried out at a trans-membrane pressure of 1.52 MPa and at a feed flow rate of 1 Lmin <sup>-1</sup> , corresponding to the laminar crossflow of Reynolds number Re=730	38
3.3	Average water flux and SN ratio for each level of each control factor	40
3.4	Average salt rejection and SN ratio for each level of each control factor	40
3.5	FESEM surface and TEM cross-section images of confirmation test membranes: PES support, C1 (MPD 1 wt.%, TMC 0.15 wt.%) and C3 (MPD 1 wt.%, TMC 0.35 wt.%) to study the effect of TMC concentration. The levels of other parameters are presented in Table 3.3	44
3.6	FESEM surface morphologies of Taguchi base membrane M1 (cured at 25°C) and confirmation test membranes C1 (cured at 55 °C) and C5 (cured at 85	46

	°C) to study the effect of curing temperature. The levels of other parameters are presented in Table 3.3	
3.7	Two-way interaction plot for MPD and TMC concentration (reaction time: 15 s, curing temperature: 55 °C)	48
3.8	Surface images of confirmation membranes C2 & C4 (MPD concentration 2 wt.%) and C7 & C8 (MPD concentration 3 wt.%). The microporous structure of PES support is clear for C7 and C8 due to formation of thin dense layer at the surface	49
3.9	Pure water flux and salt rejection of the synthesized TFC membranes. The synthesis conditions of MM1 to MM9 membranes are presented in Table 3.6. MM0 is a reference (base) TFC PA membrane prepared without using any additive in water solution	53
3.10	Marginal mean graphs showing the effect of additive concentration on water permeability of the TFC membranes with the corresponding SN ratio	55
3.11	Marginal mean graphs showing the influence of additive concentration on salt rejection of the synthesized TFC membranes with the corresponding SN ratio	55
3.12	FESEM Surface morphology of PES support, unmodified MM0, and modified TFC membranes. The concentration of additives for the preparation of the modified TFC membranes was presented in Table 3.6	59
3.13	AFM surface topography images of unmodified (MM0) and modified TFC membranes. The concentration of additives in the synthesis of modified TFC membranes are presented in Table 3.6	59
3.14	FESEM Surface morphology of confirmation membranes. The synthesis conditions of the modified TFC membranes are presented in Table 3.6	60
3.15	Cross-sectional images of confirmation membranes. The synthesis conditions of the confirmation TFC membranes are presented in Table 3.6	60
3.16	AFM surface topography images of confirmation membranes. The concentrations of additives used in the MPD-solution to modify the TFC membranes are presented in Table 3.6	61
3.17	TEM cross-sectional images of TFC membranes prepared with different concentration of SDS in water solution. Synthesis conditions: 2.0 wt.% MPD in water, 0.15 wt.% TMC in hexane, 30 sec reaction, 4 min thermal curing at 60 °C. No other additive was used in the MPD solution	62
3.18	FESEM surface morphology of the PES substrate, unmodified PA membrane (TFC0), and modified TFC membranes by ethanol (TFC1, TFC2), ethylene glycol (TFC3, TFC4), and xylitol (TFC5, TFC6) prepared at 1.0 and 6.0	69

	wt.% concentration of these alcohols in the MPD-aqueous solution	
3.19	TEM cross-sectional images of the modified TFC membranes prepared at 1.0 and 6.0 wt.% concentration of ethanol (TFC1, TFC2), ethylene glycol (TFC3, TFC4), and xylitol (TFC5, TFC6) in the MPD-aqueous solution	71
3.20	C 1s deconvolution of high resolution spectra of base (M0) and modified (M2) TFC membranes	74
3.21	Addition stage of the hydrolysis (nucleophilic) reaction of a TMC molecule	74
3.22	Elimination stage of the hydrolysis (nucleophilic) reaction of a TMC molecule	75
3.23	AFM 3D surface topography of the modified TFC membranes	79
3.24	Effect of alcohol concentration in MPD solution on water permeation and salt rejection of the synthesized membranes. Experimental conditions: feed solution: distilled water for water flux test and 2000 ppm NaCl solution for salt rejection measurement, operating pressure: 1.52±0.04 MPa (220±5 psi), temperature: 25±1 °C, pH: 6.5-7	84
4.1	Surface FESEM, cross-sectional TEM and 3D AFM images of the TFC membranes. The synthesis conditions were the same for all TFC membranes except the temperature of the heptane solution which was -20 °C for TFC1, 1 °C for TFC2, 25 °C for TFC3 and 50 °C for TFC4	89
4.2	FESEM images of TFC membranes prepared in 0.2%-hexane solution. The temperature of the hexane solution for TFC5 to TFC8 was changed as -20 °C, 1 °C, 25 °C and 50 °C, respectively. All other synthesis conditions were the same as TFC1 to TFC4	90
4.3	FESEM images of TFC membranes prepared in 0.2%-cyclohexane solution. The temperature of the cyclohexane solution for TFC9 to TFC12 was changed as 8 °C, 25 °C, 35 °C and 50 °C respectively. All other synthesis conditions were the same as TFC1 to TFC4. Since the melting temperature of the cyclohexane is about 6.7 °C, synthesis of PA membranes at sub-zero temperature was not possible with this solvent	90
4.4	(a) FTIR spectra (PES support and TFC1 to TFC4), (b) XPS survey spectrum (TFC 1) along with high resolution C (1s) and O (1s) spectra, (c) convoluted high resolution C (1s) and (d) convoluted high resolution O (1s) spectra (TFC 1 & TFC4). FTIR shows additional peaks associated with the PA to the PES support. The survey spectrum indicates the presence of O, N and C elements and the absence of S on the surface of the membranes indicating all membranes are integrally skinned. The convoluted high resolution C (1s) and O (1s) peaks provide information about the PA chemical bonds that helps to quantify C=O/C-N ratio	91

4.5	(a) Convolved high resolution C (1s) and O (1s) spectra of TFC2, (b) convolved high resolution C (1s) and O (1s) of TFC3 membrane	92
4.6	Water flux and salt rejection of the TFC membranes prepared at different temperature in 0.2 wt.% TMC-heptane solution. The surface and cross-sectional images of the membranes synthesized at -20 °C and 50 °C are presented to justify the permeation properties. Test conditions: feed solutions: pure water and 2000 ppm NaCl solution, pressure: 1.52 MPa (220 psi), temperature: 25 °C, pH: 6.5-7	95
4.7	Water flux and salt rejection of the TFC membranes prepared at different temperature in hexane and cyclohexane solutions. Test conditions: feed solutions: pure water and 2000 ppm NaCl solution, pressure: 1.52 MPa (220 psi), temperature: 25 °C, pH: 6.5-7	95
4.8	FESEM images of (a) TFC I membrane prepared with 2 wt. % MPD and 0.15 wt. % TMC, $\text{NH}_2/\text{COCl}=21.1$ , in hexane at 25 °C; (b) TFC II membrane prepared with 2 wt. % MPD and 0.35 wt. % TMC, $\text{NH}_2/\text{COCl}=9.0$ , in hexane at 25 °C; (c) TFC 3 membrane prepared with 2 wt. % MPD and 0.2 wt. % TMC, $\text{NH}_2/\text{COCl}=15.8$ , in heptane at 25 °C; and (d) TFC 1 membrane prepared with 2 wt. % MPD and 0.2 wt. % TMC, $\text{NH}_2/\text{COCl}=15.8$ , in heptane at -20 °C	98
4.9	FO performance of lab-made and commercial TFC membranes at different osmotic pressure difference between draw and feed solutions. Test conditions: draw solution: 0.25, 0.5, 1, 1.5, 2 and 3 M NaCl solutions; Feed solution: DI water; velocity: 0.22 m/s for feed and draw solutions	99
4.10	Reverse solute flux and specific solute flux of lab-made and commercial TFC membranes. Test conditions: Draw solution: 1 M NaCl solutions; Feed solution: DI water; velocity: 0.22 m/s for feed and draw solutions	101
4.11	FESEM top surface images of (a) active-side; (b) cross-sectional image; (c) support side of the TFC-HTI; (d) high magnification image of the woven fabric inside the support layer	103
4.12	Water permeation of lab-made and commercial TFC membranes. Test conditions: Feed solution: conventionally-treated SAGD BFW; Draw solution: 0.5 M NaCl solution; Cross-flow velocity: 0.22 m/s	105
5.1	FESEM images of ITO NPs along with the diameter of the NPs which was obtained using image processing ( $19.0 \pm 1.9$ nm) and XRD peak fit ( $18.9 \pm 0.11$ nm)	110
5.2	FESEM cross-sectional (a & b) and surface (c & d) SEM images of PES/ITO nanocomposite membrane. EDX spectra of PES/ITO membrane and ITO nanoclusters are added to panel (c) and (d), respectively	111



5.3	Leaching of ITO NPs in water solutions at pH=2, 7 and 12	112
5.4	TGA analysis of the PES/ITO and base PES membrane. The plot shows the weight loss of membrane as a function of temperature	113
5.5	Weight loss of different nanocomposite membranes as well as bare PES membrane as a function of temperature measured by TGA	114
5.6	I-V characteristics of PES/ITO nanocomposite membrane and bare PES membrane	115
5.7	Pure water flux through synthesized PES/ITO nanocomposite and bare PES membranes as a function of transmembrane pressure. Each membrane was initially tested at 700 kPa for 1 h; the permeation flux at lower operating pressures was obtained after 15 minutes	116
5.8	Fouling characteristics of PES/ITO membrane and pristine PES membrane. Flux decline represents fouling of membranes during filtration of WLS inlet water	117
5.9	Fouling characteristics of PES/ITO membrane and pristine PES membrane. $DR_t$ is total flux decline ratio, $DR_r$ is reversible flux decline ratio, $DR_{ir}$ is irreversible flux decline ratio, and FRR is flux recovery ratio.	118
5.10	Flux decline after fouling of nanocomposite membranes by WLS water	118
5.11	Organic matter rejection by PES/ITO and pristine PES membranes during filtration of WLS inlet water	120
5.12	(a) and (b): TEM images of the synthesized $TiO_2$ NPs presenting the size of dried nanoparticles, (c) XRD spectrum of $TiO_2$ NPs showing their anatase crystalline structure, (d) DLS measurement of $TiO_2$ NPs capped with OA presenting their stability and size distribution in heptane	124
5.13	(a) and (b): FESEM images of the base TFC membrane; (c): TEM images of the TFC membrane; (d), (e) and (f): FESEM images of TFN4 membrane; (g) and (h): FESEM images with BSE detector of the TFN4 membrane showing the $TiO_2$ -rich spots brighter than the other regions ; (i): EDX color map of Ti element at the surface of TFN4 membrane; (j), (k) and (l): TEM images of the TFN4 membrane	125
5.14	(a) The ATR-FTIR spectroscopy of the synthesized TFC and TFN membranes; (b) PA characteristic peaks emerge at $1541\text{ cm}^{-1}$ , $1611\text{ cm}^{-1}$ , and $1667\text{ cm}^{-1}$ attributing to N-H bending and C-N stretching vibration of amide II (-CONH-) group, aromatic ring breathing and C=O stretching vibration of amide I bands, respectively; (c) The broad peak at $3300\text{ cm}^{-1}$ is formed to stretching vibration of the N-H groups in the PA layer	126

- 5.15 (a) and (b) FESEM image with BSE detector of TFN2 and TFN4 membranes, respectively; (c) and (d) EDX spectra at TiO<sub>2</sub> rich (point A) and lean (point B) spots at the surface of TFN2 and TFN4 membranes, respectively 127
- 5.16 Water permeation and salt rejection of the synthesized TFC and TFN membranes at 25 °C and 65 °C showing the effect of TiO<sub>2</sub> NPs on permselectivity and thermal stability of the TFN membranes. Operating conditions: 220±5.0 psi of transmembrane pressure and 1.0±0.1 LPM of feed flow rate 129
- 5.17 (a) Schematic view of the measurement of the antibacterial activity of TFN membranes; (b) Images of the E. coli colonies formed in the plate of UV-treated (i) TFC, (ii) TFN2 and (iii) TFN4 membranes; (c) Mechanism for PCT activity of TiO<sub>2</sub> NPs under UV irradiation; (d) Number of E. coli colonies counted on the plate of TFC, TFN2 and TFN4 membranes after 30 minutes of UV irradiation 131

# Nomenclature

$A_m$	Effective surface area
$A_P$	Water permeability coefficient
$B$	Salt permeability coefficient
$C_{i,f}$	Salt concentration in the feed solution
$C_{im}$	Salt concentration at membrane surface
$C_{i,p}$	Salt concentration in the permeate solution
$D_i$	Diffusion coefficients of salt ions in water
$DOF_A$	Degree of freedom of factor A
$DR_t$	Total flux decline ratio
$DR_r$	Reversible flux decline ratio
$DR_{ir}$	Irreversible flux decline ratio
$F$	F-statistics
$F_{di}$	Molar attraction constants for dispersion forces of a specific group i
$F_{pi}$	Molar attraction constants for dipole forces of a specific group i
$E_{hi}$	Hydrogen bonding energy of a specific group i
$J_s$	Reverse salt flux
$J_W$	Pure water flux
$J_{W1}$	Permeate flux with DI water as feed
$J_{Wf}$	Permeate flux with SAGD water as feed
$J_{W2}$	Permeate flux after hydraulic washing with DI water as feed
$k_i$	Mass transfer coefficients of salt ions in water
$m$	Cross-linked structure in polyamide matrix
$n$	Linear part in polyamide matrix, number of experimental trials
$N$	Number of points on surface
$P$	Percent of contribution

$Ra$	Average roughness
$R_c$	Cake layer hydrodynamic resistance
$R_m$	Hydrodynamic resistance
$R_o$	Observed salt rejection
$Rq$	Root mean square roughness
$R_{TOC}$	TOC separation percentage
$S$	Structural parameter
$SS_T$	Total sum of squares
$SS_A$	Sum of squares of factor A
$t$	Membrane thickness
$T$	Sum of all experimental observations
$TOC_p$	TOC concentration in the permeate solution
$TOC_f$	TOC concentration in the feed solution
$V$	Molar volume
$V_A$	Variance of factor A
$y$	Experimental observation
$Z$	Surface height

## Greek Letters

$\alpha$	Levels of significance
$\delta$	Thickness of the mass boundary layer
$\delta_d$	Solubility parameter components due to dispersion forces
$\delta_p$	Solubility parameter components due to permanent dipole forces
$\delta_h$	Solubility parameter components due to hydrogen bonding
$\varepsilon$	Support porosity
$\mu$	Dynamic viscosity
$\rho_D$	Density of the draw solution
$\tau$	Tortuosity
$\pi_{D,b}$	Osmotic pressures of the bulk draw solution

$\pi_{F,m}$	Osmotic pressures of the feed solution
$\Delta P$	Transmembrane pressure
$\Delta P_t$	Total hydraulic pressure
$\Delta P_c$	Trans-cake hydraulic pressure
$\Delta P_m$	Trans-membrane hydraulic pressure
$\Delta t$	Time period of the experiment
$\Delta m$	Weight of water

## Abbreviation

AFM	Atomic force microscopy
Al <sub>2</sub> O <sub>3</sub>	Aluminum oxide
ATR-FTIR	Attenuated total reflectance-Fourier transform infrared
BBD	Boiler blow-down
BFW	Boiler feed water
BST	Biphasic solvothermal
CP	Concentration polarization
CSA	Camphorsulfonic acid
DI	Deionized water
DLS	Dynamic light scattering spectroscopy
DMSO	Dimethyl sulfoxide
DOM	Dissolved organic matter
ECP	External concentration polarization
EDX	Energy-dispersive X-ray spectroscopy
FESEM	Field emission scanning electron microscopy
FO	Forward osmosis
FRR	Flux recovery ratio
ICP-OES	Inductively coupled plasma-optical emission spectroscopy
IP	Interfacial polymerization

ITO	Indium tin oxide
IX	Ion exchanger
MF	Microfiltration
MMM	Mixed matrix membranes
MPD	m-phenylenediamine
NF	Nanofiltration
NMP	N-Methyl-2-pyrrolidone
NP	Nanoparticle
OA	Oleic acid
OTSG	Once through steam generator
PA	Polyamide
PES	Polyethersulfone
RO	Reverse osmosis
SAGD	Steam assisted gravity drainage
SDS	Sodium dodecyl sulfate
SiO <sub>2</sub>	Silicon Oxide
SN	Signal to noise ratio
TDS	Total dissolved solids
TEA	Triethylamine
TEM	Transmission electron microscopy
TFC	Thin film composite
TFN	Thin film nanocomposite
TGA	Thermal gravimetric analysis
TiO <sub>2</sub>	Titanium dioxide
TMC	Trimesoyl chloride, (xxx)
TMOP	Transmembrane osmotic pressure
TOC	Total organic carbon
UF	Ultrafiltration

WLS	Warm lime softener
XPS	X-ray photoelectron spectroscopy
XRD	X-ray diffraction spectroscopy

# Chapter 1

## Introduction



## 1.1 Water demand

Water crisis, according to the Global Risks Report by World Economic Forum in 2015, is the foremost global risk to social, environmental, and economical development of many countries in the next ten years [1]. Over the past decade, demand for fresh water has drastically increased with rapid growth in the world's population, advancement in industrialization, global climate change and growing scarcity of surface and ground water resources [2]. Today, more than 1.8 billion people, around one-fifth of the world's population, live in the areas with severe water shortage where poor access to clean and safe drinking water causes several million deaths every year [3,4]. The lack of fresh water has thus accelerated efforts toward improvement of the current treatment processes and development of novel techniques to sustainably produce potable water from sea water desalination and industrial and municipal waste waters reclamation [5]. Canada's oil sands industry is an example which needs urgent improvement in water management as it uses approximately 0.5 to 0.9 barrel of water consumed per barrel of oil produced in steam assisted gravity drainage (SAGD) operation. Hence, the sustainability of Alberta oil sands industry requires the recycling and reuse of process-affected water.

## 1.2 Overview of SAGD operation

A great amount of research and development is currently ongoing in the Canadian oil sands industry to improve the water treatment processes for higher levels of water recycle and to reduce the energy associated with water treatment and steam generation. A part of this effort to reduce the oil sands water consumption is focused on the SAGD operation. SAGD is a thermally enhanced heavy oil recovery technique which is widely practiced for bitumen extraction from oil sands in Alberta, Canada.

In this process, steam is injected through a horizontal well into the bitumen-rich region to decrease the viscosity of the bitumen and facilitates its extraction. An emulsion of steam condensate and heated bitumen flows down along the periphery of the steam chamber to the production well which is located below the injection well. This emulsion is then pumped to the surface where the bitumen and water are separated and the water is treated for reuse as boiler feed water. In a typical SAGD surface treatment plant (Figure 1.1), the produced emulsion is first sent through a series of gravity separation vessels to remove the gases, and

separate the bitumen and water. The de-oiled produced water then mixes with make-up water and recycled boiler blow-down (BBD) and is sent to a warm lime softener (WLS) to remove silica as well as the ion exchangers (IX) to remove  $\text{Ca}^{2+}$  and  $\text{Mg}^{2+}$  to make the treated water suitable for boiler feed water (BFW). The treated water is used as BFW in a steam generator, known as a once through steam generator (OTSG), which can tolerate relatively high amounts of dissolved solids and organic matter. To compensate for the relatively low-quality BFW, however, OTSGs typically produce only a low quality steam (75-80%), resulting in a large volume of BBD. A portion of the BBD is recycled back to the WLS and the rest is sent to disposal.

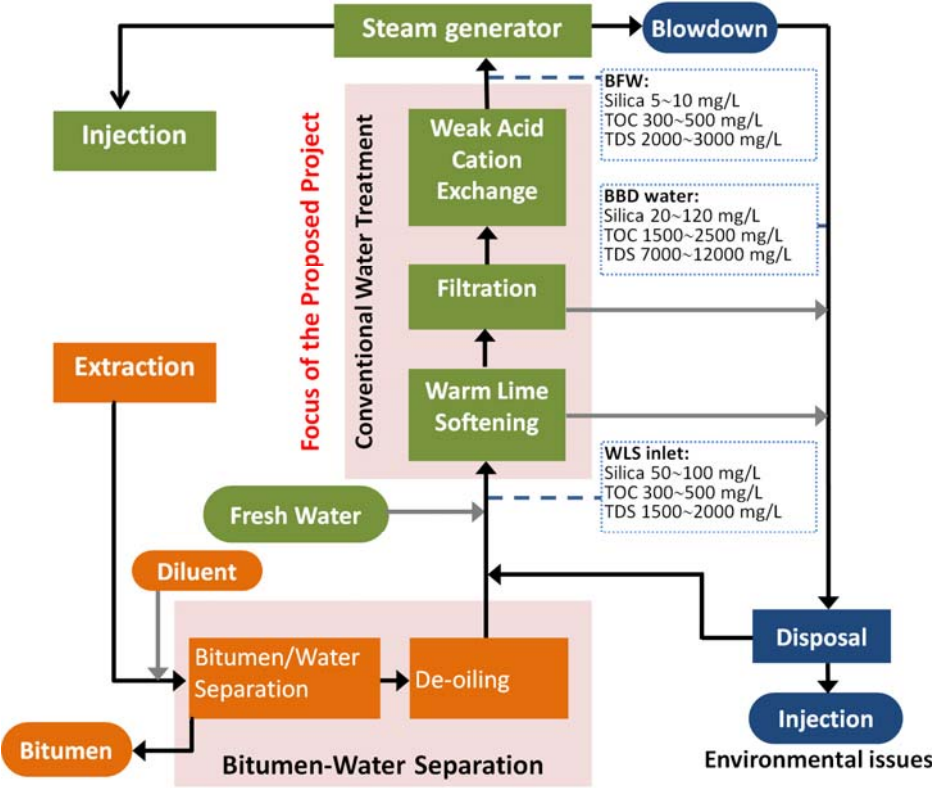


Figure 1.1: Process flow diagram of a SAGD process.

The conventional WLS-IX water treatment configuration does not reduce the amount of dissolved organic matter (DOM) or total dissolved solids (TDS) in the boiler feed water. The high levels of DOM and TDS in the OTSG feed water can cause numerous operational problems like fouling of pipelines and equipment, and clogging of injection wells [6-8]. To reduce the volume of disposal water, evaporators are sometimes used as a downstream BBD recovery process.

Evaporators have also been used to directly desalinate produced water to make high-quality boiler feed water, but energy use is high. High boiler feed water TDS and DOM results in higher blowdown volumes and necessitates recycling more low quality BBD water back to the process [8]. In light of the above, it is of interest to compare the WLS-IX scheme with emerging membrane-based process which can separate almost all silica and divalent ions and reject more than 90% of DOM and TDS in a single step operation [9]. In addition to improving operation of the current OTSGs, a membrane-based desalination process would allow the production of high-quality BFW suitable for higher efficiency drum boilers, while consuming less energy than if desalination evaporators were used.

### **1.3 Membrane technology for water treatment**

Membrane separation technologies have secured an important role in available water purification processes as a promising single step technique for removing multiple sized solutes and organic pollutants from contaminated water. Membrane technology inherits distinct advantages over traditional method such as distillation, evaporation, ion exchange, and lime softening that includes primarily lower operating expenses and energy consumption. In addition, membrane processes provide higher separation efficiency and smaller footprint than conventional processes. The required energy for the filtration in a membrane process can be provided as a driving force such as applied pressure, temperature and concentration gradient, or external electric field. Among different membrane processes, pressure-driven membranes are widely used for purification of the liquids from dissolved/dispersed contaminations. These membranes are typically classified as microfiltration (MF), ultrafiltration (UF), nanofiltration (NF), and reverse osmosis (RO). The MF membranes contain a distribution of pore size in the range of 0.05  $\mu\text{m}$  to 10  $\mu\text{m}$  and are capable to isolate large particulate and colloidal, organic matter. The UF membranes, which have smaller pores than MF membranes in the range of 10  $\mu\text{m}$  to 100 nm, are widely used to remove bacteria, viruses and macromolecules such as proteins. NF membranes possess pore size range between UF and RO membranes (1 to 10 nm). These membranes are commonly utilized for water softening or separating divalent ions and minerals from the wastewater. Finally, the RO membrane which is considered the densest membranes, has a pore size less than 1 nm [10]. The RO membranes are mainly used to separate monovalent ions to produce high quality water from sea and brackish waters.

In terms of the internal structure, membranes can be categorized into symmetric and asymmetric. The symmetrical membranes contain uniform pore size distribution in their cross-section. In contrast, the asymmetric membranes have smaller pores close to the top surface and larger pores at the bottom [11]. These membranes consist of a dense skin layer with the thickness less than 500 nm on a microporous sublayer with the thickness about 200  $\mu\text{m}$ . Asymmetric membranes often provide higher permeation rate compared to symmetric membrane of comparable thickness [12]. In general, the permeation rate across a membrane is inversely proportional to the membrane thickness. High permeation rate is highly desirable to reduce the energy consumption, thus an ideal membrane should be as thin as possible without sacrificing the quality of the filtered permeate [10].

Based on the internal free volumes, membranes can be divided into dense and porous membrane. The transport mechanism through a dense and porous membrane depends on the relative size and connectivity of the pores. In the case of a dense membrane such as NF and RO membranes, the transport of solute and solvent molecules occurs based on solution-diffusion mechanism through the membrane [13]. The molecules of the component (solvent or solute) which is going to transfer through the membrane are first dissolved into the membrane surface, then diffuse across the membrane, and finally desorbed at the permeate side. The very small pores of RO and NF membranes are in the scale of random thermal motion of the polymer chains which form the membrane [10]. Regarding that, the separation of components in NF/RO membranes is based on the difference in solubility and diffusivity of the species within the membranes. In the case of porous membranes such as MF and UF, the transport mechanism is well explained based on pressure-driven convection through the pores. The separation of the species in MF and UF membranes is mainly occurs based on the size of species, which is so called molecular sieve mechanism [10].

## **1.4 Synthesis techniques of porous and dense membranes**

Different methods are used to fabricate synthetic polymeric membranes. The widely used methods are listed in Figure 1.2 [12]. The selection of a proper technique to fabricate the membranes highly depends on the desired properties of the resulting membranes. Solution casting and interfacial polymerization reaction are often employed to prepare dense NF/RO and gas separation membranes.

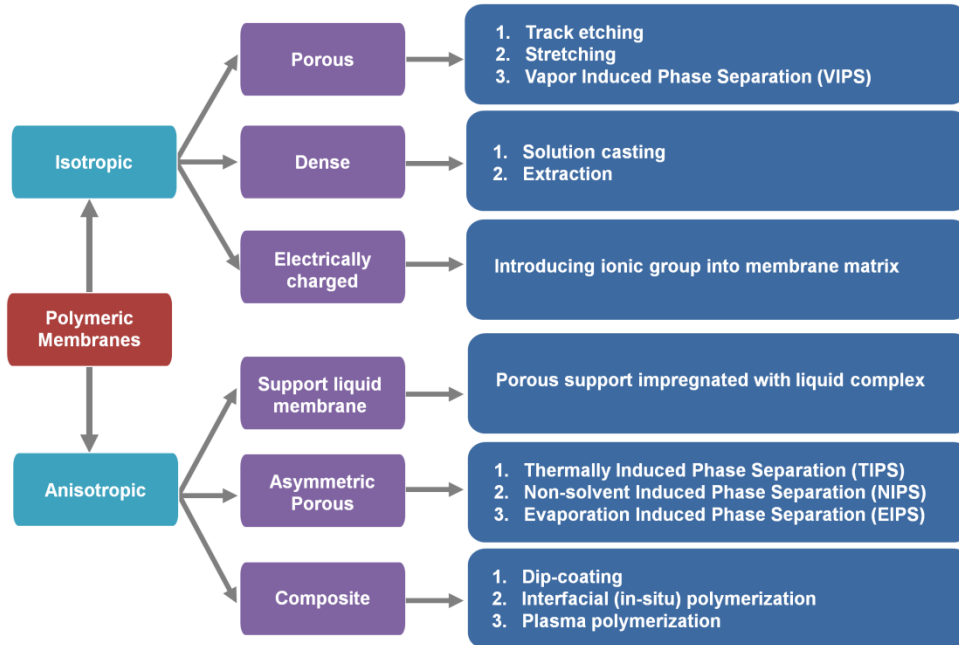


Figure 1.2: Fabrication techniques for preparation of the polymeric membranes.

Phase inversion is the most commonly used method for the fabrication of the porous polymeric membranes. This process works relies on the separation of solvent and non-solvent in a polymer solution, producing a porous polymer film. During the phase inversion process, a thermodynamically stable polymer solution experiences a liquid-liquid demixing and then separates into a polymer rich and polymer lean phase. [14]. Phase inversion process can be carried out by multiple methods including (i) immersion of cast polymer film into nonsolvent bath, (ii) evaporation of the volatile solvent from the cast polymer film, (iii) lowering the temperature of the casting solution below a threshold, and immersing the polymer film in a non-solvent vapor phase [15].

Non-solvent induced immersion precipitation method is widely used to fabricate porous sublayer for the NF/RO composite membranes. In this method, a polymer solution is cast on a flat glass plate and then immersed into a nonsolvent bath, so called coagulation bath (mainly water). The phase inversion process is controlled by diffusion of low molecular weight components. Due to the exchange of solvent in the polymer solution and non-solvent in the coagulation bath, the resulting composition in the polymer film is changed. After some time, the composition of the polymer rich phase reaches the glass transition composition and the system solidifies. As a result of solidification process, the film's morphology is frozen at that point and polymer film with porous structure forms [16].

Currently, most of the commercial desalination plants employ RO and NF with thin film composite (TFC) membranes at the heart of the separation processes [17,18]. The TFC membranes are also widely-used in other membrane-based filtration applications including food, pharmaceutical and chemical industries [19,20]. These membranes typically consist of at least two compositional layers, (i) a top thin selective layer and (ii) a bottom porous sublayer which are of different structure and material [21]. The porous support provides the required mechanical stability for the TFC membranes to operate under high pressures while the ultrathin top layer plays the principal role in water filtration. The top selective thin layer is typically fabricated from polyamide (PA) using an in-situ interfacial polymerization (IP) reaction between two reacting monomers (diamine and polyacyl chloride), at the surface of the porous support (such as polyethersulfone (PES), backed by a polyester fabric mesh). The multilayer feature of TFC membranes exploits the highly desirable advantage that each layer in the composite membrane can be independently optimized with the proper choice of materials and preparation methods for the specific application of interest [22]. A schematic representation of a TFC PA membrane with surface and cross-sectional images of the PA selective layer and PES substrate are illustrated in Figure 1.3.

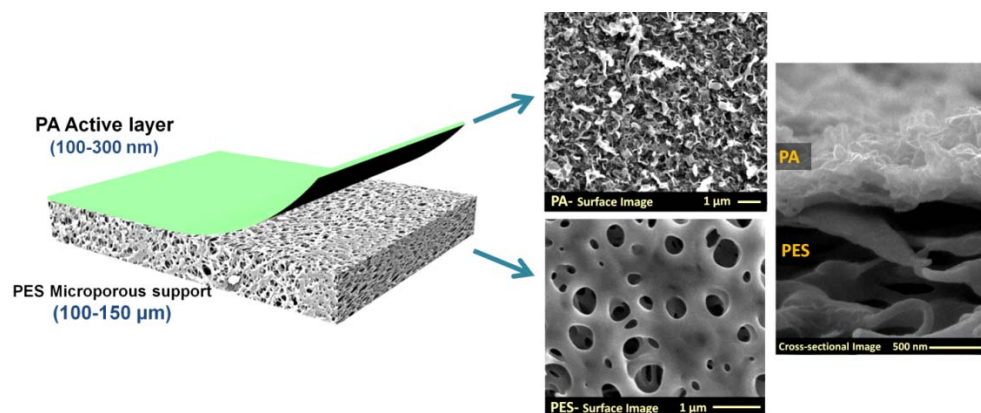


Figure 1.3: Schematic view of a TFC PA membrane along with the surface and cross-sectional images of the top PA and bottom PES layers.

## 1.5 Transport mechanism through NF/RO membranes

In the case of dense membranes such as NF and RO where the membranes show high percentage of salt rejection, the concentration polarization (CP) by ions and fouling by colloidal particles, organic matter, and microorganisms are two interconnected phenomena which lower the water permeation rate through the membranes. The resistance toward water passage through these membranes is made up of three major components, namely (i) the hydrodynamic resistance of the membrane in the absence of foulants, (ii) the resistance due to the accumulation of ions at the membrane surface (CP), and (iii) the resistance due to the accumulation of foulants at the membrane surface (fouling).

The hydrodynamic resistance ( $R_m$ ) of the membrane can be calculated by measuring the pure water flux ( $J_w$ ,  $m^3/(m^2s)$ ) at different transmembrane pressure. The membrane hydrodynamic resistance is then calculated using the following equation:

$$J_w = \frac{\Delta P}{\mu R_m} \quad (1.1)$$

where  $\mu$  is the dynamic viscosity of the water (Pa s) and  $\Delta P$  is the transmembrane pressure (Pa). The resistance caused by accumulation of salt ions at the membrane surface (CP), in the absence of fouling material, is determined by the generated transmembrane osmotic pressure (TMOP). The TMOP lowers the effective driving force for the transport of water molecules and is obtained by measuring the permeate flux, pressure, and salt concentration over time using a salt water solution with a specific NaCl concentration. The observed salt rejection ( $R_o$ ) and the TMOP ( $\Delta\pi$ , Pa) can be determined using the following equations:

$$R_o = 1 - \frac{C_{i,p}}{C_{i,f}} \quad (1.2)$$

$$J_w^S = \frac{\Delta P - \Delta\pi}{\mu R_m} \quad (1.3)$$

where  $C_{i,f}$  and  $C_{i,p}$  ( $mol/m^3$ ) are the salt concentration in the feed and permeate solutions, respectively. Using the evaluated  $R_o$  and  $\Delta\pi$ , the initial electrolyte mass transfer coefficient in the salt CP layer ( $k_i$ ,  $m/s$ ) can be calculated by employing the van't Hoff equation and film theory. Schematic diagram of the CP layer formed on the membrane is demonstrated in Figure 1.4. Applying the mass balance equation for the salt ions on a control volume shown in this figure gives the following equation [23–25]:

$$J_W^S C_i - J_W^S C_{i,p} + D \frac{dC_i}{dx} = 0 \quad (1.4)$$

The appropriate boundary conditions are as follows:

$$\begin{aligned} x = 0 \quad C_i &= C_{i,f} \\ x = \delta \quad C_i &= C_{i,m} \end{aligned} \quad (1.5)$$

where  $\delta$  is the thickness of the mass boundary layer. Utilizing these boundary conditions, the boundary layer film model is derived as:

$$\frac{C_{i,m} - C_{i,p}}{C_{i,f} - C_{i,p}} = \exp\left(\frac{J_W^S \delta}{D_i}\right) = \exp\left(\frac{J_W^S}{k_i}\right) \quad (1.6)$$

where  $D_i$  and  $k_i$  are the diffusion and mass transfer coefficients of salt ions in water, respectively, and  $C_{i,m}$  is the salt concentration at the surface of the membrane surface. The van't Hoff equation gives the osmotic pressure difference for the simple case of dilute monovalent electrolyte as:

$$\Delta\pi = 2RT(C_{i,m} - C_{i,p}) \quad (1.7)$$

where  $R$  is the universal gas constant (J/mol K) and  $T$  is the absolute temperature of water (K). Plugging in  $C_{i,m} - C_{i,p}$  from Equation (6) into Equation (7) results:

$$\Delta\pi = 2RT(C_{i,f} - C_{i,p}) \exp\left(\frac{J_W^S}{k_i}\right) \quad (1.8)$$

Finally, the TMOP can be calculated by replacing  $C_{i,f} - C_{i,p}$  using the Equation (2) as following:

$$\Delta\pi = 2RTC_{i,f}R_o \exp(J_W^S/k_i) \quad (1.9)$$

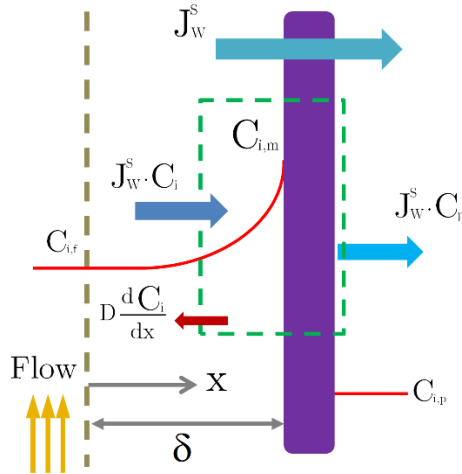


Figure 1.4: Schematic diagram of the CP layer.



The cake layer hydrodynamic resistance ( $R_c$ ) which is caused by accumulation of colloidal particles as well as organic matter at the membrane surface can be evaluated by the film theory. Considering  $R_c$ , the permeate flux can be written as:

$$J_W^F = \frac{\Delta P_c}{\mu R_c} = \frac{\Delta P_m}{\mu R_m} = \frac{\Delta P_t - \Delta \pi_m}{\mu (R_m + R_c)} \quad (1.10)$$

where  $\Delta P_t$ ,  $\Delta P_c$ , and  $\Delta P_m$  (Pa) are the total, trans-cake, and trans-membrane hydraulic pressures, respectively. The total applied pressure ( $\Delta P_t$  as the driving force of transport through the membrane) includes the trans-cake hydraulic pressure ( $\Delta P_c$ ), the trans-membrane pressure ( $\Delta P_m$ ), and TMOP ( $\Delta \pi_m$ ).

## 1.6 Literature review

Since the early invention of TFC by Cadotte [26,27], a significant amount of research and development has been underway to modify these membranes in terms of water flux, salt rejection and fouling resistance. In general, conventional membranes are subject to a trade-off relationship between permeability and selectivity, i.e. high water flux membranes show a low rejection percentage and vice versa. Therefore, one of the hoped-for goals of the research in the field of membrane fabrication has always been to develop high throughput membranes with high separation efficiency.

Recent advances in TFC membrane technology were mainly focused on (i) improving the membrane synthesis protocols [28,29], (ii) developing new polymeric material for the selective and support layers [30], (iii) modifying the surface properties of the TFC membrane [31,32] and (iv) developing nanocomposite membranes by the incorporation of multifunctional nanofillers [33–37]. The main objectives are to synthesize more water permeable membranes with tunable surface and bulk properties in order to provide enhanced thermomechanical, electrical, chemical and anti-fouling characteristics hydrophilic. Although most of these efforts have shown promising results in the lab-scale, they are still faced with the challenges of cost-efficient synthesis process and easy scale-up for high volume industrial practices [38].

## 1.7 Research objectives

The main goal of the present research is to fabricate high performance thin film nanocomposite (TFN) PA membranes with improved thermal, electrical and antifouling characteristics for water purification processes. To reach this goal, the current work is based on the following two themes:

(i) Modifying the membrane synthesis procedure via optimization of the IP reaction conditions and addition of chemical additives. It is generally accepted that the final transport properties of a TFC PA membrane strongly depend on multiple synthesis parameters such as the chemical structure and concentration of reacting monomers, presence of chemical additives in the monomers' solution, reaction time and temperature, post-treatment method, porosity of the porous sublayer. The literature does not form a clear consensus about the influence of these synthesis parameters on the final properties of the TFC membranes. Hence, further research is needed to investigate the effects of these parameters in order to fabricate energy-efficient membranes with enhanced range of permeation and selectivity. The findings at this step are used to develop a base line for further modifications of the TFC membranes by integration of the functional nanoparticles (NPs).

(ii) Developing robust and high performance nanocomposite membranes by incorporation of metal oxide NPs to the pristine membrane. The incorporation of NPs to a polymer film, with the aim of enhancing the permeation and antifouling properties, may not induce the desired functionality to the host membrane and even deteriorate its permeation properties. The major challenges that need to be addressed are the severe aggregation of the NPs in the monomer solutions as well as the weak compatibility of encapsulated NPs with the polymer linkage. In the case of TFN PA membranes, large clusters of NPs cannot be accommodated in a thin PA layer of 100-300 nm, which makes the agglomeration effect even more severe. The non-uniform dispersion of NPs within the host polymer forms non-selective voids within the PA matrix, which significantly reduces the rejection percentage. Therefore, effective synthesis protocols for robust fabrication of nanocomposite membranes are aimed to be developed to impart multiple functionalities such as thermal stability, electrical conductivity and antifouling propensity to the host membrane.

## 1.8 Thesis structure

The present dissertation is organized in a paper-based format. Chapters 3, 4 and 5 each are written based on submitted/published articles. Chapter 2 provides the list of materials, synthesis protocols and characterization techniques used for the preparation of the NPs and membranes. The TFC membranes in the present research consist of a thin PA layer over a micropores PES substrate. The PA layer was made from m-phenylenediamine (MPD) and 1,3,5-benzenetricarbonyl trichloride (TMC, also known as trimesoyl chloride) using IP reaction.

Chapter 3 presents the outcomes of a series of systematic studies on the effect of synthesis conditions and chemical additives on the final properties of TFC membranes. The concentration of reacting monomers, the time of the IP reaction and the temperature of curing treatment were the influential parameters that were studied. Also the effect of adding different chemical additives namely SDS, CSA, TEA, DMSO, ethanol, isopropanol, xylitol, glycerol on the resulting characteristics of the TFC membranes was investigated systematically.

Chapter 4 provides the results of thermally modulated IP reaction for the synthesis of high throughput TFC membranes for forward osmosis (FO) applications. The innovative adjustment relies on lowering the temperature of organic-monomer solution to sub-zero temperatures prior to the IP reaction. The substantial changes in the physicochemical properties of the resulting PA layer due to thermal adjustment of the monomer containing organic solution were discussed in this chapter.

Chapter 5 presents the findings of developing two types of nanocomposite membranes. First, ITO NPs were integrated into PES matrix in order to improve the electrical conductivity and thermal stability of the PES membranes. The antifouling propensity of the PES-ITO membranes was evaluated using SAGD produced water and compared with unmodified PES membrane. Furthermore, a robust method developed to integrate  $\text{TiO}_2$  NPs to the PA layer via in-situ polymerization process. A well-dispersed  $\text{TiO}_2$  NPs was first synthesized in heptane using biphasic solvothermal (BST) reaction and then the stable NP suspension added to TMC solution prior to IP reaction. Using this technique, TFN PA membranes with enhanced thermal stability and antibacterial activity were prepared.

Chapter 6 summarizes the major findings of all parts of this research and provides a concluding discussion. Moreover, suggestions and recommendations for further advancement of the ongoing research are provided.

## 1.9 Thesis contribution

The permeation performance of a TFC PA membrane strongly depends on its physicochemical properties (such as hydrophilicity, surface charge, and roughness) and its internal structure (e.g. free volume distribution, cross-linking density, and thickness). These characteristics are highly desirable to be controlled using IP reaction in order to tune the final performance of the TFC membranes. Regarding that, a series of studies were conducted systematically in order to develop a fundamental understanding of the effect of the synthesis conditions and chemical additives on the permeation characteristics of the TFC membranes. Guidelines for fabrication of high performance TFC membrane with a wide range of water permeation and salt rejection were presented in chapter 3. To reduce the thickness of the PA selective layer and thus improve the water permeability of the TFC membranes, an innovative adjustment of IP reaction was proposed in chapter 4. By lowering the temperature of the organic-monomer solution prior to IP reaction, TFC membranes with remarkably higher permeability were fabricated for osmotically-driven filtration processes. Finally, systematic attempts were made successfully in chapter 5 to improve the thermal stability, electrical conductivity and fouling resistivity of the TFC membranes by incorporation of ITO and  $\text{TiO}_2$  nanoparticles into the membrane matrix. A novel membrane synthesis protocol was also developed for in-situ incorporation of  $\text{TiO}_2$  NPs into the PA layer which can be widely used for robust fabrication of TFN PA membranes.

# Chapter 2\*

## Materials and methods

---

\* This chapter is organized based on references [39-45].

## 2.1 Materials

Flat sheet microporous PES membranes with the average pore size of 100 nm and 200 nm were purchased from Sterlitech Co. (WA, USA) and used as support layer for the synthesis of TFC membranes. PES polymer (molecular weight of 58 kDa) was obtained from BASF and used as for preparation of the microfiltration (MF)/ultrafiltration (UF) membranes casting solutions. The fabricated MF/UF membranes were utilized either for pretreatment of industrial produced water or as the support layer for the synthesis of TFC membranes [39].

MPD ( $\geq 99\%$ ) and TMC ( $\geq 98\%$ ) were obtained from Sigma Aldrich and used as reacting monomers for the synthesis of PA films. N-Methyl-2-pyrrolidone (NMP), ammonium hydroxide, cyclohexane, hexane, heptane ( $\geq 99\%$ ) were purchased from Fisher Scientific. Camphorsulfonic acid (CSA), triethylamine (TEA) and sodium dodecyl sulfate (SDS) were obtained from Fisher Scientific and added into MPD-water solution as chemical additives. Ethanol, ethylene glycol, xylitol and dimethyl sulfoxide were obtained from Sigma Aldrich and utilized as co-solvents in the MPD-aqueous solution [40,41].

Indium chloride ( $\text{InCl}_3$ ) and tin chloride ( $\text{SnCl}_4$ ) were purchased from Strem Chemicals Inc. (Newburyport, MA, USA) and used for synthesis of ITO NPs. Titanium (IV) isopropoxide was purchased from Sigma Aldrich and used as a precursor for synthesis of  $\text{TiO}_2$  NPs. Commercial silicon oxide ( $\text{SiO}_2$ ),  $\text{TiO}_2$  and aluminum oxide ( $\text{Al}_2\text{O}_3$ ) NPs were supplied from Skyspring Nanomaterials Inc. (Houston, TX, USA). Chemical dispersing agents, namely oleic acid (OA), hexylamine, dodecylamine and oleylamine (Sigma Aldrich) and proprietary BYK-106 and BYK-107 (Altana AG, Wesel, Germany) were used to make monodispersed suspension of NPs in different solvents. All the materials were used as they were received from the suppliers [42].

The industrial produced water used for testing the fouling propensity of the synthesized membranes was SAGD produced water provided from a SAGD water treatment plant located in the Athabasca oil sands region of Alberta, Canada. SAGD is a thermally enhanced heavy oil recovery method which is widely practiced for bitumen extraction from oil sands in Alberta, Canada. In this process, steam is injected through a horizontal well into the bitumen-containing formation to decrease the viscosity of the bitumen and effect its extraction. An emulsion of steam condensate and heated bitumen flows down along the periphery of the steam chamber to the production well which is located below the injection well. This emulsion is then pumped to the surface where the bitumen and water are separated

and the water is treated for reuse. In a conventional SAGD plant, the produced water is de-oiled and treated by warm lime softening (WLS) and ion exchange to reduce inorganic scalants, and then used as boiler feed water (BFW) in a steam generator known as a once through steam generator (OTSG), which can tolerate relatively high amounts of dissolved solids, but is limited to low quality steam (70-85%). The properties of WLS and BFW are summarized in Table 2.1 and 2.2 [43,44].

Table 2.1: Properties of WLS inlet water.

Parameter	Unit	WLS inlet water
pH	-	10.0
TOC	mg/L	480
TDS	mg/L	1100
Conductivity	$\mu$ S/cm	1750
Na <sup>+</sup>	mg/L	380
Cl <sup>-</sup>	mg/L	205
Mg <sup>2+</sup>	mg/L	0.7
Ca <sup>2+</sup>	mg/L	1.6
Iron, total	mg/L	0.45
SiO <sub>2</sub> , dissolved	mg/L	90

Table 2.2: Properties of conventionally-treated SAGD BFW.

Parameter	Unit	Specification
Conductivity	mS/cm	1.8 – 2.2
pH	---	9.8 – 10.5
TDS	mg/L	1800 – 2000
TOC	mg/L	450 – 550
Silica (as SiO <sub>2</sub> )	mg/L	30 – 40
Calcium	mg/L	0.4 – 0.5
Iron	mg/L	0.2 – 0.3

## 2.2 Synthesis of ITO NPs

The ITO NPs were synthesized in water solution with the following procedure: indium chloride and tin chloride were first reacted in water in the presence of ammonium hydroxide to make a complex of tin oxide–indium hydroxide and ammonium chloride. The solution was then centrifuged and washed several times with deionized (DI) water in order to remove ammonium chloride and make a white compound of tin oxide–indium hydroxide. Following this, water was removed by crystallization of this compound at 700 °C when the yellow ITO crystals were formed. Finally, the yellow ITO crystals were hydrogenated with 10% H<sub>2</sub> and 90 %

Ar gas at 350 °C to produce conductive blue ITO crystals [45]. Figure 2.1 illustrates the hydrothermal route for the synthesis of ITO NPs.

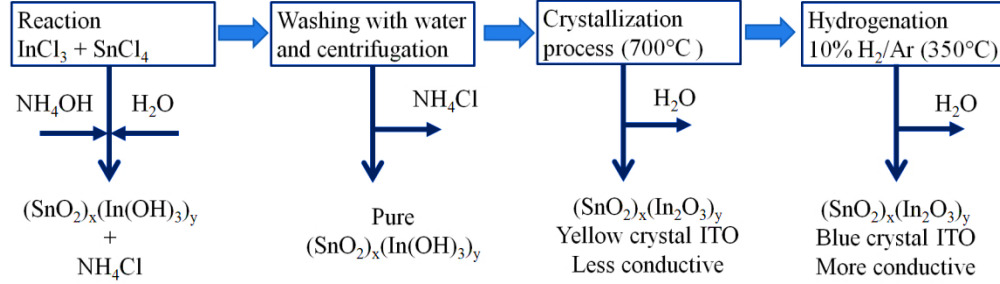


Figure 2.1: Schematic route for synthesis of ITO NPs.

## 2.3 Synthesis of TiO<sub>2</sub> NPs

TiO<sub>2</sub> NPs were prepared using a biphasic solvothermal (BST) reaction where the reaction takes place at the interface of water and organic solutions at an elevated temperature [46,47]. First, a water solution consisting of 20 ml of DI water and 200 µl of TEA (as a pH regulator) was added into a PTFE Teflon liner. Afterward, the organic solution was prepared by adding 800 µl of titanium (IV) isopropoxide and 1200 µl OA to 20 ml of heptane. The heptane solution was sonicated for 30 minutes in an ultrasonic bath (FS30H, Fisher Scientific) and then poured gently over the water phase in the PTFE liner. The Teflon vessel was placed into a stainless steel autoclave, then sealed and heated in a vacuum oven (Thermo Scientific Heratherm™, USA) for 8 hours at 200 °C. Titanium (IV) isopropoxide reacted with water at the water/heptane interface to generate TiO<sub>2</sub> as follows [48]:



Afterwards, the autoclave was cooled down for 12 hours at room temperature and the supernatant organic solution which contained TiO<sub>2</sub> NPs capped with OA was carefully extracted. Assuming 100% conversion for the progress of the above reaction, the produced TiO<sub>2</sub> was found to be 0.01 mg/µl. Figure 2.2 schematically illustrates the synthesis route of the TiO<sub>2</sub> NPs using BST reaction.



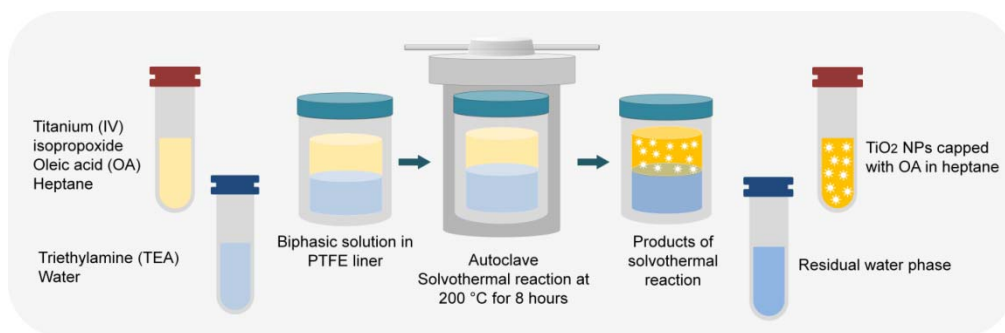


Figure 2.2: Schematic synthesis route for making TiO<sub>2</sub> NPs.

## 2.4 Synthesis of PES support layer

The PES substrate was prepared by phase inversion method with NMP and water as solvent and nonsolvent, respectively. First, PES-NMP solution was stirred for 24 h at room temperature. Then the solution was sonicated in an ultrasonic bath (Fisher Scientific FS30H) to remove any air bubbles from the solutions. Afterwards, the prepared homogeneous solution was cast using an automatic film applicator (Gradco, FL, USA) with 200  $\mu\text{m}$  clearance gap on a glass plate or a polyester (PS) fabric. The cast film was subsequently immersed in a DI water bath for 24 h to complete the phase separation process.

## 2.5 Synthesis of PES-ITO nanocomposite membrane

In order to add ITO NPs to the PES matrix, first a mono-dispersed suspension of ITO NPs in NMP was prepared with the use of a proper dispersing agent. The dispersing agents are basically surfactant molecules which have both hydrophilic and hydrophobic groups (amphiphilic molecules) [49,50]. The amphiphilic surfactants bound to the NPs surface by a number of attractive interactions (e.g. chemisorption, electrostatic attraction, hydrophobic interaction and hydrogen bonding) [51]. The surface modified NPs are then less prone to aggregation due to repulsive forces between them which originate from electrostatic repulsion, ligand-solvent and ligand-ligand (steric) interactions, or a hydration/solvation layer on the surface [52]. However, the final stability of the NPs suspension depends significantly on the interaction of the surfactant molecule with both NPs surface and carrier solvent. Very weak bonding between dispersing agent and the NPs surface leads to easier detachment of longer chain surfactant molecules from the surface of the NPs [53,34]. Furthermore, utilization of dispersing agents with low solubility in the carrier solvent intensifies formation of

surfactant micelles in the solution which might deteriorate the suspension stability and ultimately cause aggregation and precipitation of NPs [54]. For synthesis of nanocomposite PES-ITO membranes, after testing the six dispersing agents and comparing the size distribution of ITO/NMP system, BYK-106 was selected to be the most suitable dispersing agent that yielded the most stable mono-dispersion of ITO NPs in NMP. The viscosity of the dispersing agent and its concentration in the casting solution was very low which didn't affect the viscosity of the casting solution and subsequently the demixing of solvent and nonsolvent in the phase inversion process [55]. In the second step, the PES polymer was added to the suspension and sonicated for 2 h. Subsequently, the prepared homogeneous PES/ITO suspension was cast on a glass plate using an automatic film applicator (TQC AB3120, Gradco). The casting speed and clearance gap of micrometer film applicator were adjusted to 20 mm/s and 200  $\mu\text{m}$ , respectively. Other nanocomposite membranes (PES-TiO<sub>2</sub>, PES-SiO<sub>2</sub> and PES-Al<sub>2</sub>O<sub>3</sub>) were fabricated following the same procedure.

## 2.6 Synthesis of TFC membranes

The TFC PA membranes were prepared via IP reaction between MPD and TMC monomers, which were dissolved separately into an immiscible solvent, at the surface of PES microporous support. First, the PES support was placed between a rubber gasket and a plastic frame and then the MPD-aqueous solution was poured into the frame and allowed to fully penetrate into the support for 15 minutes before draining the MPD solution. The frame and the gasket were then disassembled and the excess amine solution was removed from the surface using a rubber roller. Afterwards, the impregnated PES support was again mounted between frame and gasket and this time TMC-organic (e.g. cyclohexane, hexane, or heptane) solution is poured at the surface to allow the IP reaction to take place for a desired period of time. The resulting TFC membranes were then thermally treated in a digital oven at certain times and temperatures. Finally, to remove any residual solution from the surface, the TFC membranes were washed several times with DI water and kept in the water bath at room temperature until the characterization tests were performed. The schematic view of the interfacial polymerization reaction and the chemical formula of the resulting PA film are presented in Figure 2.3.

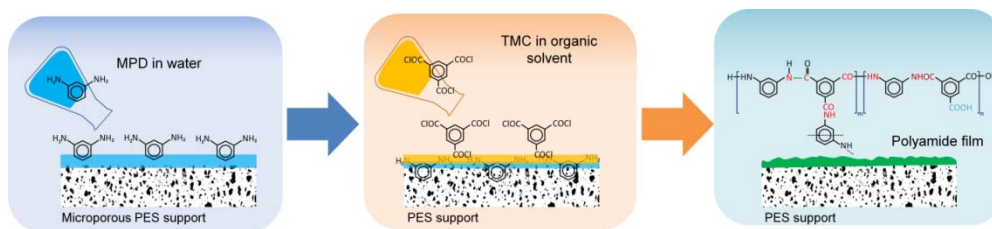


Figure 2.3: Schematic representation of the IP reaction between MPD and TMC at the surface of the microporous PES support.

## 2.7 Characterization of synthesized NPs and membranes

Different characterization techniques were employed to evaluate the physiochemical and structural properties of the synthesized NPs and membranes.

### 2.7.1 Analysis of the surface and cross-sectional morphology

The surface morphology of the membranes was examined using field emission scanning electron microscope (FESEM, Zeiss Sigma 300 VP and JEOL 6301F). The samples were carbon coated and imaged at an accelerating voltage of 10 kV. The microscope was also equipped with energy-dispersive X-ray spectroscopy acquisition system (EDX, Bruker) for elemental mapping and phase identification. The cross-sectional images of the membranes and NPs were obtained using transmission electron microscopy (TEM, Philips/FEI Morgagni 268, The Netherlands) at acceleration voltage of 80 kV. Regarding the polymeric samples, the preparation protocol included first staining in uranyl acetate and lead citrate, then embedding in spurr's resin, and finally sectioning using ultramicrotome (Reichert-Jung Ultracut E, USA). In order to obtain the TEM image of the NPs, a drop of dilute suspension of NPs was poured on the TEM grid. After evaporation of the carrying solvent, the sample was inserted into the TEM machine.

### 2.7.2 Evaluation of the chemical composition

The functional groups present at the surface of the synthesised membranes were investigated using attenuated total reflectance-Fourier transform infrared (ATR-FTIR) spectroscopy. The ATR-FTIR microscope (Thermo Nicolet Nexus 670, USA) was equipped with a mercury-cadmium-tellurium (MCT) detector. The

spectrum of each membrane was averaged from 512 scans and collected over the range of 600–4000  $\text{cm}^{-1}$  at 4  $\text{cm}^{-1}$  resolution.

X-ray photoelectron spectroscopy (XPS) is used for analyzing elemental composition (C, O, N) for the top 1–10 nm of the membranes surface. The TFC membranes analyzed using a Kratos AXIS ULTRA spectrometer equipped with a monochromatic Al K $\alpha$  X-ray source. The source was run at a power of 210 W (14 mA, 15 kV) and a hybrid lens with a spot size of 700  $\mu\text{m} \times 400 \mu\text{m}$ . Survey spectra were collected with a pass energy of 160 eV, step size of 0.4 eV, and sweep time of 100 s in the range of 0–1100 eV. High resolution spectra for C, O and N elements were collected with pass energy of 20 eV, step size of 0.1 eV, and sweep time of 200 s.

### 2.7.3 Analysis of surface topography

The surface topography and roughness of the TFC PA membranes were studied using Atomic force microscopy (AFM, Bruker Dimension Icon, USA). The surface topography of the membranes was obtained using tapping mode at scan rate of 1.0 Hz at ambient conditions of temperature and humidity. Nanoscope analysis software V.1.40 was used for processing the AFM data, removing the noise and calculating the average (Ra) and the root mean square (Rq) roughness values. The Ra and Rq roughness of the membranes were calculated using:

$$R_a = \frac{1}{N} \sum_{i=1}^N |Z_i| \quad (2.2)$$

$$R_q = \sqrt{\frac{\sum Z_i^2}{N}} \quad (2.3)$$

where  $Z_i$  is the surface height and  $N$  is the number of points on the surface of the membrane.

### 2.7.4 Evaluation of the membrane surface wettability

The surface wettability of the fabricated membranes was evaluated by measuring the contact angle data using Krüss DSA 100 (Krüss GmbH, Germany) and FTÅ200 (First Ten Angstroms, Inc.) instruments. A sessile drop of DI water was placed on the surface of the TFC membranes and the static contact angle was measured. The contact angle was measured at 5 different locations for each sample in order to minimize the experimental error.

## 2.7.5 Measurement of the degree of cross-linking of the PA film

The degree of cross-linking for an interfacially polymerized PA film is referring to the ratio of the cross-linked (branched part,  $m$ ) to the linear (part  $n$ ) structures as shown in Figure 2.4.

$$\text{Degree of cross-linking} = \frac{m}{m+n} \times 100 \quad (2.4)$$

The values of  $m$  and  $n$  can be obtained based on experimental O/N ratio measured by XPS analysis using [56]:

$$\frac{O}{N} = \frac{3m+4n}{3m+2n} \quad (2.5)$$

Theoretically, O/N ratio varies between 1.0 for fully cross-linked ( $C_{18}H_{12}N_3O_3$ ,  $n=1$  and  $m=0$ ) and 2.0 for fully linear ( $C_{15}H_{10}O_4N_2$ ,  $n=0$  and  $m=1$ ) structure.

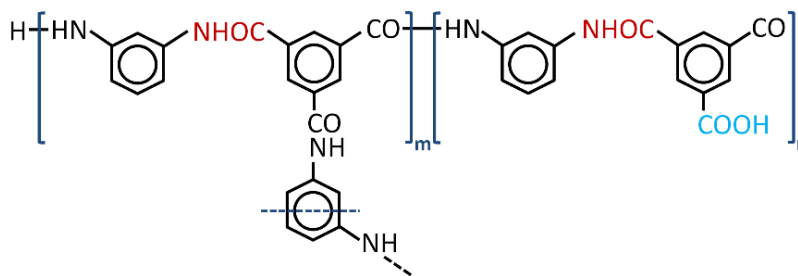


Figure 2.4: Chemical structure of polyamide film.  $m$  and  $n$  represents the cross-linked and the linear parts, respectively ( $m+n=1$ ).

## 2.7.6 Measurement of total organic carbon

The concentration of organic matter in the industrial produced water was done using a combustion type TOC analyzer (Shimadzu, model TOC-V; detection range 3–25,000 mg/L). The concentration of inorganic elements such as silica,  $Ca^{+2}$ ,  $Mg^{+2}$  was measured using inductively coupled plasma-optical emission spectroscopy (ICP-OES) (Agilent 735 ICP-OES).

### **2.7.7 Evaluation of crystalline structure and size of the solid NPs**

The size of the solid ITO NPs was examined by X-ray powder diffraction (XRD) and SEM techniques. The XRD profiles of ITO NPs were obtained using INEL XRG 3000 X-ray diffractometer equipped with a Cu K $\alpha$  radiation source ( $\lambda = 1.54 \text{ \AA}$ ) from  $2\theta=20^\circ$  to  $2\theta=90^\circ$  at a step of  $0.02^\circ$ . The SEM images of ITO nano-powder were taken by Hitachi S4800 high resolution SEM device. By the use of image processing software (Image J), the size distribution of NPs was obtained. The crystalline structure of the TiO<sub>2</sub> NPs was examined by XRD technique (Rigaku XRD Ultima IV, Cu-K $\alpha$  source, 40 kV, 44 mA). The collected spectrum was analyzed using JADE software.

### **2.7.8 Measurement of size and stability of NPs in solution**

Particle size and stability of the dispersed NPs in solvent (such as water, NMP, heptane) were measured by dynamic light scattering (DLS) technique (ALV/CGS-3 compact goniometer, ALV-GmbH, Langen, Germany). Particle size distribution (PSD) of NPs was extracted by CONTIN analysis through scattering results obtained from He-Ne laser at 632.8 nm.

### **2.7.9 Evaluation of the thermal stability of the membranes**

Thermal stability of the synthesized membranes was examined using thermal gravimetric analysis (TGA), which determines the changes in the weight of the sample in relation to changes in temperature. 10 mg of membrane samples were placed in the sample holder and loaded into the TGA Q500 (TA Instruments). The temperature was increased to 1000 °C with a ramp of 1 °C/min and the sample weight reduction was recorded.

### **2.7.10 Measurement of the surface potential of the membranes**

The surface (zeta) potential of the nanocomposite membranes was measured using Surpass Electrokinetic Analyzer (Anton Paar). The zeta potential values were measured at pH 10 and 25 °C using 0.001 M KCl solution.

### **2.7.11 Measurement of the electrical conductivity of the membranes**

The surface and bulk electrical conductivity of the synthesized PES-ITO membranes were evaluated by measuring the current versus potential (I-V) characteristics of the membranes using a potentiostat/galvanostat (model 263 A, Princeton Applied Research). The applied potential increased from 0 to 1 V with the increment of 0.01 V and the current passed through the membrane was recorded.

### **2.7.12 Evaluation of the leaching of NPs from nanocomposite membrane**

The possible release of ITO NPs from the nanocomposite PES-ITO membranes was examined by inductively coupled plasma-optical emission spectroscopy (Agilent 735 ICP-OES). Samples of ITO nanocomposite membranes with the same weight were soaked in three aqueous solutions at different pH of acidic (pH=2), neutral (pH=7) and basic (pH=12). 15 ml water samples were taken up to 14 days to find the leaching of ITO NPs in the water solution. The concentration of indium in the water was measured using ICP-OES and used as a criterion for leaching of ITO NPs. The higher leaching rate indicates poorer binding of the NPs with the polymer matrix which implies that the nanocomposite membrane will lose its modified properties faster. In contrast, the lower leaching rate confirms the preparation of a more stable nanocomposite membrane.

### **2.7.13 Evaluation of the water flux and salt rejection of the membranes in RO operation**

The water permeability of the membranes was examined using a cross-flow filtration setup (Sterlitech Corporation, USA) which is shown schematically in Figure 2.5. The setup consists of a stainless steel feed tank, membrane cell, a constant flow diaphragm pump of maximum capacity 6.8 LPM (1.8 GPM) from Hydra-Cell, a chiller/heater (Isotemp 3013, Fisher Scientific) to maintain the feed temperature at 25 °C, a bypass valve and a back pressure regulator to control applied pressure and cross flow velocities (Swagelok). A digital weighing balance (Mettler Toledo) was used to measure the permeate flow rate and the data were directly collected in a computer using LabVIEW (National Instruments) data acquisition software. The filtration tests were conducted at a trans-membrane

pressure of 1.52 MPa and at a feed flow rate of 1 L min<sup>-1</sup>, corresponding to a constant cross-flow velocity of 0.25 m/s and a laminar crossflow of Reynolds number Re=730.

The water flux ( $J_w$ ) at steady state was calculated by measuring the weight of water ( $\Delta m$ ) passed through the effective surface area ( $A_m$ ) of membrane over a specific time ( $\Delta t$ ) as follows:

$$J_w = \frac{\Delta m}{\rho A \Delta t} \quad (2.6)$$

where  $\rho$  is water density. Apparent salt rejection was calculated by measuring the salt concentration in permeate solution after 3 h filtration of 2000 ppm NaCl solution at 25 °C as follows:

$$R_o = \left(1 - \frac{C_p}{C_f}\right) \times 100 \quad (2.7)$$

where  $C_p$  and  $C_f$  are the NaCl concentration in permeate and feed (2000 ppm NaCl) solutions, respectively, measured after 3 h filtration process. The salt concentration in each solution was obtained based on a calibration curve of solution conductivity. Pure water permeability coefficient ( $A_p$ ) was determined at different applied pressure (1.52, 1.24, 0.96, and 0.69 MPa). The flux was allowed to stabilize at each pressure for 30 min. The flux values were plotted against pressure where the slope of the linear regression gave the pure water permeability of the membrane. Salt permeability coefficient ( $B$ ) was calculated by  $B = J_w (1/R - 1)$  at 1.52 MPa and 2000 ppm NaCl solution.

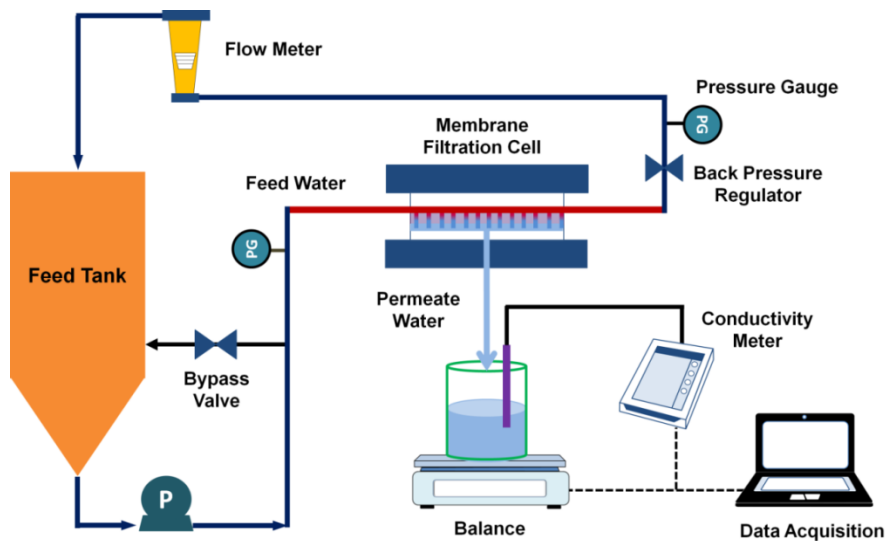


Figure 2.5: Schematic view of the cross-flow RO filtration setup.



### 2.7.14 Evaluation of the fouling propensity of the membrane in RO operation

The fouling experiments consisted of three consecutive steps: (i) pure water filtration, (ii) industrial produced water, and (iii) pure water filtration after hydraulic washing of the membrane surface. Each of these filtration steps lasted for 3 h and the permeate flux was measured at each step. The fouling evaluating parameters, namely total flux decline ratio ( $DR_t$ ), which is the sum of reversible flux decline ratio ( $DR_r$ ) and irreversible flux decline ratio ( $DR_{ir}$ ) as well as flux recovery ratio (FRR) were calculated using the following equations [57,58].

$$DR_t = 1 - \frac{J_{WF}}{J_{W1}} \quad (2.8)$$

$$FRR = \frac{J_{W2}}{J_{W1}} \quad (2.9)$$

$$DR_r = \frac{(J_{W2} - J_{WF})}{J_{W1}} \quad (2.10)$$

$$DR_{ir} = 1 - \frac{J_{W2}}{J_{W1}} \quad (2.11)$$

where,  $J_{W1}$ ,  $J_{WF}$  and  $J_{W2}$  are pure water flux, water flux during filtration of SAGD water, and pure water flux after hydraulic washing of the membranes, respectively. The rejection of organic matter was calculated by measuring the TOC in the collected permeate during the filtration of SAGD water at 25 °C as follows:

$$R_{TOC} = \left(1 - \frac{TOC_p}{TOC_f}\right) \times 100 \quad (2.12)$$

where  $TOC_p$  and  $TOC_f$  are the TOC concentration in the permeate and feed solutions, respectively.

### 2.7.15 Evaluation of the permeation performance of the composite membranes in FO process

The permeation performance of TFC membranes was evaluated using a cross-flow FO filtration setup which is illustrated schematically in Figure 2.6. The membrane cell was designed with channels on both sides of the membrane. The

length, width and height of both channels were 145 mm, 96 mm, and 2 mm, respectively, providing an effective filtration area of 140 cm<sup>2</sup>. Thin plastic mesh spacers were used on both sides of the membrane to provide mechanical support to the membrane and to induce better mixing in the channel to reduce external concentration polarization (ECP).

Water permeation of the membrane in FO unit was measured using salt water with different NaCl concentrations (ranging from 0.25 M to 3 M) as draw solution and DI water as feed solution. The test was first conducted with DI water on both sides of the membranes for 15 min. The volumes of initial draw and feed solutions were 2 L and 2.5 L, respectively. Afterwards, in a series of stepwise experimental runs, the concentration of the draw solution was increased to desired values by adding proper amount of concentrated (5M) NaCl solution. The temperature of the feed and draw solutions were maintained at 21±2 °C using Isotemp water bath (Polyscience, model: MX-CA11B and model: 6560M11A120C, USA). Variable speed gear pumps were used to maintain the flow of both solutions at 2.5 L/min (0.22 m/s cross flow velocity). The draw solution tank was placed over a digital weighing balance (Mettler Toledo) and the change in the weight of the solution was recorded continuously. For all experiments, the initial volumes of draw and feed solutions were 2 L and 2.5 L, respectively. During the test, the conductivity of the feed and draw solutions was monitored using in-line conductivity sensors and recorded automatically every minutes.

The water flux through the membrane was calculated by measuring the change in the weight of the draw solution passed through the effective surface area of the membrane over a specific time period of the experiment using equation 2.6. The reverse salt flux,  $J_s$ , in gm<sup>-2</sup>h<sup>-1</sup> (gMH) was calculated by dividing the mass flow rate of NaCl (obtained via measuring the feed conductivity) by the membrane effective surface area. The ratio of reverse solute flux to pure water flux,  $J_s/J_w$ , was considered as specific flux ratio. The FO filtration of BFW was carried out with 0.5 M NaCl salt water as the draw solution and BFW as the feed solution. The FO tests were conducted over a time period of 6 hours under similar operating conditions.

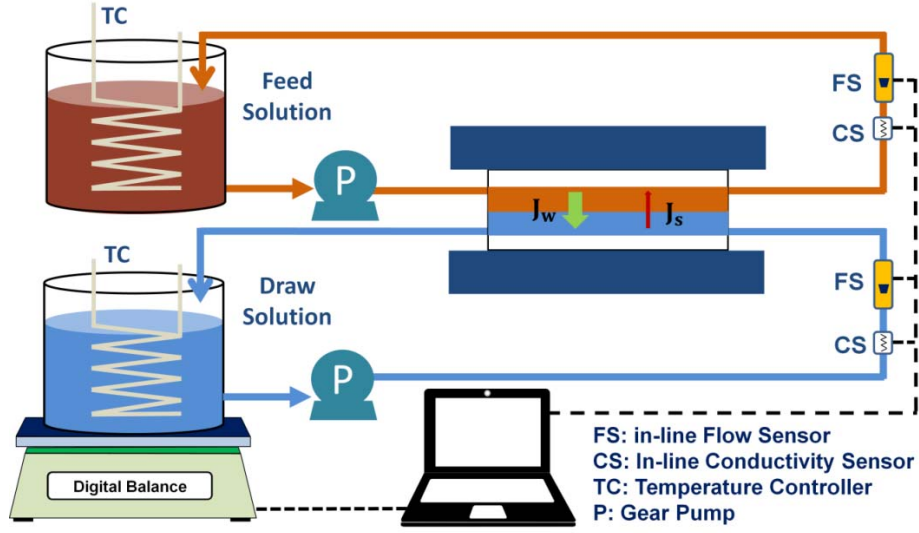


Figure 2.6: Schematic view of the FO setup. All the TFC membranes were tested in active layer toward feed side (AL-FS) orientation.

### 2.7.16 Determination of the FO membrane structural parameter

The structural parameter ( $S$ ) is one of the most important properties of a FO membrane, and is used as a measure to evaluate the vulnerability of the membrane to the ICP. The structural parameter is basically a property of the support layer and depends on the support porosity ( $\varepsilon$ ), tortuosity ( $\tau$ ) and thickness ( $t$ ) ( $S = t\tau/\varepsilon$ ). The structural parameter can be obtained using the following equation [59,60]:

$$S = \left( \frac{D}{J_W} \right) \ln \frac{B + A\pi_{D,b}}{B + J_W + A\pi_{F,m}} \quad (2.13)$$

where  $D$  is the salt (NaCl) diffusion coefficient,  $\pi_{D,b}$  is the osmotic pressures of the bulk draw solutions, and  $\pi_{F,m}$  is the osmotic pressures of the feed solution on the membrane interface. For high salt rejecting membranes,  $B$  is typically assumed to be zero [61]. The structural parameters of the lab-made and commercial membranes were evaluated using 1 M NaCl solution and DI water as draw and feed solution, respectively. The cross-flow velocity of both draw and feed solutions was maintained at 0.22 m/s. Using DI water as feed Eq. (2.14) is simplified to:

$$S = \left( \frac{D}{J_W} \right) \ln \frac{B + A\pi_{D,b}}{B + J_W} \quad (2.14)$$

## 2.8 Design of experiment (DOE) using Taguchi method

The synthesis of TFC membranes were designed using the Taguchi method which primarily emphasizes on conducting a minimum number of experiments by using tables of orthogonal arrays while studying the simultaneous influence of several control factors on a target response. The Taguchi method utilizes the plots of “marginal means” which provide a visual interpretation of the “trend of influence” of a control factor on a response variable [62]. The key feature of the Taguchi design, which is highly desirable in the membrane fabrication by IP reaction, is the reduction of the response variability by providing an optimum experimental design that is robust against uncontrollable conditions. The variability of a response due to signal (controllable) and noise (uncontrollable) factors can be evaluated by calculating the signal to noise (SN) ratio. The method of evaluation of the SN ratio depends on the target of the experiment. The three standard SN ratios which are commonly used for assessment of the response quality include the larger-the-better, smaller-the-better, and nominal-the-best [63]. In all these cases, a bigger SN ratio indicates the better quality of the result (permeate water in this study) as well as smaller variation in the response caused by noise factors. In the present study, the larger-the-better SN ratio was employed using the following equation:

$$SN = -10 \log \left( \frac{1}{n} \sum_{i=1}^n \frac{1}{y_i^2} \right) \quad (2.15)$$

where  $y_i$  is the observation at each experimental trial and  $n$  is the total number of experiments. Three main stages to employ the Taguchi method include (i) establishing the quality characteristic (response), (ii) selecting the matrix of experiment by identifying control variables and their corresponding levels, (iii) conducting the experiments and performing analysis of variance and (iv) conducting more experiments to confirm the Taguchi results.

## 2.9 Analysis of Variance (ANOVA)

When manipulating a series of experimental data, it is always informative to determine the contribution weight of different factors and to recognize the most influential one(s). ANOVA is a useful statistical technique to determine the

contribution and significance of each parameter to the total variation of the results. Instead of analyzing each single data, the ANOVA test evaluates the variability (variance) of the control and noise factors to provide the level of confidence and statistical significance of the experimental results. The analysis first starts with the calculation of the total sum of squares ( $SS_T$ ) and the factors sum of squares ( $SS_A$ ) to quantify the deviation of the experimental results from their mean values using the following equations [62]:

$$SS_T = \sum_{i=1}^N Y_i^2 - \frac{T^2}{N} \quad (2.16)$$

$$SS_A = \sum_{i=1}^{K_A} \left( \frac{A_i^2}{n_{A_i}} \right) - \frac{T^2}{N} \quad (2.17)$$

In these equations,  $Y_i$  is an experimental data, e.g., water flux,  $N$  is the total number of experimental observations,  $T$  is the sum of all  $N$  observations,  $A_i$  is the experimental observations at level  $i$  of factor  $A$ ,  $K_A$  is the number of levels of factor  $A$ , and  $n_{A_i}$  is the total number of trials that includes  $A_i$ . The sum of squares of error ( $SS_e$ ) will be the difference of total sum of squares and the factors sum of squares as:

$$SS_e = SS_T - (SS_A + SS_B + \dots) \quad (2.18)$$

where  $A$  and  $B$  are the control variables. It must be noted that the term “error” here not only accounts for experimental measurement errors but also represents the contribution of all other unknown or uncontrollable parameters that may affect the response variable. To measure the distribution of the experimental results about their mean value for each control factor,

In general, the variance ( $V$ ) of a collection of data presents the distribution of individual observations about the mean value. For the experimental results involving a control factor  $A$ ,  $V_A$  can be calculated as follows:

$$V_A = SS_A / DOF_A \quad (2.19)$$

where  $DOF_A$  is the degree of freedom of factor  $A$  and is equal to one less than the level number of the variable  $A$  ( $DOF_A = K_A - 1$ ). Similarly, the variance of error is obtained by  $V_e = SS_e / DOF_e$  where  $DOF_e$  is the degree of freedom of error given by  $DOF_e = DOF_T - (DOF_A + DOF_B + \dots)$ .  $DOF_T$  in this equation is the total degree of freedom which equals to one less than total number of observations ( $DOF_T = N - 1$ ). The variance ratio for a particular control factor, which is also known as F-

statistics, compares the variance because of the effect of the control factor with the variance caused by the effect of noise factors ( $F_A = V_A/V_e$ ). F-statistics is commonly used to assess the significance of a control factor on the target response. The computed F-statistic from experimental data is compared with a standard F-table for a particular level of significance. The standard F-tables can be found in most textbooks of statistics for different levels of significance ( $\alpha$ ) and degrees of freedom. If the value of the calculated F-statistics for a control variable is larger than the extracted one from the F-table, a conclusion can be drawn that the influence of the control variable of interest on the response is significant and must be taken into account.

## 2.10 Performance prediction using Taguchi method

Using the Taguchi method, a prediction model (transfer function) can be employed to predict the permeation performance (water flux and salt rejection) of the synthesized TFC membranes. The prediction model exploits a linear interpolation between the levels of control factors by the following equation:

$$\text{Response} = \left( \overline{A}_i + \overline{B}_j + \overline{C}_k + \overline{D}_l + \dots \right) - 3 \times \frac{T}{N} \quad (2.20)$$

where the response can be water flux or salt rejection and  $\overline{A}_i, \overline{B}_j, \overline{C}_k$ , and  $\overline{D}_l$  are the average values of observations (flux or rejection) for the control factors (A, B, C, ...). at i, j, k and l levels of these variables.

# Chapter 3<sup>†</sup>

## Effect of synthesis conditions and chemical additives on the properties of TFC PA membranes

---

<sup>†</sup> This chapter is organized based on references [39-41].

## **3.1 Systematic study on the influence of monomer concentration, reaction time and curing temperature on the properties of the TFC PA membranes**

### **3.1.1 Introduction**

Over the past decades, TFC PA membranes has attracted great attention in desalination and water purification applications [5,29]. The PA film is often synthesized by an IP reaction between polyfunctional amine and acyl chloride monomers at the surface of a porous sublayer [32,38]. Demands to improve the productivity of composite membranes have triggered much research to understand and optimize the properties of the top layer which is responsible for the final productivity and selectivity of these types of membranes. The reported results reveal the significant importance of the synthesis condition on the permselectivity of the resulting PA film. However, the experimental results in the literature do not form a clear consensus about the trend of influence of the synthesis parameters on the final properties of the PA membranes. This is mainly due to (i) the complex nature and fast polymerization rate of the PA selective layer which make the full characterization of the resulting PA film very challenging and (ii) different experimental methodologies and conditions used by the researcher. Therefore, further research is needed in order to produce definitive practical conclusions leading to the robust and high performance membrane designs. Particular research challenges in this field are (i) to fundamentally and systematically understand the effects of reaction conditions on the characteristics of fabricated thin films, and (ii) to identify the most influential parameters affecting transport properties of the membranes.

A brief overview of earlier studies on the influence of synthesis conditions on the structure and transport properties of TFC membranes is presented in Table 3.1 [64–73]. Although the reported studies in the literature have demonstrated the significant role of individual chemical additives on the variation of the final properties of TFC membranes, the simultaneous effects of multiple additives have not been well studied [17,73–80]. All previous studies have used one-factor-at-a-time (OFAT) experimentation methods in which only one variable (control factor) was varied in each experiment. The major drawbacks of the OFAT approach are



that the chance of testing the optimum condition is very low, and the covariance between influential parameters cannot be verified [81,82]. Also, OFAT is not able to find the level of significance of each parameter and predict the level setting that leads to the less variability of the results with noise factors. Thus, existing results should be interpreted with caution, and the widely accepted hypotheses for the effect of synthesis conditions require further reevaluation to be extrapolated to novel practices.

Table 3.1: Overview of experimental studies regarding the effects of synthesis conditions on performance of TFC membranes [39].

Reference	Studied Parameters	Performance <sup>1</sup> Flux (LMHbar) Rejection(%)	Major Results
Chai and Krantz, 1994 [64]	Monomers conc. <sup>2</sup> , reaction time	$\frac{0.39 - 0.74}{96.7 - 98.5}$	- PA thickness increased with increase in TMC conc. and reaction time, but did not change with MPD conc. - Water flux substantially decreased with increase in reaction time.
Rao et al., 1997 [65]	Reaction time, curing time and temperature	$\frac{0.68 - 1.33}{74 - 97.5}$	- Flux and rejection increased with increase in reaction time up to 60 sec, but rejection decreased dramatically for higher reaction time - Increasing curing temp up to 75 °C improved both flux and rejection; higher curing temperature lowered the flux considerably.
Rao et al. 2003 [66]	Reaction & curing time and temperature	$\frac{1.1 - 2.57}{92 - 95}$	- Lowering the reaction time and curing temperature resulted in thinner membranes with higher water flux. - Salt rejection was not sensitive to modified conditions
Song et al. 2005 [67]	Monomers conc., reaction time	$\frac{0.3 - 2}{50 - 98}$	- Water flux increased with increase in reaction time at low TMC conc.; the opposite trend was reported at higher TMC conc. - Increasing MPD conc. improved salt rejection but lowered the flux.
Roh et al., 2006 [68]	Monomers conc.	$\frac{0.78 - 1.17}{75 - 97}$	- PA film thickness increased with increase in both MPD and TMC conc. -Surface hydrophilicity increased by increasing TMC conc., but decreased as MPD conc. increased.
Ghosh et al. 2008 [69]	Organic solvent properties, curing time and temperature	$\frac{0.76 - 1.8}{93 - 98}$	- High surface tension, low viscosity solvents led to higher permeation performance for membranes -Flux and rejection increased with increase in curing temperature.
Liu et al. 2008 [70]	Reaction time, pH of MPD solution, curing time and temperature	$\frac{0.38 - 0.7}{64.6 - 99.4}$	- Increasing reaction time reduced permeation flux and improved salt rejection. - Water permeation increased with increase in TMC concentration. - Both water flux and rejection increased with increase in curing temperature.

Jin and Su 2009 [71]	Monomers conc., reaction time and temperature	NA	Increasing MPD/TMC conc. ratio and reaction time resulted in PA film with more hydrophilic -COOH group at the surface.
Xie et al. 2012 [72]	Monomers conc., thermal treatment method	$\frac{1.35 - 2.65}{99.4 - 99.7}$	- There was an optimum range for monomer conc. to obtain high water flux - Salt passage was not sensitive to change in monomer conc. - Thermal treatment did not cause any significant effect on transport properties of membranes
Klaysom et al. 2013 [73]	Monomers conc., reaction time	$\frac{0.6 - 1.2}{78 - 95}$	- Water flux decreased with increase in MPD conc. and reaction time - Membranes performance did not changed with TMC conc. except for low values where water flux dropped with increase in TMC conc.

<sup>1</sup>All reports used RO test cell to study membranes performance except reference [71] which used FTIR spectroscopy for membrane characterization.

<sup>2</sup>Reacting monomers are MPD and TMC for all studies except reference [70] which used 5-chloroformyloxyisophthaloyl chloride (CFIC) in organic solution.

Here, a systematic study was conducted to investigate the effect of simultaneous changes in the MPD concentration in water, TMC concentration in hexane, IP reaction time and heat curing. The experimental trials were arranged using a robust DOE method known as Taguchi to minimize the number of experiments, quantifying the significance of each parameter, and obtaining valuable information about the inter-relationship between the parameters.

### 3.1.2 Materials and methods

TFC PA membranes were prepared via IP reaction between MPD-water and TMC-cyclohexane solutions at the surface of PES microporous (0.2  $\mu\text{m}$ ) support. The MPD-water solution contained 2 wt. % CSA, 1 wt. % TEA and 0.2 wt. % SDS as additive. The concentration of these additives was kept constant in all trials. Table 3.2 presents the control variables investigated in the present study and their corresponding levels and arrangement in the  $L_9$  (4 three-level factors) array. Each run was replicated twice (18 membranes were synthesized in total) to evaluate the repeatability of membrane formation.

Table 3.2: Control factors (synthesis parameters) and their corresponding levels in Taguchi L<sub>9</sub> design.

Synthesized TFC membrane	Control factors			
	MPD conc. (wt.%)	TMC Conc. (wt.%)	Reaction Time (s)	Curing Temperature (°C)
M1	1	0.15	15	25
M2	1	0.25	30	55
M3	1	0.35	60	85
M4	1.5	0.15	30	85
M5	1.5	0.25	60	25
M6	1.5	0.35	15	55
M7	2	0.15	60	55
M8	2	0.25	15	85
M9	2	0.35	30	25

### 3.1.3 Results and discussion

#### 3.1.3.1 Chemical composition of the TFC membranes

The chemical composition of prepared membranes was analysed by ATR-FTIR and the spectra are presented in Figure 3.1. The spectra of PES support layer showed three peaks at 1410, 1485 and 1580 cm<sup>-1</sup> due to presence of aromatic ring (benzene) skeletal vibration [83,84]. These peaks were also identified in all synthesized TFC membranes due to high penetration depth of IR beam (>300 nm) at this region (1350-1750 cm<sup>-1</sup>). However, the three new peaks at 1667, 1611, 1541 cm<sup>-1</sup> in the spectra of the TFC membranes revealed the presence of interfacially polymerized PA film at the surface of the PES support. These peaks were associated with C=O stretching of amide I bond, aromatic amide ring breathing and N-H bending of amide II in -CO-NH- group, respectively [84]. According to Figure 3.1, the similar spectra characteristics of the TFC membranes suggest the presence of PA layer with similar basic structure in spite of different synthesis conditions.

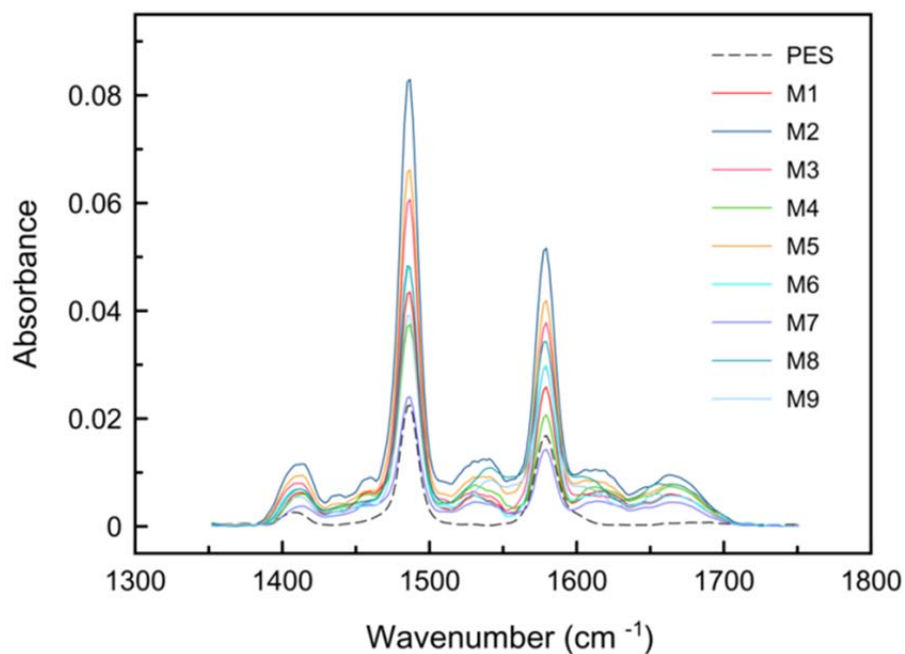


Figure 3.1: ATR-FTIR spectra of TFC membranes and base PES support.

### 3.1.3.2 Water flux and salt rejection

Figure 3.2 presents the average water flux and salt rejection of the synthesized TFC membranes (M1 to M9 membranes). As it is shown in this figure, the water flux and salt rejection of all membranes were in a mutually exclusive relationship, so that when the water flux increased, the salt rejection decreased and vice versa. While the rejection percentage of the membranes varied in the range of 94-98% the water flux changed remarkably in the range of 7-68 L/(m<sup>2</sup>h) (LMH) which indicates a greater influence of synthesis parameters on water permeability leaving the rejection rate at consistently high and desirable value.

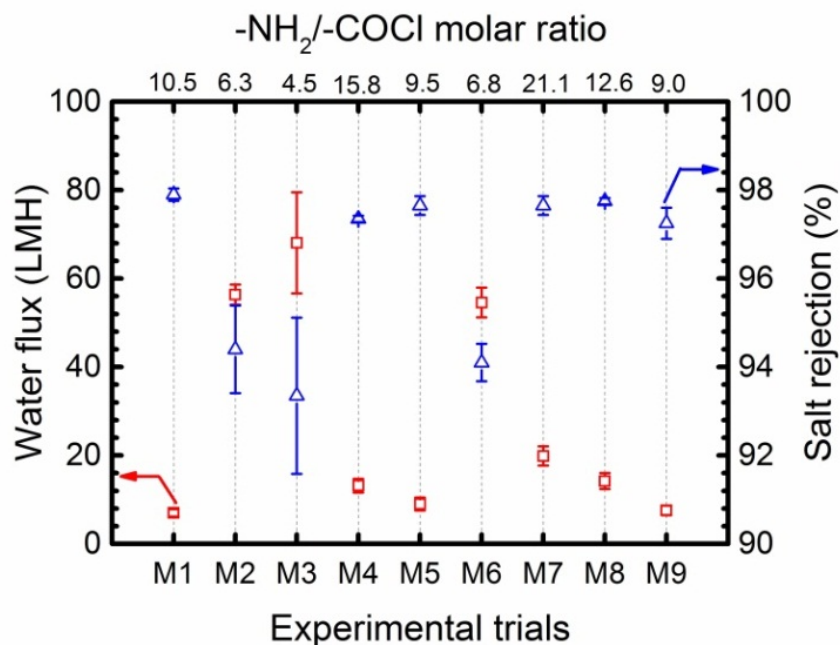


Figure 3.2: Water flux and salt rejection of all synthesized membranes. The performance measurements were carried out at a trans-membrane pressure of 1.52 MPa and at a feed flow rate of 1 L min<sup>-1</sup>, corresponding to the laminar crossflow of Reynolds number Re=730.

The amine/acyl chloride ( $-\text{NH}_2/-\text{COCl}$ ) molar ratio in Figure 3.2 is a criterion showing the amount of reactive functional groups present in polymerization reaction. This ratio is calculated by converting the initial mass concentration of MPD and TMC in their corresponding solvents to molar concentration considering the numbers of  $-\text{NH}_2$  and  $-\text{COCl}$  functional group in each monomer (two  $-\text{NH}_2$  and three  $-\text{COCl}$  groups). According to Figure 3.2, the membranes with low molar ratio ( $-\text{NH}_2/-\text{COCl} < 7$ ) showed significantly different flux/rejection behaviour compared to other membranes. As will be shown later, very high molar ratio ( $-\text{NH}_2/-\text{COCl} > 30$ ) also changes the separation performance of composite membranes considerably. The  $-\text{NH}_2/-\text{COCl}$  molar ratio directly affects the rate of monomers diffusion and polymerization reaction at the surface, which subsequently changes the resulting morphology and water permeation of membranes. The detailed explanation of the effect of monomer concentration on the properties of synthesized PA films is discussed in the following section.

### **3.1.3.3 Influence of control factors on the properties of the resulting TFC membranes**

#### **3.1.3.3.1 Effect of MPD and TMC concentration**

The plot of “marginal means” for water flux, salt rejection and their corresponding SN ratios at different levels of each control factor are shown in Figure 3.3 and Figure 3.4. The marginal graphs are plotted by averaging the results of experimental trials at a specified value of a parameter. For example, the mean water flux for the membranes made with 1 wt.% MPD concentration is the average of the results of M1 to M3 where MPD concentration is 1 wt.%. Although more than one factor is varying at each run of Table 3.2, the arrays orthogonality in this table allows an independent estimation of the influence of each factor on the response. Figures 3.3a and 3.4a show that the average influence of increasing MPD concentration in the aqueous solution was the formation of TFC membranes with higher salt rejection but lower water flux. Exactly the opposite trend was observed by increasing the TMC concentration as indicated in Figure 3.3b and Figure 3.4b. SN ratios in these figures account for response variability, so that the higher the SN ratio the lower the variability of the response, thus the better the quality of the product. According to Figure 3.3 and Figure 3.4, the mean responses and SN ratio followed the same trend, implying that the optimum condition would also provide the least variability in response and maximum robustness. Furthermore, the relatively high SN ratios in these graphs show that the levels of control factors were adjusted properly so that the effects of the uncontrollable or unknown noise factors on the response were minimized. The extracted trends using Taguchi marginal graphs can be verified by comparing the performances of membranes synthesized by only changing the levels of one specific factor when all other factors maintained constant. Since no two runs in the L9 matrix are comparable, 11 extra confirmation membranes were prepared at combinations, which were not considered in Table 3.2. The synthesis conditions and permeation performance of these confirmation membranes are presented in Table 3.3. Taguchi predicted flux and rejection in this table are calculated by Taguchi transfer function (a linear model) that will be explained in ANOVA section. By comparing the permeation results of C1 vs. C2 and C3 vs. C4, it is confirmed that membranes prepared at higher MPD concentration showed lower water flux and higher salt rejection.

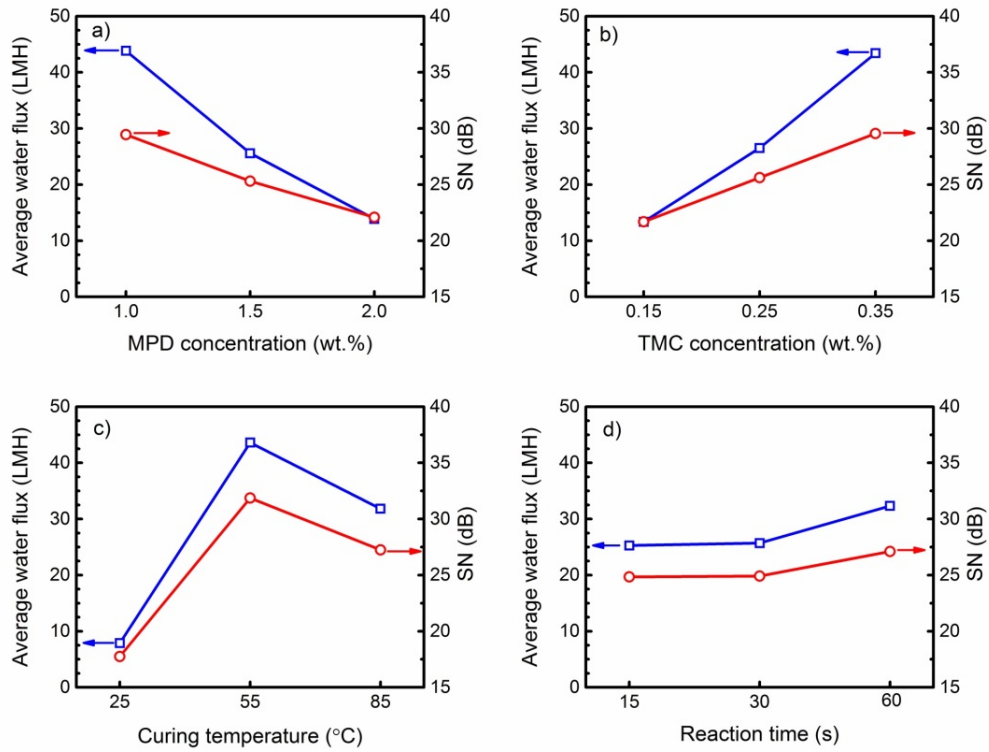


Figure 3.3: Average water flux and SN ratio for each level of each control factor.

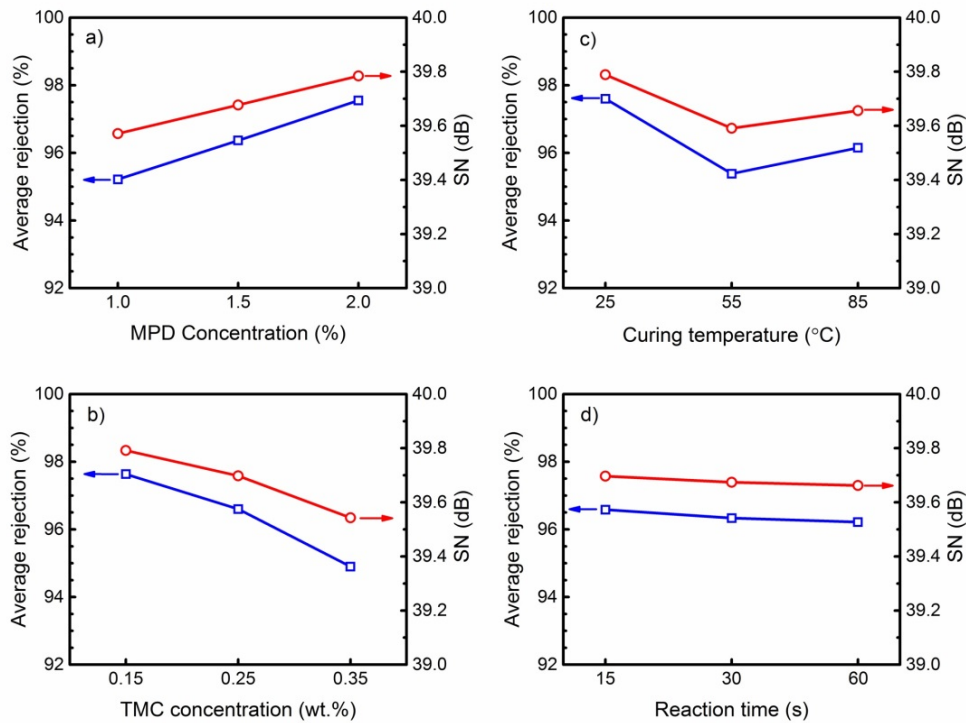


Figure 3.4: Average salt rejection and SN ratio for each level of each control factor.

Table 3.3: Synthesis conditions and permeation performance of the confirmation experiments.

Confirmation membrane	Controllable factors				Results			
	MPD conc. (wt.%)	TMC conc. (wt.%)	Reaction time (s)	Curing temperature (°C)	Average water flux (LMH)	Taguchi predicted flux (LMH)	Average salt rejection (%)	Taguchi predicted rejection (%)
C1	1	0.15	15	55	20.9	42.8	96.9	95.7
C2	2	0.15	15	55	19.6	12.8	97.4	98
C3	1	0.35	15	55	79.1	72.8	91.4	93
C4	2	0.35	15	55	42.5	42.8	96.2	95.3
C5	1	0.15	15	85	15.6	31	97.5	96.4
C6	2	0.15	30	55	19.4	13.3	97.6	97.8
C7	3	0.15	15	55	110.5	NA	72.1	NA
C8	3	0.35	15	55	30.6	NA	96.7	NA
C9	1	0.25	15	55	46.0	56	95.2	94.6
C10	2	0.25	15	55	26.0	25	96.4	97
C11	3	0.25	15	55	15.3	-	97.1	-

In order to explain the observed trends in Figure 3.3 and Figure 3.4, the mechanism of PA formation via interfacial polymerization should be understood. The IP reaction initiates at the surface when the MPD/water impregnated PES support is brought into contact with TMC/organic solvent solution. Since water and organic solvent are immiscible, the polymerization reaction occurs at the water/organic interface [22,85,86]. In most IP reactions, the MPD concentration in water is much larger than the TMC concentration in the organic solvent, due to negligible solubility, vigorous reaction of the acyl chloride monomer with water and good solubility of amine in organic solvent [64,69]. Thus the IP reaction is believed to be mainly controlled by diffusion of MPD molecules to the reaction zone and thus the polymer film grows from the water/organic interface toward the bulk of the organic solution [87,88]. However, the growth of the PA film does not follow a linear increase over the reaction time. Immediately after the contact of the two monomers solution the water/organic interface provides an empty platform for fast reaction of MPD and TMC molecules to form an ultrathin incipient (core) PA film at the PES surface. After that, polymerization shifts to a slow growth stage where the MPD diffusion and thus reaction rate slows down significantly due to presence of the incipient layer [89]. The result of polymerization at this stage is the formation of a second layer with the so-called ridge-and-valley morphology which covers the core layer [69,72,88]. The separation performance of the final PA layer



depends not only on the overall film thickness (The thicker the film is, the lower the water permeates), but also on the cross-link density of the internal structure [72]. It is worth mentioning that, other than thickness and density of the core layer, its crystallinity also plays a major role in determining the permeability of the membrane [90]. In general, the crystallites of the polymers have highly packed structure, and the transport of water only takes place through the amorphous part. Hence, the higher the crystallinity the lower is the permeation flux. Crystallinity is primarily determined by the chain flexibility and the volume fraction of polymer, thereby directly depends on the density of polymer. Polyamide in TFC RO membranes is a semi-crystalline polymer which its degree of crystallinity couldn't be measured directly. This is due to the fact that, the very thin layer of PA, synthesized by in-situ polymerization, is not detachable from the PES support to be used for further tests on crystallinity. In the present work, the discussions on the density and/or crystallinity of the membranes are provided based on the pure water flux and salt rejection results, knowing that the crystallinity of the polymer affect the space between the polymer chains and thus the diffusion rate [91]. It was shown by Freger [92] that the cross-link density of the PA film is not uniform across the cross-section where the incipient thin film is proposed to be the densest and actual selective layer over the whole structure [92,93]. Since the monomer diffusion and reaction rate in the slow growth stage strongly depend on the mass transfer resistance of the core layer, any factor which changes the properties of this layer (in terms of the thickness and cross-link density) will affect the final morphology and separation performance of the resulting films.

Regarding the Figure 3.3a, the flux decline with the increase in MPD concentration could be attributed to the increase in the overall thickness of the PA film during the course of polymerization. At higher MPD concentration, there will be a larger driving force for MPD to diffuse through the initially formed PA film. The increase in the number of available MPD molecules in the reaction zone promotes polymerization, thus increases the membrane internal resistance toward water passage by forming a thicker PA film with bigger ridge-and-valley structure at the surface [72].

The observed trend for the influence of the TMC concentration was also confirmed by comparing the permeation flux of confirmation membranes C1 vs. C3 and C2 vs. C4 as presented in Table 3.3. It is a widely held view that in a typical IP reaction, an increase in the TMC concentration decreases the

amine to acyl chloride molar ratio ( $-\text{NH}_2/-\text{COCl}$ ) and results in a thinner but denser PA active film with lower water flux in overall [72,93]. Surface images of the membranes made at high TMC concentration (C3) in this study also confirmed the formation of a thin and dense film at the surface (based on more resemblance of PES and C3 surface morphology). However, significant increase in the water flux with increasing in TMC concentration (from 20.9 LMH in C1 to 79.1 LMH in C3), not predicted by the above hypothesis, reveals the complex influence of the film thickness and density on the transport properties of membranes. The thickness and cross-link density of PA layer were measured by TEM and XPS analyses, respectively to approve above discussion. For example, for the C1 and C3 membranes shown in Figure 3.5, the XPS results are presented in Table 3.4. As can be seen, the cross-linking density of C1 and C3 are 28% and 69%, respectively, which confirms our hypothesis about the higher density of C3 membrane. However, it must be noted that, the density of the core layer, which is commonly used to justify conclusions (e.g. change in surface morphology) cannot be measured with characterization tests because it is covered by the outer loose layer. In the present study, we qualitatively discussed and compared the density of core layer for different membranes by noting that the mass transfer resistance of the incipient layer to MPD diffusion is directly related to its density. As mentioned earlier, in the case of denser core layer, the mass transfer resistance against diffusion of MPD diffusion is larger and less ridge-and-valley morphology forms on the surface.

Table 3.4: Atomic concentration of C, O and N in PA layer of C1 and C3 membranes obtained by XPS analysis.

Sample	Atomic Concentration (%)				Cross-linking Density (%)
	O 1s	N 1s	C 1s	S 2p	
C1	14.74	9.03	75.97	0.25	28
C3	12.75	10.31	76.72	0.23	69

The surface FESEM and cross-section TEM images of two confirmation test membranes along with PES substrate are shown in Figure 3.5. Unlike microporous PES supports which have a relatively smooth and featherless morphology, C1 had a tortuous and ridge-and-valley structure at its surface [22]. However, by increasing the TMC concentration from 0.1 wt. % (C1) to 0.35 wt. % (C3), the morphology changed to a nodular structure with small

microprotuberances at the surface. This again confirms formation of a denser PA core layer which hindered diffusion of MPD, thereby prevented film growth and formation of ridge-and-valley features on the surface. Moreover, the TEM images illustrate that increasing the TMC concentration results in a marked decrease in PA film thickness which is highly desirable for reducing the hydraulic resistance of membrane against water permeation.

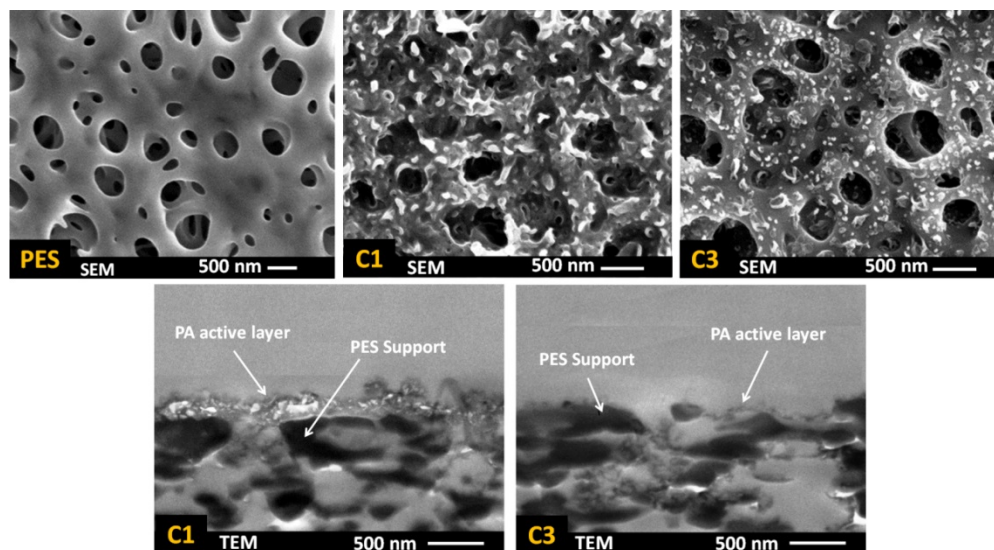


Figure 3.5: FESEM surface and TEM cross-section images of confirmation test membranes: PES support, C1 (MPD 1 wt.%, TMC 0.15 wt.%) and C3 (MPD 1 wt.%, TMC 0.35 wt.%) to study the effect of TMC concentration. The levels of other parameters are presented in Table 3.3.

The substantial change in surface morphology and the absence of ridge-and-valley structure at the surface by increasing TMC concentration is a proof of concept for formation of a thin and dense core layer at the early stage of IP reaction. At higher TMC concentration, due to the presence of a higher number of TMC molecules in the reaction zone, the incipient PA layer became dense enough that hindered MPD molecules to diffuse to organic phase and form a thick ridge-and-valley structure during the time of IP reaction. There are two likely causes for such a significant increase in permeation flux by increasing the TMC concentration: First, there is a marked decrease in the thickness of the PA active layer as it is shown by TEM images in Figure 3.5, which decreases membrane resistance against mass transfer and eventually increases the water flux. Second, a thinner active layer is more prone to be affected by the subsurface morphology (e.g. porosity and roughness of the support) than the thicker ones; the presence of

any open nanopores at the substrate due to incomplete coverage by the thin film may manifest themselves by increasing the water flux and lowering the salt rejection.

The typical trade-off behaviour between salt rejection and water flux was also observed in confirmation experiments. According to Table 3.3, increasing TMC concentration from 0.1 wt.% (C1) to 0.35 wt.% (C3) increased water flux significantly (almost four times), but decreased the salt rejection slightly from 96.9% to 91.4%. The salt rejection results from the confirmation experiments (C1-C4) show the dramatic role of monomers concentration. The range of results varies from high rejection/low flux RO membranes to low rejection/high flux NF membranes.

#### **3.1.3.3.2 Effect of curing temperature**

Heat curing is primarily performed to speed up evaporation of both water and organic solvent from the membrane surface and to help termination of the polymerization reaction [69]. The average effect of curing temperature on the performance of TFC membranes is presented in Figure 3.3c and Figure 3.4c. According to these figures, curing at room temperature (25 °C) resulted in TFC membranes with a high rejection but poor water flux. Raising the temperature to 55 °C increased the flux roughly 5 times with only a 2% reduction in rejection. Further increase in the curing temperature slightly decreased the flux and improved the rejection. This result is confirmed by comparing the performance of base membrane M1 (Table 3.2) and by confirmation experiments C1 and C5 (Table 3.3). The observed variation in water permeation and salt rejection of the membranes can be justified by monitoring the change in surface morphology at various curing temperatures. The surface images of M1, C1 and C5 (Figure 3.6) indicates that the PA film underwent a surface densification with increasing curing temperature. The thin ear-like PA ridges at the surface of M1 (cured at 25°C) merged together and became larger in C1 (cured at 55 °C). This change in morphology increased water permeation from 7.1 LMH in M1 to 20.9 LMH in C1. However, further increase in the curing temperature to 85°C (above the boiling point of cyclohexane) resulted in film shrinkage due to the fast evaporation of solvent residue from the C5 membrane which could explain the slight decrease in the water flux for this membrane [69,72].

### 3.1.3.3.3 Effect of reaction time

Figure 3.3d and Figure 3.4d present the average effect of the reaction time on the transport properties of the TFC membranes. It can be observed that changing the polymerization time from 15 s to 60 s did not result in an appreciable change in the average flux and rejection. The observed trend was also verified by the performance results of confirmation membranes C2 and C6 (Table 3.3) and base membrane M7. A very narrow range of water flux (19.4-19.9 LMH) and salt rejection (97.4-97.7%) indicated a trivial effect of reaction time on the membrane properties. Based on the IP reaction mechanism, prolonging the reaction time should increase film thickness and thus membrane resistance to water flow. However, a negligible shift in flux and rejection with the change in reaction time reveals that the growth of the PA film after 15 s was insignificant and implies that the permeation was mainly controlled by the dense core layer which was rapidly formed at the surface.

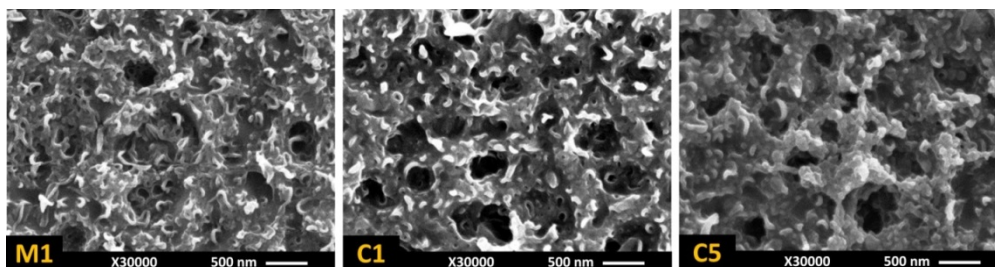


Figure 3.6: FESEM surface morphologies of Taguchi base membrane M1 (cured at 25°C) and confirmation test membranes C1 (cured at 55 °C) and C5 (cured at 85 °C) to study the effect of curing temperature. The levels of other parameters are presented in Table 3.3.

### 3.1.3.4 Interaction between MPD and TMC concentration

The interaction between two factors, in a simple explanation, accounts for a condition where a factor shows different behavior at different levels of the other factor [62]. Identifying the possible interactions between synthesis parameters can be quite helpful as it not only improves the basic understanding of the PA formation via interfacial polymerization reaction, but also increases the efficiency and output quality of the preparation process. Although exploiting saturated orthogonal arrays (like L9) eliminates the chance of extracting the interactions directly from OA table, it can provide guidance to track probable interactions between influential

parameters. According to Figure 3.3 and Figure 3.4, the average trends of the influence of TMC and MPD concentrations are in opposite directions, which suggest a possible interaction between these two factors. The interaction between two factors can be visually represented by plotting the impact of one of these factors on the response at different level of the other factor. In general, an interaction exists when the straight lines are not parallel [62]. Employing the water flux data in Table 3.3, a two way interaction plot for the TMC and MPD concentrations is presented in Figure 3.7. The intersecting lines in this figure reveal the existence of a mutual interaction between the TMC and MPD concentrations.

Figure 3.7 shows that MPD concentration induced different effects on permeation flux when TMC changed from 0.15 wt.% to 0.35 wt.% in organic solution. At MPD concentration of 1 wt.%, the water flux significantly improved from 20.9 LMH (C1) to 79.1 LMH (C3) with the increase in TMC concentration. When MPD concentration in aqueous phase increased to 2 wt.%, the rate of flux enhancement decreased, which supports the accepted hypothesis that membranes become thicker with higher internal resistance at higher MPD concentrations. However, at 3 wt.% MPD, the trend was different: water flux first dropped dramatically from 110.5 LMH in C7 to 15.3 LMH in C11, then increased to 30.6 LMH in C8 with further increase in the TMC concentration.

The SEM images of C2, C4, C7 and C8 membranes (Figure 3.8) provide clear evidence that the unexpected shift in water flux was the result of a significant change in the surface structure of the membranes. The C7 membrane, prepared at high MPD (3 wt. %) and low TMC (0.15 wt. %) concentrations, had completely different morphology from previously seen ridge-and-valley and nodular structures. The markedly thick and fully formed PA film at the surface of this membrane reveals that due to the lack of sufficient TMC molecules, the incipient core layer was not dense enough to slow down the polymer growth at the surface. Therefore, rapid diffusion of MPD molecules to the reaction zone in the organic phase resulted in a thick but loose structure with high water flux and low salt rejection. By increasing the TMC concentration to 0.35 wt.% in C8, the active layer became dense again and the surface morphology transformed to a nodular structure, similar to C3 and C4 membranes which were similarly prepared at high TMC concentration.

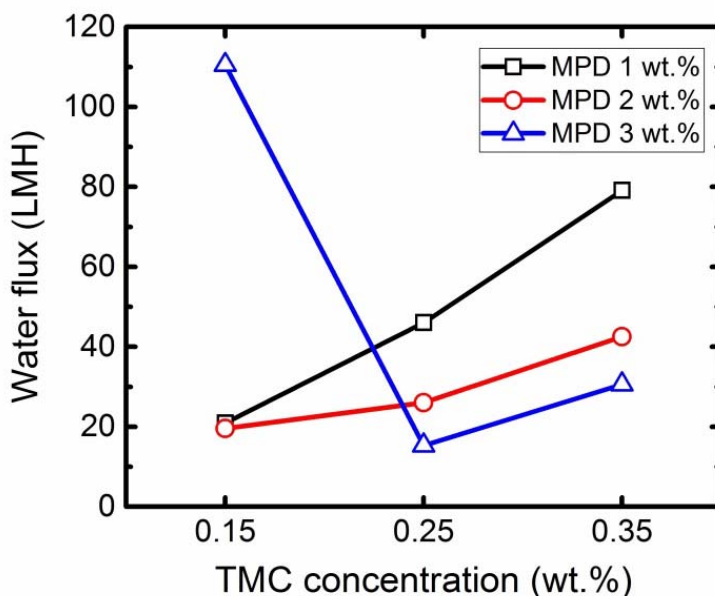


Figure 3.7: Two-way interaction plot for MPD and TMC concentration (reaction time: 15 s, curing temperature: 55 °C).

According to the interaction plot (Figure 3.7), it can be concluded the widely accepted view that the lower amine/acyl chloride molar ratio (closer to unity) results in a denser polyamide film with lower water flux [72,89,93,94], cannot be simply generalized to all practices. The flux and rejection of the PA films is directly related to the surface structure and more specifically to the cross-link density of the core layer which are controlled by initial concentration of both monomers at the beginning of IP reaction rather than a single molar ratio. The very high (31.6 in C7) and low (4.51 in C2) molar ratio in our experiments resulted in high flux membranes at the expense of salt rejection decline, suggesting that there is an acceptable range of monomer concentration which yields salt rejecting NF and RO membranes with desirable water flux (>90%). In order to make TFC membranes with tailored properties, this range must be first identified by considering the monomer concentration interaction at very high and low molar ratios.

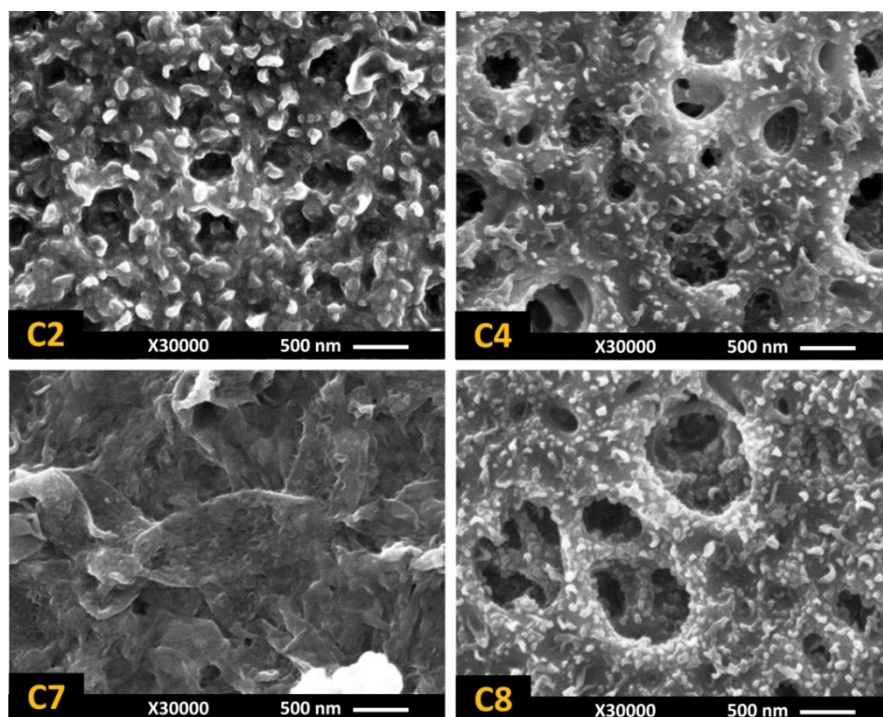


Figure 3.8: Surface images of confirmation membranes C2 & C4 (MPD concentration 2 wt.%) and C7 & C8 (MPD concentration 3 wt.%). The microporous structure of PES support is clear for C7 and C8 due to formation of thin dense layer at the surface.

### 3.1.3.5 ANOVA analysis

Table 3.5 presents the analysis of variance of experimental results based on water flux data. According to this table, the calculated  $F$ -ratio for all factors was greater than the extracted  $F$ -table ( $F=4.26$ ) with 95% confidence ( $\alpha=0.05$ ) which means all factors had significant effect on the response.

The percent contribution of each factor (P) can also be evaluated by considering the sum of squares (SS) values using the equation  $P_A = SS_A/SS_T \times 100$ . According to the P values presented in Table 3.5, curing temperature had the highest contribution (40.7 %) to the variance in the water permeation in comparison to other factors. The MPD and TMC concentrations had similar contribution to permeate flux, 28% and 27.8%, respectively. Reaction time, as was observed in the marginal plots (Figure 3.3d), had the minimum contribution (1.9%) on the response. It must be noted that the extracted contribution values are limited to the levels of control factors considered in this study and could be different for a different set of factor combinations.



Table 3.3 presents the predicted water flux and salt rejection of confirmation membranes. Note that the prediction data for C7, C8 and C11 membranes were not presented in this table as the monomers concentration for these trials were not within the range of initial levels. As can be seen in Table 3.3, the Taguchi prediction model predicts the permeation flux pretty well for the high flux membranes (C3 and C4) where the monomers concentration, particularly TMC, are set to the highest level. However, it fails to precisely predict the flux of C1 and C5 membranes which are prepared at the lowest level of TMC and MPD concentration. The relatively high prediction error for the flux of C1 and C5 membranes can be due to simplicity of the prediction model, as it assumes that the change in the results follows a linear behaviour. From the other point of view, it can be indicative of complexity and nonlinearity of film formation by IP reaction when the TMC concentration in the organic solution is low (0.15 wt. %). However, as the TMC concentration increases (0.35 wt. %), the model prediction and experimental results match very well, suggesting a more predictable mechanism for the polymerization reaction at the surface.

Table 3.5: Analysis of variance based on water permeation data.

Factor	SS <sup>1</sup>	DOF <sup>2</sup>	Variance	F-ratio <sup>3</sup>	P <sup>4</sup> (%)
Curing Temperature (°C)	3977	2	1988	111.0	40.7
MPD Concentration (%)	2733	2	1366	76.3	28.0
TMC Concentration (%)	2720	2	1360	75.9	27.8
Reaction Time (s)	187	2	94	5.2	1.9
Error (%)	161	9	18	----	----

<sup>1</sup> Sum of squares

<sup>2</sup> Degree of freedom

<sup>3</sup> F-table for  $\alpha$  (risk) =0.05 is F=4.26

<sup>4</sup> Percent contribution of each factor on response ( $SS_A/SS_T$ )

## **3.2 Systematic study on the influence of chemical additives on the properties of the TFC PA membranes**

### **3.2.1 Introduction**

In order to improve the physicochemical and permeation properties of the TFC PA membranes, extensive research has been carried out by utilizing different types of additives such as surfactants [74,80], phase-transfer catalysts [73,75], and co-solvents [76–78] in amine aqueous solution to tune the physicochemical and structural properties of the resulting membranes. The presence of these additives in the water solution is believed to alter the partitioning and diffusion rate of the amine molecules into the reaction zone by changing the properties of the water-organic interface.

Although the reported studies in the literature have demonstrated the significant role of individual chemical additives on the variation of the final properties of TFC membranes, the simultaneous effects of multiple additives have not been well studied. Hence, the objective of the present work is to systematically study the synergistic effects of four commonly used additives, namely SDS, CSA, TEA and DMSO on the permeation performance of the resulting TFC membranes. The experimental trials were designed using Taguchi method to quantify the significance and contribution of each additive on the surface characteristics and transport properties of the synthesized membranes while minimizing the number of experimental runs.

### **3.2.2 Materials and methods**

The TFC membranes were fabricated by the IP reaction between 2.0 wt.% MPD in water and 0.15 wt.% TMC in hexane at the surface of a PES microporous (0.1  $\mu\text{m}$ ) support. In order to elucidate the impact of chemical additives, a reference membrane without any additive (M0) was also synthesized following the same procedure. The control variables considered in the present study, their levels of variation in the L9 array (4 three-level factors) are given in Table 3.6. The chemical additives introduced in this table, were added into MPD-water solutions. All the membranes were synthesized twice based on the designed conditions to evaluate the repeatability of the experimental results.

Table 3.6: The list of control factors and their corresponding levels of variation in the designed experimental trials.

Membrane	Control factors			
	SDS conc. (wt.%)	CSA conc. (wt.%)	TEA conc. (wt.%)	DMSO conc. (wt.%)
MM1	0.1	0.5	0.5	0.5
MM2	0.1	1	1	1
MM3	0.1	2	2	2
MM4	0.2	0.5	1	2
MM5	0.2	1	2	0.5
MM6	0.2	2	0.5	1
MM7	0.4	0.5	2	1
MM8	0.4	1	0.5	2
MM9	0.4	2	1	0.5

### 3.2.3 Results and discussion

#### 3.2.3.1 Trend of influence of additives based on Taguchi marginal mean graphs

Figure 3.9 presents the pure water flux and salt rejection of the TFC membranes synthesized based on the Taguchi design (Table 3.6). The flux/rejection data of the base membrane (MM0), as a baseline membrane, is also provided in this figure to demonstrate the significant effect of chemical additives on the permeation performance of the synthesized membranes. As can be seen, the water flux and salt rejection of the modified TFC membranes varied in the range of 30.6–119.2 LMH and 90.9–98.2%, while the base TFC membrane (MM0) provided 6.0 LMH and 91.1% rejection under the same operating condition. This observation implies the critical role of chemical additives in the fabrication of high-performance and energy-efficient membranes.

The results presented in Figure 3.9 show the overall performance of the modified TFC membranes where all the control factors simultaneously contributed to the variation of the final performance. In order to demonstrate the trend of influence of the individual factors, the “marginal mean” graphs for water flux and rejection results are presented in Figure 3.10 and Figure 3.11, respectively. Each data point in these graphs is obtained by averaging the results of all the experimental trials conducted at each level of the additive of interest. For example, the mean water flux for the membranes made with 0.1 wt.% SDS concentration is the average of experimental results corresponding to MM1, MM2 and MM3 membranes for which the SDS concentration was set to 0.1 wt.% in the synthesis process.

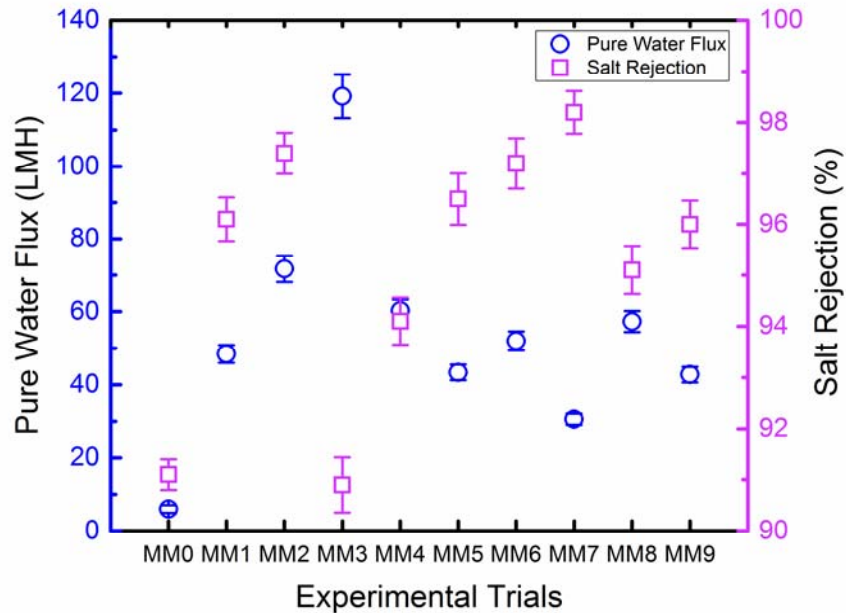


Figure 3.9: Pure water flux and salt rejection of the synthesized TFC membranes. The synthesis conditions of MM1 to MM9 membranes are presented in Table 3.6. MM0 is a reference (base) TFC PA membrane prepared without using any additive in water solution [40].

It is worth noting that although more than one factor is varying at each row of Table 3.6, the orthogonality of the Taguchi arrays allows an independent estimation of the mean influence of each control factor on the response [63]. Orthogonality here means that there are equal numbers of level settings at each column of the design table. In Taguchi OAs, each factor column is also mutually orthogonal to any other column which implies that all possible ordered pairs of two columns appear just once. Assigning the levels 1, 2, and 3 in Table 3.6 to weighing factors of -1, 0, and 1, respectively, the inner product of these weighing factors for any two columns will be zero. This property leads to the primary assumption of using Taguchi method that the main effects of independent variables on response are separable. The Taguchi OAs are also suitable designs when there is a fixed number of levels for each control factor. Also, in Taguchi method, the interaction between the control factors is assumed to be minimal which means that the impact of each control factor on the target response is independent of the influence of the other factors. Although, Taguchi method may suggest an accurate optimum combination of the factors for experiments with multi-level and dependent factors, however, the estimated response variable at this conditions can be significantly inaccurate [63].

The general approach in using the graphs of marginal means is to examine the trends and pick the levels that optimize the response. According to Figure 3.10, to maximize the water flux, SDS concentration should be set to its low level (0.1 wt.%), whereas the concentration of other additives should be adjusted at their high level (2.0 wt.%). This level setting, however, minimizes the salt rejection (Figure 3.11). The maximum salt rejection was achieved at the high level of SDS concentration, the medium level of DMSO and CSA concentration, and the high level of TEA concentration. The marginal mean plots also provide a graphical representation of the significance of each factor. The larger the difference between the low and high levels the longer the line and more significant is that factor. Based on the Figure 3.10 and Figure 3.11, SDS and DMSO were more influential on permeation properties than CSA and TEA. The TEA was found to be the less significant factor on response compared to the other additives within the studied concentration levels ( see Table 3.6).

The observed trends in Figure 3.10a and Figure 3.11a show that the mean influence of increasing the SDS concentration in amine solution was the formation of TFC membranes with lower water flux and higher salt rejection. The effect of SDS was found to be more significant at lower concentrations (i.e. from 0.1 wt.% to 0.2 wt.%). In contrast to SDS, the addition of other additives improved the water permeation through the membrane (see panel b, c, and d in the Figure 3.10 and Figure 3.11). The water flux increased steadily by increasing the concentration of CSA and TEA over the whole range, while DMSO appeared to have a more significant effect at higher concentrations (1.0 wt.% to 2.0 wt.%).

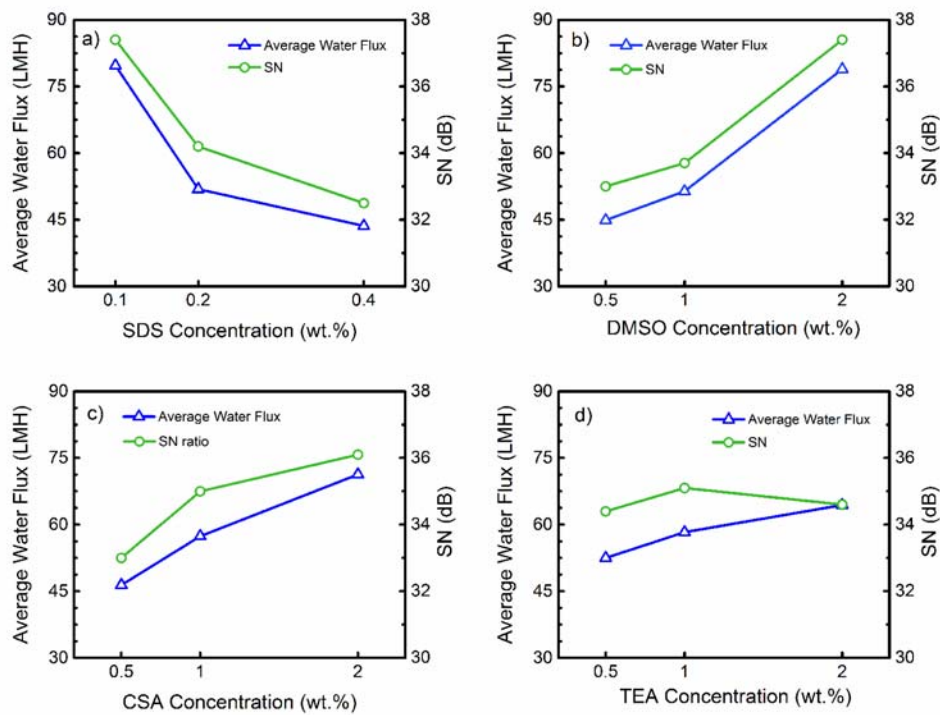


Figure 3.10: Marginal mean graphs showing the effect of additive concentration on water permeability of the TFC membranes with the corresponding SN ratio.

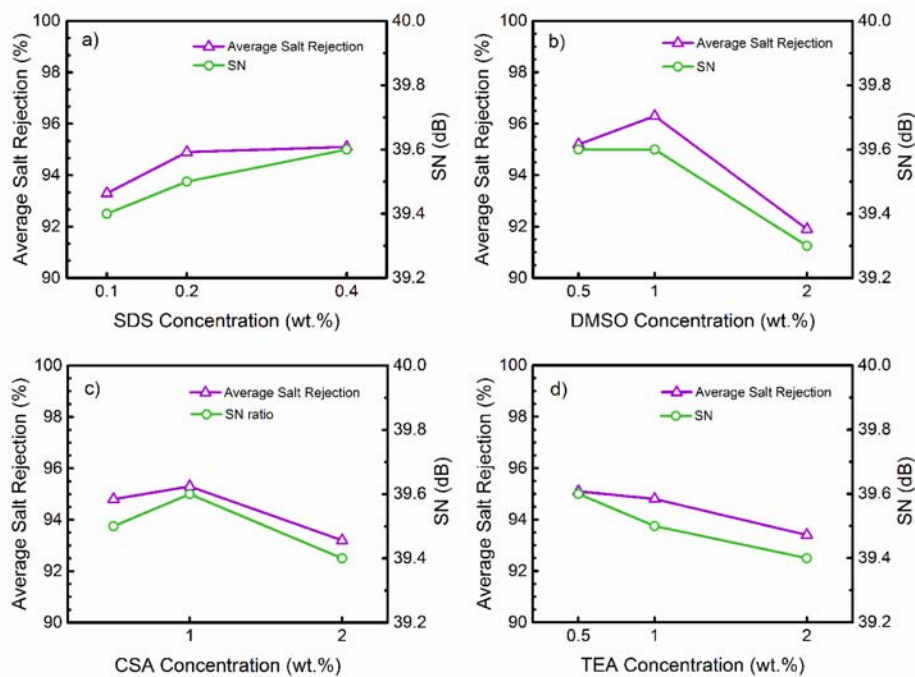


Figure 3.11: Marginal mean graphs showing the influence of additive concentration on salt rejection of the synthesized TFC membranes with the corresponding SN ratio.

The salinity of the permeate water also changed when the different concentration of additives was added into the aqueous solution. Figure 3.11b shows the addition of low concentration of DMSO in MPD solution favourably led to a slight improvement of salt rejection at 1.0 wt.%. However, the rejection decreased significantly with further increase in its concentrations up to 2.0 wt.%. Similarly, Figure 3.11c illustrates that at lower concentrations of CSA (0.5 wt.% to 1.0 wt.%), the salt rejection increased slightly, then decreased at higher concentrations (up to 2.0 wt.%). Contrary to DMSO and CSA, the variation in the TEA concentration resulted in a smooth decline in salt rejection, as shown in Figure 3.11d.

The IP reaction for the synthesis of TFC membranes is very sensitive to numerous factors which some of them are not easily controllable even by elaborate automation of membrane fabrication process. Hence, one of the hoped-for goals in the field of membrane manufacturing has been making robust membranes with identical permeation properties. Taguchi advocates the claim that utilizing the SN ratio enables exploring a combination of levels that minimizes both the influence of noise factors and the standard deviation in response. The SN ratio in Figure 3.10 and Figure 3.11 measures the sensitivity of the experimental results to different noise conditions. In general, a higher SN ratio represents a lower variability of the response due to the noise factors. Thus, as the second stage of Taguchi optimization, a factor setting that provides a maximum SN ratio must be identified. Based on Figure 3.10 and Figure 3.11, the mean responses and SN ratio followed the same trend, suggesting that (1) response variability can be minimized applying the same level setting that gives optimum responses (flux and rejection), and (2) the SN ratio changes in direct proportion to the signal variable with a constant noise portion (with the insignificant effect of noise conditions).

### 3.2.3.2 ANOVA analysis

Table 3.7 provides the analysis of variance for the water flux results of the synthesized TFC membranes. Since the computed F-statistics for each control variable is larger than the extracted F-statistics from standard statistical tables (F-table) at 95% confidence level ( $\alpha=0.05$ ), it is concluded that the addition of all additives into the MPD-water solution had a significant effect on the water flux of the resulting TFC membranes.

The percent contribution (P) of each control variable was also calculated by dividing the factors sum of squares by total sum of squares. The percent contribution values in Table 3.7 shows that the concentration of SDS and DMSO had a significantly higher contribution (40.8 % and 37.0%, respectively) to the water flux in comparison to the other control factors. The CSA concentration had a modest contribution to permeate flux (17.7 %). Finally, the addition of TEA into the amine solution had the minimum contribution (4.1%) on the response, as was also observed in the marginal plots (Figure 3.10d). It is worth noting that the present analysis of variance of water flux only applies to the experimental trials which were done within the considered range of variation of the control factors, and any extrapolation to different levels of control factors needs to be interpreted with caution.

Table 3.7: ANOVA based on water permeation results. F-table for  $\alpha = 0.05$  is 4.26.

Factor	SS	DOF	Variance	F-statistic	P (%)
SDS concentration (wt.%)	4305.8	2	2152.9	444.6	40.8
DMSO concentration (wt.%)	3919.2	2	1959.6	404.6	37.0
CSA concentration (wt.%)	1872	2	936.0	193.3	17.7
TEA concentration (wt.%)	420.3	2	210.2	43.4	4.1
Error (%)	43.6	9	4.8	---	0.4

### 3.2.3.3 Prediction of permeation properties of TFC membranes

The permeation properties (water flux and salt rejection) of the synthesized membranes were predicted using equation 2.22. To evaluate the accuracy of the prediction model four new confirmation membranes (CM1 to CM4) were synthesized at the conditions that were not previously considered in the Taguchi design.

Table 3.8 presents the synthesis conditions and the predicted permeation performance of the confirmation membranes. The results show that the Taguchi model is able to provide a reliable prediction of the water flux and salt rejection with a maximum error of 9.8% and 1.9% for the flux and rejection, respectively. It can also be inferred that there is minimal interaction between the control variables (i.e. chemical additives) which



allowed the Taguchi model to predict the permeation properties of the resulting membrane with satisfying accuracy. Cost-benefit analyses using the estimated performance of various additive blends by this prediction model can be used to guide membrane development efforts.

Table 3.8: Predicted water flux and salt rejection of confirmation membranes using Taguchi model.

Confirmation membrane	Control factors: Additives conc. in MPD solution (wt.%)				Results					
	SDS	CSA	TEA	DMSO	Measured flux (LMH)	Predicted flux (LMH)	Prediction error (%)	Measured rejection (%)	Predicted rejection (%)	Prediction error (%)
CM1	0.2	2	0.5	2	72.4	79.5	9.8	93.6	91.8	1.9
CM2	0.2	1	1	1	48.1	43.8	9.0	96.9	98.0	1.1
CM3	0.1	1	2	1	75.8	77.8	2.6	94.1	95.0	0.9
CM4	0.2	2	1	1	55.3	57.7	4.3	96.2	95.8	0.4

### 3.2.3.4 Characterization of structural and physicochemical properties of TFC membranes

The establishment of a precise correlation between the physicochemical properties and the permeation performance of the modified TFC membranes is not within the scope of the present work. However, it is worth presenting some of the characterization results obtained for the synthesized TFC membranes.

Figure 3.12 illustrates the FESEM images of the PES microporous support, the unmodified M0, M2 and M6 membranes. The significant role of additives on changing the surface morphology of the membrane is evident in panel b & c where the modified M2 and M6 membranes had remarkably larger surface features compared to nodular structure of the unmodified M0 membrane. Furthermore, the addition of the chemical additives into MPD solution resulted in thicker PA film as it is shown in the TEM cross-sectional images of the M2 and M6 membranes compared to a very thin PA film at the surface of the M0 membrane.

The 3D AFM images in Figure 3.13 show a more illustrative comparison between the surface topography of the modified and unmodified TFC membranes. Confirming the previous observations by FESEM, AFM images

showed that the modified TFC membranes by using chemical additives possessed a rougher surface compared to the unmodified MM0 membrane.

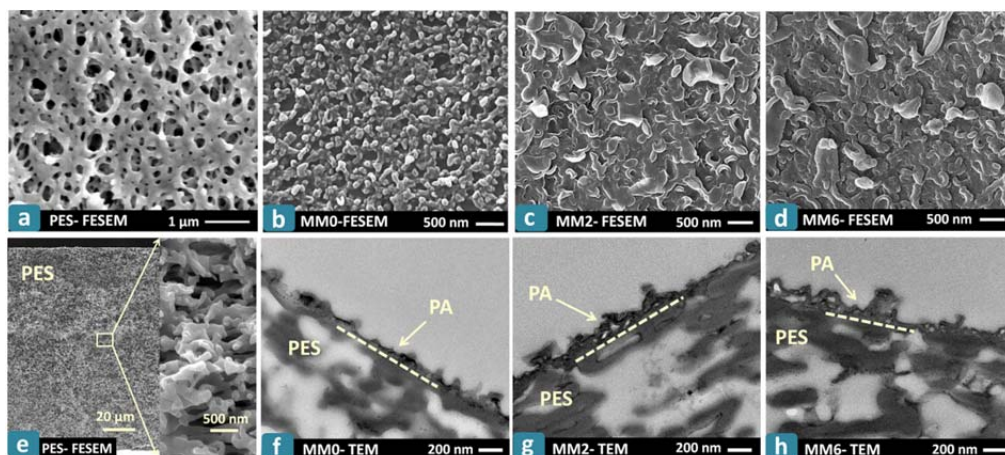


Figure 3.12: FESEM Surface morphology of PES support, unmodified MM0, and modified TFC membranes. The concentration of additives for the preparation of the modified TFC membranes was presented in Table 3.6.

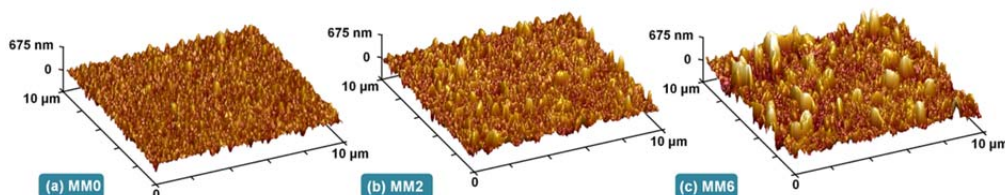


Figure 3.13: AFM surface topography images of unmodified (MM0) and modified TFC membranes. The concentration of additives in the synthesis of modified TFC membranes are presented in Table 3.6.

The surface and cross-sectional images of the confirmation membranes are presented in Figures 3.14 to 3.16. These images provide useful information to exclusively examine the effect of individual additives.

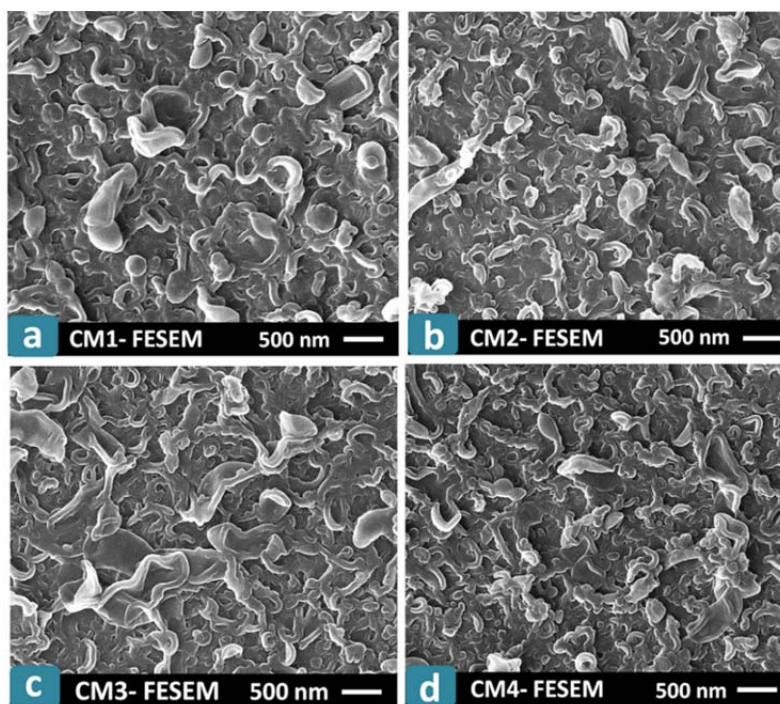


Figure 3.14: FESEM Surface morphology of confirmation membranes. The synthesis conditions of the modified TFC membranes are presented in Table 3.6.

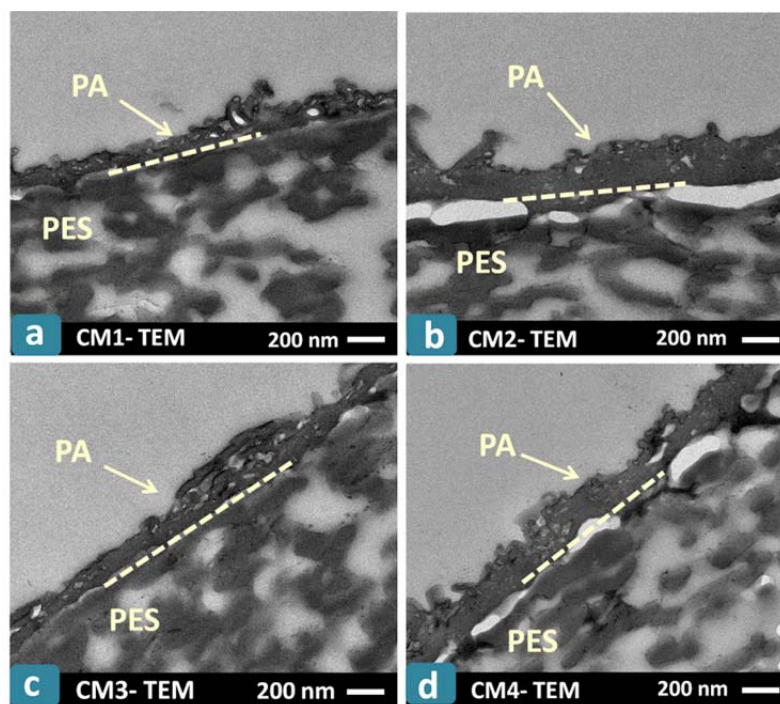


Figure 3.15: Cross-sectional images of confirmation membranes. The synthesis conditions of the confirmation TFC membranes are presented in Table 3.6.

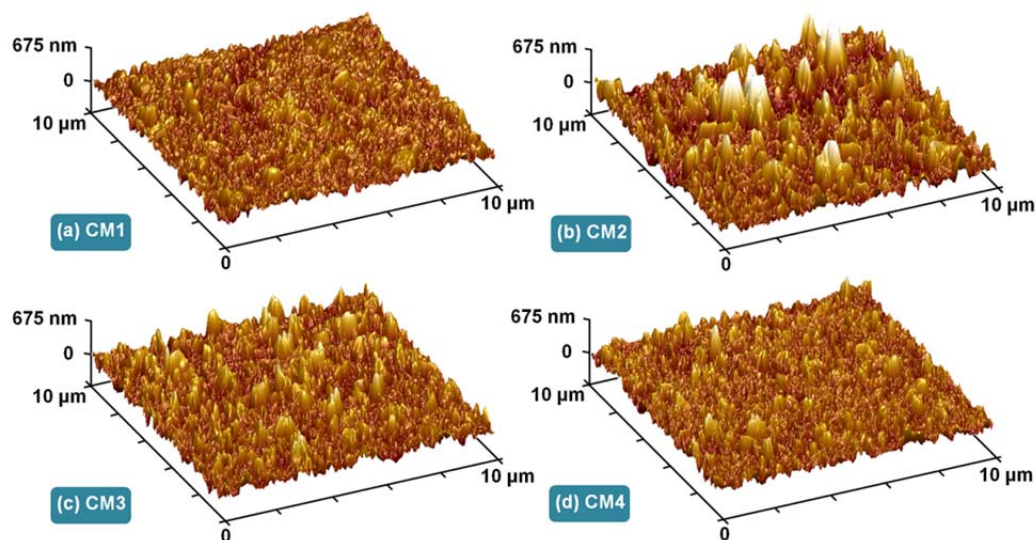


Figure 3.16: AFM surface topography images of confirmation membranes. The concentrations of additives used in the MPD-solution to modify the TFC membranes are presented in Table 3.6.

Table 3.9 presents the chemical composition, surface roughness and contact angle data of the unmodified and modified TFC membranes. Since the synthesis protocol and the underlying PES support was identical for all membranes, the substantial change in the structural morphology and the physicochemical properties of the resulting PA films can be attributed to the variation of the interfacial properties of the aqueous-organic interface due to the presence of the chemical additives. Lowering the interfacial tension of the water-hexane interface, for instance by adding SDS into the MPD solution, results in a faster diffusion and partitioning of MPD molecules into the organic phase. As a result, the number of available MPD in the reaction zone may increase, as compared to that of TMC molecules, which consequently promotes the polymerization rate and enlarges the thickness of the PA film [39,42,80,95].

Table 3.9: Degree of cross-linking, surface roughness and contact angle data of the synthesized TFC membranes.

Membrane	Degree of Cross-linking	Contact Angle (°)	Surface Roughness (nm)	
			Ra	Rq
MM0	72.7	82±2	46±2	61±5
MM2	32.6	70±4	60±3	78±5
MM6	40.0	82±4	85±8	115±9
CM1	46.9	72±3	59±5	75±6
CM2	38.1	59±2	100±7	140±10
CM3	37.2	68±3	72±6	95±8
CM4	28.1	57±3	59±5	77±5

Figure 3.17 presents the TEM cross-sectional images of four TFC membranes that were prepared with different concentrations of SDS in MPD solution. It can be observed that the PA film thickness dramatically increased with an increase in the concentration of the SDS in the water solution.

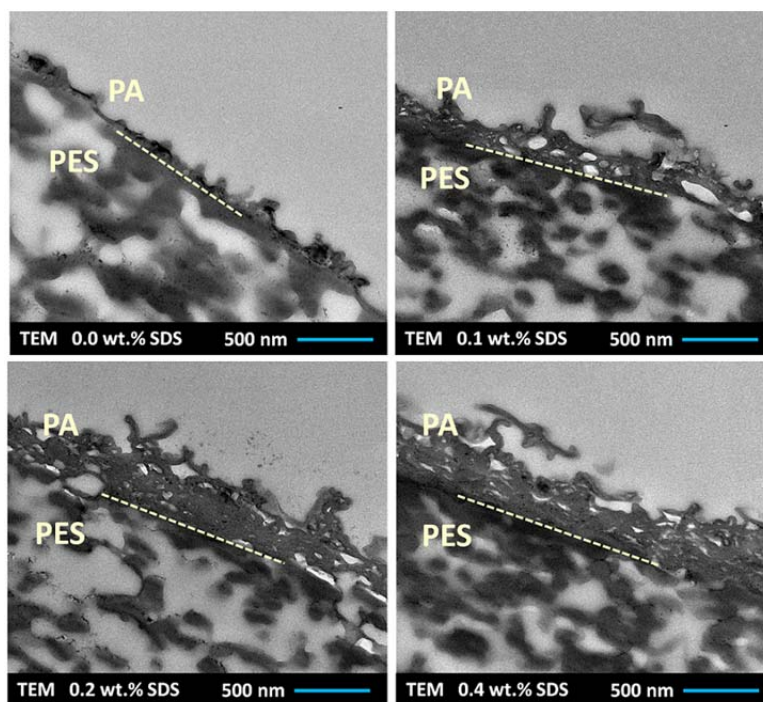


Figure 3.17: TEM cross-sectional images of TFC membranes prepared with different concentration of SDS in water solution. Synthesis conditions: 2.0 wt.% MPD in water, 0.15 wt.% TMC in hexane, 30 sec reaction, 4 min thermal curing at 60 °C. No other additive was used in the MPD solution.

The comparison between the characteristics of the M2 and C2 membranes in Table 3.9 provides more details about the effect of SDS on the properties of the prepared PA films. The synthesis conditions of these two membranes differ only in SDS concentration (0.1 wt. % in M2 to 0.2 wt. % in C2, see Table 3.6 and Table 3.8). The results revealed that a thicker and rougher PA film with more degree of cross-linking and higher surface wettability was formed when more SDS was added to the MPD solution. The combination of these effects resulted in a decrease in the water flux and enhancement of salt rejection by the addition of SDS into the MPD solution as shown in Figure 3.10a and Figure 3.11a.

M6 and C1 membranes can be considered as a pair where only DMSO concentration was changed in their preparation process (1.0 wt. % in M6 and 2.0 wt. % in C1). Based on the data presented in Table 3.9, the membrane prepared with higher DMSO concentration possessed a smoother PA film with a higher degree of cross-linking and surface wettability. A thicker PA film was obtained when higher concentration of the DMSO was added into MPD solution (see Figure 3.12 and Figure 3.15) which can be attributed to the higher miscibility of the water-hexane interface at higher DMSO concentration. DMSO has a solubility parameter ( $26.7 \text{ MPa}^{1/2}$ ) between water ( $47.8 \text{ MPa}^{1/2}$ ) and hexane ( $14.9 \text{ MPa}^{1/2}$ ) [96]. Therefore, DMSO reduces the miscibility gap between water and hexane solutions and thus improves the partitioning of MPD molecules into the reaction zone. Furthermore, DMSO partially swells the incipient PA film which is formed during the initial stage of IP reaction. Hence, MPD molecules can migrate to the organic phase and react with TMC molecules at higher rates and form a thicker PA film when DMSO is present in the solution. The permeation results in Figure 3.10b and Figure 3.11b showed that the addition of the DMSO into MPD solution at lower concentration (0.5 wt. % to 1.0 wt. %) favorably improved both water flux and salt rejection, whereas at higher concentrations (1.0 wt. % to 2.0 wt. %) the flux enhancement was accompanied by a slight sacrifice in salt rejection.

The observed permeation results of the modified TFC membranes with DMSO is quite interesting, as it is generally considered that the water flux and salt rejection follow a mutually exclusive relationship. Also, a TFC membrane with a thicker PA film and a higher degree of cross-linking is typically expected to provide lower water flux compared to a membrane with thinner and less cross-linked PA layer. However, caution should be exercised

while drawing a conclusion based on the characterization results for a dense RO membrane where the transport mechanism is principally based on solution-diffusion phenomenon. In TFC RO membranes, the surface and structural characteristics of the membranes such as surface roughness, thickness, charge density, degree of cross-linking, size and configuration of the complex internal free volumes within the PA structure may significantly affect the final performance of the TFC membrane [88,95,97–102]. For example, just considering the overall thickness of the PA film (obtained by SEM or TEM) as a measure of the film resistance toward water passage can be misleading due to the presence of numerous nano- and microvoids within the PA structure [95,103–108]. Although the formation mechanism of these multiscale voids during IP reaction is not still clear, they can significantly contribute to the enhancement of water passage through the PA film, particularly when the voids are internally connected [88,99,100,109,110].

Regarding the effect of DMSO, recent studies attributed the enhancement of water flux, in spite of formation of thicker and higher cross-linked PA film, to an increase in the number and size of the network and aggregate pores within the PA matrix, as well as, formation of more favorable spots for hydrogen bonding by amide linkages [76,104,108,111]. A possible explanation for the improvement of both water flux and salt rejection of the membranes at low concentration of DMSO and CSA might be the reconfiguration of the size and number of free volumes within the PA network that provided more surface area for the permeation of water molecules without any sacrifice in salt rejection. Indeed, more characterization at nanoscale resolution must be conducted to draw a solid conclusion about the physicochemical-permeation relationship of the modified TFC membranes at low DMSO concentration. Similarly, the addition of CSA into MPD solution desirably improved both water flux and salt rejection at lower concentrations of CSA (0.5 – 1.0 wt.% ), as shown in Figure 3.10c and Figure 3.11c. The comparison between the physicochemical properties of C2 and C4 membranes in Table 3.9 reveals that an increase in CSA concentration resulted in a considerably smoother PA film with a slightly less degree of crosslinking.

A similar comment can be made about the N/O ratio obtained by the XPS analysis. In general, a high N/O ratio represents a highly cross-linked PA film with low water flux and high salt rejection. However, it should be noted that XPS is commonly used to analyze the elemental composition of

the top 5-10 nm of the PA surface and it is not expected to give detailed information about the inner structure of the PA layer. Hence, a high N/O ratio alone does not guarantee a high degree of cross-linking or uniform distribution of the microvoids over the entire cross-section of the PA layer. This is particularly correct for the unmodified membrane (M0) where both the water flux and salt rejection were lower than the modified TFC membranes despite the formation of a thinner and more cross-linked PA film over the PES surface (see Figure 3.12 and Table 3.9).

Comparing M2 and C3 membranes provides insight into the effect of TEA concentration (1.0 wt.% in M2 to 2.0 wt.% in C3). The addition of more TEA into the MPD solution resulted in the formation of a thicker PA film with a slightly greater degree of cross-linking and a higher surface roughness in C3 compared to M2. However, the membranes prepared at higher TEA concentration provided more water flux and less salt rejection (Figure 3.10d and Figure 3.11d). A possible explanation for this result might be due to the restructure of the internal free volumes within the PA network by incorporation of higher TEA to the organic solvent which develops pathways for easier transport of both water and solute molecules. Overall, the experimental results revealed a less significant influence of TEA compared to the other additives which supports the results of formerly reported studies [87,112,113].



## **3.3 Investigation of the influence of monohydric and polyhydric alcohol additives on the properties of the TFC PA membranes**

### **3.3.1 Introduction**

It is a widely held view that the permeation properties of a synthesized TFC membrane are highly influenced by the conditions of the membrane synthesis reaction. For an IP reaction where the concentration of the amine monomer is considerably larger than the acyl chloride monomer (often 10 to 20 times higher), the IP reaction is essentially controlled by the diffusion of amine molecules to the organic phase, and thus the reaction mainly happens on the organic side of the interface [87,88]. Therefore, any variation in miscibility of the water-organic interface is expected to affect the diffusion and partitioning of the amine molecules into the reaction zone and thus change the rate of the polymerization reaction.

A common approach for changing the miscibility of water and organic phases is to incorporate chemical additives in either of the aqueous and organic phases. Although extensive research has been conducted to improve transport properties of the TFC membranes using surfactants, phase transfer catalysts and co-solvents [17,112,114,115], a few efforts have been made to explore the effect of polar alcohols on permselectivity and morphology of the resulting membranes [116–120]. Utilization of alcohols with polarity and miscibility between water and the organic solvent is anticipated to alter the solubility and diffusion of the reacting monomers through the water-organic interface. As a result, the rate of the polymerization reaction changes which consequently affects the surface morphology, thickness and physicochemical properties of the synthesized PA selective layer. Jegal et al. [121] studied the effect of different concentration of n-propanol in amine-water solution on permeation properties and morphology of PA TFC membranes. The addition of n-propanol up to 20 wt% in amine-water solution increased the water flux with a constant rejection of polyethylene glycol (PEG) 200 Da (~90 %). However, higher concentrations of n-propanol in aqueous solution resulted in dramatic decrease in salt rejection (~25 %). The change in permeation properties of the synthesized membranes was attributed to a change in the miscibility of water and organic solvent (hexane) that affected the polymerization reaction and the final structure of the polymerized

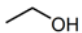
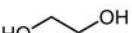
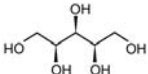
membrane. Liu et al. [122] used different concentration of isopropyl alcohol in aqueous solution in order to modify the IP reaction between MPD and 5-chloroformyloxyisophthaloyl chloride (CFIC). It is reported that the water permeability and salt rejection of the synthesized membranes improved at lower concentration of the isopropyl alcohol (less than 6 wt.%). In contrast, at higher isopropyl concentration, the increase in water flux was accompanied with dramatic decrease in salt rejection. The reason behind the observed decrease in salt rejection was ascribed to formation of a loose PA film due to high concentration of alcohol additive during the IP reaction. Qui et al. [123] reported that the incorporation of isopropanol into the amine-water solution enhanced the permeation flux, while the salt rejection remained constant. The increase in water flux was mainly attributed to the fast reaction between hydroxyl groups of the alcohol and the functional groups of the acid chloride monomer that led to the formation of ester structure within the PA network. Furthermore, the swelling of PA film with isopropanol alcohol as well as change in polarity of the water-alcohol system were also mentioned as the possible reasons for water flux enhancement of the modified membranes. However, in spite of the existing reports in the literature regarding the modification of IP reaction using alcohol additives, more investigation is required to provide a clear understanding of the influence of size and functionalities of alcohols (i.e. number of hydroxyl groups and chain length) on the kinetics of the IP reaction and consequently the physicochemical properties of the resulting TFC membranes.

Here, the effect of using monohydric and polyhydric alcohol additives with different chain length and hydroxyl group on the final properties of the TFC PA membrane was studied. Different concentrations of ethanol ( $C_2H_6O$ ), ethylene glycol ( $C_2H_6O_2$ ), and xylitol ( $C_5H_{12}O_5$ ) were added into the MPD-aqueous solution. The physicochemical characteristics of synthesized TFC PA membranes such as surface morphology, wettability, and chemical composition were analysed and linked to their permselectivity (pure water flux and salt rejection) properties. The addition of alcohols into MPD-aqueous solution was found to enhance the water flux by changing the miscibility of water and the organic phase during IP reaction which significantly altered the surface morphology and permeation characteristics of the PA active layer. The number of hydroxyl groups and the chain length of the alcohols were also identified as significant influential factors on the permeation properties of the synthesized membranes.

### 3.3.2 Materials and methods

TFC PA membranes were prepared via IP reaction between 2.0 wt.% MPD in water and 0.15 wt.% TMC in hexane at the surface of the PES microporous (0.1  $\mu\text{m}$ ) substrate. The MPD solution contained 0.2 wt.% SDS and 1.0 wt.% TEA and different concentration (1.0-6.0 wt.%) of alcohol (ethanol, ethylene glycol and xylitol). The list of the synthesized TFC membranes and the concentration of the alcohols used as the additives in the MPD-water solution are presented in Table 3.10.

Table 3.10: List of the synthesized TFC membranes with corresponding monomer and alcohol concentration in MPD-water solution [41].

Membrane	Monomer conc. (wt%)		Alcohol in MPD solution	Alcohol Chemical Formula	Alcohol Chemical Structure	Alcohol Density (g/cm <sup>3</sup> )	Alcohol Molar volume (g/mol)	Concentration of alcohol (wt.%)
	MPD	TMC						
TFC0	2	0.15	---		-	-	-	-
TFC1	2	0.15	Ethanol	C <sub>2</sub> H <sub>6</sub> O		0.79	46.07	1.0
TFC2	2	0.15						6.0
TFC3	2	0.15	Ethylene glycol	C <sub>2</sub> H <sub>6</sub> O <sub>2</sub>		1.11	62.07	1.0
TFC4	2	0.15						6.0
TFC5	2	0.15	Xylitol	C <sub>5</sub> H <sub>12</sub> O <sub>5</sub>		1.52	152.15	1.0
TFC6	2	0.15						6.0

### 3.3.3 Results and discussion

#### 3.3.3.1 Surface morphology of synthesized TFC membranes

The FESEM surface images of the PES microporous support, unmodified (base) membranes, and the modified TFC membranes with the minimum and maximum concentrations of alcohols (ethanol, ethylene glycol and xylitol) are presented in Figure 3.18. According to this figure, the active surface of all TFC membranes has the typical “ridge-and-valley” structure of the PA-based TFC membranes. However, taking a closer look at Figure 3.18 reveals that larger ridges and valleys were formed at the polyamide surface when the film was prepared at lower concentration (1.0 wt.%) of alcohols (TFC1, TFC3, and TFC5).

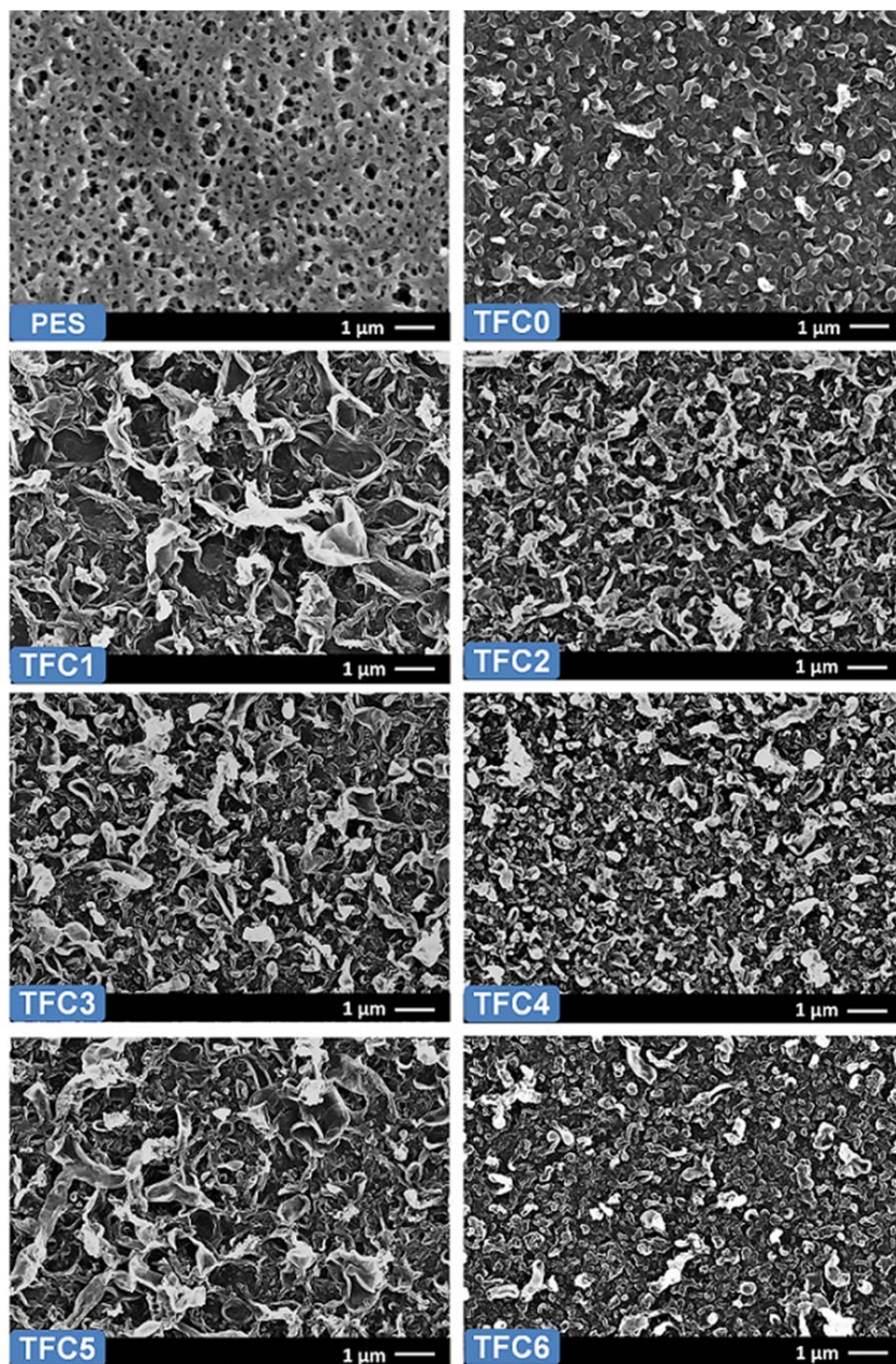


Figure 3.18: FESEM surface morphology of the PES substrate, unmodified PA membrane (TFC0), and modified TFC membranes by ethanol (TFC1, TFC2), ethylene glycol (TFC3, TFC4), and xylitol (TFC5, TFC6) prepared at 1.0 and 6.0 wt.% concentration of these alcohols in the MPD-aqueous solution.

The cross-sectional TEM images of the unmodified and modified TFC membranes in Figure 3.19 show the significant influence of alcohols on the internal structure and thickness of the PA skin layer. According to this figure, all the modified TFC membranes had a thicker PA layer than the unmodified membrane. Furthermore, the PA films modified with 1.0 wt.% alcohol had multiple voids within the ridge-and-valley structure (see TFC1, TFC3, and TFC5). In contrast, by increasing the concentration of alcohols to 6.0 wt.%, especially for the case of ethanol and ethylene glycol, the synthesized PA layers became thicker and fuller with the fewer voids inside the PA structure (TFC2, TFC4, and TFC6).

The observed change in surface and the cross-sectional structure of the modified TFC membranes implies a significant change in the kinetics of the IP reaction caused by the addition of alcohols into the MPD solution. Basically, the polymerization reaction between MPD and TMC molecules starts immediately when the TMC-hexane solution is brought into contact with the MPD-impregnated PES support. In the absence of any chemical additives, water and organic solvent are immiscible, restricting the polymerization reaction to occur at the interface of water and organic solution [22,86,124]. The IP reaction is mainly controlled by the diffusion of MPD molecules to the organic phase which is attributed to (1) higher concentration of MPD than TMC in their relevant solvents and (2) better solubility of MPD in the organic solvent rather than TMC in water [87,88]. Hence, any change in the property of water/organic interface (such as miscibility and interfacial tension) significantly affects the diffusion rate of MPD molecules to the organic phase and thus alters the kinetics of IP reaction [44,108].

The change in the miscibility of water and hexane solution by the addition of alcohols can be evaluated through comparing the Hansen solubility parameters of the two phases. This parameter is calculated as follows:

$$\delta^2 = \delta_d^2 + \delta_p^2 + \delta_h^2 \quad (3.1)$$

where  $\delta_d$ ,  $\delta_p$  and  $\delta_h$  are the solubility parameter components due to (atomic) dispersion forces, (molecular) permanent dipole forces, and (molecular) hydrogen bonding (electron exchange or in general donor-acceptor interactions), respectively.

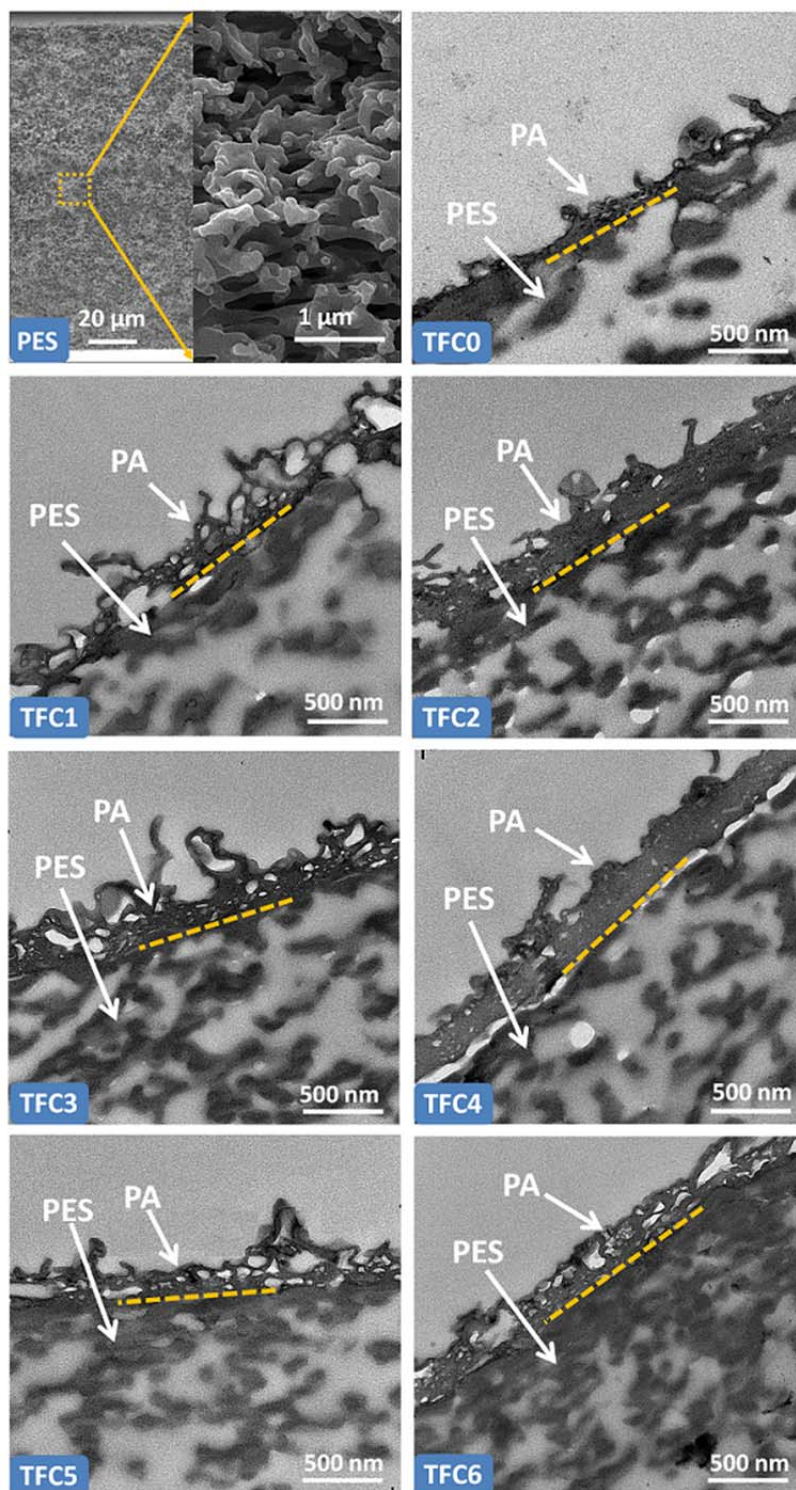


Figure 3.19: TEM cross-sectional images of the modified TFC membranes prepared at 1.0 and 6.0 wt.% concentration of ethanol (TFC1, TFC2), ethylene glycol (TFC3, TFC4), and xylitol (TFC5, TFC6) in the MPD-aqueous solution.

These components can be predicted from group contributions using the method proposed by Hoftyzer and Van Krevelen [125]:

$$\begin{aligned}\delta_d &= \frac{\sum F_{di}}{V} \\ \delta_p &= \frac{\sqrt{\sum F_{pi}^2}}{V} \\ \delta_h &= \frac{\sqrt{\sum E_{hi}}}{V}\end{aligned}\tag{3.2}$$

where  $F_{di}$ ,  $F_{pi}$  are the molar attraction constants for the dispersion and dipole forces of a specific group  $i$ , respectively,  $E_{hi}$  represents the hydrogen bonding energy of each group, and  $V$  is the molar volume of the molecule [126]. The values of the structural group contributions ( $F_{di}$ ,  $F_{pi}$  and  $E_{hi}$ ) of water, alcohols and organic solvent used in this study are presented in Table 3.11.

Table 3.11: Values of group contributions for solubility parameter component for some structural groups.

Structural group	$F_{di}$ , (MJ/m <sup>3</sup> ) <sup>1/2</sup> mol <sup>-1</sup>	$F_{pi}$ , (MJ/m <sup>3</sup> ) <sup>1/2</sup> mol <sup>-1</sup>	$E_{hi}$ , J/mol
-CH <sub>3</sub>	420	0	0
-CH <sub>2</sub> -	270	0	0
>CH-	80	0	0
-OH	210	500	20000

The solubility parameter of the water-alcohol mixture  $\delta_{mix}$  at different concentrations is calculated using the volume fraction ( $\phi$ ) of each component by the following equation [127–129]:

$$\delta_{mix} = \phi_{comp1} \delta_{comp1} + \phi_{comp2} \delta_{comp2}\tag{3.3}$$

The volume fraction of each component can be obtained using [96]:

$$(\text{Vol.Fraction})_{comp1} = \frac{(\text{Wt.Fraction})_{comp1}}{\text{Density}} \bigg/ \left( \frac{(\text{Wt.Fraction})_{comp1}}{\text{Density}} + \frac{(\text{Wt.Fraction})_{comp2}}{\text{Density}} \right)\tag{3.4}$$

Table 3.12 presents the solubility parameter components of water, hexane and water-alcohol mixtures. According to this table, the addition of all alcohols into water phase increased the miscibility of water and organic

solvent as the difference in the total solubility parameter between the aqueous and organic solutions decreased by the increase in the concentration of alcohol in the water. Comparing the three components of the solubility parameter in Table 3.12, it can be concluded that the major variation in the total solubility parameter of alcohol-water mixture was due to hydrogen bonding contribution ( $\delta_h$ ) in the solution which itself decreased by the decrease in the number of hydroxyl groups of the alcohol. Therefore, among the three alcohols, the miscibility of water-hexane phases increased more by ethanol, followed by ethylene glycol and then xylitol. The increase in the miscibility of water and hexane solutions facilitates the migration of MPD molecules to reach the organic phase. The presence of more MPD molecules in the reaction zone speeds up the rate of the polymerization reaction, thereby producing thicker PA film at the surface as it can be observed for the case of TFC2, TFC4 and TFC6 membranes in Figure 3.19 [39,42,72].

Table 3.12: Solubility parameter components of water, hexane and water-alcohol mixtures.

Solubility parameter (MPa <sup>1/2</sup> )	Water	Hexane	Ethanol	Ethylene glycol	Xylitol	Ethanol conc. in water		Ethylene glycol conc. in water		Xylitol conc. in water	
						1	6	1	6	1	6
						wt%	wt%	wt%	wt%	wt%	wt%
$\delta_d$	15.6	14.9	15.4	17.2	18.3	15.6	15.6	15.6	15.7	15.6	15.7
$\delta_p$	16.0	0	8.56	12.7	11.2	15.9	15.4	16.0	15.8	16.0	15.8
$\delta_h$	42.3	0	18.5	26.8	31.6	42.0	40.5	42.2	41.5	42.2	41.9
$\delta$	47.8	14.9	25.6	34.3	38.2	47.5	46.1	47.7	47.1	47.8	47.4

### 3.3.3.2 Chemical composition of the PA active layer

The elemental composition and chemical bonding information of PA active layer of the synthesized TFC membranes were evaluated using XPS analysis. Figure 3.20 illustrates the deconvolution of C (1s) high resolution XPS spectra of the modified TFC membranes which involved four peaks: (1) a peak at 285 eV which is assignable to the single-bond carbon (aliphatic/aromatic C–C and C–H), (2) two peaks at 285.7 and 286.5 eV which are associated with carbon attached to weak electron withdrawing atoms (carbons in C–N and C–O, respectively), and (3) a peak at 288.6 eV which corresponds to carbons adjacent to strong electron withdrawing atoms (carbon atoms in carboxylic O=C–O and amide O=C–N groups) [130].



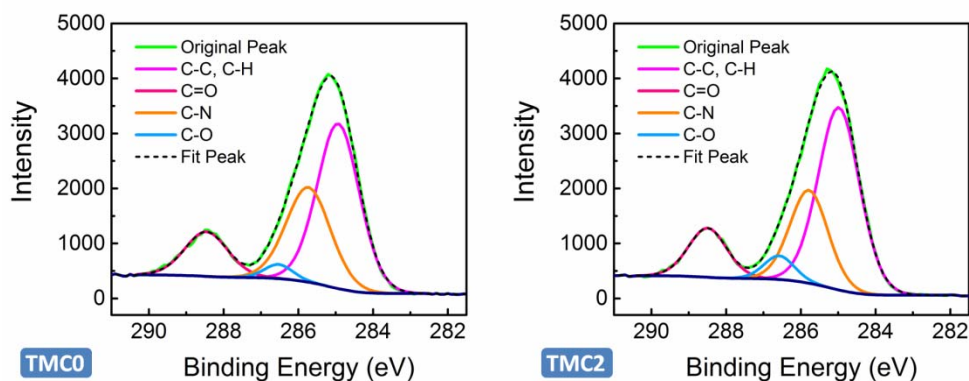


Figure 3.20: C 1s deconvolution of high resolution spectra of base (M0) and modified (M2) TFC membranes.

The extent of cross-linking of the synthesized membranes can be compared by considering the ratio of the surface area under C–O peak over the C=O peak. Theoretically, a fully cross-linked PA film ( $C_{18}H_{12}N_3O_3$ ) does not have any C–O covalent bond in the structure. In contrast, the C–O bond appears in the linear chain of PA structure. Therefore, a higher C–O/C=O ratio represents a lower extent of cross-linking of the synthesized PA film. By this measure, all the modified TFC membranes (TFC1 to TFC6) had higher C–O/C=O ratio and thus were less cross-linked than the unmodified membrane (TFC0) as presented in Table 3.13. This observation can be attributed to the neutralization of TMC monomers by the penetrated water and alcohol molecules via a nucleophilic addition/elimination reaction [131]. The carbon atom in acyl chloride group has partial positive charge due to higher electronegativity of the oxygen and the chlorine atoms which makes the carbon atom to be easily attacked by nucleophile molecules like water or alcohols. Regarding that, the first stage (i.e. the addition stage of the nucleophilic reaction) of the hydrolysis reaction of TMC molecules is a nucleophilic attack on carbon atom of the acyl chloride by a lone pair on the oxygen atom of water or alcohol molecule as it is shown in Figure 3.21.

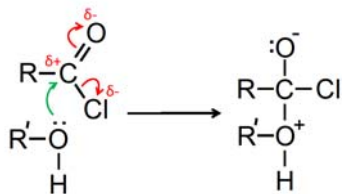


Figure 3.21: Addition stage of the hydrolysis (nucleophilic) reaction of a TMC molecule.

The hydrolysis reaction then moves to second (elimination) stage where hydrogen chloride will be produced in two successive stages: first, the covalent double bond between the carbon and oxygen atoms reforms and then hydrogen will be removed by the chloride ion to give carboxylic ( $\text{O}=\text{C}-\text{OH}$ ) or ester linkage ( $\text{O}=\text{C}-\text{O}-\text{C}$ ) and hydrogen chloride (see Figure 3.22) [131].

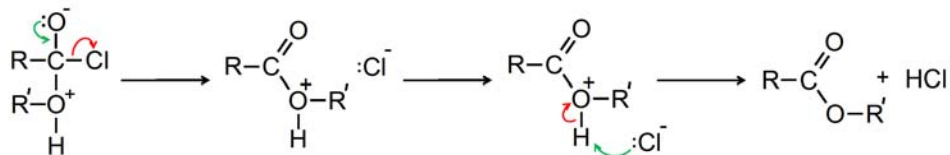


Figure 3.22: Elimination stage of the hydrolysis (nucleophilic) reaction of a TMC molecule.

Therefore, the addition of alcohol additive into MPD solution intensifies the neutralization reaction of the carboxylic groups of the TMC molecules and result in more participation of water and alcohol molecules during the IP reaction. As a result, a PA film with more linear structure than the cross-linked network forms at the surface of the PES support [42]. Comparing the  $\text{C}-\text{O}/\text{C}=\text{O}$  ratio of the modified TFC membranes with ethanol and ethylene glycol, the network cross-linking of these membranes decreased with increase in alcohol concentration (see TFC2 and TFC4 compared to TFC1 and TFC3, respectively). This result suggests that more hydrolysis and nucleophilic reactions take place at the higher concentration of these alcohols. In contrast, for the membrane modified by xylitol,  $\text{C}-\text{O}/\text{C}=\text{O}$  ratio significantly increased at lower concentration of this alcohol (1.0 wt.%, TFC1 compared to unmodified TFC0 membrane), then decreased by the addition of more alcohol suggesting a highly cross-linked PA film at high xylitol concentrations.

Table 3.13: Elemental compositions, chemical bonding peak area of the synthesized TFC membranes.

Sample	Atomic Concentration (%)			Chemical Bonding Peak Area				$\frac{C-O}{C=O}$	$\frac{C-O}{C-N}$
	O (1s)	N (1s)	C (1s)	C-C, C-H Peak at 285 eV	C-N Peak at 285.7 eV	C-O Peak at 286.5 eV	O-C-O, O=C-N Peak at 288.6 eV		
TFC0	13.42±1.59	12.16±1.14	74.42±1.82	51.68±4.02	14.22±0.5	2.96±2.87	31.15±6.66	0.10	0.21
TFC1	13.95±1.43	12.29±0.73	73.77±1.63	50.13±4.23	13.0±0.50	4.44±2.85	32.43±6.69	0.14	0.34
TFC2	15.45±1.93	12.01±1.09	72.55±2.08	55.11±3.07	13.74±0.44	5.24±3.48	25.91±5.61	0.20	0.38
TFC3	14.45±1.70	12.46±0.86	73.09±2.42	56.32±3.48	13.71±0.48	4.00±2.19	25.96±4.99	0.15	0.29
TFC4	15.97±1.34	12.26±0.99	71.77±1.94	52.61±3.76	14.32±0.49	6.27±4.27	26.80±6.95	0.23	0.44
TFC5	14.74±1.19	11.99±0.85	73.27±1.50	55.26±3.36	13.88±0.55	5.26±2.41	25.60±4.68	0.21	0.38
TFC6	15.01±1.16	11.93±0.77	73.06±1.50	56.47±3.79	13.56±0.47	2.91±2.42	27.37±5.68	0.11	0.21

### 3.3.3.3 Surface wettability and roughness of the synthesized membranes

The contact angle data of the synthesized TFC membranes is presented in Table 3.14. In general, the contact angle measurement is conducted to evaluate the surface wettability of the synthesized membranes. A lower value of the contact angle is often interpreted as higher surface hydrophilicity which can lead to the enhancement of water permeation and antifouling properties of the membrane. According to Table 3.14, the surface wettability of the TFC membranes was increased by the addition of all alcohols into MPD-water solution. In the case of ethanol and ethylene glycol, the contact angle decreased significantly with increase in their concentration. For xylitol, however, the contact angle first decreased notably to  $\sim 35^\circ$  at 1.0 wt.%, and then increased, suggesting lower wettability of resulting TFC membranes at higher xylitol concentration. Among all the synthesized membranes, the ones prepared with 6.0 wt.% of ethylene glycol and xylitol had the lowest and highest surface wettability with contact angles of  $31^\circ$  and  $62^\circ$ , respectively. The change in surface hydrophilicity is related to the presence of hydrophilic functional groups (such as hydroxyl, ester, and amide linkage) in the PA network. For monohydric and polyhydric alcohols with smaller chain length, e.g., ethanol and ethylene glycol, the surface hydrophilicity increased by an increase in the number of hydrophilic C–O bond at the surface (due to

neutralization of TMC molecules via nucleophilic reaction) as it is evidenced by XPS (Table 3.13). However, for the case of membranes modified by polyhydric alcohol with high molar volume, e.g., xylitol, the trade-off relationship between the number of the hydrophilic –OH groups and hydrophobic C–C bonds of alcohol governs the wettability. At low concentration of xylitol (TFC5), the number of –OH groups is dominant, and the surface hydrophilicity of the resulting membranes is improved. This result aligns well with the XPS result of C–O/C=O ratio as presented in Table 3.13. At higher xylitol concentration (TFC6), however, there was a negligible improvement in the surface wettability of the polymerized films compared to the original membranes, due to presumably lower rate of hydrolysis reaction and the adverse effect of hydrophobic C–C bonds on wettability.

Table 3.14: Contact angle and surface roughness of the synthesized TFC membranes.

Sample	Contact Angle (°)	Surface Roughness (nm)	
		R <sub>a</sub>	R <sub>q</sub>
TFC0	62.5±3.7	122±9	156±12
TFC1	54.4 ±3.4	160±10	201±11
TFC2	49.0±4.1	98±11	131±12
TFC3	44.1±1.5	127±16	169±14
TFC4	31.9±4.0	87±8	117±10
TFC5	34.9±1.7	133±10	174±13
TFC6	62.0±4.1	41±6	56±9

It must be noted that the contact angle of the synthesized membranes is partially affected by their surface roughness. Adding surface roughness is reported to enhance the wettability caused by the chemistry of the surface [132]. The AFM 3D surface topography of the modified TFC membranes is displayed in Figure 3.23. According to this figure, the membranes synthesized using a higher concentration of alcohol in water solution (TFC2, TFC4, and TFC6) had a smoother surface with smaller surface features. The comparison between the surface roughness data of modified and unmodified membrane in Table 3.14, show that the addition of 1.0 wt. % alcohol into MPD solution increased the surface roughness of the resulting TFC membranes. The synergistic effect of the increased roughness and improved chemistry (C–O/C=O ratio measured by XPS) decreased the contact angle of these modified membranes compared to the unmodified base membrane. Further addition of alcohol into MPD solution, however, effectively reduced

the roughness of PA active layer. In the case of ethylene and ethylene glycol, despite the reduction of roughness, the contact angle decreased which clearly shows the dominant effect of the polymer chemistry improvement. For the TFC6 which was synthesized with 6.0 wt.% xylitol in water solution, the integrated effect of diminished roughness ( $\sim 42$  nm compared to  $\sim 133$  nm in TFC5) and reduced hydrophilic groups in polymer structure ( $0.11$  C–O/C=O compared to  $0.22$  in TFC5) increased the contact angle significantly. It is also worth mentioning that the AFM roughness results are in good agreement with the observed FESEM surface and TEM cross-section morphologies of the membranes.

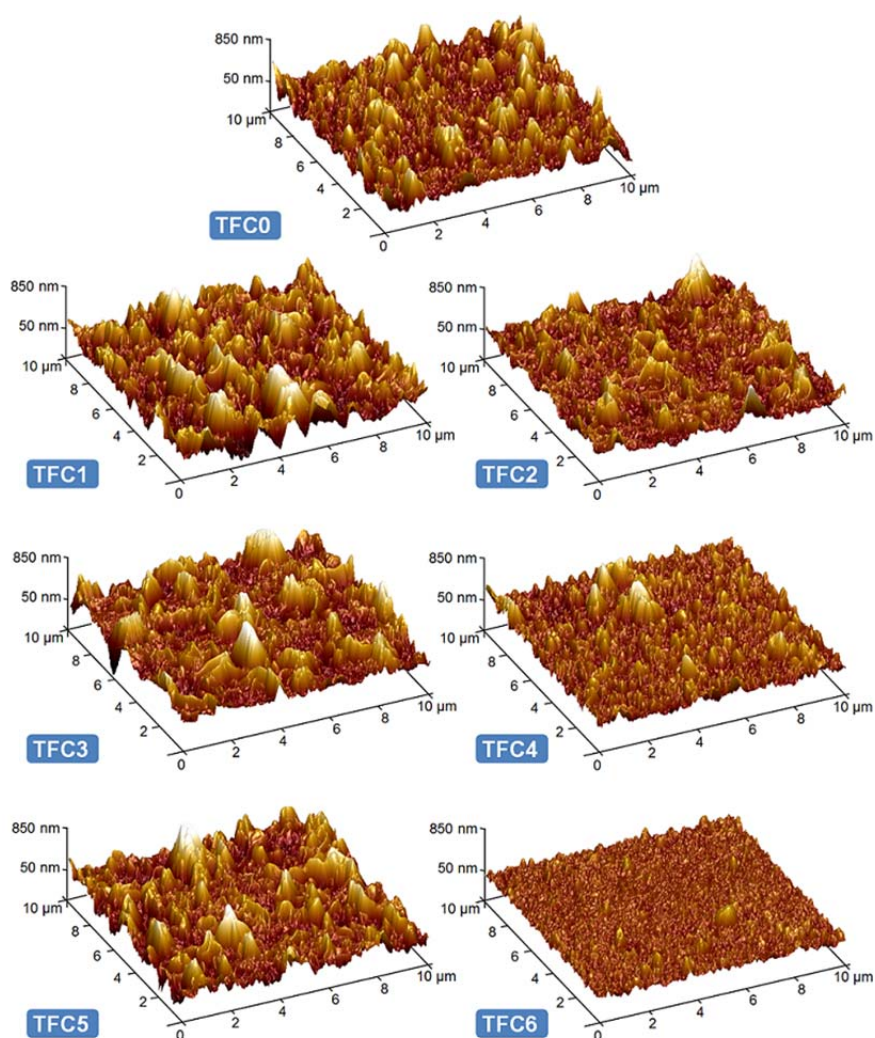


Figure 3.23: AFM 3D surface topography of the modified TFC membranes.

### 3.3.3.4 Water flux and salt rejection of TFC membranes

Figure 3.24 presents pure water flux and salt (NaCl) rejection of the TFC membranes. It can be observed that the addition of ethanol and ethylene glycol into the MPD-aqueous phase resulted in a significant enhancement in water permeation from ~14 LMH to ~30 LMH. However, the addition of xylitol up to 1.0 wt.% concentration in the aqueous solution first significantly increased the water flux to 28.5 LMH, then decreased the flux gradually at higher concentrations (up to 6.0 wt.%). It is also worth mentioning that the salt rejection of all modified TFC membranes almost remained unchanged with the addition of alcohol into amine solution.

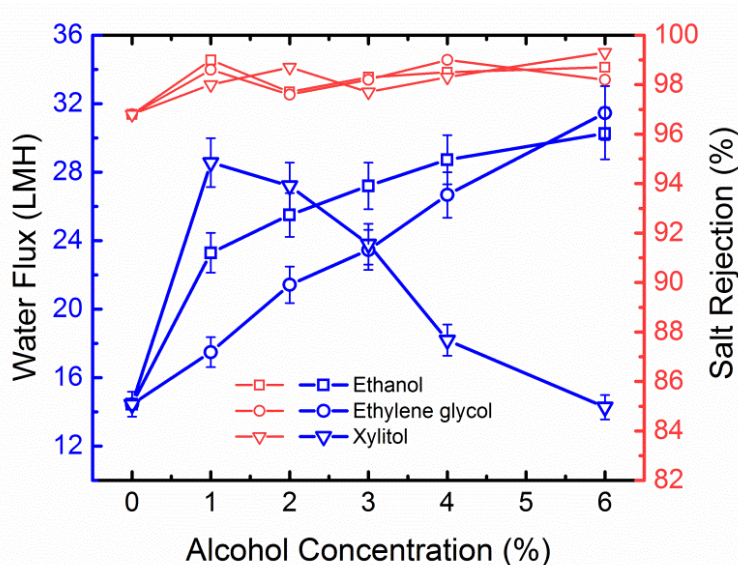


Figure 3.24: Effect of alcohol concentration in MPD solution on water permeation and salt rejection of the synthesized membranes. Experimental conditions: feed solution: distilled water for water flux test and 2000 ppm NaCl solution for salt rejection measurement, operating pressure:  $1.52 \pm 0.04$  MPa ( $220 \pm 5$  psi), temperature:  $25 \pm 1$  °C, pH: 6.5-7.

The water permeation through the PA active layer of a TFC membrane is strongly related to both structural properties (such as thickness, cross-link density, network pore size) and surface characteristics (like roughness, hydrophilicity/hydrophobicity) of the membrane. Therefore, the observed variation in water flux and the salt rejection of the synthesized membranes needs to be rationalized by considering all these influential properties. In the case of modified membranes with ethanol and ethylene glycol, the enhancement in water flux can be mainly attributed to the higher surface

wettability (Table 3.14) and lower cross-linking of the PA layers (Table 3.13) which could compensate the negative impact of an increase in the film thickness. Similarly, the low concentration of xylitol in amine solution also resulted in higher permeability and salt rejection compared to the unmodified membrane. However, at higher xylitol concentration the triple effects of a decrease in surface wettability, as well as an increase in the network cross-linking and the thickness of the PA film, resulted in a remarkable decline in the water flux. This result shows the complex influences of polyhydric alcohols with larger chain length on physicochemical and permeation properties of the resulting TFC membranes. Furthermore, since the salt rejection of the modified TFC membranes remained constant, it can be concluded that the addition of hydrophilic alcohols into the amine-water solution did not result in an undesirable enlargement of free volume within the PA network, and consequently the salt rejection of the membranes was not sacrificed by the flux enhancement. One of the most significant findings to emerge from this study is that there is no straightforward correlation between the number of hydroxyl groups in an alcohol and the permeation properties of the synthesized membranes. As a matter of fact, polyhydric alcohols are not necessarily providing higher hydrophilicity of the surface and therefore, other important properties including the molar volume (chain length), solubility parameter, miscibility in aqueous and organic solutions, as well as the tendency of alcohol to participate in nucleophilic reaction with carboxylic acids of the PA, must be accounted. All these properties affect the miscibility of the organic and the aqueous phase and the diffusion of water, MPD monomer and alcohol additive to the reaction zone, thereby changing the properties of the synthesized PA layer.

### 3.4 Conclusion

Here, the effect of synthesis conditions and chemical additives on the physicochemical and permeation properties of interfacially polymerized TFC PA membranes was systematically investigated. The concentration of reacting monomers, reaction time and curing temperature were considered as synthesis parameters. Furthermore, different chemical additives, namely SDS as a surfactant, TEA as an acid acceptor, DMSO as a co-solvent, and CSA as a pH regulator were added into MPD solution in order to control and modulate the permeation properties of the resulting TFC membranes. The experimental trials were designed using Taguchi method (L9 orthogonal arrays) in order to investigate the synergistic effects of the influential parameters.

Regarding the effect of synthesis conditions, the plot of marginal means showed that the average influence of increasing the MPD concentration was to lower water flux and to improve salt rejection, whereas increasing the TMC concentration resulted in more permeable membranes with lower rejection. Furthermore, a strong interaction was found between MPD and TMC concentrations, suggesting the importance of monomer concentration (or molar) ratio rather than on individual concentration. The ANOVA revealed that the water flux through synthesized membranes was most dramatically affected by curing temperature. The MPD and TMC concentration also had significant effect whereas changing the reaction time beyond one minute was found to have the lowest influence on water permeation.

Regarding the effect of chemical additives, it was found that the average effect of adding TEA, CSA, and DMSO to the MPD-aqueous solution was to improve water permeation of the resulting TFC membranes whereas increasing SDS concentration lowered the permeability of the TFC membranes. Based on the results, to maximize the water flux, the high level of TEA, CSA, and DMSO concentration and low level of SDS concentration was suggested. Also, to make the results less sensitive to noises and enhance the robustness, the same level setting was proposed. The ANOVA revealed that the change in the SDS and DMSO concentrations had the most significant influence on water flux of the membranes. Increasing the CSA concentration moderately improved the water permeation through the



membranes. Finally, TEA concentration was found to be the least significant parameter on water permeation.

The effect of addition of monohydric and polyhydric alcohols into MPD-aqueous solution on the final properties of the TFC membranes was studied using ethanol, ethylene glycol, and xylitol. The experimental results showed that inclusion of alcohols in the water solution improved the permeation properties as compared to the based TFC membrane. In addition, increasing the concentration of ethanol and ethylene glycol increased the water flux continuously, while, in the case of xylitol, a maximum flux was obtained at ~1.0 wt.% concentration and then the flux decreased by further addition of this alcohol. Furthermore, the addition of alcohols showed a promising effect on the membrane selectivity as all the modified membranes possessed higher salt rejection percentage than the unmodified TFC membranes. Applying hydrophilic alcohols in amine-water solution during the IP reaction was found to overcome the trade-off relationship between permeability (water recovery) and selectivity (water quality) normally observed in polymeric membranes. This study shows the significant role of the four considered influential parameters on the final properties of TFC membranes. The findings can be used as guidelines for the synthesis of NF/RO membranes possessing a broad range of water permeation and salt rejection characteristics.

## Chapter 4<sup>‡</sup>

Thermally modulated IP reaction for  
fabrication of high throughput TFC PA  
membrane for FO application

---

<sup>‡</sup> This chapter is organized based on references [42] and [44].

## 4.1 Introduction

Forward osmosis (FO) has attracted increasing interest in the past decade as an alternative to conventional pressure-driven membrane processes for various applications including seawater desalination [133], wastewater treatment [134], food processing [135] and clean energy generation [136]. The transport mechanism in a FO membrane is based on the osmotic pressure gradient between a low concentration solution, known as “feed”, and a high concentration solution which is referred to as “draw”. Applying a semi-permeable membrane between the draw and the feed solutions provides pathways for water molecules while restricting the passage of solutes from one side of the membrane to the other side.

An ideal FO membrane exhibits high water permeability, high solute rejection, low concentration polarization, low fouling propensity and high chemical and mechanical stability [137,138]. The majority of the recent advances in the FO process is devoted to membrane materials development with the aim of fabricating high performance FO membranes [139]. Commonly used commercial FO membranes are made from asymmetric cellulose triacetate (CTA) [140–142] which became popular due to its hydrophilic nature and relatively low cost [143]. However, the major drawbacks of the CTA membranes are their low permselectivity and poor stability in harsh acidic and basic environment [144]. These limitations have diverted attention from single layer cellulose based membranes toward TFC PA based membranes.

The TFC membranes are very popular in pressure-driven separation processes such as NF and RO processes, however, their application in the FO processes is at the early stage [145]. These membranes exhibit low permeation flux when tested for the FO process, as in the absence of hydraulic pressure, the dense active layer hinders the permeation flux through the membrane [135,140,146]. Additionally, the thick and dense support layer provides a large resistance against the diffusion of the draw solute to the back side of the active layer, contributing to internal concentration polarization (ICP) phenomenon, thereby adversely affecting the water permeation of the membranes [147]. The ICP generally occurs inside the pores of the porous support layer and depends mainly upon the thickness, porosity and tortuosity of the support layer rather than the hydrodynamics of the flow [147]. Ideally, the support layer should be thin, highly porous with low tortuosity [147,148]. To date, numerous efforts have been made on modification of TFC membranes in terms of the physicochemical characteristics of both the active and support layers to make them efficient for the FO process. Much of these efforts

were dedicated to improve the support layer permeability by the following strategies:

- (i) modifying the support layer morphology [142,145,149–152]
- (ii) increasing the hydrophilicity of the common support materials (i.e. PES or PSf), either by blending them with more hydrophilic materials such as sulfonated polysulfone (SPSf) [137], polyphenylsulfone (PPSU) [150], carboxylated polysulfone (CPSf) [153], Montmorillonite (MMT)-sulfonated polyethersulfone (SPES) [154] or by coating them with hydrophilic polymers like polydopamine [140] or sodium dodecyl sulfate (SDS) [155]
- (iii) using alternative hydrophilic support materials like cellulose acetate (CA) [156], cellulose acetate propionate (CAP) [157], polyacrylonitrile (PAN) [73], polyketone (PK) [158], sulfonated poly(ether ketone) (SPEK) [159], and sulfonated polyphenylenesulfone (sPPSU) [160]
- (iv) incorporating organic and inorganic nanofillers LDH and TiO<sub>2</sub> NPs into the support matrix [161,162]
- (v) using a highly porous electrospun nanofiber matrix such as polyvinylidene fluoride (PVDF), PES and PAN as support layer [163–166].

In spite of vast research on the properties of support layer, there are only a few studies focused on modifying the characteristics of the active thin layer of the TFC membranes for FO application, and these are mainly focused on incorporating nanoparticles like Zeolite, SiO<sub>2</sub> and multi-walled carbon nanotube (MWCNT) into the active layer of the TFC membrane [167–170]. However, the addition of nanoparticles in a thin film with the aim of fabricating a thin film nanocomposite (TFN) membrane is more complicated than it appears, due to (i) severe aggregation of the nanoparticles in the monomer solutions during the IP reaction, and (ii) weak compatibility of the nanoparticles with the host polymer matrix. It is well known that non-uniform dispersion of nanoparticles forms non-selective voids at the interface of the polymer and the nanoparticles, which significantly reduces the rejection percentage [53,171]. The uncertainties related to the formation of an integrally-skinned and defect-free thin film due to the presence of nanoparticles limit further development of the TFN membranes.

In the present study, a novel and efficient method is proposed to enhance the water permeation of the TFC membranes by performing the PA synthesis reaction at sub-zero temperatures of organic solution. Investigation of the effect of organic solution temperature on the properties of the resulting PA membranes has been limited to a few studies. Ghosh et al. [69] investigated the effect of variation in the

temperature of the organic solution from 8 °C to 38 °C, on the surface morphology and permeation performance of the TFC membranes. The TFC PA membranes were made by IP reaction between m-Phenylenediamine (MPD) in water and trimesoylchloride (TMC) in Isopar-G solution. It was demonstrated that the synthesis of the TFC membranes at lower temperatures decreased water permeation of the membranes by formation of thicker and denser PA films. In contrast, at higher temperatures of organic solution, thinner, rougher and more water permeable films with higher hydrophilicity were produced. Yu et al.[172] reported the same trend for their synthesized TFC membranes by the reaction of MPD-aqueous solution and 5-chloroformyloxyisophthaloyl chloride (CFIC) in Isopar-G solution at different temperatures ranging from 10 °C to 40 °C. However, the aforementioned studies did not capture the influence of the organic solution temperature, which becomes critical at sub-zero temperatures. In the present work, the variation range of organic solution temperature is broadened from -20 °C to 50 °C using three different solvents (hexane, cyclohexane and heptane). It was anticipated that the change in the temperature of the organic solution would change the transfer rate of monomers to the reaction zone and thus alter the rate of polymerization reaction, final physicochemical and permeation properties of the resulting TFC membranes. Additionally, in order to evaluate the separation performance of the synthesized TFC membranes for treatment of industrial water with different types of contaminants, FO tests were carried out using BFW of SAGD process.

## 4.2 Materials and methods

TFC PA membranes were prepared via IP reaction between MPD-aqueous solution (2 wt.% MPD, 0.2 wt.% SDS, 2 wt.% CSA and 1 wt.% TEA) and TMC-organic solution (0.2 wt.% TMC in cyclohexane, hexane, and heptane). Polyethersulfone (PES, 0.2  $\mu\text{m}$ ) was used as porous substrate. The temperature of the organic solution was changed from -20 °C to 50 °C using isothermperature water bath and freezer. The organic solution was kept in sealed glass vials to ensure no loss of solvent and change in monomer concentration at elevated temperatures. Table 4.1 presents the temperature of the organic solution used for preparation of TFC membranes.

Table 4.1: Synthesized TFC membranes, organic solution used for dissolving TMC monomer, temperature of the organic solution during the IP reaction. The IP reaction was allowed to proceed for 30 secs and after that, the membranes were thermally treated at 70 °C for 5 min.

Membrane	Organic solvent	Organic solution temperature (°C)
TFC1	Heptane	-20
TFC2	Heptane	+1
TFC3	Heptane	+25
TFC4	Heptane	+50
TFC5	Hexane	-20
TFC6	Hexane	+1
TFC7	Hexane	+25
TFC8	Hexane	+50
TFC9	Cyclohexane	-20
TFC10	Cyclohexane	+1
TFC11	Cyclohexane	+25
TFC12	Cyclohexane	+50

The surface tension and viscosity of three organic solvents namely cyclohexane, hexane and heptane at different temperatures are presented in Table 4.2 [173–176]. For all solvents, both the surface tension and viscosity decrease with increase in temperature vice versa. The observed change in these properties is believed to be the principle reason for the substantial change in the final chemical and physical characteristics of the polymerized film.

Table 4.2: Selected properties of the organic solvents used for making TFC membranes.

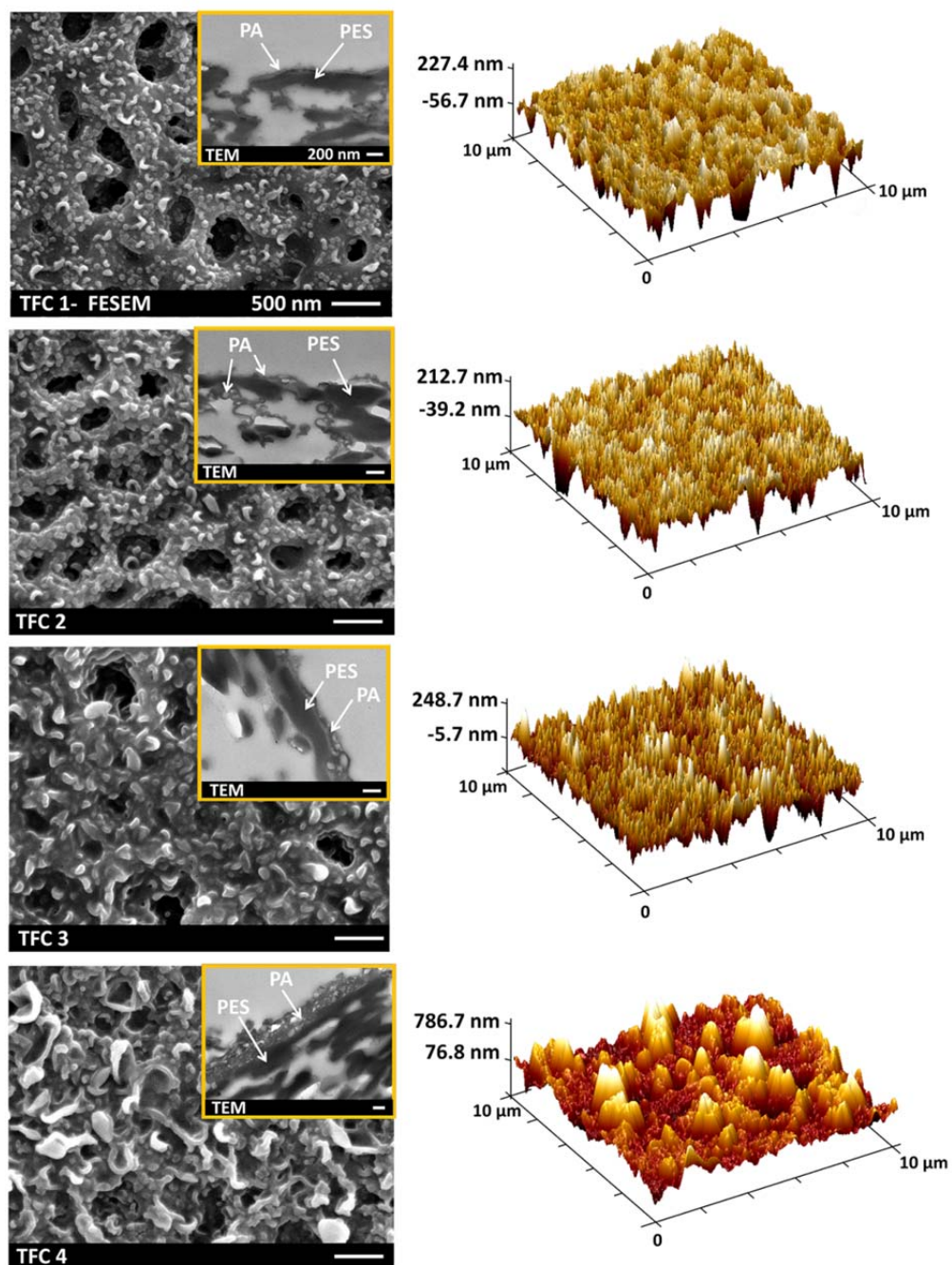
Solvent (chemical formula)	Melting Point[173] (°C)	Boiling Point[173] (°C)	Surface Tension (mN.m <sup>-1</sup> ) [173,174]					Viscosity (mPa.s) [173,176]				
			-20 °C	-10 °C	1 °C	25 °C	50 °C	-20 °C	-10 °C	1 °C	25 °C	50 °C
Cyclohexane (C <sub>6</sub> H <sub>12</sub> )	6.7	80.7	NA	NA	NA	24.16	21.26	NA	NA	NA	0.894	0.615
Hexane (C <sub>6</sub> H <sub>14</sub> )	-95.3	68.7	22.48	21.46	20.34	17.89	15.33	0.48	0.42	0.38	0.3	0.24
Heptane (C <sub>7</sub> H <sub>16</sub> )	-90.55	98.38	24.06	23.08	22	19.66	17.19	0.69	0.6	0.52	0.39	0.3

## 4.3 Results and discussion

### 4.3.1 Membrane morphology

Figure 4.1 illustrates the FESEM, TEM and AFM images of TFC1 to TFC4 membranes which were prepared in heptane at different temperatures. These images provide useful information about the surface structure, thickness and roughness of the PA films, respectively. Based on the FESEM images, the surface morphology of the PA skin layer is noticeably different for the synthesized membranes. The surface of the TFC3 membrane, which was prepared at room temperature 25 °C, has several wrinkled features which are well-known as ridge-and-valley structures [177]. By increasing the organic solution temperature to 50 °C (see TFC4), the wrinkled protuberances enlarged and resulted in a thicker PA layer as it is more evident in the TEM cross-section image. In contrast, for the membranes synthesized at lower temperatures (see TFC1 and TFC2 which were prepared at -20 °C and 1 °C, respectively), the size of the ridges and valleys decreased remarkably and a thinner PA film was produced at the surface. The 3D AFM image of TFC4 membrane also confirmed the formation of rougher PA films at high temperature of organic solution compared to the other membranes. It is worth mentioning that the apparent holes in the FESEM image of TFC1 and TFC2 correspond to PES substrate, not the PA skin layer. These holes are visible in TFC1 and TFC2 due to formation of an ultrathin layer of the PA on the support surface, whereas they are completely covered by a thicker PA film in TFC3 and TFC4 membranes. Taking a closer look at the TEM images of TFC1 and TFC2 in Figure 4.1, it is found that the support holes are internally closed by the PA layer otherwise the membrane selectivity would fall down drastically.

Figure 4.2 and Figure 4.3 illustrate the FESEM images of the membranes prepared using hexane and cyclohexane as organic solvent, respectively. The similar surface morphologies at the surface of these membranes also reveal the significant influence of the solution temperature on the structure of the resulting PA films.





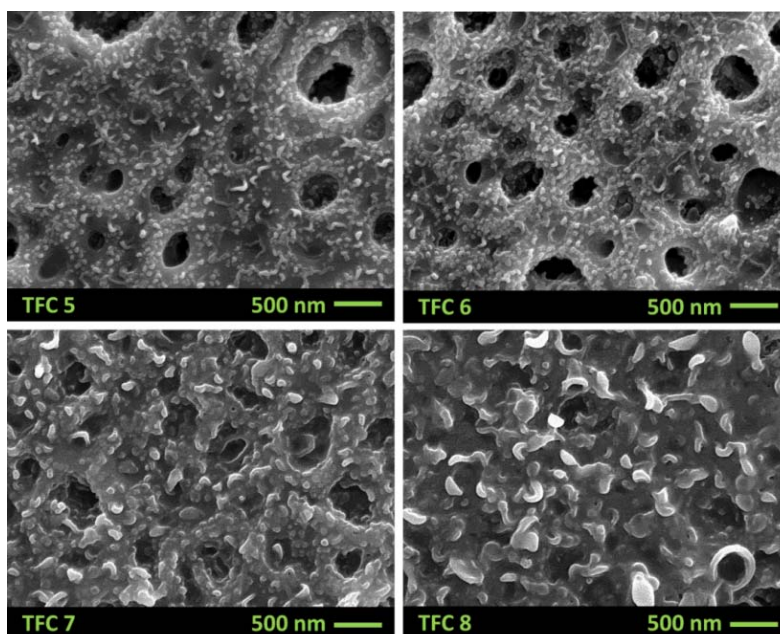


Figure 4.2: FESEM images of TFC membranes prepared in 0.2%-hexane solution. The temperature of the hexane solution for TFC5 to TFC8 was changed as -20 °C, 1 °C, 25 °C and 50 °C, respectively. All other synthesis conditions were the same as TFC1 to TFC4.

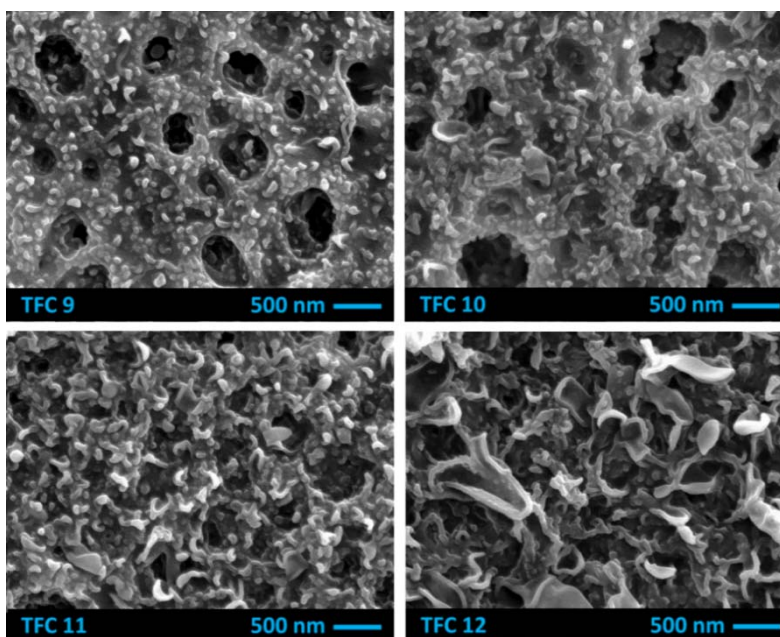


Figure 4.3: FESEM images of TFC membranes prepared in 0.2%-cyclohexane solution. The temperature of the cyclohexane solution for TFC9 to TFC12 was changed as 8 °C, 25 °C, 35 °C and 50 °C respectively. All other synthesis conditions were the same as TFC1 to TFC4. Since the melting temperature of the cyclohexane is about 6.7 °C, synthesis of PA membranes at sub-zero temperature was not possible with this solvent.

### 4.3.2 Chemical composition and elemental analysis

Figure 4.4 presents the result of ATR-FTIR and XPS analysis of the membranes which provide information about compositional elements and functional groups of the polyamide skin layer. The ATR-FTIR spectra of the TFC1 to TFC4 membranes (Figure 4.4a) confirm the successful formation of a PA skin layer at the surface of the PES support by the IP reaction. According to this figure, the FTIR spectrum of the base PES substrate had three peaks at 1410, 1485, and 1580  $\text{cm}^{-1}$  due to the aromatic ring (benzene) vibration [178,179]. However, for the composite membranes, three new peaks at 1541, 1611, and 1667  $\text{cm}^{-1}$  were identified which are attributed to the PA skin layer over the PES support. These peaks are related to C=O stretching of the amide I bond, aromatic amide ring breathing and N-H bending of amide II in the -CO-NH- group, respectively [83,84,180,181].

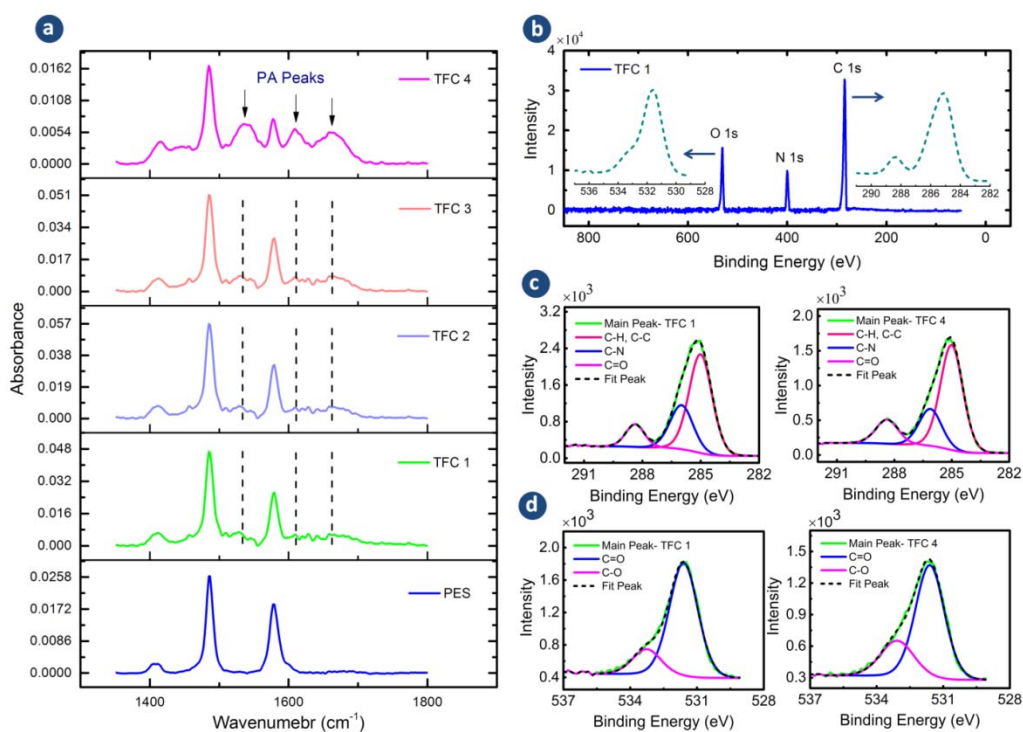


Figure 4.4: (a) FTIR spectra (PES support and TFC1 to TFC4), (b) XPS survey spectrum (TFC 1) along with high resolution C (1s) and O (1s) spectra, (c) convoluted high resolution C (1s) and (d) convoluted high resolution O (1s) spectra (TFC 1 & TFC4). FTIR shows additional peaks associated with the PA to the PES support. The survey spectrum indicates the presence of O, N and C elements and the absence of S on the surface of the membranes indicating all membranes are integrally skinned. The convoluted high resolution C (1s) and O (1s) peaks provide information about the PA chemical bonds that helps to quantify C=O/C-N ratio.

The XPS survey spectra of TFC1, which has the thinnest PA skin layer (Figure 4.4b), shows the presence of only three elements, namely oxygen (O 1s), nitrogen (N 1s) and carbon (C 1s) at the membrane surface. The absence of a sulfur peak, which is the principle peak of the PES support, implies the formation of an integrally skinned PA layer at the support surface for all TFC membranes. The XPS survey spectra of the other TFC membranes were similar to TFC1 and thus were not shown here. The high resolution spectra of the C (1s) and O (1s) of TFC2 and TFC3 membranes are presented in Figure 4.5.

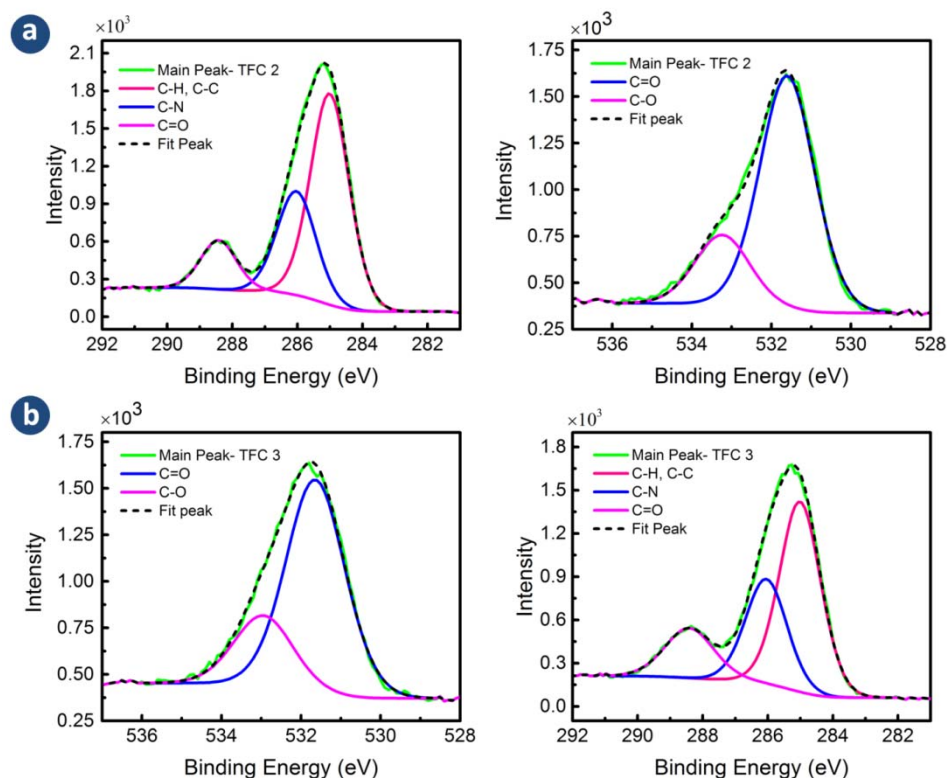


Figure 4.5: (a) Convolved high resolution C (1s) and O (1s) spectra of TFC2, (b) convolved high resolution C (1s) and O (1s) of TFC3 membrane.

Table 4.3 summarizes the XPS analysis of the synthesized TFC1 to TFC4 membranes. The results of the elemental compositions show that by decreasing the temperature of the organic solution, the experimental O/N ratio nears the theoretical values for fully cross-linked PA films which is comparable with that of commercial XLE, LE, ESPA3 and SWC4 Hydranautics membranes [84]. In contrast, by elevating the organic solution temperature to 50 °C, the O/N ratio of the synthesized TFC membranes increased to 1.42, implying formation of more linear structures in the polyamide network similar to commercial NF90 and FT-30

Filmtec membranes [76,182]. The information of chemical bonding was obtained by deconvolution of C (1s) and O (1s) high resolution XPS spectra as shown in Figure 4.4c. The C (1s) high resolution spectra for all TFC membranes showed three peaks: a major peak at 285 eV which is assignable to a carbon atom without adjacent electron withdrawing atoms (carbons in aliphatic/aromatic C–C and C–H), an intermediate peak at 286.5 eV that is associated with carbon in weak electron withdrawing atoms (carbons in C–N) and a minor peak at 288.5 eV which corresponds to carbons attached to strong electron withdrawing atoms (carbons in carboxylic O=C–O and amides O=C–N) [130] The C=O/C–N ratio can also be used for comparing the degree of cross-linking of the synthesized membranes. Theoretically, for every aromatic carbon attached with a single bond to nitrogen there is one carbon in amide group which makes the O=C–N/C–N ratio equal to 1.0. Therefore, for a highly cross-linked PA film, the C=O/C–N and O=C–O/O=C–N must approach 1.0 and 0.0, respectively, due to the lower number of carboxylic groups in the polymer structure. Based on Table 4.3, it can be concluded that the membranes prepared at lower temperatures of the organic solution had a higher degree of cross-linking. High resolution O (1s) spectra have two peaks (Figure 4.4d), which illustrate the presence of two types of oxygen in the PA layer: O=C at 531.6 eV and O–C at 533.0 eV [183,184]. The ratio of O=C/O–C for TFC1-4 membranes was calculated to be 4.53, 3.35, 3.04, and 2.78, respectively. This again confirms that synthesis of TFC membrane at low temperatures results in more cross-linking in the polyamide network, while elevating the reaction temperature decreases the cross-linking density of the PA layer.

Table 4.3: Elemental compositions, O/N ratio, chemical bonding peak area and degree of cross-linking of the TFC1 to TFC4 membranes.

Sample	Atomic Concentration (%)			Chemical Bonding Peak Area			$\frac{C=O}{C-N}$	O/N ratio	Cross-link Density (%)
	O	N	C	C–C, C–H	C–N Peak at 286.5 eV	O=C–O, O=C–N Peak at 288.5 eV			
	(1s)	(1s)	(1s)	Peak at 285 eV					
TFC 1	12.92	12.61	74.47	44.99	22.64	32.37	1.42	1.02	97
TFC 2	14.93	12.94	72.13	42.62	22.51	34.87	1.54	1.15	79
TFC 3	17.40	12.98	69.61	41.72	20.75	37.53	1.80	1.34	56
TFC 4	17.09	11.61	71.30	40.06	20.22	39.72	1.96	1.47	42

### 4.3.3 Surface roughness and wettability of TFC membranes

Table 4.4 presents the contact angle and surface roughness of TFC1 to TFC4 membranes. Contact angle measurement is commonly carried out for evaluating the wettability of the membrane surface. A lower value of the contact angle is often interpreted as enhancement of water permeation through the membrane [185]. For a non-smooth polymeric film like a TFC polyamide membrane, the contact angle measurement can be influenced by both surface chemical composition (hydrophilic/hydrophobic functional groups) and morphology (roughness) [186]. Compared to TFC3 which had the contact angle of 81.2°, the other membranes had a substantially lower contact angle, suggesting that the variation of temperature of the organic solution (either decrease or increase from the 25 °C) resulted in a TFC membrane with higher wettability. The average roughness ( $R_a$ ) and the root mean square ( $R_q$ ) roughness data in Table 4.4 show that the TFC1, TFC2 and TFC3 membranes had comparable surface roughness. However, the roughness of TFC4 membrane (prepared at 50 °C) was notably higher (almost three times) than the other membranes, implying that synthesis of TFC membrane at higher temperature of organic solution will increase the surface roughness of the resulting PA film.

Table 4.4: Contact angle and surface roughness of synthesized TFC membranes.

Sample	Contact Angle (°)	Surface Roughness (nm)	
		$R_a$	$R_q$
TFC1	53.3 ±1.2	49.5 ±2.1	65.1 ±2.2
TFC2	56.9 ±1.1	54.2 ±2.3	71.0 ±3.8
TFC3	81.2 ±1.6	53.0 ±1.6	66.3 ±2.4
TFC4	66.2 ±1.0	130.7 ±15.2	168.8 ±12.1
TFC-HTI	46.3±1.8	56.7±2.3	24.0±1.3

### 4.3.4 RO permeation performance of the membranes

Figure 4.6 presents the RO performance of TFC membranes prepared at different temperatures of TMC-heptane solution. The TFC3 membrane, prepared at 25 °C, had the lowest water flux among the other TFC membranes with 10.7 LMH and 98.8% salt rejection. When a TMC-heptane solution at -20 °C used, the water permeation of the resulting TFC membrane improved significantly to 92.1 LMH with just 4 % sacrifice in rejection percentage. Moderate enhancement in water flux and salt rejection up to 27.9 LMH and 99.1%, respectively, was also observed by increasing the organic solvent temperature from 25 °C to 50 °C.

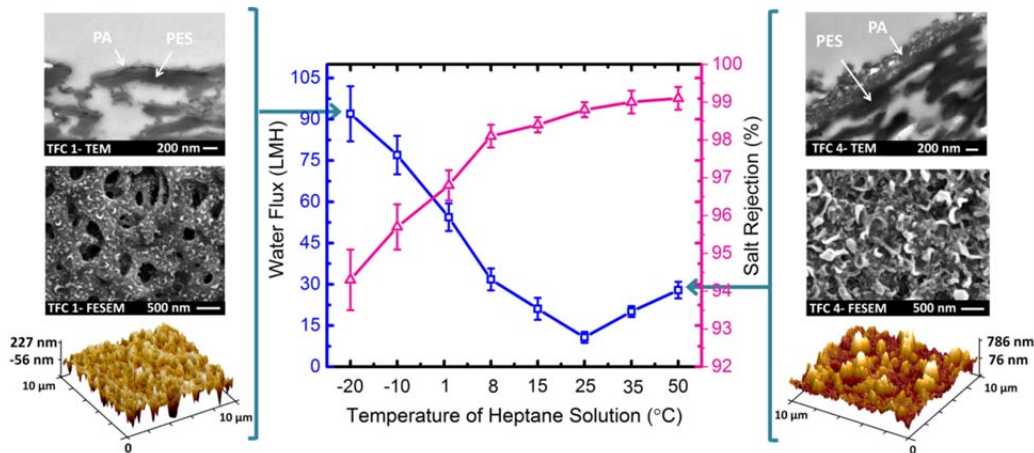


Figure 4.6: Water flux and salt rejection of the TFC membranes prepared at different temperature in 0.2 wt.% TMC-heptane solution. The surface and cross-sectional images of the membranes synthesized at -20 °C and 50 °C are presented to justify the permeation properties. Test conditions: feed solutions: pure water and 2000 ppm NaCl solution, pressure: 1.52 MPa (220 psi), temperature: 25 °C, pH: 6.5-7.

The water flux and salt rejection of the TFC membranes prepared with hexane and cyclohexane solution were shown in Figure 4.7. As can be observed, the TFC membranes prepared at different temperatures of hexane and cyclohexane solution, presented a similar trend of variation of water flux and salt rejection to the membranes prepared in heptane. This observation implies the significant influence of the temperature of organic solution on the transport properties of the resulting TFC membranes.

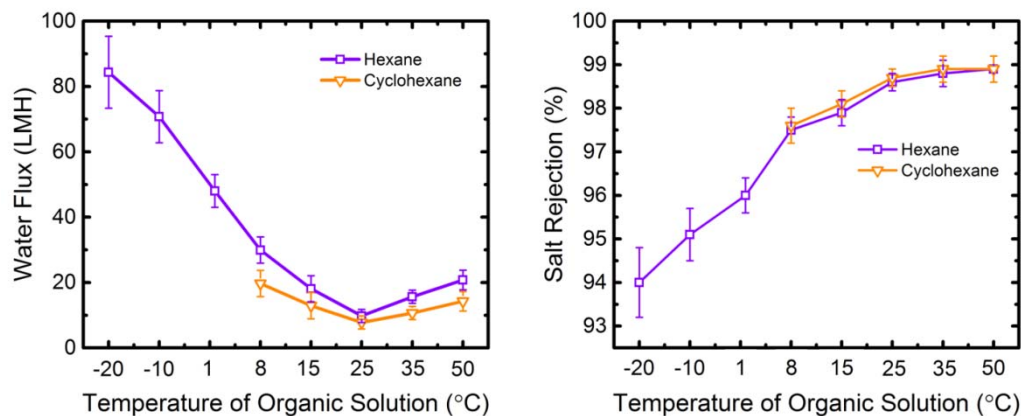


Figure 4.7: Water flux and salt rejection of the TFC membranes prepared at different temperature in hexane and cyclohexane solutions. Test conditions: feed solutions: pure water and 2000 ppm NaCl solution, pressure: 1.52 MPa (220 psi), temperature: 25 °C, pH: 6.5-7.

Table 4.5 compares the permeation properties of the two most permeable TFC membranes, prepared at -10 °C and -20 °C in heptane, with three commercially available RO membranes namely Filmtec BW30, TriSep RO, and Hydranautics ESPA membranes. The experimental results show that the lab-made TFC membranes prepared at sub-zero temperatures provided higher water flux than commercial RO membranes with comparable salt rejection percentage.

Table 4.5: Permeation properties of the commercial RO membranes compared with the lab-made TFC membranes. Test conditions: feed solutions: pure water and 2000 ppm NaCl solution, pressure: 1.52 MPa (220 psi), temperature: 25 °C.

Membrane	Water flux (LMH)	Salt rejection (%)	$A_p$ (LMH/bar)	$B$ (LMH)
Filmtec BW30	69.7	94.3	4.26	3.54
Hydranautics ESPA	59	95.1	3.7	2.4
TriSep RO	41.1	93.2	2.4	2.1
Lab-made TFC prepared at -10 °C	77	95.7	4.8	2.8
Lab-made TFC prepared at -20 °C	92	94.3	5.78	4.96

The significant change in the surface characteristics of the TFC membranes due to the variation of organic solution temperature can be attributed to the changes in the solubility and diffusivity of the MPD molecules into the reaction zone. At higher temperatures of the TMC-organic solution, the surface tension and the viscosity of the organic solvent decrease which allows the MPD molecules to have more solubility and diffusivity into the organic phase. Additionally, more swelling of the initially formed PA layer at high temperature will facilitate migration of the MPD molecules from the aqueous solution to organic phase. The more available MPD molecules in the reaction zone increases the amine to acyl chloride molar ratio ( $\text{NH}_2/\text{COCl}$ ) and thus speed up the rate of polymerization and produce thicker PA film at the surface. Furthermore, higher thermal energy, imparted by surrounding organic solvent to MPD molecules, increases their local movement to reach TMC-rich spots in the reaction zone which results in formation of larger ridges and valleys and thus rougher PA film as it is observable in the case of TFC 4 which was prepared at 50 °C. However, the miscibility of water and organic solvent increases with increase in temperature [96,187–189]. Since the TMC molecules can be readily hydrolyzed by water, the diffusion of water molecules into the reaction zone is considered as an important competitive reaction which alters the cross-linking density of polyamide film by reducing the number of reacting

carboxyl groups of TMC [124]. Therefore, the resulting PA layer has less extent of cross-linking as confirmed for TFC4 by C=O/C-N and O/N ratio in Table 4.3. In contrast, at very low temperatures of organic solution, the MPD solubility and diffusivity into the reaction zone decreases due to the higher surface tension and viscosity of the solvent. Furthermore, the low temperature of organic solution quenches the incipient PA layer and hinders further diffusion of MPD molecules from aqueous solution to organic phase. Therefore, the transport rate of MPD molecules to the organic side of the interface and thus the ratio of available amine/acyl chloride in the reaction zone decreases. As a result, a thinner PA skin layer with smaller ridges and valleys, more cross-linking density and higher water permeation forms over the PES surface. It is worth noting that the changes in amine/acyl chloride ratio in the reaction zone due to different organic solution temperature is very similar to the changes imparted by the different initial monomer concentration in water and organic solutions, reported earlier by the authors [39]. Figures 4.8a and 4.8b illustrate the surface morphology of the TFCI and TFCII membranes which were prepared in hexane at room temperature (25 °C) but with different MPD and TMC concentrations (thus different amine/acyl chloride ratio). For comparison, the surface images of the TFC3 and TFC1 membranes which were prepared at different organic solution temperature but with identical monomer concentration are presented in Figures 4.8c and 4.8d. Based on Figure 4.8a, at higher amine/acyl chloride ratio (TFC I,  $\text{NH}_2/\text{COCl}=21.1$ ), the PA surface has the wrinkled ridges and valleys, similar to the surface structure of TFC3 (Figure 8d, membrane prepared at 25 °C with  $\text{NH}_2/\text{COCl}=15.8$ ). However, when the amine/acyl chloride ratio decreased in TFCII (Figure 4.8b, membrane prepared at 25 °C with  $\text{NH}_2/\text{COCl}=9.0$ ), the structure noticeably changed to a fine morphology with small micro-protuberances which is quite similar to the surface morphology of TFC1 synthesized at -20 °C (Figure 4.8d,  $\text{NH}_2/\text{COCl}=15.8$ ).



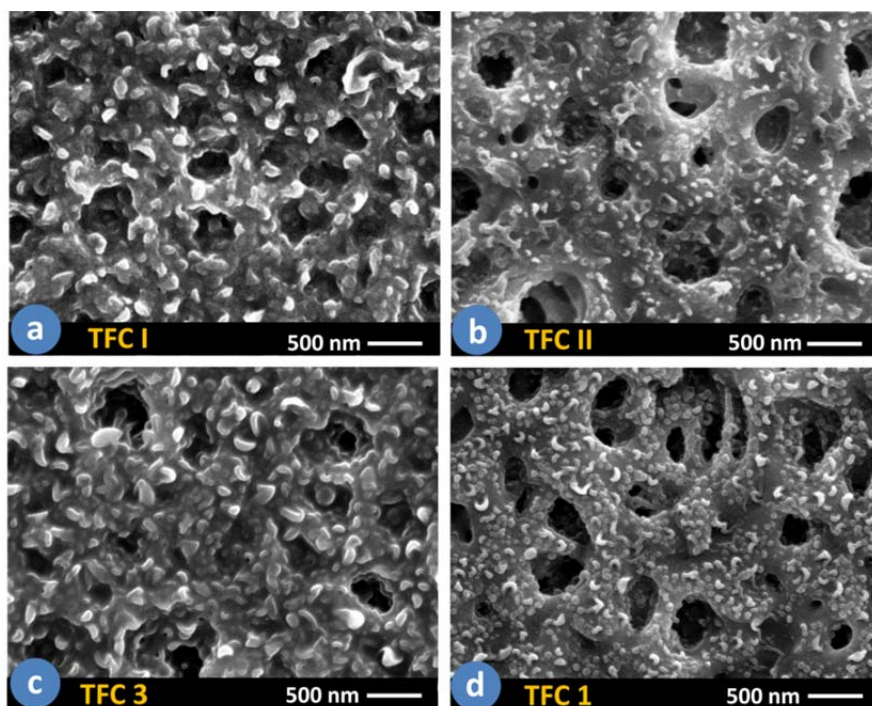


Figure 4.8: FESEM images of (a) TFC I membrane prepared with 2 wt. % MPD and 0.15 wt. % TMC,  $\text{NH}_2/\text{COCl}=21.1$ , in hexane at 25 °C; (b) TFC II membrane prepared with 2 wt. % MPD and 0.35 wt. % TMC,  $\text{NH}_2/\text{COCl}=9.0$ , in hexane at 25 °C; (c) TFC 3 membrane prepared with 2 wt. % MPD and 0.2 wt. % TMC,  $\text{NH}_2/\text{COCl}=15.8$ , in heptane at 25 °C; and (d) TFC 1 membrane prepared with 2 wt. % MPD and 0.2 wt. % TMC,  $\text{NH}_2/\text{COCl}=15.8$ , in heptane at -20 °C.

The above described changes in physico-chemical properties of PA active layer manifest their effects through altering the permeation performance of the synthesized TFC membranes. In general, water permeability of a TFC membrane is strongly related to both structural (thickness, density, pore size) and surface physico-chemical (roughness, hydrophilicity/hydrophobicity) properties of the membrane [12]. As the water flux results of the synthesized TFC membranes at different temperatures followed a curve with a minimum at room temperature, it can be concluded that there exist competing factors suggesting that the final water permeation of the membrane needs be rationalized by considering the important influential parameters. Regarding the TFC membranes prepared at sub-zero temperatures of organic solutions, the significant enhancement in water flux can be attributed to the marked decreases in the thickness of PA active layer, although these membranes showed higher degree of cross-linking. The consistent decrease in water flux with increases in organic solution temperature up to 25 °C, due to formation of thicker PA layer is an evidence for dominant impact of the PA thickness on water flux. The moderate increase in water flux for the TFC

membranes prepared above room temperatures, may be ascribed to the presence of larger ridges and valley at the surface which may contribute to the enhancement of water permeation by providing more effective contact area between water molecules and membrane surface [90]. These observations clearly demonstrate the significant effect of the organic solution temperature on the physico-chemical characteristics of the synthesized TFC membranes. The results can be easily employed (i) to fabricate cost-efficient TFC membrane by eliminating the requirement for high concentration of monomers, (ii) to facilitate robust fabrication of high-flux membranes by replacing two influential factors (concentrations of both monomers) with one factor (temperature of organic solution) in the membrane synthesis process. The latter reduces the uncertainties associated with fabrication of the TFC membranes and consequently increases the repeatability (which commercially equates to quality) of membrane properties.

### 4.3.5 FO separation performance

The FO performance of the lab-made TFC membranes was evaluated by FO filtration setup over a range of osmotic pressure difference and the results are presented in Figure 4.9. For comparison, a commercially available TFC-FO membrane (called TFC-HTI here) was also test under the same operating condition.

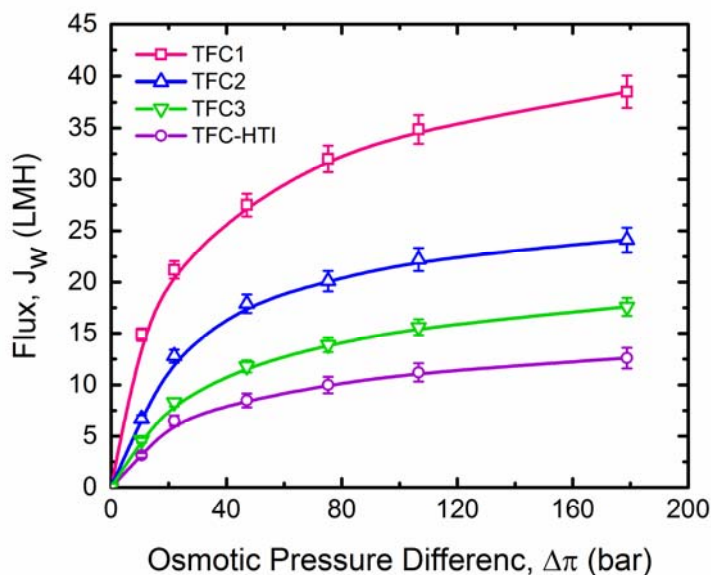


Figure 4.9: FO performance of lab-made and commercial TFC membranes at different osmotic pressure difference between draw and feed solutions. Test conditions: draw solution: 0.25, 0.5, 1, 1.5, 2, 3 M NaCl solutions; Feed: DI water; velocity: 0.22 m/s for feed and draw solutions [44].

The osmotic pressure was calculated by the following polynomial equation as a function of NaCl concentration (mol Lit<sup>-1</sup>) [190]:

$$\pi = 6.2971 C^2 + 40.714 C \quad (4.1)$$

The calculated osmotic pressure by this equation increases non-linearly with increase in NaCl concentration, especially at higher concentrations. Based on the results in Figure 4.9, the water permeability of all TFC membranes increased with increases in the osmotic pressure difference between the draw and the feed solutions. However, the rate of flux enhancement was initially high at lower values of osmotic driving forces and then declined at higher osmotic pressure difference, mainly due to the more significant dilutive ICP phenomenon within the porous support layer. Comparing the performance of the membranes reveals that all the lab-made membranes showed higher water permeation than the commercial membrane. The TFC1 membrane which was prepared at the lowest organic solution temperature (-20 °C), outperformed the other membranes with a high permeation rate of 38.5 LMH at osmotic pressure of 179 bar. The TFC2 (prepared at +1 °C) and TFC3 (prepared at +25 °C) showed water permeation of 17.6 LMH and 24.1 LMH, respectively, implying that the water permeability of the membrane significantly improved by decreasing the temperature of the organic solution during the interfacial polymerization reaction. The high permeation rate of the TFC1 membrane is primarily attributed to the formation of a thinner PA selective layer at the surface of the PES support, as illustrated in FESEM and TEM images, which provided lower mass transfer resistance toward water passage through the membrane.

The reverse solute flux and the specific salt flux through the lab-made and commercial TFC membranes are shown in Figure 4.10. The reverse solute flux takes place due to the imperfection of the active layer of the TFC membrane. An ideal selective membrane would allow no draw solute to pass through and reach the feed side. The specific solute flux is a caliber indicating how much salt passes through the membrane per unit volume of permeated water. In general, a lower value of both reverse salt flux and specific solute flux is desirable for development of high performance membranes [191]. With respect to Figure 4.10, the reverse salt flux of the synthesized membranes decreased from TFC1 to TFC3. This can be attributed to the formation of a thinner active layer with lower selectivity by using organic solution at lower temperatures. Comparing with TFC-HTI membrane, the TFC2 membrane showed superior performance with two times higher water permeation and 50% less reverse salt flux.

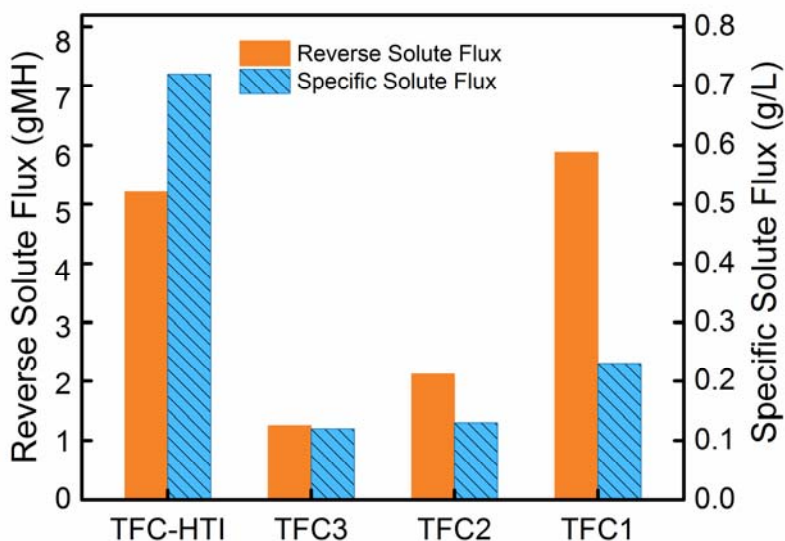


Figure 4.10: Reverse solute flux and specific solute flux of lab-made and commercial TFC membranes. Test conditions: Draw solution: 1 M NaCl solutions; Feed solution: DI water; velocity: 0.22 m/s for feed and draw solutions.

Although TFC1 had slightly higher reverse salt flux, its specific salt flux was significantly lower than the TFC-HTI membranes. The specific solute flux of the other two lab-made membranes was also remarkably lower than TFC-HTI. The specific solute flux results clearly indicate that all lab-synthesized membranes perform more efficiently than the commercial membrane in a FO process.

Tables 4.6 provides a comparison between the intrinsic permeation properties of lab-made TFC membranes and the literature PA TFC flat sheet membranes under both RO and FO conditions. According to this table, the TFC3 membrane exhibited the highest pure water permeability coefficient ( $A$ ) among all the other membranes. The water permeability of this membrane is two folds higher than that of the commercial TFC-HTI (5.78 LMH/bar compared to 2.48 LMH/bar) with comparable salt rejection percentage (93.4% for TFC1 and 95% for TFC-HTI). This result again confirms the significant effect of organic solution temperature for controlling the thickness of the PA active layer and thereby enhancing the water permeability. Although TFC1 and TFC2 membranes showed lower water permeability coefficient than the TFC-HTI membrane under RO test conditions, they provided more water flux in FO experiment (Figure 4.9) which can be presumably attributed to their significantly lower structural parameter than the TFC-HTI membrane ( $451 \pm 13 \mu\text{m}$  for lab-made TFC membranes compared to 1770 for TFC-HTI membrane).

Table 4.6: Permeation performance of TFC PA flat-sheet membranes in AL-FS orientation.

Membrane, Material	Modified Layer	FO Performance			RO Performance			S( $\mu\text{m}$ )	Reference
		Feed Solution	Draw Solution	Water Flux (LMH)	A (LMH/bar)	B (LMH)	R (%)		
TFC1, PA/PES	Active	DI Water	1 M NaCl	11.0	0.66	0.35	97.8	460	Present Work
TFC2, PA/PES	Active	DI Water	1 M NaCl	17.0	1.80	1.00	97.5	458	Present Work
TFC3, PA/PES	Active	DI Water	1 M NaCl	26.5	5.78	4.96	93.4	436	Present Work
TFC-HTI, PA/PSf	-	DI Water	1 M NaCl	7.5	2.48	0.82	95.0	1770	Present Work
PA/PSf	Support	DI Water	1 M NaCl	15.8	1.16	0.47	97.4	492	[142]
PA/PSf	Support	DI Water	1 M NaCl	25.0	1.90	0.33	98.6	312	[149]
PA/PES- co-sPPSU	Support	DI Water	1 M NaCl	20.0	0.73	0.25	91.0	324	[150]
PA/PES	Support	DI Water	1 M NaCl	47.0	1.70	NA	97.0	80	[163]
PA/PES- SPSF	Support	DI Water	1 M NaCl	32.0	0.77	0.11	93.5	238	[137]
PA/CAP	Support	DI Water	1 M NaCl	10.0	1.82	0.19	89.2	789	[157]
PA/PSf- SPEK	Support	DI Water	1 M NaCl	23.0	0.75	0.07	89.5	107	[159]
PA/PVDF	Support	DI Water	1 M NaCl	28.0	3.15	2.33	84.4	325	[166]
PA/PK	Support	DI Water	1 M NaCl	27.0	2.50	0.18	NA	280	[158]
Zeolite NaY- PA/PSf	Active	DI Water	1 M NaCl	11.0	2.57	1.57	77.6	782	[168]
PA/PVDF	Support	DI Water	1 M NaCl	22	1.28	0.28	NA	193	[192]
PA/PSf- LDHs	Support	DI Water	1 M NaCl	18.1	0.61	0.27	NA	148	[162]

From the FESEM images of the TFC-HTI membrane (Figure 4.11), it is noticed that a polyester woven fabric is used to provide extra mechanical support to the membrane. The use of this woven fabric might be the main reason for the high structural parameter of the TFC-HTI membrane by adding extra resistance against solute transport inside the porous support. Furthermore, the asymmetric structure of the PSf support with a dense skin layer in the TFC-HTI membrane could enhance the ICP phenomenon and thus decrease the flux. In general, an ideal support layer for FO separation process needs to be very thin and hydrophilic, with high porosity and low tortuosity in order to facilitate draw solution passage toward the membrane active layer [142]. A lower value of the structural parameter is highly desirable for a membrane to counter the negative impact of ICP during the FO process.

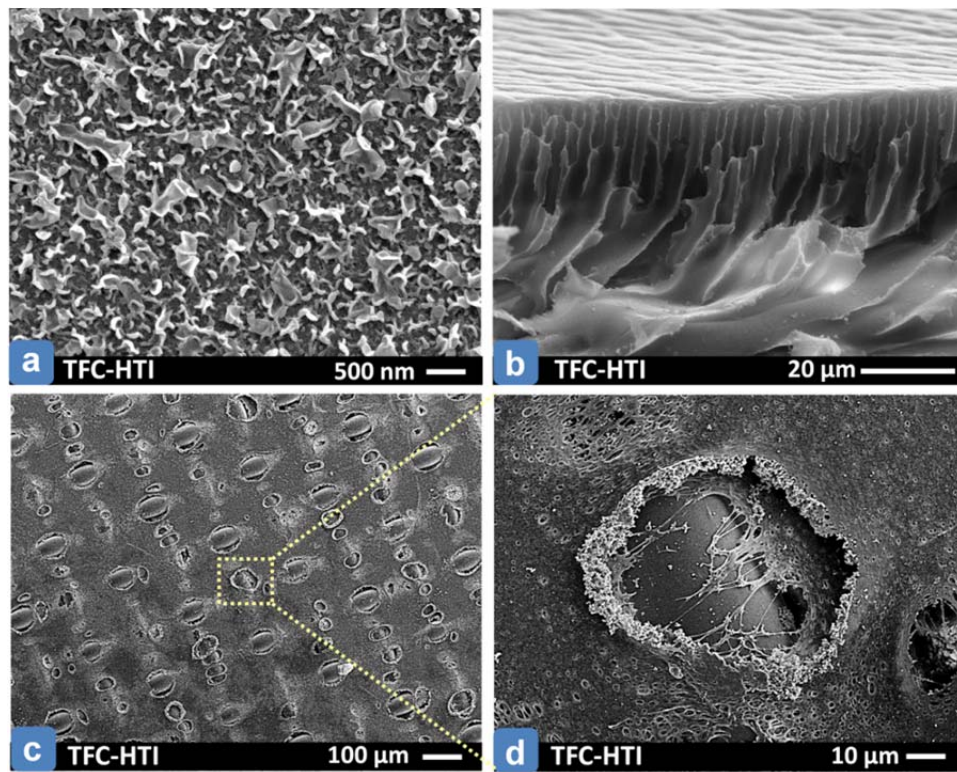


Figure 4.11: FESEM top surface images of (a) active-side; (b) cross-sectional image; (c) support-side of the TFC-HTI; (d) high magnification image of the woven fabric inside the support layer.

As previously discussed, the flux through a TFC membrane in a pressure-driven process is mainly governed by a compromise between the hydrophilicity and the thickness of the PA skin layer, whereas in FO process, another influential factor, i.e. the structural parameter, is also brought to action. With a low structural parameter along with an ultra-thin selective layer, the TFC3 membrane provided the highest water permeability, whereas the water flux through TFC1 and TFC2 was compromised by the increased thickness of the active layer. It must be noted that the reduction of the active layer thickness in the TFC3 is accompanied by a slight reduction in the rejection percentage of the membrane (93.4% for TFC3 compared to 97.5% in TFC2). Furthermore, the larger B value of the TFC3 compared to the other lab-made membranes can be presumably attributed to the formation of ultra-thin PA layer. In spite of the fact that, employing support layer with large pores can be beneficial to yield a lower structural parameter, it can make the top layer more prone to fail when working under high applied pressure of RO process due to the lack of sufficient supporting area [165]. It has been reported that the pore size distribution of the support layer has a significant influence on the physicochemical properties (e.g. degree of cross-linking, surface morphology, mechanical stability and permselectivity) of the PA active layer [193–195]. Considering a series of hydrophilic microporous supports with average pore sizes of 0.025, 0.1, 0.2 and 0.45  $\mu\text{m}$ , Huang and McCutcheon found that water permeability increases gradually with increase in the support pore size up to 0.2  $\mu\text{m}$  while the salt rejection slightly decreases following the permselectivity trade-off relationship [193]. Regarding that, at higher pore sizes (>100 nm), proper adjustment of the synthesis parameters in interfacial polymerization reaction, particularly the monomers concentration ratio and drying process, becomes important for making a defect-free PA selective layer [73]. However, unlike the RO operation, the FO process does not require a large hydraulic pressure that allows more flexibility in the synthesis and modification of both active and support layers in terms of mechanical stability.

#### **4.3.6 FO separation performance with BFW**

The performance of the lab-made and commercial TFC membranes is also evaluated for filtration of a real wastewater (SAGD BFW) and the reduction of water flux and the draw solution concentration is plotted over time, as shown in Figure 4.12. Similar to the trend observed in Figure 4.9, the lab-made TFC membranes displayed higher water flux than the commercial membrane under

identical test conditions. The initial flux for TFC1 (18.1 LMH) and TFC2 (12.6 LMH) was about three and two times higher than the TFC-HTI (6.4 LMH) membrane, respectively. The water permeation of the TFC1 membrane declined rapidly from 18.1 LMH to 12.8 LMH after 6 hours operation. There are two likely causes for such a sharp water flux decline: First, fouling of membrane by deposition of the BFW contaminants, such as organic matters, dissolved and suspended solids on the surface induces extra resistance against water transport through the membranes. Second, the high permeation rate of TFC1 membrane quickly dilutes the draw solution and at the same time concentrates the feed solution which results in a significant reduction in osmotic pressure difference. Based on Figure 4.12, the draw solution concentration of TFC1 membrane decreased about 30% and diluted from 0.46 M to 0.3M during the test. In contrast, for TFC3 and TFC-HTI membranes, where the permeate flux was comparatively low, there was not a significant change in the osmotic driving force (around 14% reduction in draw solution concentration), leading to a relatively slow decline in the water flux with time. The separation performance of the TFC membranes was evaluated by establishing a mass balance between the concentration of TOC, silica and divalent ions (calcium and magnesium) in the final and initial feed solutions. All the TFC membranes showed very good rejection percentages (~99%) toward the removal of organic matter, silica and divalent ions.

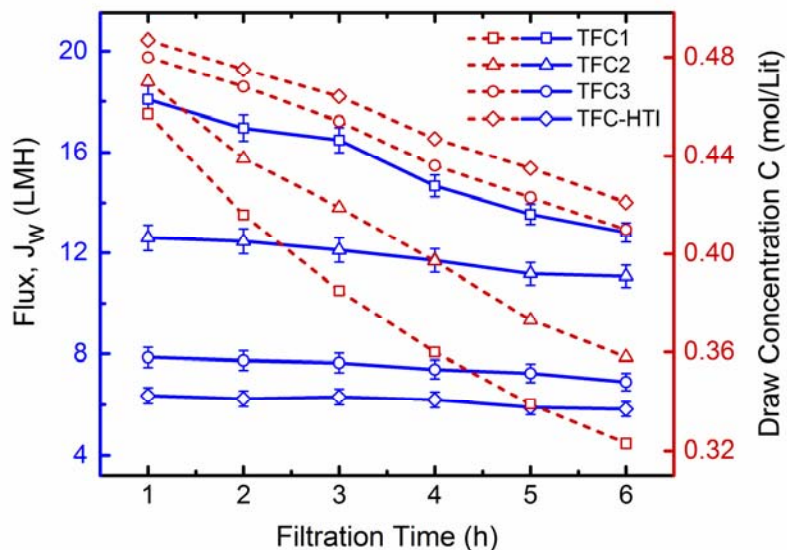


Figure 4.12: Water permeation of lab-made and commercial TFC membranes. Test conditions: Feed solution: conventionally-treated SAGD BFW; Draw solution: 0.5 M NaCl solution; Cross-flow velocity: 0.22 m/s.



## 4.4 Conclusion

In the present work, high throughput TFC PA membranes were fabricated for the FO operation by controlling the thickness of PA selective layer via temperature adjustment of organic solution during the IP reaction. It was found that by reducing the temperature of the organic solution down to  $-20\text{ }^{\circ}\text{C}$ , an ultra-thin layer of PA film was formed at the support surface. The synthesized TFC membranes, prepared via thermally-tuned IP reaction, demonstrated higher permeation performance compared to the unmodified as well as commercial TFC membranes. The results obtained in this study demonstrate the significant role of the active layer properties (thickness and morphology) on performance of a FO membrane. The microporous support used in this work had a thickness of about  $140\text{ }\mu\text{m}$  with a structural parameter of  $451\pm 13\text{ }\mu\text{m}$ . For further improvement, the support layer can be modified either in terms of structure or material to provide a lower structural parameter and minimize the negative impact of the ICP, thus maximizing the permeation flux. FO trials using conventionally-treated SAGD boiler feed water indicate that high performance TFC membranes show promise for the production of desalinated boiler feed water from SAGD produced water. Furthermore, the method proposed in this report to control the thickness of the PA active layer can be effectively applied for energy- and cost-efficient development of high performance nanofiltration, reverse osmosis and forward osmosis membranes.

# Chapter 5<sup>§</sup>

## Fabrication of thermally stable and antifouling nanocomposite membranes

---

<sup>§</sup> This chapter is organized based on reference [43] and a submitted manuscript entitled “A novel approach for the fabrication of thin film polyamide-TiO<sub>2</sub> nanocomposite membranes with enhanced thermal stability and anti-biofouling propensity” to the journal of Scientific Reports.

## 5.1 Background

Fouling is the major challenge of almost all membrane-based filtration systems which results in lower throughput, shorter membrane lifecycle, and higher cleaning cost and energy demand [196,197]. In practical water treatment applications, synergistic fouling by multiple entities, involving mechanisms such as scaling, colloid deposition (cake formation), adsorption and pore-blocking are the norm [198–200]. Practically, the key recourse of fouling mitigation is recurrent cleaning through several mechanisms such as back washing [201], air scouring [202], chemically enhanced cleaning [203], and clean in place [204]. Ceramic and metallic membranes are robust materials as they can be cleaned efficiently using combinations of high temperature and strong cleaning agents [205,206]. However, polymeric membranes are not resistant to high temperatures or harsh cleaning agents which often limits their application for treatment of fouling prone waters [207,208]. The synthesis of mixed matrix membranes (MMM)s via embedding inorganic NPs into the polymer matrix, is one of the most promising techniques to overcome the above mentioned limitations [36,209–213]. This new generation of polymeric membranes, also referred to as nanocomposite membranes as well as hybrid organic/inorganic membranes, combine the superior advantages of high mechanical and thermal stability of inorganic nanomaterials with the low cost and easy processability of commodity polymers [171,214–216]. Multiple studies investigated the effect of a variety of nanofillers including porous nanofillers (e.g. carbon nanotubes, graphene oxide, zeolites and mesoporous silica) and nonporous particles (e.g. metal/metal oxide like Ag, TiO<sub>2</sub>, MgO, ZnO, Al<sub>2</sub>O<sub>3</sub>, ZrO<sub>2</sub>, Fe<sub>2</sub>O<sub>3</sub>, and SiO<sub>2</sub>) on the structural morphology, surface characteristics and transport properties of the resulting nanocomposite membranes [33–35,217–223]. In general, the rationale behind the incorporation of nanofillers within the polymer matrix is to introduce different functionalities into to the membrane material in order to develop (smart and) stimuli-responsive membranes with enhanced permselectivity, stability and anti-fouling-properties characteristics [224–229]. For example, developing a high temperature tolerant MMMs renders polymeric membranes more versatile, cost and energy-efficient and makes them competitive with inorganic membranes in several industrial applications where separation and cleaning are required to be done at high temperature. Furthermore, the surface charge and electrical conductivity of the MMMs can also be efficiently tuned for electro-filtration process [230,231]. In the following sections, the results of adding ITO NPs to the PES support and TiO<sub>2</sub> NPs to the top PA layer are presented.

## 5.2 Thermally resistant and electrically conductive PES/ITO nanocomposite membrane

### 5.2.1 Introduction

Polyethersulfone is one of the most common polymeric materials for the synthesis of symmetric/asymmetric single/composite membranes [12,21]. The chemical and mechanical stability of PES makes it a good choice for MF and UF membranes for treatment of contaminated water [232,233]. However, the inability of the PES-based membranes to maintain the separation efficiency at high temperatures and their susceptibility to fouling due to their hydrophobic nature, limit the applications of these membranes in water purification processes [197,234].

Previous reports have shown that application of electric field across the membrane surface can reduce the accumulation of charged foulant at the surface of membrane by electrostatic repulsion [235–238]. However, the major drawback of the electro-filtration processes is their low efficiency due to the presence of electrically-insulated membrane between the two electrodes which dramatically reduces the electric field intensity and increases the energy demand and power consumption of the process [239,240]. This limitation can be effectively mitigated by improving the electrical conductivity of the membrane via embedding metal and metal oxide NPs within the polymer network. The use of conductive MMMs in electro-filtration processes can effectively reduce the membrane interference with electric field propagation in the system which results in lower power consumption and higher filtration efficiency.

Here, the effect of incorporation of ITO NPs on physicochemical characteristics and permeation properties of PES membranes was studied. ITO or tin-doped indium oxide is a solid ceramic oxide (typically 90 wt.%  $\text{In}_2\text{O}_3$ , 10 wt.%  $\text{SnO}_2$ , melting point 1526-1926 °C, density 7120–7160  $\text{kg/m}^3$ ) which is widely used for fabrication of conducting films in electronic devices [241,242]. The ITO-coated plates are usually made by vapor deposition techniques, magnetron sputtering or plasma ion-assisted evaporation which is expensive processes and cannot be applied for particle coating on large surface areas. Recently, the in-situ synthesis of nanocomposite ITO films has received considerable attention which makes it possible to assemble different nanocomposite materials including films and membranes [243–246]. The present work explores the feasibility of the utilization of ITO NPs for the synthesis of multifunctional composite membrane [43].

## 5.2.2 Synthesis of PES-ITO

The detailed description of the synthesis of PES-ITO membrane is provided in chapter 2. Briefly, the PES-ITO membrane was prepared by phase inversion method using NMP and water as solvent and nonsolvent, respectively. First, ITO NPs were dispersed in NMP using BYK106 dispersing agent. Then, PES polymer was added to the suspension. Afterwards, the prepared homogeneous PES/ITO suspension was cast on a glass plate. The water permeation of PES/ITO membrane was also compared with four other nanocomposite membranes prepared with titanium oxide ( $\text{TiO}_2$ ), aluminum oxide ( $\text{Al}_2\text{O}_3$ ), silicon oxide ( $\text{SiO}_2$ ) NPs in PES substrates. Finally, the fouling propensity of the nanocomposite membranes was evaluated using warm lime softener (WLS) inlet water of steam assisted gravity drainage (SAGD) process.

## 5.2.3 Results and discussion

### 5.2.3.1 Size of solid ITO NPs

Figure 5.1 illustrates the FESEM image of the synthesized ITO NPs. Based on size distribution histogram obtained by XRD peaks and image processing; it was found that the average diameter of ITO NPs was about  $\sim 19$  nm.

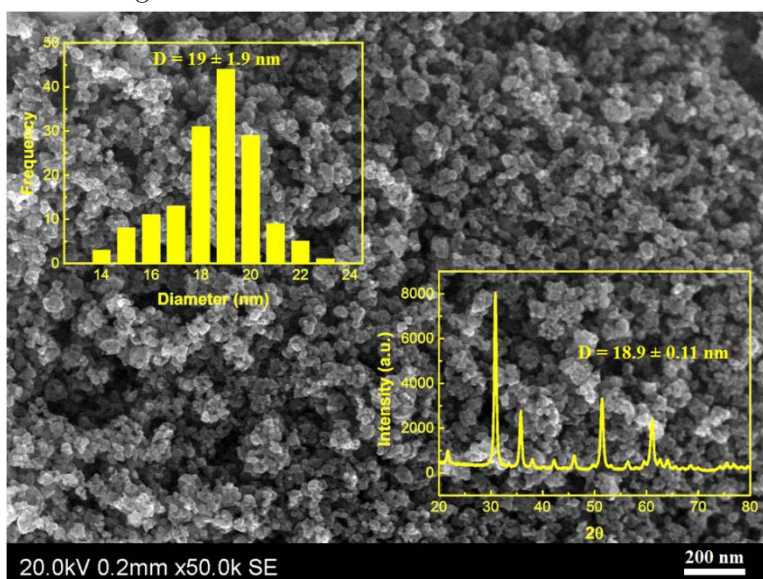


Figure 5.1: FESEM images of ITO NPs along with the diameter of the NPs which was obtained using image processing ( $19.0 \pm 1.9$  nm) and XRD peak fit ( $18.9 \pm 0.11$  nm).

### 5.2.3.2 Surface and internal structure of PES/ITO membrane

Figure 5.2 illustrates the internal and surface morphology of the nanocomposite PES/ITO membrane. Based on the cross-sectional FESEM images (Figures 5.2a and 5.2b), the PES membrane has a thin skin layer with a porous finger-like architecture which is typical for the membranes made by non-solvent induced phase separation (NIPS) method. More importantly, it can be seen that the ITO NPs were homogeneously distributed over the internal structure of the PES layer which is highly desirable for tuning the bulk properties of the PES membrane. The successful incorporation of ITO NPs at the surface was also evidenced by EDX spectra which are presented in Figures 5.2c and 5.2d for the PES/ITO surface and ITO nanocluster, respectively. Furthermore, the surface image of the nanocomposite membranes (Figure 5.2c) also exhibits the uniform dispersion of nanoclusters of the ITO particles at the surface.

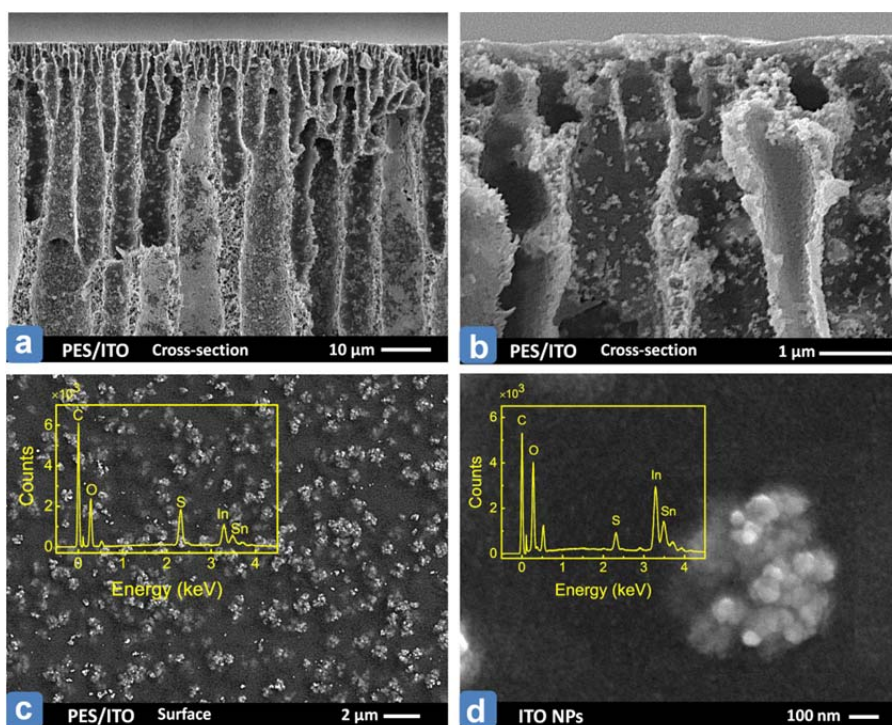


Figure 5.2: FESEM cross-sectional (a & b) and surface (c & d) SEM images of PES/ITO nanocomposite membrane. EDX spectra of PES/ITO membrane and ITO nanoclusters are added to panel (c) and (d), respectively.

### 5.2.3.3 Leaching of ITO NPs from PES substrate

It is important to examine that the embedded ITO NPs remain associated with the PES membrane matrix during water treatment applications. Figure 5.3 presents the results of leaching of ITO NPs from the PES substrate into acidic, neutral, and alkaline water solution. The results revealed that the leaching ITO NPs is more prominent under acidic condition (pH=2), resulting in the increase of the concentration ITO NPs in the leachate to 90 ppm after about 14 days. The extent of leaching is much lower for alkaline and neutral pH. This indicates that the present methodology of phase inversion produces nanocomposite membranes which will retain the embedded NPs more effectively in the polymer matrix under alkaline and neutral conditions. The poor leaching characteristics under acidic conditions are not a severe concern with the nanocomposite PES-ITO membranes, as the majority of PES membranes for water treatment are often used in neutral or slightly alkaline pH conditions rather than highly acidic waters.

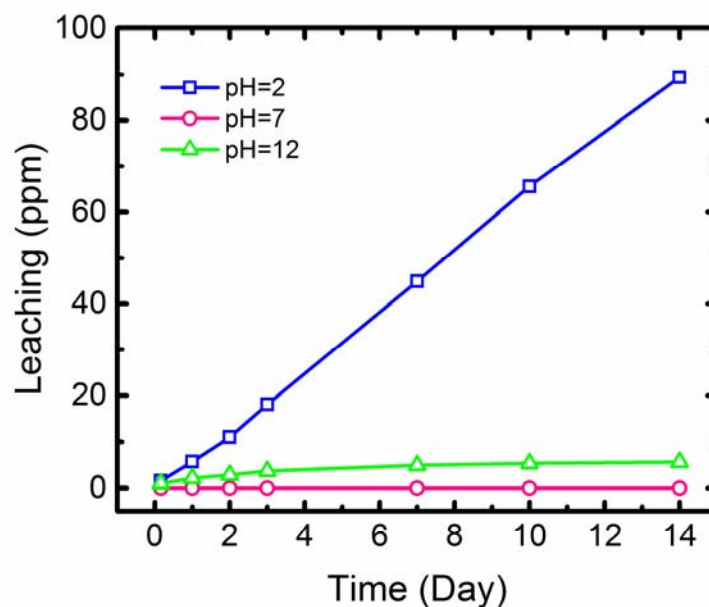


Figure 5.3: Leaching of ITO NPs in water solutions at pH=2, 7 and 12.

### 5.2.3.4 Thermal stability of PES/ITO membranes

Figure 5.4 illustrates the results of TGA analysis of the nanocomposite PES/ITO membrane and the bare PES film. It can be observed that the weight-loss curves of the two membranes show different characteristics as temperature is raised. The initial weight loss of the PES/ITO membrane is conservatively observed at temperatures around 100 °C above the corresponding temperature for the pristine PES membrane (decomposition temperature of 500 °C for PES/ITO nanocomposite membrane compared to 400 °C virgin PES film). Moreover, the overall weight loss is more modest for PES/ITO membrane in comparison with bare PES film which implies that the incorporation of the ITO NPs within the matrix of PES polymer makes it thermally more stable than the original PES film. This observation can be attributed to the fact that the presence of the inorganic NPs within the polymer matrix decreases the chain mobility of host polymer and thus enhances its resistance against thermal decomposition [247–249].

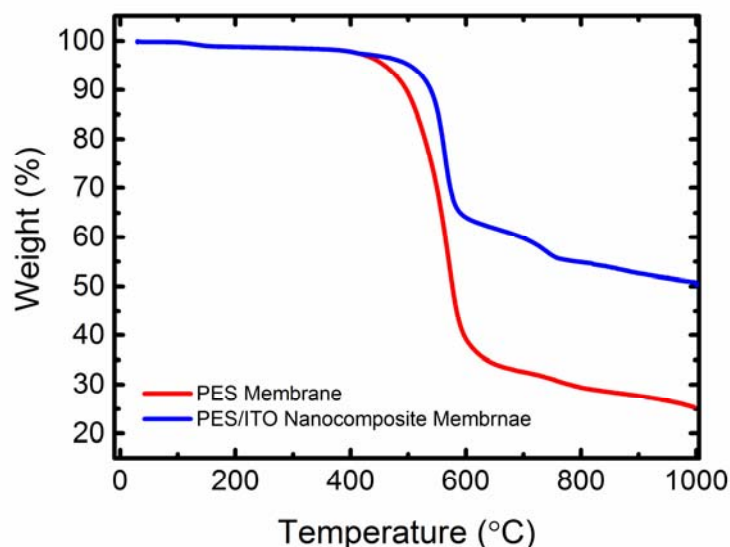


Figure 5.4: TGA analysis of the PES/ITO and base PES membrane. The plot shows the weight loss of membrane as a function of temperature.

Figure 5.5 compares the TGA results of bare PES film with four nanocomposite membranes which are made with ITO, TiO<sub>2</sub>, SiO<sub>2</sub>, and Al<sub>2</sub>O<sub>3</sub> NPs. According to this figure, the overall weight loss of all nanocomposite membranes is higher than the bare PES film. Among the nanocomposite membranes, the PES/ITO membrane has the highest decomposition temperature. A slightly higher thermal stability of PES/ITO nanocomposite membranes than other



nanocomposite membranes can be attributed to the induced IR reflectance and thermal conductive properties by ITO NPs. The PES/ITO membrane is believed to have very high reflectance compared to the native PES membrane and other nanocomposite membranes in a broad range of near IR (NIR) and IR wavelengths. Furthermore, presence of ITO NPs imparts higher thermal conductivity to the PES/ITO membrane compared to other nanocomposite membranes. This attests to the original hypothesis that use of ITO NPs can deflect heat from the core of the membrane, effectively keeping the interior of the polymer membrane relatively shielded from external heat. This can increase the longevity of a polymeric membrane under high temperature conditions.

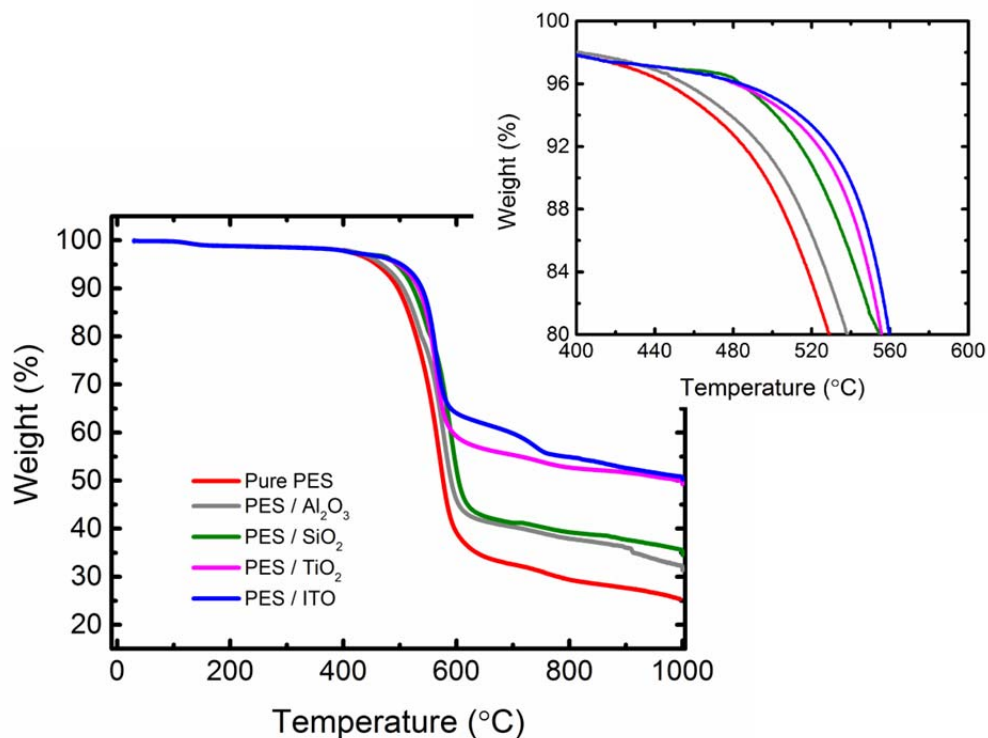


Figure 5.5: Weight loss of different nanocomposite membranes as well as bare PES membrane as a function of temperature measured by TGA.

### 5.2.3.5 Electrical conductivity of PES/ITO membrane

The I-V characteristics of the PES/ITO nanocomposite membrane and the base PES membrane are demonstrated in Figure 5.6. The linear response of the PES/ITO membrane to the applied electric potential implies that the inclusion of ITO NPs into the PES matrix has significantly enhanced the electrical conductivity of the resulting nanocomposite membrane.

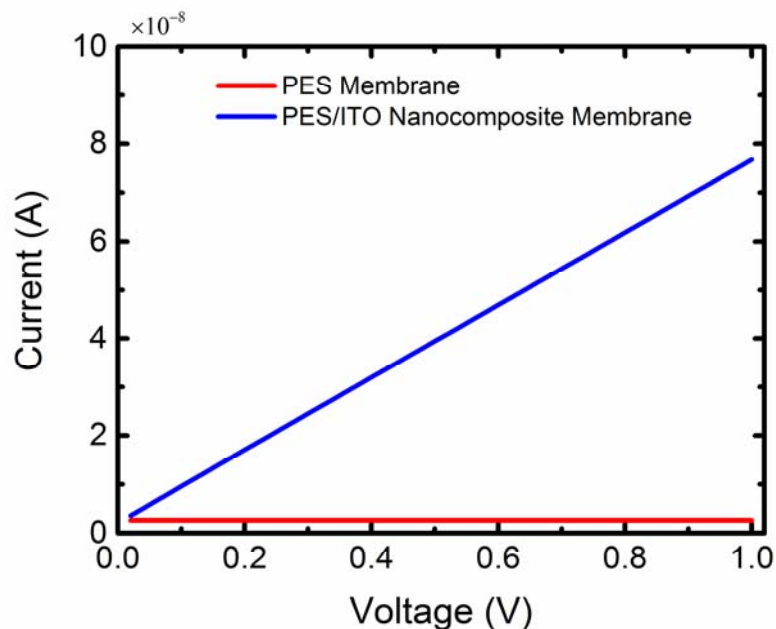


Figure 5.6: I-V characteristics of PES/ITO nanocomposite membrane and bare PES membrane.

### 5.2.3.6 Separation performance and fouling characteristics

Figure 5.7 depicts pure water permeability of the PES/ITO nanocomposite membrane and the bare PES film as a function of transmembrane hydraulic pressure. According to this figure, the water permeation of the two membranes was comparable at low values of applied pressure (100-200 kPa). However, their water flux deviated at higher pressure where the PES/ITO nanocomposite membrane showed 500 LMH higher water flux at 700 kPa (100 Psi).

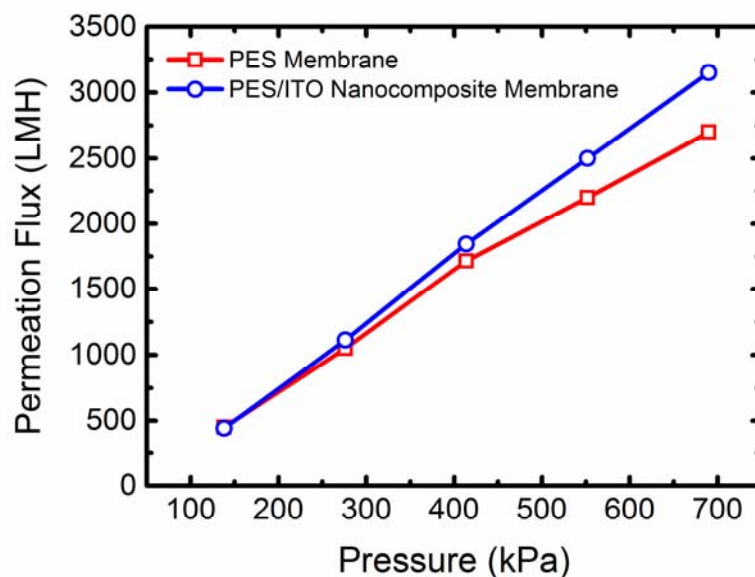


Figure 5.7: Pure water flux through synthesized PES/ITO nanocomposite and bare PES membranes as a function of transmembrane pressure. Each membrane was initially tested at 700 kPa for 1 h; the permeation flux at lower operating pressures was obtained after 15 minutes.

The fouling characteristics of the PES/ITO nanocomposite membrane during the filtration of the WLS inlet water is presented in Figure 5.8 where the rate of the water flux decline over time indicates the fouling tendency of the membrane [250]. It is worth mentioning here that the fouling characteristics of a membrane can be influenced by several parameters including (i) hydrodynamic conditions (feed flow rate, feed channel dimensions, and permeation drag, which is related to permeation flux), (ii) feed water chemistry (concentration of salt and organic matter, and pH), and (iii) the membrane material properties (hydrophilicity, zeta potential, and surface roughness) [251,252]. In order to solely explore the effect of the modification in the membrane material by addition of ITO NPs, the first two parameters were kept constant during the fouling test [253]. Regarding that, the feed temperature and flow rate, and the initial flux of permeate were maintained at 25 °C, 1 LPM and 120 LMH, respectively. The initial permeate flux of 120 LMH was obtained by adjusting the transmembrane pressure to 275 and 345 kPa for the PES/ITO nanocomposite and base PES membranes, respectively.

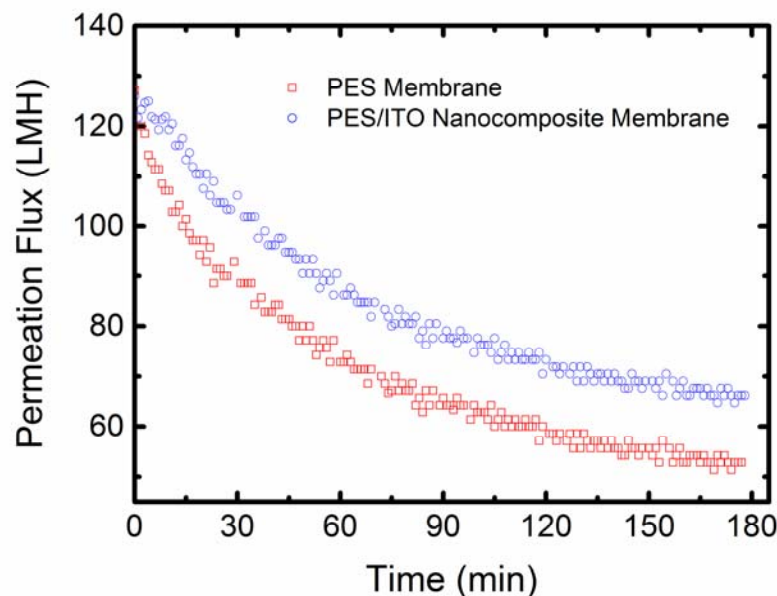


Figure 5.8: Fouling characteristics of PES/ITO membrane and pristine PES membrane. Flux decline represents fouling of membranes during filtration of WLS inlet water.

Based on Figure 5.8, the flux decline of the PES/ITO nanocomposite membrane was 10% less than the bare PES membrane which indicates that at identical conditions, the inclusion of ITO in the PES matrix significantly improved the anti-fouling properties of the PES membrane. Moreover, the lower flux decline of PES/ITO membrane suggests that the PES polymer impregnated with ITO NPs was mechanically more stable and had experienced less compaction than the bare PES membrane. The water flux decline and the recovery ratio of the PES/ITO and base PES membranes during filtration of WLS inlet water are illustrated in Figure 5.9. As can be seen, both membranes showed a drastic  $DR_t$  (90.0% and 88% for pristine PES and PES/ITO membranes, respectively) upon filtration of WLS inlet water which was expected due to high concentration of organic matters, dissolved and suspended solid materials in the feed solution. However, the irreversible flux decline due to severe adsorption of fouling materials on the surface and inside the pores of membrane was lower for PES/ITO membrane (29%) than the pristine PES (44%). Additionally, the PES/ITO membrane showed 15% more flux recovery ratio than the base PES membrane (71% for PES/ITO compared to 56% for PES membrane), which implies an improvement in antifouling properties of the base membrane by incorporation of ITO NPs.

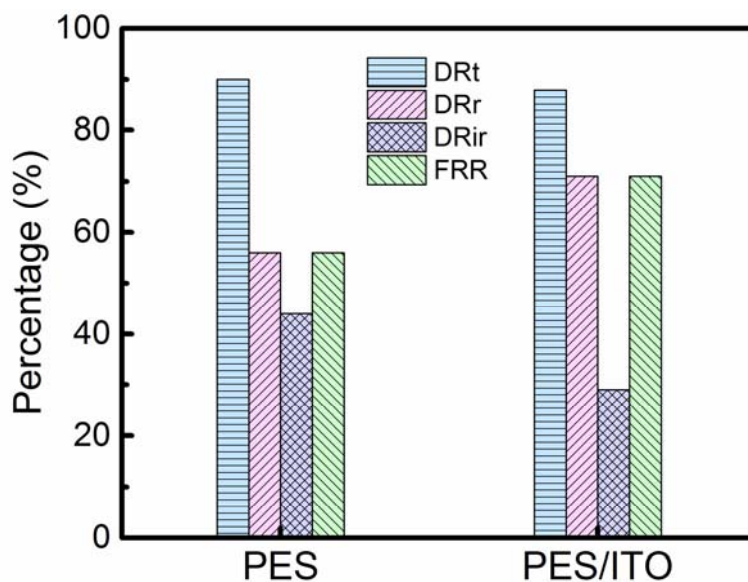


Figure 5.9: Fouling characteristics of PES/ITO membrane and pristine PES membrane. DR<sub>t</sub> is total flux decline ratio, DR<sub>r</sub> is reversible flux decline ratio, DR<sub>ir</sub> is irreversible flux decline ratio, and FRR is flux recovery ratio. Fouling evaluation test: 180 min, washing duration: 30 min, all data were collected at the end of measurement.

Performance of the PES/ITO nanocomposite membrane was also compared with the other nanocomposite membranes impregnated with TiO<sub>2</sub>, SiO<sub>2</sub>, and Al<sub>2</sub>O<sub>3</sub> in Figure 5.10.

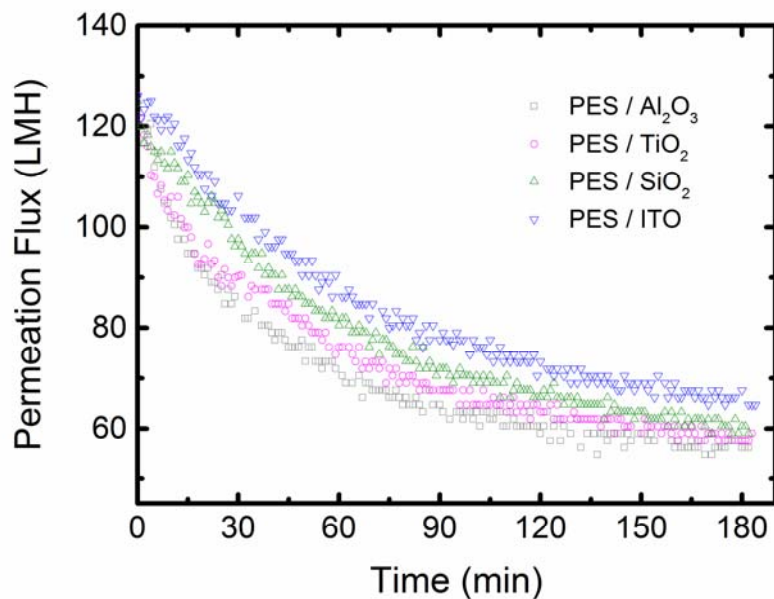


Figure 5.10: Flux decline after fouling of nanocomposite membranes by WLS water.

As can be observed, the rate of flux decline and the final permeation flux at the steady stage (after the 180 min) were higher for PES/ITO nanocomposite membranes compared to other membranes. These results can be rationalized by comparing the surface (zeta) potential and hydrophilicity of membranes which are presented in Table 5.1.

It is a widely held view that the membranes with a higher negative surface charge and greater hydrophilicity are less prone to fouling due to fewer interactions between the chemical groups in the organic solute and the polar groups on the membrane surface [200,254]. In general, the more negatively charged membranes, particularly with acidic functional groups, exhibit lower fouling propensity to dispersed foulants, which are typically negatively charged colloids and/or organic molecules. However, it must be taken into account that the fouling tendency of the membranes is also strongly affected by the surface hydrophilicity. The membranes with more hydrophilic surface are less prone to fouling, especially by organic matters, due to the lower hydrophobic interaction between the foulants and the membrane surface [255–257]. Therefore, the overall antifouling property is governed by the complex interaction of surface charge and hydrophilicity. Based on the data presented in Table 5.1, the surface potential of nanocomposite membranes was lower than the pristine PES membranes. The reason behind this observation can be attributed to the presence of the inorganic dispersing agent within the polymer matrix. Although the solid NPs may contain higher (negative) surface potential compared to the polymer substrate, their encapsulation in the dispersing agent presumably moderates their surface properties and thus results in a nanocomposite membrane with lower surface potential compared to the unmodified membrane. However, the PES/ITO membrane had the highest surface (negative) potential compared to other nanocomposite membranes. Furthermore, the contact angle values of all nanocomposite membranes were lower than the bare PES membranes, implying that the incorporation of the metal oxide NPs within the polymer matrix can bring more hydrophilicity to the PES membrane. However, in the special case of PES/ITO membrane, the surface contact angles were significantly decreased to  $46.2^\circ$  which was about half of the bare PES membrane ( $85.9^\circ$ ). The combination of the very high surface potential and hydrophilic properties of the PES/ITO nanocomposite membrane makes it favorable for water treatment application and less prone to fouling by organic compounds.

Table 5.1: Surface potential and contact angle of nanocomposite and pristine PES membranes.

Membrane	Zeta potential (mV)	Contact angle ( $\theta^\circ$ )
Pure PES	-40.4 $\pm$ 2.2	85.9 $\pm$ 3.5
PES/ITO	-30.9 $\pm$ 1.8	46.2 $\pm$ 3.1
PES/SiO <sub>2</sub>	-28.6 $\pm$ 1.4	61.5 $\pm$ 1.5
PES/TiO <sub>2</sub>	-30.1 $\pm$ 1.4	66.3 $\pm$ 2.1
PES/Al <sub>2</sub> O <sub>3</sub>	-25.3 $\pm$ 2.6	70.9 $\pm$ 1.8

Figure 5.11 depicts the rejection of dissolved organic matter (DOM) by the PES and PES/ITO membranes over a three hours filtration of WLS inlet water. Low rejection values (start from 31% and 33% for pristine PES and PES/ITO nanocomposite membranes, respectively) suggest presence of low molecular weight organic matter in the WLS inlet feed. According to our prior studies on the characterization of the DOM in the boiler water, the majority of the molecules constituting the DOM are <1000 Da [8,258]. Based on the MWCO of the synthesized membranes it can be concluded that almost 30% of organic matter have molecular weight higher than 2500 $\pm$ 250 Da. This result matches well with our earlier study where 75% of organic matter passed through a membrane with MWCO of 3 kDa [8]. As it is shown in Figure 5.11, the DOM rejection of both membranes increased with time, a behavior that is typically representative of formation of a fouling layer on the membrane surface, which hinders the permeation of DOM through the membrane. However, the rejection percentage of the PES/ITO membrane was always higher than the bare PES membrane during the filtration process which implies that the selectivity of the nanocomposite membrane is improved upon the addition of the ITO NPs.

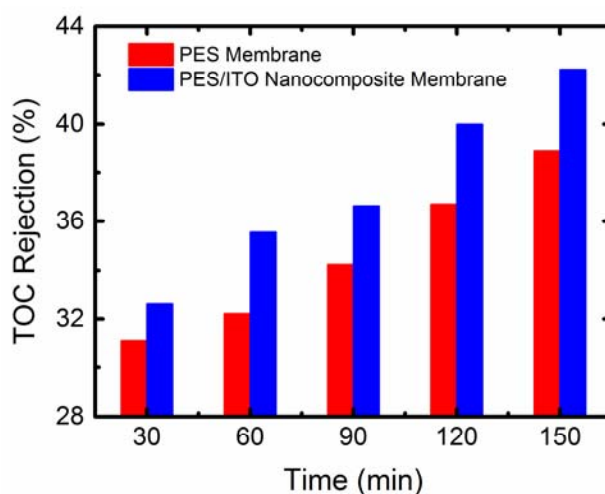


Figure 5.11: Organic matter rejection by PES/ITO and pristine PES membranes during filtration of WLS inlet water.

## 5.3 Fabrication of TFN PA-TiO<sub>2</sub> with enhanced thermal stability and anti-biofouling propensity

### 5.3.1 Introduction

Recently, considerable effort has been devoted to the integration of the advances in nanotechnology with the classical synthesis procedure of the polymeric membranes with the aim of fabricating multifunctional nanocomposite membranes [259,260]. The first instance of such work was reported for gas separation by adding zeolite nanofillers into silicone rubber in 1973 [261]. Later, in 2005, the application was extended to water filtration with the incorporation of zeolite-A NPs into a thin-film nanocomposite (TFN) PA membrane [262]. Since then, a variety of nanoparticles (NPs), including organic (carbon-based nanomaterials such as carbon nanotube, graphene, and graphene oxide) and inorganic (zeolite, silica, metal and metal oxide) nanofillers, have been utilized to fabricate TFN membranes for diverse applications of gas separation, pervaporation, and water purification processes [34,35,43,171,263,264].

Titanium dioxide (TiO<sub>2</sub>) which is a natural oxide of titanium has attracted considerable attention for improving the permselectivity and antifouling properties of the TFN PA membranes owing to its low synthesis cost, high chemical and thermal stability and, most importantly, its photocatalytic (PCT) activity upon UV irradiation [265–267]. There are two main approaches that have been widely utilized to incorporate TiO<sub>2</sub> NPs in TFN PA membranes: (i) attachment via self-assembly to the PA surface [268–270] and (ii) in-situ integration into PA matrix during the IP reaction [271–273]. The former involves dip coating of a prepared TFC membrane into a TiO<sub>2</sub> NP suspension. In the second method the TiO<sub>2</sub> NPs are directly dispersed in one of the reacting monomer (either MPD-aqueous or TMC-organic) solutions prior to polymerization reaction [274]. The self-assembly is highly efficient in modifying the surface properties of the membrane with easy implementation since the NPs are directly deposited on the membrane surface [275]. However, the weak attachment between the TiO<sub>2</sub> NPs and the host PA membrane surface causes the leaching of the NPs during the filtration process and thus limits its application for a long-term operation [276].

The significant advantage of the in-situ integration method is to resolve this problem by the entrapment of the TiO<sub>2</sub> NPs within the PA matrix during the IP reaction [217]. However, the critical challenge with this method is that the synthesis of a defect-free PA film requires first, synthesis of nanosized TiO<sub>2</sub> NPs



and second, preparation of a stable dispersion of the TiO<sub>2</sub> NPs in the reacting monomers (MPD or TMC) solutions [53]. When the concentration of TiO<sub>2</sub> NPs in the monomer solutions increases, they become more prone to aggregation and thus form large clusters, especially during IP reaction when there is a minimal agitation in the solution [277]. The presence of these NPs clusters within the resulting PA film causes an unfavorable decrease in the separation efficiency of the membrane by creating large empty [278].

In recent years, researchers have investigated a variety of approaches to effectively incorporate NPs in the thin PA layer via the in-situ polymerization [279,280]. Due to the strong interaction of most nanomaterials with polar solvents, much of these research has been restricted to the dispersion of NPs in MPD-aqueous solution [281]. A serious weakness of this approach, however, is that NPs cannot be integrated into the topmost PA layer and, as a result, their properties are not present in the membrane/water interface [282]. Given that, it is preferable to have NPs dispersed in TMC-organic solvent (e.g. heptane). In such cases, however, the aggregation of TiO<sub>2</sub> NPs becomes more challenging as the thermodynamics of the resulting multiphase system are inherently unstable. Hence, it is essential to modify the surface properties of the NPs using dispersing agents, which are typically surfactant with polar and non-polar end functional groups [283]. Surface modification of the NPs lowers the free energy of the NPs-solvent system and results in stable suspension of NPs in organic solvents [54,284].

In the present work, we report a highly robust and efficient method for the dispersion of TiO<sub>2</sub> NPs in an organic solvent (heptane) and their incorporation into the PA matrix.

### 5.3.2 Synthesis of TFN PA-TiO<sub>2</sub> membranes

The synthesis and surface modification of the NPs were carried out simultaneously using oleic acid (OA) in heptane via a biphasic solvothermal (BST) reaction. The complete details of synthesis conditions of TiO<sub>2</sub> NPs as well as the TFC membrane were provided in chapter 2. After making the TiO<sub>2</sub> suspension in heptane, certain amount of it was added to TMC-heptane solution prior to IP reaction. Afterwards, the resulting suspension was brought into contact with MPD solution at the surface of PES support to fabricate TFN Pa-TiO<sub>2</sub> membranes. Table 5.2 presents the synthesis conditions for fabrication of TFC and TFN membranes.

Table 5.2: Concentration of MPD, TMC and TiO<sub>2</sub> NPs for the fabrication of TFC and TFN membranes. The invariant synthesis conditions were: 0.2 wt.% SDS, 1 wt.% CSA, 1 wt.% TEA in MPD-water solution, 30 sec IP reaction, 4 minutes heat curing at 60 °C.

Membrane	MPD conc. in DI water (wt.%)	TMC conc. in heptane (wt.%)	Volume of TiO <sub>2</sub> NP suspension added to TMC- heptane solution (µl)	Estimated conc. of TiO <sub>2</sub> NPs in TMC-heptane solution (wt.%)
TFC	2	0.2	0	0
TFN1	2	0.2	125	0.006
TFN2	2	0.2	250	0.0124
TFN3	2	0.2	375	0.0185
TFN4	2	0.2	500	0.0245

### 5.3.3 Results and discussion

#### 5.3.3.1 Characterization of TiO<sub>2</sub> NPs

Figure 5.12 illustrates the TEM, XRD and DLS analysis of the TiO<sub>2</sub> NPs. Based on panels (a) and (b), it can be observed that the TiO<sub>2</sub> NPs have a nano size core in the range of 5 to 10 nm. Regarding crystalline shape, TiO<sub>2</sub> NPs are generally available in three structures, namely anatase, rutile, and brookite. The prepared TiO<sub>2</sub> NPs mainly have the anatase structure as evidenced by the characteristic peaks at 2θ degree of 25.3°, 37.8°, and 48.1° in the XRD spectra (panel c). These peaks correspond to the (101), (004) and (200) planes, respectively [265]. The anatase structure is known to provide higher PCT activities, as will be discussed in section 3.2.4. The size distribution and aggregation rate of dispersed TiO<sub>2</sub> NPs in heptane were evaluated by DLS technique. The size measurement was conducted three times over a period of 30 minutes. Panel (d) in Figure 5.12 demonstrates that the TiO<sub>2</sub> NPs were highly stable in heptane with the average size of less than 10 nm, starting from 7.1 nm (after 1 minute) and reaching to 8.5 nm after 30 minutes. The high stability of the TiO<sub>2</sub> NPs in heptane is essential for the synthesis of defect-free PA films.

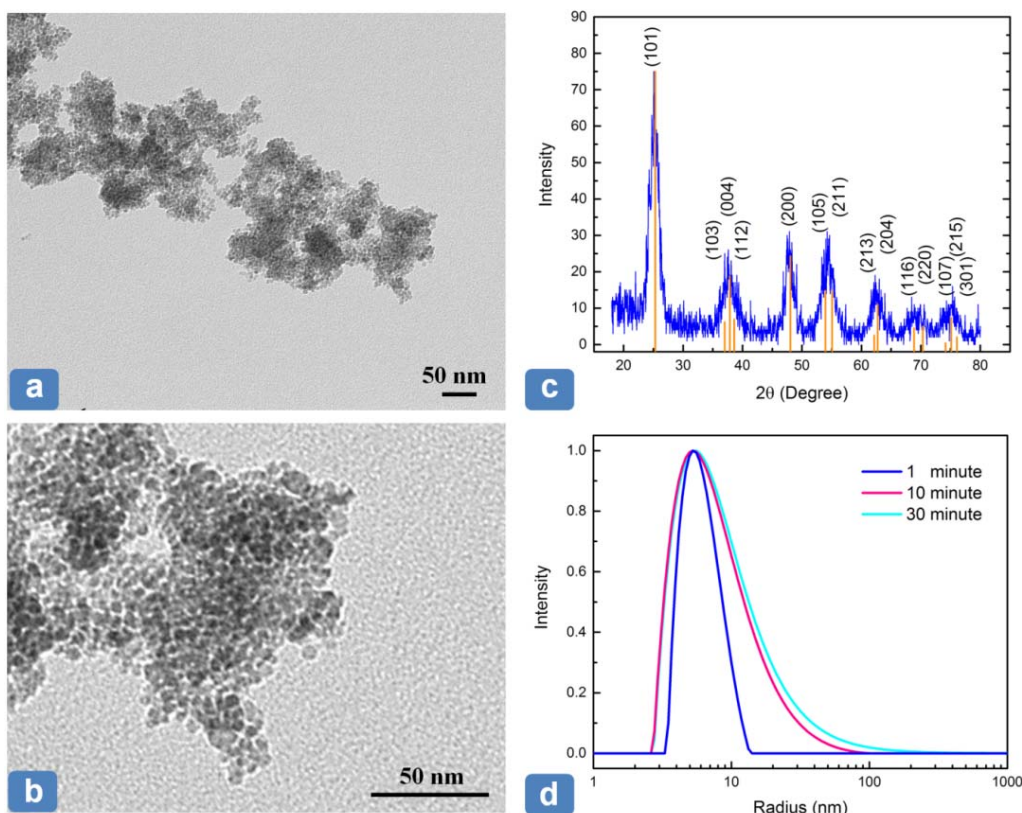


Figure 5.12: (a) and (b): TEM images of the synthesized  $\text{TiO}_2$  NPs presenting the size of dried nanoparticles, (c) XRD spectrum of  $\text{TiO}_2$  NPs showing their anatase crystalline structure, (d) DLS measurement of  $\text{TiO}_2$  NPs capped with OA presenting their stability and size distribution in heptane.

### 5.3.3.2 Characterization of PA- $\text{TiO}_2$ TFN membranes

Figure 5.13 illustrates the surface and cross-sectional images of the base TFC and TFN4 membranes. The FESEM and TEM images in panels (a), (b), and (c) demonstrate that the PA layer of the base TFC membrane possesses a ridge-and-valleys morphology with multiple internal nano- and microvoids [95,105]. These complex multiscale voids are the typical characteristic of the PA-based membranes; however, their formation process and the mechanism by which they contribute to the improvement of the PA permeation properties are not well-established yet and have been the focus of several studies in the recent years [99,100,109,110]. In contrast to the homogeneous surface feature of the base TFC membrane, the FESEM images of TFN4 membrane in panels (d), (e), and (f) reveal the formation of multiple islands at the membrane surface. The images obtained using back-

scattered electron detector (BSE) in panel (g) and (h) showed that these islands were blends of PA with a high concentration of TiO<sub>2</sub> NPs. The elemental color map in panel (i), which was obtained by energy-dispersive X-ray spectroscopy (EDX), also confirmed a good distribution of TiO<sub>2</sub> NPs within the observed clusters. The TEM cross-sectional images of the TFN4 membrane (panel j, k, and l) show that the TiO<sub>2</sub> NPs were mainly integrated into the topmost layer of the PA film. It is highly desirable to have the NPs at the topmost interface of the membrane as it enables tuning of the surface and bulk properties of the nanocomposite membranes.

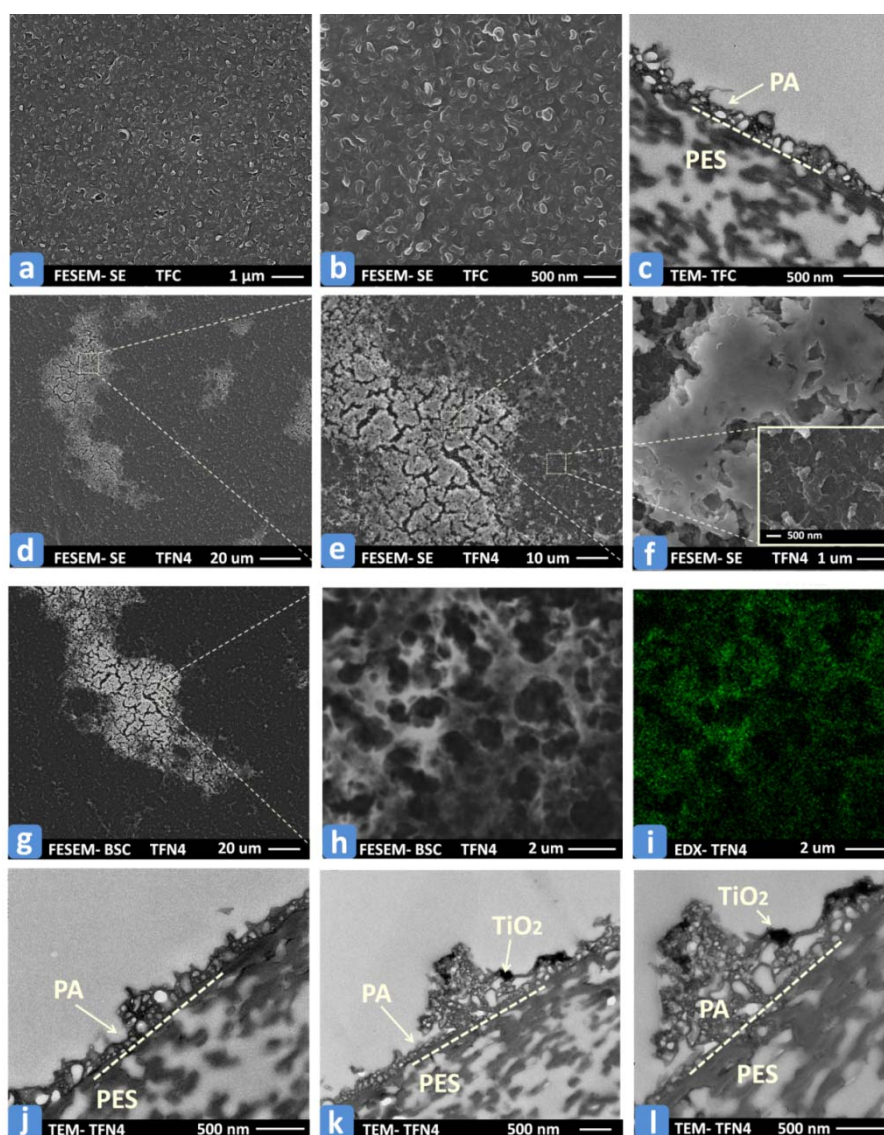


Figure 5.13: (a) and (b): FESEM images of the base TFC membrane; (c): TEM images of the TFC membrane; (d), (e) and (f): FESEM images of TFN4 membrane; (g) and (h): FESEM

images with BSE detector of the TFN4 membrane showing the  $\text{TiO}_2$ -rich spots brighter than the other regions ; (i): EDX color map of Ti element at the surface of TFN4 membrane; (j), (k) and (l): TEM images of the TFN4 membrane.

The chemical properties of the synthesized membranes were evaluated using ATR-FTIR spectroscopy and EDX technique. Figure 5.14 presented the ATR-FTIR spectra of the TFC and TFN membranes. These spectra demonstrate the chemical functional groups present in both top PA skin layer and the bottom PES substrate due to the high penetration depth of the IR beam, particularly in the range of  $600\text{ cm}^{-1}$ - $2000\text{ cm}^{-1}$ . However, there are three peaks at between  $1500\text{ cm}^{-1}$  and  $1700\text{ cm}^{-1}$  which are merely related to the PA layer. These PA characteristic peaks were highlighted in a separate window in panel (b). The peak at  $1667\text{ cm}^{-1}$  is attributed to C=O stretching vibration (amide I bands), the peak at  $1611\text{ cm}^{-1}$  belongs to aromatic amide ring breathing, and the peak at  $1541\text{ cm}^{-1}$  is associated (mainly) with N-H bending as well as the C-N stretching vibration (amide II bands) of the -CO-NH-group [84]. The broad peak at  $3300\text{ cm}^{-1}$  is due to stretching vibration of the N-H groups in the PA layer [56,83].

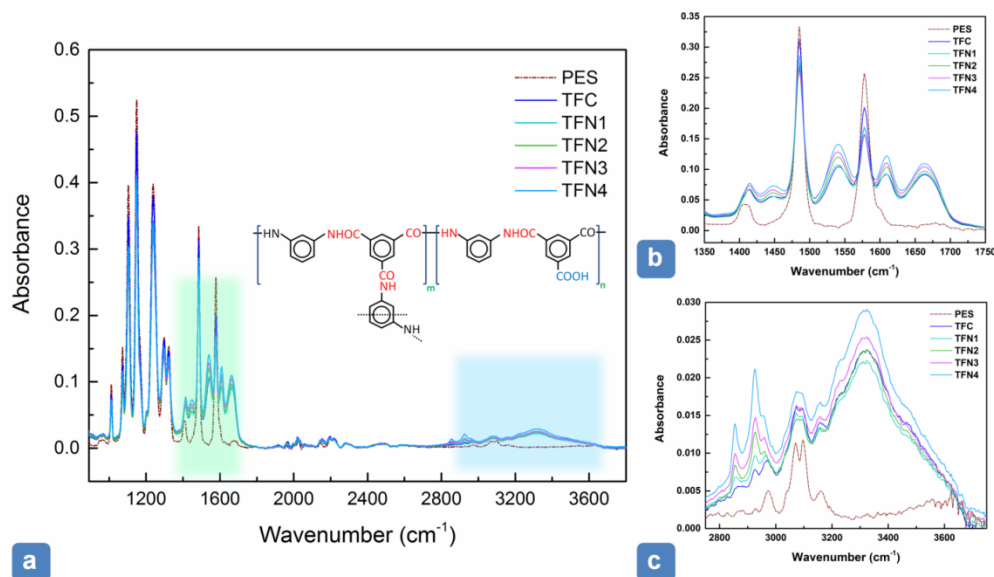


Figure 5.14: (a) The ATR-FTIR spectroscopy of the synthesized TFC and TFN membranes; (b) PA characteristic peaks emerge at  $1541\text{ cm}^{-1}$ ,  $1611\text{ cm}^{-1}$ , and  $1667\text{ cm}^{-1}$  attributing to N-H bending and C-N stretching vibration of amide II (-CONH-) group, aromatic ring breathing and C=O stretching vibration of amide I bands, respectively; (c) The broad peak at  $3300\text{ cm}^{-1}$  is formed to stretching vibration of the N-H groups in the PA layer.

EDX spectroscopy was utilized to analyze the chemical composition of the TFN membranes, and the results are presented in Figure 5.15 for TFN2 and TFN4 membranes. In addition, the elemental composition was evaluated at two different spots: TiO<sub>2</sub> rich (point A, white region in the FESEM image with BSC detector); and lean (Point B, dark region in the FESEM image with BSC detector) spots at the surface of TFN2 and TFN4 membranes. The EDX spectra illustrate a distinct peak for titanium at the membrane surface, particularly at point A where the blend of PA and TiO<sub>2</sub> NPs formed large clusters at the surface. A comparison between the composition results of the TFN2 and TFN4 membranes shows that the weight percentage of the TiO<sub>2</sub> NPs at the PA surface increased with rise in the concentration of the TiO<sub>2</sub> NPs in the TMC solution. This result implies the effective integration of the TiO<sub>2</sub> NPs during the IP reaction.

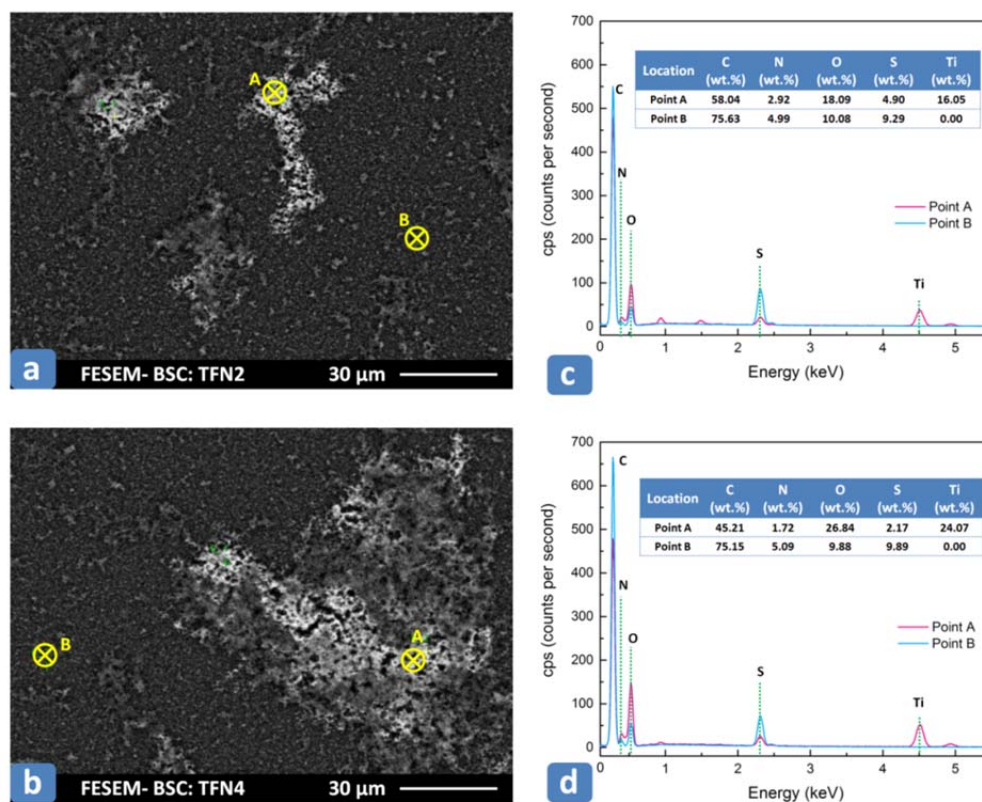


Figure 5.15: (a) and (b) FESEM image with BSE detector of TFN2 and TFN4 membranes, respectively; (c) and (d) EDX spectra at TiO<sub>2</sub> rich (point A) and lean (point B) spots at the surface of TFN2 and TFN4 membranes, respectively.

### 5.3.3.3 Water flux and salt rejection of TFN membranes

The permeation performance of a TFC membrane highly depends on its physicochemical and structural characteristics such as the thickness and crosslinking density of the PA layer, the complex interior free volumes, the surface charge, and hydrophilicity of the membrane [41,42,88,108]. In the case of TFN membranes, the surface and bulk properties of the incorporated nanomaterials as well as their interaction with the host polymer matrix have also a significant influence on the final transport properties of the TFN membranes.

The water flux and salt rejection of the synthesized TFC and TFN membranes are presented in Figure 5.16. To evaluate the thermal stability of the membranes, filtration tests were initially conducted at room temperature (25 °C) and then elevated to 65 °C. The comparison between the water permeation results at room temperature revealed that the addition of TiO<sub>2</sub> NPs into the PA layer initially improved the water flux of the resulting TFN membrane (22.7 LMH and 24.3 LMH for TFN1 and TFN2, respectively, compared to 21.5 LMH for base TFC membrane). Further incorporation of TiO<sub>2</sub> NPs, however, resulted in TFN membranes with lower water flux (10.7 LMH and 10.0 LMH for TFN3 and TFN4 membranes, respectively). The higher water flux of the TFN1 and TFN2 membranes than that of TFC membrane suggests the existence of an optimum loading of the TiO<sub>2</sub> NPs for the fabrication of high throughput TFN membranes. Regarding salt rejection, all the synthesized membranes provided greater selectivity than 97% of NaCl in water. The salt rejection of the base TFC membrane and TFN1 and TFN2 membranes were almost similar; however, TFN3 and TFN4 membranes provided a higher salt rejection following the typical trade-off relation between the water flux and salt rejection. The lower water flux and higher salt rejection of TFN3 and TFN4 can be attributed to the reduced internal free volumes within the PA matrix by the integration of well-dispersed nanosize TiO<sub>2</sub> particles. The presence of these NPs may have restricted the pathways for the transport of water and solute molecules through the TFN membranes.

By increasing the temperature of the feed solution (2000 ppm NaCl), all the synthesized membranes provided more water flux with a maximum value at 65 °C. The progressive increase in the permeation rate of the membranes with temperature can be attributed to the swelling of the PA layer as well as the higher diffusion coefficient of water molecules through the swelled membrane. When the filtration test continued for a longer time at 65 °C, the base TFC membrane

showed a stepwise flux decline from 43.5 LMH to 33 LMH over 6 hours of filtration test. The observed flux decline became milder for the case of the TFN1 and TFN2 and was completely overcome in the case of TFN3 and TFN4 in which higher concentration of TiO<sub>2</sub> NPs was integrated. A possible explanation for this stepwise flux decline may be the compaction of the swelled PA film under high temperature and pressure (65 °C and 220 psi, respectively). Hence, it can be concluded that the addition of the TiO<sub>2</sub> NPs could effectively improve the thermomechanical stability of the TFN membranes by limiting the chain mobility of the PA matrix at high temperatures. Regarding the salt rejection, all the synthesized membranes showed higher rejection percentage at 65 °C as compared to room temperature, particularly for the case of TFN3 and TFN4 where the salt rejection was as high as 99.2% and 99.4%, respectively. The high salt rejection and stable water permeation of TFN3 and TFN4 are highly desirable for the applications that robust membrane performance and high-quality water is required under high temperatures of feed streams. Such an application can be found in SAGD process of oil recovery where the temperature of the produced water is as high as ~150 °C. In order to reuse and recycle the produced water, a significant amount of energy is wasted by cooling down the produced water to ~60 °C in water treatment processes, followed by re-heating to ~200 °C in steam generators [44,250]. Thermally tolerant membranes have the potential to integrate into water treatment facilities and reduce the boiler heating requirements and greenhouse gas production in oil recovery plants.

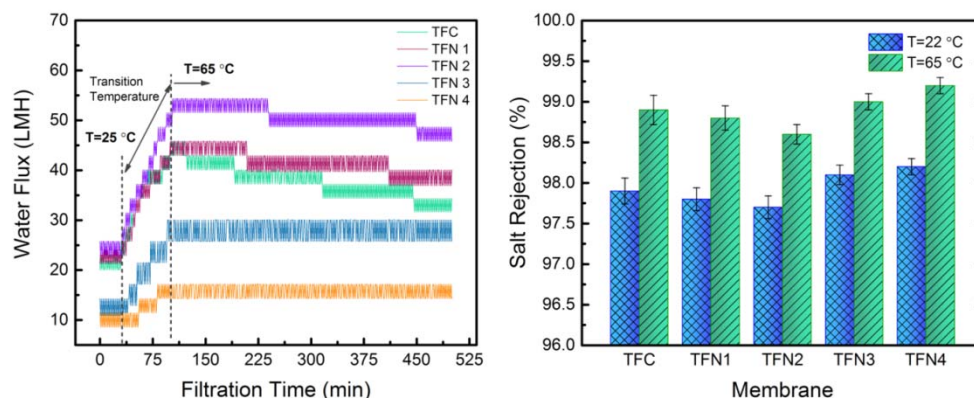


Figure 5.16: Water permeation and salt rejection of the synthesized TFC and TFN membranes at 25 °C and 65 °C showing the effect of TiO<sub>2</sub> NPs on permselectivity and thermal stability of the TFN membranes. Operating conditions: 220±5.0 psi of transmembrane pressure and 1.0±0.1 LPM of feed flow rate.



#### 5.3.3.4 Antibacterial activity of TFN membranes

The PCT activity of  $\text{TiO}_2$  has made it a potent material to be used in a wide range of applications including food and medical industry, solar energy conversion and water purification. Under the UV light, the  $\text{TiO}_2$  NPs generate active radical species (such as hydroxyl and superoxide radicals) which decompose organic matter and inactivate living organisms like bacteria in the water (Figure 5.17c) [285,286]. A moderate band gap ( $\sim 3.2$  eV) along with low toxicity has made  $\text{TiO}_2$  NPs promising nanofillers for water treatment applications, particularly for mitigating the bio- and organic fouling [287–289]. The antibacterial activity of the synthesized TFN membranes in this study was evaluated by counting the number of bacteria (*E. coli*) colonies formed over the UV-illuminated membranes [290,291]. Figure 5.17b illustrates the image of three plates of base TFC, TFN2 and TFN4 membranes after 30 minutes of UV irradiation. As can be observed, the exposure of the UV light on TFN membranes effectively lowered the viability of the *E. coli* bacteria. The number of bacteria colonies dramatically decreased from  $12.2 \log_{10}(\text{cfu/ml})$  for the base TFC membrane to  $10.7 \log_{10}(\text{cfu/ml})$  for the TFN2 membrane as presented in Figure 5.17d. Further increase in the concentration of  $\text{TiO}_2$  NPs in TFN4 membranes provided a slightly higher antibacterial efficiency compared to TFN2 membrane. The distinct difference between the numbers of bacteria colonies on the surface of the TFN membranes compared to the base TFC membrane shows the high PCT activity and thus the antibacterial efficiency of the integrated  $\text{TiO}_2$  NPs within the PA network. This property is highly beneficial for those membrane-based separation processes where mitigation of biofouling and organic deposition at the membrane surface is essential.

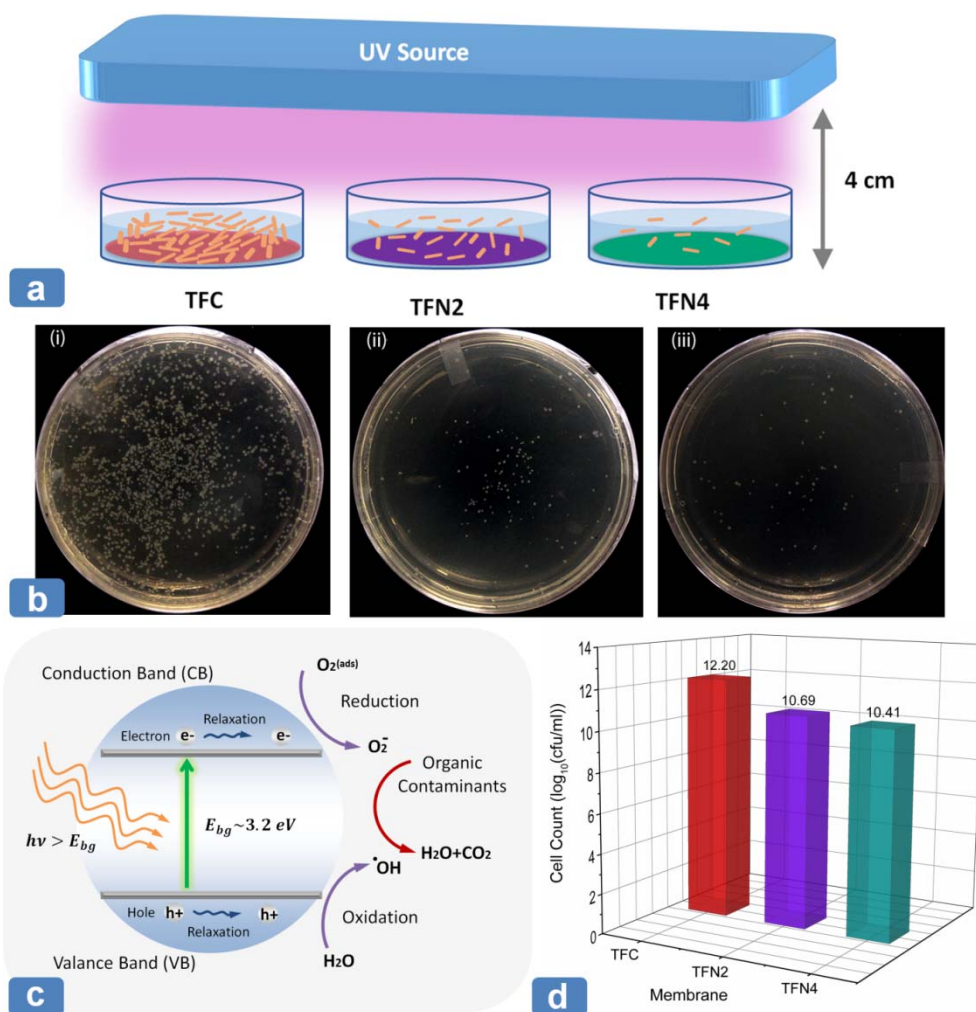


Figure 5.17: (a) Schematic view of the measurement of the antibacterial activity of TFN membranes; (b) Images of the E. coli colonies formed in the plate of UV-treated (i) TFC, (ii) TFN2 and (iii) TFN4 membranes; (c) Mechanism for PCT activity of  $\text{TiO}_2$  NPs under UV irradiation; (d) Number of E. coli colonies counted on the plate of TFC, TFN2 and TFN4 membranes after 30 minutes of UV irradiation.

## 5.4 Conclusion

In the present work, it we demonstrated that phase inversion casting of PES membranes with ITO NPs resulted in a hybrid membrane with improved thermal, electrical and antifouling properties with respect to unmodified PES membrane. The PES/ITO membrane showed also superior characteristics in comparison to PES/TiO<sub>2</sub>, PES/SiO<sub>2</sub>, and PES/Al<sub>2</sub>O<sub>3</sub> nanocomposite membranes. These attributes of the novel PES/ITO nanocomposite membrane can render it more suitable for high temperature filtration applications. Furthermore, the electrical properties of the membranes make them suitable for a variety of membrane based applications that involve beneficial use of electric fields for flux enhancement and fouling mitigation. A robust method of fabrication of TFN membrane was also presented by incorporation of the TiO<sub>2</sub> NPs into the PA layer. The fabrication process includes synthesis of highly stable TiO<sub>2</sub> NPs using BST reaction in heptane and then employing the NPs suspension as an additive to TMC solution during the IP reaction. The resulting TFN PA-TiO<sub>2</sub> membranes showed and enhanced thermal stability and anti-biofouling properties compared to unmodified TFC PA membranes. These features make the synthesized TFN membranes as potential candidates for applications where the treatment of high-temperature streams containing biomaterials is desirable.

# Chapter 6

## Conclusion and future work

## 6.1 Conclusions

The development of nano-enabled composite materials has led to a paradigm shift in the manufacture of high-performance nanocomposite membranes with enhanced permeation, thermo-mechanical, and antibacterial properties. The major challenges to the successful incorporation of NPs to the polymer films are (i) the severe aggregation of the NPs in the monomer containing solutions and (ii) the weak compatibility of NPs with the host polymer matrix. These two phenomena lead to the formation of non-selective voids at the interface of the polymer and NPs, which adversely affect the separation performance of the nanocomposite polymer films. To overcome these challenges, systematic studies were conducted in this research to fabricate robust TFC and TFN membranes with enhanced permeation, thermomechanical, electrical and antifouling properties.

Initially, the synergistic effects of the monomers (MPD and TMC) concentration, IP reaction time and curing temperature was studied using a robust design of experiment method know as Taguchi. The main objectives in this part were to (i) fundamentally understand the role of each synthesis parameters, (ii) to identify the most influential parameters affecting the physicochemical characteristics of the membranes, and (iii) to control and optimize the final permeation performance of the resulting membranes. By varying the considered control parameters simultaneously using a Taguchi design, it was found that monomer concentration and curing temperature significantly affect water permeation by creating a substantial change in both internal and surface morphology of the PA films. More importantly, a strong interaction between monomer concentration was observed, which demonstrates the importance of smart adjustment of these parameters in the preparation process. Based on analysis of variance, the contribution of the synthesis parameters towards change in water permeation was determined as: curing temperature > MPD concentration ~ TMC concentration > reaction time (see chapter 3 for complete discussion). Similar approach was taken to investigate the effect of different types of chemical additives to improve the permeation performance of the TFC PA membranes. Based on the designed table of experimentations, certain concentration of SDS as a surfactant, TEA as an acid scavenger, DMSO as a co-solvent, and CSA as a pH regulator were added into the amine solution. The experimental results showed that increasing the concentration of CSA, DMSO and TEA in the MPD solution enhanced the water permeation of the membranes. In contrast, addition of higher concentrations of SDS resulted in denser TFC membranes with lower water flux and higher salt

rejection. Based on the analysis of variance, the contribution of the additives to the variation of the water flux was in the order of SDS > DMSO > CSA > TEA (see chapter 3 for more results). In addition to the above mentioned chemical additives, the effect of adding monohydric and polyhydric alcohols into the MPD solution on the surface morphology and permeation properties of the TFC PA membranes was studied. The experimental results revealed that addition of alcohols with low molar volumes such as ethanol and ethylene glycol significantly improved the water flux of the modified TFC membranes. However, in the case of alcohols with large molar volumes, such as polyhydric xylitol, the water flux enhanced by increasing the alcohol concentration up to ~1.0 wt.%, and then decreased, suggesting the presence of an optimum concentration of xylitol. This observation indicated the presence of a complex interaction between the hydrophilic hydroxyl groups and hydrophobic aliphatic carbon chain in the structure of large alcohol molecules. Most importantly, all the modified membranes showed higher salt rejection percentage than the original membrane which is highly desirable for fabrication of high-performance TFC membranes (see chapter 3 for complete discussion). The findings of this study provide useful guidelines for the development of high performance TFC PA membranes by adjusting the synthesis conditions as well as the additives concentration in the amine-aqueous solution.

In order to control and enhance the water permeability of TFC PA membranes, an innovative thermal adjustment to IP reaction was proposed. It was found that reducing the temperature of the TMC-organic solution down to -20 °C prior to IP reaction effectively reduced the thickness of the PA selective layer and thus significantly enhanced water permeability of the resulting TFC membranes. The results confirmed that the TFC membranes, synthesized at sub-zero temperatures of organic solution, had thinner and smoother PA layer with a greater degree of cross-linking and wettability compared to the PA films prepared at 50 °C. The most water permeable membrane was prepared at -20 °C and exhibited nine times higher water flux compared to the membrane synthesized at room temperature. The performance of lab-synthesized TFC membranes was also evaluated for the treatment of boiler feed water of SAGD process using FO filtration setup. The results showed superior permeation properties of lab-made membranes to commercially available TFC-FO membranes. The greater performance of the lab-made TFC membranes attributed to the thinner PA selective layer and lower structural parameter ( $451 \pm 13$ ) of the lab-made membranes compared to the commercial membrane ( $1770 \mu\text{m}$ ) which alleviated the effect of internal concentration polarization (ICP) remarkably (see chapter 4 for

complete discussion). The method proposed here can be effectively applied for energy- and cost-efficient development of high throughput TFC FO membranes.

To develop nanocomposite membranes, the effect of incorporation of metal oxide NPs to the top PA layer as well as bottom PES sublayer was studied separately. First, the effect of addition of conductive ITO NPs into PES casting solution to form an ITO doped phase inversion PES membrane was studied. The experimental results showed that the incorporation of ITO NPs into the PES matrix improved thermal and electrical properties of the resulting nanocomposite membrane. Also, the PES-ITO membrane demonstrated an enhanced antifouling propensity without any loss in separation efficiency compared to unmodified PES membrane. The combination of ITO NPs and the PES membranes provides a pathway to develop antifouling microfiltration and ultrafiltration membranes with a higher thermal tolerance and tunable electrical characteristics. Regarding the addition of NPs to the top thin PA layer, an efficient method was proposed to mitigate the aggregation of the NPs in the monomer solution. This approach relies on the simultaneous synthesis and surface functionalization of  $\text{TiO}_2$  NPs in an organic solvent (heptane) via BST reaction. The resulting stable suspension of the  $\text{TiO}_2$  NPs in heptane was then utilized in the IP reaction where the NPs were entrapped within the matrix of the host membrane.  $\text{TiO}_2$  NPs of 10 nm were effectively incorporated into the thin PA layer and improved the thermal stability and anti-biofouling properties of the resulting TFN membranes. These features have made the synthesized TFN PA- $\text{TiO}_2$  membranes potent candidates for applications where the treatment of high-temperature streams containing biomaterials is desirable.

## 6.2 Future work

The systematic studies in chapter 3 on the effect of synthesis conditions and chemical additives can be extended to consider the properties of the PES sublayer. In general, the hydrophilicity and surface porosity of the support layer as well as its uniform and complete impregnation with amine solution has significant impact on the permeation characteristics of the resulting PA film. Hence, it is worth studying the synergistic effects of amine concentration, surfactant concentration and the porosity of the support layer on the final physicochemical properties of the PA film. Furthermore, the PA membranes in this research were fabricated using MPD and TMC as reacting monomers. The investigation on the effect of co-presence of two or more diamine and acyl chloride monomers in the aqueous and organic solution, respectively, may reveal valuable information for tunable fabrication of

the PA membranes. The number of reacting functional groups of the monomers, their partitioning rates and affinity to dissolve into water and organic phases may result in remarkably different structural and permeation characteristics compared to PA membranes prepared from only MPD and TFC monomers.

Regarding the studies on thermal adjustment of IP reaction in chapter 4, there is still room for further investigation of the effect of temperature on the polymerization reaction. The experimental part can be extended to other organic solvents with different physicochemical properties than heptane, hexane and cyclohexane. Moreover, the temperature of the amine solution can be altered to have more variation and flexibility for controlling the PA film formation. Also, molecular dynamic simulation can be done to elucidate how variation in the temperature of monomer solution can alter the monomers' diffusion and partitioning rate to the reaction reason during the IP reaction. The results of the MD simulation can provide useful information to correlate the final characteristics of the PA film to thermal variation during the polymerization reaction.

In chapter 5, the experimental results about imparting different functionalities to the host membrane using metal oxide NPs were presented. As a continuation of this work, the application of conductive PES-ITO membranes in an electrofiltration setup is worth being studied. The PES-ITO membranes can be placed between two metal electrodes or it can even be used as positive- or negative-polarity electrode to establish an electric field in the feed stream using externally applied voltage. The fouling propensity of the modified PES-ITO membranes can be compared with unmodified PES membrane during the electrofiltration process. Regarding the synthesis of TFN PA-TiO<sub>2</sub> membranes, further studies can be done to (i) optimize the synthesis of TiO<sub>2</sub> NPs using BST reaction in order to minimize the loading of dispersing agent without deteriorating the size distribution, stability and crystallinity of the resulting NPs in organic solvent, (ii) applying the surface functionalization technique, presented in this chapter, for the integration of the other nanofillers whenever the solvothermal reaction is a possible synthesis route, (iii) evaluate the PCT activity of the PA-TiO<sub>2</sub> membranes in purification of the feed streams which contain organic matter and bio-foulants.



## 6.3 List of contributions

The outcomes of this research is published and presented in the following journals and conferences:

### 6.3.1 Journal Papers

1. B. Khorshidi, I. Biswas, T. Thundat, M. Sadrzadeh, A novel approach for the fabrication of thin film polyamide-TiO<sub>2</sub> nanocomposite membranes with enhanced thermal stability and anti-biofouling propensity, *Scientific Reports* (under revision).
2. B. Khorshidi, T. Thundat, D. Pernitsky, M. Sadrzadeh, A parametric study on the synergistic impacts of chemical additives on permeation properties of thin film composite polyamide membrane, *J. Memb. Sci.* 535 (2017) 248–257. doi:10.1016/j.memsci.2017.04.052.
3. B. Khorshidi, B. Soltannia, T. Thundat, M. Sadrzadeh, Synthesis of thin film composite polyamide membranes: Effect of monohydric and polyhydric alcohol additives in aqueous solution, *J. Memb. Sci.* 523 (2017) 336–345. doi:10.1016/j.memsci.2016.09.062.
4. B. Khorshidi, T. Thundat, B.A. Fleck, M. Sadrzadeh, A novel approach toward fabrication of high performance thin film composite polyamide membranes, *Sci. Rep.* 6 (2016) 22069. doi:10.1038/srep22069.
5. B. Khorshidi, A. Bhinder, T. Thundat, D. Pernitsky, M. Sadrzadeh, Developing high throughput thin film composite polyamide membranes for forward osmosis treatment of SAGD produced water, *J. Memb. Sci.* 511 (2016) 29–39. doi:10.1016/j.memsci.2016.03.052.
6. B. Khorshidi, J. Hajinasiri, G. Ma, S. Bhattacharjee, M. Sadrzadeh, Thermally resistant and electrically conductive PES/ITO nanocomposite membrane, *J. Memb. Sci.* 500 (2016) 151–160. doi:10.1016/j.memsci.2015.11.015.
7. B. Khorshidi, T. Thundat, B.A. Fleck, M. Sadrzadeh, Thin film composite polyamide membranes: Parametric study on the influence of synthesis conditions, *RSC Adv.* 5 (2015) 54985–54997. doi:10.1039/C5RA08317F.

### 6.3.2 Conference presentations

1. B. Khorshidi, M. Sadrzadeh, Application of co-solvents in synthesis of high performance thin film composite membranes via interfacial polymerization reaction, 3rd International Conference on Desalination Using Membrane Technology, Gran Canaria, Spain, April 2017.
2. B. Khorshidi, A. Bhinder, T. Thundat, D. Pernitsky, M. Sadrzadeh, Fabrication of high performance thin film composite membranes for forward osmosis treatment of SAGD water, 3rd International Conference on Desalination Using Membrane Technology, Gran Canaria, Spain, April 2017.
3. Z. Almansoori, B. Khorshidi, B. Sadri. M. Sadrzadeh, Parametric study on the stability of indium tin oxide nanoparticles in organic solvent as a prerequisite for synthesizing defect-free thin film nanocomposite membranes, 3rd International Conference on Desalination Using Membrane Technology, Gran Canaria, Spain, April 2017.
4. B. Khorshidi, H. Nazaripoor, M. Sadrzadeh, Thin film composite PA/PES membrane: Parametric study on the effects of surfactant, phase-transfer catalyst and co-solvent, Desalination for the Environment: Clean Water and Energy, Rome, Italy, May 2016.
5. B. Khorshidi, B. Soltannia, M. Sadrzadeh, Synthesis of thin film composite polyamide membranes: Effect of monohydric and polyhydric alcohol additives in aqueous solution, Desalination for the Environment: Clean Water and Energy, Rome, Italy, May 2016.
6. B. Khorshidi, M. Sadrzadeh, Membranes for SAGD Produced Water Treatment, COSIA AI-EES Water Conference, Calgary, Canada, March 2016.
7. B. Khorshidi, D. Pernitsky, M. Sadrzadeh, PA/PES thin film composite membrane: Parametric study on the effects of reaction and curing conditions, 64th Canadian Chemical Society of Chemical Engineering (CSCHE), Niagara Falls, Canada, October 2014.

# Reference

- [1] Global Risks Report, 11th ed., World Economic Forum, 2016.
- [2] M. Hightower, S.A. Pierce, The energy challenge, *Nature*. 452 (2008) 285–6. doi:10.1038/452285a.
- [3] Progress on sanitation and drinking water– 2015 update and MDG assessment, World Health Organization and UNICEF Joint Monitoring Programme (JMP), n.d.
- [4] Water: a shared responsibility, UNESCO: World Water Development Report, 2006.
- [5] M.A. Shannon, P.W. Bohn, M. Elimelech, J.G. Georgiadis, B.J. Mariñas, A.M. Mayes, Science and technology for water purification in the coming decades., *Nature*. 452 (2008) 301–10. doi:10.1038/nature06599.
- [6] D.W. Jennings, A. Shaikh, Heat-exchanger deposition in an inverted steam-assisted Gravity drainage operation . Part 1 . inorganic and organic analyses of deposit samples, *Energy & Fuels*. 21 (2007) 176–184.
- [7] S. Wang, E. Axcell, R. Bosch, V. Little, Effects of chemical application on antifouling in steam-assisted gravity drainage operations, *Energy & Fuels*. 19 (2005) 1425–1429. doi:10.1021/ef049808l.
- [8] S. Guha Thakurta, A. Maiti, D.J. Pernitsky, S. Bhattacharjee, Dissolved organic matter in steam assisted gravity drainage boiler blow-down water, *Energy & Fuels*. 27 (2013) 3883–3890. doi:10.1021/ef4002154.
- [9] W.F. Heins, Technical advancements in SAGD evaporative produced water treatment, *J. Can. Pet. Technol.* 48 (2009) 27–32.
- [10] R.W. Baker, *Membrane Technology and Application*, 2nd Editio, Wiley, 2004.
- [11] H. Strathmann, K. Kock, P. Amar, R.W. Baker, The formation mechanism of asymmetric membranes, *Desalination*. 16 (1975) 179–203.
- [12] M. Mulder, *Basic Principles of Membrane Technology*, Springer Netherlands, Dordrecht, 1996. doi:10.1007/978-94-009-1766-8.
- [13] U. Zhanat, E. Sharipzhan, Mechanism of Gases Transfer through Polymer Membranes and Membrane Module Calculation Model to Separate Gases, *Procedia Technol.* 1 (2012) 356–361. doi:10.1016/j.protcy.2012.02.074.
- [14] X. Li, Y. Wang, X. Lu, C. Xiao, Morphology changes of polyvinylidene fluoride membrane under different phase separation mechanisms, *J. Memb. Sci.* 320 (2008) 477–482. doi:10.1016/j.memsci.2008.04.033.

- [15] W.T.D. Schafer, A I, Fane, A G, Nanofiltration Principles and Applications, n.d.
- [16] I.M.W. C.A. Smolders, A.J. Reuvers, R.M. Boom, Microstructures in phaseinversionmembranes .1. Formation of macrovoids, *J. Memb. Sci.* 73 (1992) 259–275.
- [17] W.J. Lau, A.F. Ismail, N. Misdan, M.A. Kassim, A recent progress in thin film composite membrane: A review, *Desalination.* 287 (2012) 190–199. doi:10.1016/j.desal.2011.04.004.
- [18] C. Fritzmann, J. Löwenberg, T. Wintgens, T. Melin, State-of-the-art of reverse osmosis desalination, *Desalination.* 216 (2007) 1–76. doi:10.1016/j.desal.2006.12.009.
- [19] A.K. Pabby, S.S.H. Rizvi, A.M.S. Requena, Handbook of Membrane Separations: Chemical, Pharmaceutical, Food, and Biotechnological Applications, CRC Press, 2008.
- [20] R.W. Baker, Membrane Technology and Applications, 3rd ed., John Wiley & Sons, Inc., 2012.
- [21] I. Pinnau, B. D. Freeman, Membrane Formation and Modification, American Chemical Society, Washington, DC, 1999. doi:10.1021/bk-2000-0744.
- [22] R.J. Petersen, Composite reverse osmosis and nanofiltration membranes, *J. Memb. Sci.* 83 (1993) 81–150. doi:10.1016/0376-7388(93)80014-O.
- [23] E.M. V. Hoek, A.S. Kim, M. Elimelech, Influence of crossflow membrane filter geometry and shear rate on colloidal fouling in reverse osmosis and nanofiltration separations, *Environ. Eng. Sci.* 19 (2002) 357–372. doi:10.1089/109287502320963364.
- [24] K. V Peinemann, S.P. Nunes, Membranes for Water Treatment, WILEY-VCH Verlag GmbH & Co. KGaA, Weinheim, Germany, 2010.
- [25] A.L. Zydney, Stagnant film model for concentration polarization in membrane systems, *J. Memb. Sci.* 130 (1997) 275–281. doi:10.1016/S0376-7388(97)00006-9.
- [26] J.E. Cadotte, Interfacially synthesized reverse osmosis membrane, U.S. Patent 4277344 A, 1981.
- [27] R.E. Larson, J.E. Cadotte, R.J. Petersen, The FT-30 seawater reverse osmosis membrane-element test results, *Desalination.* 38 (1981) 473–483. doi:10.1016/S0011-9164(00)86092-0.
- [28] F. Meng, S.-R. Chae, A. Drews, M. Kraume, H.-S. Shin, F. Yang, Recent advances in membrane bioreactors (MBRs): Membrane fouling and

- membrane material., *Water Res.* 43 (2009) 1489–512. doi:10.1016/j.watres.2008.12.044.
- [29] D. Li, H. Wang, Recent developments in reverse osmosis desalination membranes, *J. Mater. Chem.* 20 (2010) 4551. doi:10.1039/b924553g.
- [30] D. Li, Y. Yan, H. Wang, Recent advances in polymer and polymer composite membranes for reverse and forward osmosis processes, *Prog. Polym. Sci.* 61 (2016) 104–155. doi:10.1016/j.progpolymsci.2016.03.003.
- [31] A.W. Mohammad, Y.H. Teow, W.L. Ang, Y.T. Chung, D.L. Oatley-Radcliffe, N. Hilal, Nanofiltration membranes review: Recent advances and future prospects, *Desalination.* 356 (2014) 226–254. doi:10.1016/j.desal.2014.10.043.
- [32] K.P. Lee, T.C. Arnot, D. Mattia, A review of reverse osmosis membrane materials for desalination—Development to date and future potential, *J. Memb. Sci.* 370 (2011) 1–22. doi:10.1016/j.memsci.2010.12.036.
- [33] W. Salim, W.S.W. Ho, Recent developments on nanostructured polymer-based membranes, *Curr. Opin. Chem. Eng.* 8 (2015) 76–82. doi:http://dx.doi.org/10.1016/j.coche.2015.03.003.
- [34] L.Y. Ng, A.W. Mohammad, C.P. Leo, N. Hilal, Polymeric membranes incorporated with metal/metal oxide nanoparticles: A comprehensive review, *Desalination.* 308 (2013) 15–33. doi:10.1016/j.desal.2010.11.033.
- [35] X. Qu, P.J.J. Alvarez, Q. Li, Applications of nanotechnology in water and wastewater treatment, *Water Res.* 47 (2013) 3931–46. doi:10.1016/j.watres.2012.09.058.
- [36] J. Theron, J.A. Walker, T.E. Cloete, Nanotechnology and water treatment: Applications and emerging opportunities, *Crit. Rev. Microbiol.* 34 (2008) 43–69. doi:10.1080/10408410701710442.
- [37] C.H. Ahn, Y. Baek, C. Lee, S.O. Kim, S. Kim, S. Lee, et al., Carbon nanotube-based membranes: Fabrication and application to desalination, *J. Ind. Eng. Chem.* 18 (2012) 1551–1559. doi:10.1016/j.jiec.2012.04.005.
- [38] N. Misdan, W.J. Lau, A.F. Ismail, Seawater reverse osmosis (SWRO) desalination by thin-film composite membrane—current development, challenges and future prospects, *Desalination.* 287 (2012) 228–237. doi:10.1016/j.desal.2011.11.001.
- [39] B. Khorshidi, T. Thundat, B.A. Fleck, M. Sadrzadeh, Thin film composite polyamide membranes: Parametric study on the influence of synthesis conditions, *RSC Adv.* 5 (2015) 54985–54997. doi:10.1039/C5RA08317F.
- [40] B. Khorshidi, T. Thundat, D. Pernitsky, M. Sadrzadeh, A parametric study

- on the synergistic impacts of chemical additives on permeation properties of thin film composite polyamide membrane, *J. Memb. Sci.* 535 (2017) 248–257. doi:10.1016/j.memsci.2017.04.052.
- [41] B. Khorshidi, B. Soltannia, T. Thundat, M. Sadrzadeh, Synthesis of thin film composite polyamide membranes: Effect of monohydric and polyhydric alcohol additives in aqueous solution, *J. Memb. Sci.* 523 (2017) 336–345. doi:10.1016/j.memsci.2016.09.062.
- [42] B. Khorshidi, T. Thundat, B.A. Fleck, M. Sadrzadeh, A novel approach toward fabrication of high performance thin film composite polyamide membranes, *Sci. Rep.* 6 (2016) 22069. doi:10.1038/srep22069.
- [43] B. Khorshidi, J. Hajinasiri, G. Ma, S. Bhattacharjee, M. Sadrzadeh, Thermally resistant and electrically conductive PES/ITO nanocomposite membrane, *J. Memb. Sci.* 500 (2016) 151–160. doi:10.1016/j.memsci.2015.11.015.
- [44] B. Khorshidi, A. Bhinder, T. Thundat, D. Pernitsky, M. Sadrzadeh, Developing high throughput thin film composite polyamide membranes for forward osmosis treatment of SAGD produced water, *J. Memb. Sci.* 511 (2016) 29–39. doi:10.1016/j.memsci.2016.03.052.
- [45] Z. Almansoori, B. Khorshidi, B. Sadri, M. Sadrzadeh, Parametric study on the stabilization of metal oxide nanoparticles in organic solvents: A case study with indium tin oxide (ITO) and heptane, *Ultrason. Sonochem.* (2017). doi:10.1016/j.ultsonch.2017.09.012.
- [46] R. Mohan, J. Drbohlavova, J. Hubalek, Water-dispersible TiO<sub>2</sub> nanoparticles via a biphasic solvothermal reaction method, *Nanoscale Res. Lett.* 8 (2013) 503. doi:10.1186/1556-276X-8-503.
- [47] P.M. Forster, P.M. Thomas, A.K. Cheetham, Biphasic solvothermal synthesis: A new approach for hybrid inorganic–organic materials, *Chem. Mater.* 14 (2002) 17–20. doi:10.1021/cm010820q.
- [48] S. Gupta, M. Tripathi, A review on the synthesis of TiO<sub>2</sub> nanoparticles by solution route, *Open Chem.* 10 (2012) 279–294. doi:10.2478/s11532-011-0155-y.
- [49] S. Kumar, V.K. Aswal, Tuning of nanoparticle-surfactant interactions in aqueous system., *J. Phys. Condens. Matter.* 23 (2011) 35101. doi:10.1088/0953-8984/23/3/035101.
- [50] M.J. Rosen, J.T. Kunjappu, *Surfactants and Interfacial Phenomena*, 4th ed., John Wiley & Sons, Inc., 2012.
- [51] S. Paria, K.C. Khilar, A review on experimental studies of surfactant

- adsorption at the hydrophilic solid-water interface., *Adv. Colloid Interface Sci.* 110 (2004) 75–95. doi:10.1016/j.cis.2004.03.001.
- [52] K.J. Klabunde, R.M. Richards, *Nanoscale Materials in Chemistry*, 2nd ed., John Wiley & Sons, Inc., 2009.
- [53] J.W. Krumpfer, T. Schuster, M. Klapper, K. Müllen, Make it nano-Keep it nano, *Nano Today*. 8 (2013) 417–438. doi:10.1016/j.nantod.2013.07.006.
- [54] R. a Sperling, W.J. Parak, Surface modification, functionalization and bioconjugation of colloidal inorganic nanoparticles, *Philos. Trans. A. Math. Phys. Eng. Sci.* 368 (2010) 1333–1383. doi:10.1098/rsta.2009.0273.
- [55] M. Sadrzadeh, S. Bhattacharjee, Rational design of phase inversion membranes by tailoring thermodynamics and kinetics of casting solution using polymer additives, *J. Memb. Sci.* 441 (2013) 31–44. doi:10.1016/j.memsci.2013.04.009.
- [56] O. Akin, F. Temelli, Probing the hydrophobicity of commercial reverse osmosis membranes produced by interfacial polymerization using contact angle, XPS, FTIR, FE-SEM and AFM, *Desalination*. 278 (2011) 387–396. doi:10.1016/j.desal.2011.05.053.
- [57] W. Chen, Y. Su, J. Peng, X. Zhao, Z. Jiang, Y. Dong, et al., Efficient wastewater treatment by membranes through constructing tunable antifouling membrane surfaces, *Environ. Sci. Technol.* 45 (2011) 6545–6552. doi:10.1021/es200994n.
- [58] F. Gao, G. Zhang, Q. Zhang, X. Zhan, F. Chen, Improved antifouling properties of poly(ether sulfone) membrane by incorporating the amphiphilic comb copolymer with mixed poly(ethylene glycol) and poly(dimethylsiloxane) brushes, *Ind. Eng. Chem. Res.* 54 (2015) 8789–8800. doi:10.1021/acs.iecr.5b02864.
- [59] S. Loeb, Effect of porous support fabric on osmosis through a Loeb-Sourirajan type asymmetric membrane, *J. Memb. Sci.* 129 (1997) 243–249. doi:10.1016/S0376-7388(96)00354-7.
- [60] T.Y. Cath, M. Elimelech, J.R. McCutcheon, R.L. McGinnis, A. Achilli, D. Anastasio, et al., Standard methodology for evaluating membrane performance in osmotically driven membrane processes, *Desalination*. 312 (2013) 31–38. doi:10.1016/j.desal.2012.07.005.
- [61] K.L. Lee, R.W. Baker, H.K. Lonsdale, Membranes for power generation by pressure-retarded osmosis, *J. Memb. Sci.* 8 (1981) 141–171.
- [62] R.K. Roy, *Design of Experiments Using The Taguchi Approach: 16 Steps to Product and Process Improvement*, John Wiley & Sons, Inc., 2001.

- [63] R.K. Roy, A primer on the Taguchi method, Second Edi, Society of Manufacturing Engineering, 2010.
- [64] G.-Y. Chai, W.B. Krantz, Formation and characterization of polyamide membranes via interfacial polymerization, *J. Memb. Sci.* 93 (1994) 175–192. doi:10.1016/0376-7388(94)80006-5.
- [65] A. Prakash Rao, N.V. Desai, R. Rangarajan, Interfacially synthesized thin film composite RO membranes for seawater desalination, *J. Memb. Sci.* 124 (1997) 263–272. doi:10.1016/S0376-7388(96)00252-9.
- [66] A.P. Rao, S. V. Joshi, J.J. Trivedi, C. V. Devmurari, V.J. Shah, Structure–performance correlation of polyamide thin film composite membranes: Effect of coating conditions on film formation, *J. Memb. Sci.* 211 (2003) 13–24. doi:10.1016/S0376-7388(02)00305-8.
- [67] Y. Song, P. Sun, L. Henry, B. Sun, Mechanisms of structure and performance controlled thin film composite membrane formation via interfacial polymerization process, *J. Memb. Sci.* 251 (2005) 67–79. doi:10.1016/j.memsci.2004.10.042.
- [68] I.J. Roh, A.R. Greenberg, V.P. Khare, Synthesis and characterization of interfacially polymerized polyamide thin films, *Desalination*. 191 (2006) 279–290. doi:10.1016/j.desal.2006.03.004.
- [69] A.K. Ghosh, B.-H. Jeong, X. Huang, E.M.V. Hoek, Impacts of reaction and curing conditions on polyamide composite reverse osmosis membrane properties, *J. Memb. Sci.* 311 (2008) 34–45. doi:10.1016/j.memsci.2007.11.038.
- [70] M. Liu, S. Yu, J. Tao, C. Gao, Preparation, structure characteristics and separation properties of thin-film composite polyamide-urethane seawater reverse osmosis membrane, *J. Memb. Sci.* 325 (2008) 947–956. doi:10.1016/j.memsci.2008.09.033.
- [71] Y. Jin, Z. Su, Effects of polymerization conditions on hydrophilic groups in aromatic polyamide thin films, *J. Memb. Sci.* 330 (2009) 175–179. doi:10.1016/j.memsci.2008.12.055.
- [72] W. Xie, G.M. Geise, B.D. Freeman, H.-S. Lee, G. Byun, J.E. McGrath, Polyamide interfacial composite membranes prepared from m-phenylene diamine, trimesoyl chloride and a new disulfonated diamine, *J. Memb. Sci.* 403–404 (2012) 152–161. doi:10.1016/j.memsci.2012.02.038.
- [73] C. Klaysom, S. Hermans, A. Gahlaut, S. Van Craenenbroeck, I.F.J. Vankelecom, Polyamide/Polyacrylonitrile (PA/PAN) thin film composite osmosis membranes: Film optimization, characterization and performance



- evaluation, *J. Memb. Sci.* 445 (2013) 25–33. doi:10.1016/j.memsci.2013.05.037.
- [74] S. Hermans, H. Mariën, E. Dom, R. Bernstein, I.F.J. Vankelecom, Simplified synthesis route for interfacially polymerized polyamide membranes, *J. Memb. Sci.* 451 (2014) 148–156. doi:10.1016/j.memsci.2013.10.005.
- [75] J. Xiang, Z. Xie, M. Hoang, K. Zhang, Effect of amine salt surfactants on the performance of thin film composite poly(piperazine-amide) nanofiltration membranes, *Desalination*. 315 (2013) 156–163. doi:10.1016/j.desal.2012.10.038.
- [76] S.Y. Kwak, S.G. Jung, S.H. Kim, Structure-motion-performance relationship of flux-enhanced reverse osmosis (RO) membranes composed of aromatic polyamide thin films, *Environ. Sci. Technol.* 35 (2001) 4334–40.
- [77] C. Kong, M. Kanezashi, T. Yamomoto, T. Shintani, T. Tsuru, Controlled synthesis of high performance polyamide membrane with thin dense layer for water desalination, *J. Memb. Sci.* 362 (2010) 76–80. doi:10.1016/j.memsci.2010.06.022.
- [78] T. Kamada, T. Ohara, T. Shintani, T. Tsuru, Optimizing the preparation of multi-layered polyamide membrane via the addition of a co-solvent, *J. Memb. Sci.* 453 (2014) 489–497. doi:10.1016/j.memsci.2013.11.028.
- [79] A.F. Ismail, M. Padaki, N. Hilal, T. Matsuura, W.J. Lau, Thin film composite membrane — Recent development and future potential, *Desalination*. 356 (2015) 140–148. doi:10.1016/j.desal.2014.10.042.
- [80] Y. Cui, X.-Y. Liu, T.-S. Chung, Enhanced osmotic energy generation from salinity gradients by modifying thin film composite membranes, *Chem. Eng. J.* 242 (2014) 195–203. doi:10.1016/j.cej.2013.12.078.
- [81] V. Czitrom, One-factor-at-a-time versus designed experiments, *Am. Stat.* 53 (2012) 126–131.
- [82] D.D. Frey, F. Engelhardt, E.M. Greitzer, A role for “one-factor-at-a-time” experimentation in parameter design, *Res. Eng. Des.* 14 (2003) 65–74. doi:10.1007/s00163-002-0026-9.
- [83] B.C. Smith, *Infrared Spectral Interpretation: A Systematic Approach*, CRC Press, 1998.
- [84] C. Tang, Y. Kwon, J. Leckie, Probing the nano- and micro-scales of reverse osmosis membranes—A comprehensive characterization of physiochemical properties of uncoated and coated membranes by XPS, TEM, ATR-FTIR, and streaming potential measurements, *J. Memb. Sci.* 287 (2007) 146–156.

- doi:10.1016/j.memsci.2006.10.038.
- [85] P.W. Morgan, S.L. Kwolek, Interfacial polycondensation. II. Fundamentals of polymer formation at liquid interfaces, *J. Polym. Sci.* 40 (1959) 299–327. doi:10.1002/pol.1959.1204013702.
- [86] J.E. Cadotte, R.J. Petersen, R.E. Larson, E.E. Erickson, A new thin-film composite seawater reverse osmosis membrane, *Desalination*. 32 (1980) 25–31. doi:10.1016/S0011-9164(00)86003-8.
- [87] J.E. Cadotte, Evolution of composite reverse osmosis membranes, in: *Mater. Sci. Synth. Membr.*, ACS Publications, London, 1985: pp. 273–294. doi:10.1021/bk-1985-0269.ch012.
- [88] H. Yan, X. Miao, J. Xu, G. Pan, Y. Zhang, Y. Shi, et al., The porous structure of the fully-aromatic polyamide film in reverse osmosis membranes, *J. Memb. Sci.* 475 (2015) 504–510. doi:10.1016/j.memsci.2014.10.052.
- [89] A. V. Berezkin, A.R. Khokhlov, Mathematical modeling of interfacial polycondensation, *J. Polym. Sci. Part B Polym. Phys.* 44 (2006) 2698–2724. doi:10.1002/polb.20907.
- [90] B.S. Lalia, V. Kochkodan, R. Hashaikeh, N. Hilal, A review on membrane fabrication: Structure, properties and performance relationship, *Desalination*. 326 (2013) 77–95. doi:10.1016/j.desal.2013.06.016.
- [91] R.W. Baker, *Membrane Technology and Applications*, 3rd ed., John Wiley & Sons, Chichester, UK, 2012.
- [92] V. Freger, Nanoscale heterogeneity of polyamide membranes formed by interfacial polymerization, *Langmuir*. 19 (2003) 4791–4797. doi:10.1021/la020920q.
- [93] V. Freger, S. Srebnik, Mathematical model of charge and density distributions in interfacial polymerization of thin films, *J. Appl. Polym. Sci.* 88 (2003) 1162–1169. doi:10.1002/app.11716.
- [94] V. Freger, Kinetics of film formation by interfacial polycondensation., *Langmuir*. 21 (2005) 1884–94. doi:10.1021/la048085v.
- [95] M.M. Kłosowski, C.M. McGilvery, Y. Li, P. Abellan, Q. Ramasse, J.T. Cabral, et al., Micro-to nano-scale characterisation of polyamide structures of the SW30HR RO membrane using advanced electron microscopy and stain tracers, *J. Memb. Sci.* 520 (2016) 465–476. doi:10.1016/j.memsci.2016.07.063.
- [96] C.M. Hansen, *Hansen Solubility Parameters: A User's Handbook*, 2nd ed., CRC Press, Inc., Boca Raton FL, 2007.

- [97] X. Lu, S. Nejati, Y. Choo, C.O. Osuji, J. Ma, M. Elimelech, Elements provide a clue: Nanoscale characterization of thin-film composite polyamide membranes, *ACS Appl. Mater. Interfaces.* 7 (2015) 16917–22. doi:10.1021/acsami.5b05478.
- [98] V. Freger, Swelling and morphology of the skin layer of polyamide composite membranes: An atomic force microscopy study, (2004). doi:10.1021/ES034815U.
- [99] S. Karan, Z. Jiang, A.G. Livingston, Sub-10 nm polyamide nanofilms with ultrafast solvent transport for molecular separation, *Science* (80-. ). 348 (2015).
- [100] T. Fujioka, N. Oshima, R. Suzuki, W.E. Price, L.D. Nghiem, Probing the internal structure of reverse osmosis membranes by positron annihilation spectroscopy: Gaining more insight into the transport of water and small solutes, *J. Memb. Sci.* 486 (2015) 106–118. doi:10.1016/j.memsci.2015.02.007.
- [101] J. Stawikowska, A.G. Livingston, Nanoprobe imaging molecular scale pores in polymeric membranes, *J. Memb. Sci.* 413 (2012) 1–16. doi:10.1016/j.memsci.2012.02.033.
- [102] F.A. Pacheco, I. Pinnau, M. Reinhard, J.O. Leckie, Characterization of isolated polyamide thin films of RO and NF membranes using novel TEM techniques, *J. Memb. Sci.* 358 (2010) 51–59. doi:10.1016/j.memsci.2010.04.032.
- [103] T.D. Nguyen, K. Chan, T. Matsuura, S. Sourirajan, Viscoelastic and statistical thermodynamic approach to the study of the structure of polymer film casting solutions for making RO/UF membranes, *Ind. Eng. Chem. Prod. Res. Dev.* 24 (1985) 655–665. doi:10.1021/i300020a030.
- [104] T.D. Nguyen, T. Matsuura, S. Sourirajan, Effect of nonsolvent additives on the pore size and the pore size distribution of aromatic polyamide RO membranes, *Chem. Eng. Commun.* 54 (1987) 17–36. doi:10.1080/00986448708911895.
- [105] D. Dutta, A. Bhattacharyya, B.N. Ganguly, Microstructural study of aromatic polyamide membrane material, *J. Memb. Sci.* 224 (2003) 127–135. doi:10.1016/j.memsci.2003.08.001.
- [106] R.R. Sharma, S. Chellam, Temperature effects on the morphology of porous thin film composite nanofiltration membranes, *Environ. Sci. Technol.* 39 (2005) 5022–5030. doi:10.1021/es0501363.
- [107] E. Harder, D.E. Walters, Y.D. Bodnar, R.S. Faibish, B. Roux, Molecular

- dynamics study of a polymeric reverse osmosis membrane, *J. Phys. Chem. B.* 113 (2009) 10177–10182. doi:10.1021/jp902715f.
- [108] S.H. Kim, S.-Y. Kwak, T. Suzuki, Positron annihilation spectroscopic evidence to demonstrate the flux-enhancement mechanism in morphology-controlled thin-film-composite (TFC) membrane, *Environ. Sci. Technol.* 39 (2005) 1764–1770. doi:10.1021/es049453k.
- [109] F. Pacheco, R. Sougrat, M. Reinhard, J.O. Leckie, I. Pinnau, 3D visualization of the internal nanostructure of polyamide thin films in RO membranes, *J. Memb. Sci.* 501 (2016) 33–44. doi:10.1016/j.memsci.2015.10.061.
- [110] L. Lin, R. Lopez, G.Z. Ramon, O. Coronell, Investigating the void structure of the polyamide active layers of thin-film composite membranes, *J. Memb. Sci.* 497 (2016) 365–376. doi:10.1016/j.memsci.2015.09.020.
- [111] D.G. Cahill, V. Freger, S.-Y. Kwak, R.J. Petersen, G.-Y. Chai, W.B. Krantz, et al., Microscopy and microanalysis of reverse-osmosis and nanofiltration membranes, *MRS Bull.* 33 (2008) 27–32. doi:10.1557/mrs2008.11.
- [112] S. Hermans, R. Bernstein, A. Volodin, I.F.J. Vankelecom, Study of synthesis parameters and active layer morphology of interfacially polymerized polyamide–polysulfone membranes, *React. Funct. Polym.* 86 (2015) 199–208. doi:10.1016/j.reactfunctpolym.2014.09.013.
- [113] J.E. Cadotte, Reverse osmosis membrane, US4259183 A, 1979.
- [114] L. Zhao, P.C.-Y. Chang, W.S.W. Ho, High-flux reverse osmosis membranes incorporated with hydrophilic additives for brackish water desalination, *Desalination.* 308 (2013) 225–232. doi:10.1016/j.desal.2012.07.020.
- [115] T. Kamada, T. Ohara, T. Shintani, T. Tsuru, Controlled surface morphology of polyamide membranes via the addition of co-solvent for improved permeate flux, *J. Memb. Sci.* 467 (2014) 303–312. doi:10.1016/j.memsci.2014.03.072.
- [116] M. Hirose, K. Ikeda, Method of producing high permeable composite reverse osmosis membrane, US5576057 A, 1996.
- [117] M. Hirose, H. Ito, M. Maeda, K. Tanaka, Highly permeable composite reverse osmosis membrane, method of producing the same, and method of using the same, U.S. Patent 5614099 A, 1997.
- [118] M. Hirose, H. Ito, T. Ohara, Method for producing highly permeable composite reverse osmosis membrane, US5733602 A, 1998.
- [119] J.-Y.K. Koo, Y.S. Yoon, N. Kim, J.-E.K. Kim, Composite polyamide

- reverse osmosis membrane and method of producing the same, US6368507 B1, 2002.
- [120] W.S.W. Ho, Water permeable membranes and methods of making water permeable membranes, US 20080296225 A1, 2008.
- [121] J. Jegal, S.G. Min, K.-H. Lee, Factors affecting the interfacial polymerization of polyamide active layers for the formation of polyamide composite membranes, *J. Appl. Polym. Sci.* 86 (2002) 2781–2787. doi:10.1002/app.11257.
- [122] M. Liu, S. Yu, J. Tao, C. Gao, Preparation, structure characteristics and separation properties of thin-film composite polyamide-urethane seawater reverse osmosis membrane, *J. Memb. Sci.* 325 (2008) 947–956. doi:10.1016/j.memsci.2008.09.033.
- [123] S. Qiu, L. Wu, L. Zhang, H. Chen, C. Gao, Preparation of reverse osmosis composite membrane with high flux by interfacial polymerization of MPD and TMC, *J. Appl. Polym. Sci.* 112 (2009) 2066–2072. doi:10.1002/app.
- [124] P.W. Morgan, S.L. Kwolek, Interfacial polycondensation. II. Fundamentals of polymer formation at liquid interfaces, *J. Polym. Sci. Part A Polym. Chem.* 34 (1996) 531–559. doi:10.1002/pola.1996.816.
- [125] D.W. Van Krevelen, K.T. Nijenhuis, *Properties of Polymers*, 4th Ed., Elsevier, 2009. doi:10.1016/B978-0-08-054819-7.00007-8.
- [126] D.M. Koenhen, C.A. Smolders, The determination of solubility parameters of solvents and polymers by means of correlations with other physical quantities, *J. Appl. Polym. Sci.* 19 (1975) 1163–1179. doi:10.1002/app.1975.070190423.
- [127] T.-H. Young, L.-W. Chen, Pore formation mechanism of membranes from phase inversion process, *Desalination*. 103 (1995) 233–247. doi:10.1016/0011-9164(95)00076-3.
- [128] S.-G. Li, T. van den Boomgaard, C.A. Smolders, H. Strathmann, Physical gelation of amorphous polymers in a mixture of solvent and nonsolvent, *Macromolecules*. 29 (1996) 2053–2059. doi:10.1021/ma9508966.
- [129] C. Jin, C. Yang, F. Chen, Effects on microstructure of NiO–YSZ anode support fabricated by phase-inversion method, *J. Memb. Sci.* 363 (2010) 250–255. doi:10.1016/j.memsci.2010.07.044.
- [130] C.Y. Tang, Y.N. Kwon, J.O. Leckie, Effect of membrane chemistry and coating layer on physiochemical properties of thin film composite polyamide RO and NF membranes II. Membrane physiochemical properties and their dependence on polyamide and coating layers, *Desalination*. 242 (2009) 168–

182.

- [131] F.A. Carey, R.J. Sundberg, *Advanced Organic Chemistry Part A: Structure and Mechanisms*, Fifth Edit, Springer US, 2007.
- [132] R.N. Wenzel, Resistance of solid surfaces to wetting by water, *Ind. Eng. Chem.* 28 (1936) 998–994.
- [133] S. Zhao, L. Zou, C.Y. Tang, D. Mulcahy, Recent developments in forward osmosis: Opportunities and challenges, *J. Memb. Sci.* 396 (2012) 1–21. doi:10.1016/j.memsci.2011.12.023.
- [134] K. Lutchmiah, A.R.D. Verliefde, K. Roest, L.C. Rietveld, E.R. Cornelissen, Forward osmosis for application in wastewater treatment: a review., *Water Res.* 58 (2014) 179–97. doi:10.1016/j.watres.2014.03.045.
- [135] T. Cath, A. Childress, M. Elimelech, Forward osmosis: Principles, applications, and recent developments, *J. Memb. Sci.* 281 (2006) 70–87. doi:10.1016/j.memsci.2006.05.048.
- [136] T.-S. Chung, X. Li, R.C. Ong, Q. Ge, H. Wang, G. Han, Emerging forward osmosis (FO) technologies and challenges ahead for clean water and clean energy applications, *Curr. Opin. Chem. Eng.* 1 (2012) 246–257. doi:10.1016/j.coche.2012.07.004.
- [137] K.Y. Wang, T.-S. Chung, G. Amy, Developing thin-film-composite forward osmosis membranes on the PES/SPSf substrate through interfacial polymerization, *AIChE J.* 58 (2012) 770–781. doi:10.1002/aic.12635.
- [138] I. Pinnau, B. D. Freeman, Formation and Modification of Polymeric Membranes: Overview, in: I. Pinnau, B.D. Freeman (Eds.), *Membr. Form. Modif.*, American Chemical Society, Washington, DC, DC, 1999: pp. 1–22. doi:10.1021/bk-2000-0744.
- [139] M. Qasim, N.A. Darwish, S. Sarp, N. Hilal, Water desalination by forward (direct) osmosis phenomenon: A comprehensive review, *Desalination.* 374 (2015) 47–69. doi:10.1016/j.desal.2015.07.016.
- [140] J.T. Arena, B. McCloskey, B.D. Freeman, J.R. McCutcheon, Surface modification of thin film composite membrane support layers with polydopamine: Enabling use of reverse osmosis membranes in pressure retarded osmosis, *J. Memb. Sci.* 375 (2011) 55–62. doi:10.1016/j.memsci.2011.01.060.
- [141] C.H. Tan, H.Y. Ng, A novel hybrid forward osmosis - nanofiltration (FO-NF) process for seawater desalination: Draw solution selection and system configuration, *Desalin. Water Treat.* 13 (2010) 356–361. doi:10.5004/dwt.2010.1733.

- [142] N.Y. Yip, A. Tiraferri, W.A. Phillip, J.D. Schiffman, M. Elimelech, High performance thin-film composite forward osmosis membrane, *Environ. Sci. Technol.* 44 (2010) 3812–8. doi:10.1021/es1002555.
- [143] C. Klaysom, T.Y. Cath, T. Depuydt, I.F.J. Vankelecom, Forward and pressure retarded osmosis: potential solutions for global challenges in energy and water supply, *Chem. Soc. Rev.* 42 (2013) 6959–89. doi:10.1039/c3cs60051c.
- [144] J. Ren, J.R. McCutcheon, A new commercial thin film composite membrane for forward osmosis, *Desalination.* 343 (2014) 187–193. doi:10.1016/j.desal.2013.11.026.
- [145] J. Wei, C. Qiu, C.Y. Tang, R. Wang, A.G. Fane, Synthesis and characterization of flat-sheet thin film composite forward osmosis membranes, *J. Memb. Sci.* 372 (2011) 292–302. doi:10.1016/j.memsci.2011.02.013.
- [146] W.A. Phillip, J.D. Schiffman, M. Elimelech, High Performance Thin-Film Membrane, 44 (2010) 3812–3818.
- [147] J.R. McCutcheon, M. Elimelech, Influence of concentrative and dilutive internal concentration polarization on flux behavior in forward osmosis, *J. Memb. Sci.* 284 (2006) 237–247. doi:10.1016/j.memsci.2006.07.049.
- [148] J.R. Mccutcheon, M. Elimelech, Modeling water flux in forward osmosis: Implications for improved membrane design, *AIChE J.* 53 (2007) 1736–1744. doi:10.1002/aic.11197.
- [149] A. Tiraferri, N.Y. Yip, W. a. Phillip, J.D. Schiffman, M. Elimelech, Relating performance of thin-film composite forward osmosis membranes to support layer formation and structure, *J. Memb. Sci.* 367 (2011) 340–352. doi:10.1016/j.memsci.2010.11.014.
- [150] N. Widjojo, T.S. Chung, M. Weber, C. Maletzko, V. Warzelhan, The role of sulphonated polymer and macrovoid-free structure in the support layer for thin-film composite (TFC) forward osmosis (FO) membranes, *J. Memb. Sci.* 383 (2011) 214–223. doi:10.1016/j.memsci.2011.08.041.
- [151] Y. Yu, S. Seo, I.-C. Kim, S. Lee, Nanoporous polyethersulfone (PES) membrane with enhanced flux applied in forward osmosis process, *J. Memb. Sci.* 375 (2011) 63–68. doi:10.1016/j.memsci.2011.02.019.
- [152] L. Huang, J.R. Mccutcheon, Impact of support layer pore size on performance of thin fi lm composite membranes for forward osmosis, *J. Memb. Sci.* 483 (2015) 25–33. doi:10.1016/j.memsci.2015.01.025.
- [153] Y.H. Cho, J. Han, S. Han, M.D. Guiver, H.B. Park, Polyamide thin-film

- composite membranes based on carboxylated polysulfone microporous support membranes for forward osmosis, *J. Memb. Sci.* 445 (2013) 220–227. doi:10.1016/j.memsci.2013.06.003.
- [154] Y. Wang, T. Xu, Anchoring hydrophilic polymer in substrate: An easy approach for improving the performance of TFC FO membrane, *J. Memb. Sci.* 476 (2015) 330–339. doi:10.1016/j.memsci.2014.11.025.
- [155] J.R. McCutcheon, M. Elimelech, Influence of membrane support layer hydrophobicity on water flux in osmotically driven membrane processes, *J. Memb. Sci.* 318 (2008) 458–466. doi:10.1016/j.memsci.2008.03.021.
- [156] I.L. Alsvik, K.R. Zodrow, M. Elimelech, M.-B.B. Hägg, Polyamide formation on a cellulose triacetate support for osmotic membranes: Effect of linking molecules on membrane performance, *Desalination.* 312 (2013) 2–9. doi:10.1016/j.desal.2012.09.019.
- [157] X. Li, K.Y. Wang, B. Helmer, T.S. Chung, Thin-film composite membranes and formation mechanism of thin-film layers on hydrophilic cellulose acetate propionate substrates for forward osmosis processes, *Ind. Eng. Chem. Res.* 51 (2012) 10039–10050. doi:10.1021/ie2027052.
- [158] M. Yasukawa, S. Mishima, M. Shibuya, D. Saeki, T. Takahashi, T. Miyoshi, et al., Preparation of a forward osmosis membrane using a highly porous polyketone microfiltration membrane as a novel support, *J. Memb. Sci.* 487 (2015) 51–59. doi:10.1016/j.memsci.2015.03.043.
- [159] G. Han, T.S. Chung, M. Toriida, S. Tamai, Thin-film composite forward osmosis membranes with novel hydrophilic supports for desalination, *J. Memb. Sci.* 423–424 (2012) 543–555. doi:10.1016/j.memsci.2012.09.005.
- [160] N. Widjojo, T.-S. Chung, M. Weber, C. Maletzko, V. Warzelhan, A sulfonated polyphenylenesulfone (sPPSU) as the supporting substrate in thin film composite (TFC) membranes with enhanced performance for forward osmosis (FO), *Chem. Eng. J.* 220 (2013) 15–23. doi:10.1016/j.cej.2013.01.007.
- [161] D. Emadzadeh, W.J. Lau, T. Matsuura, M. Rahbari-Sisakht, A.F. Ismail, A novel thin film composite forward osmosis membrane prepared from PSf–TiO<sub>2</sub> nanocomposite substrate for water desalination, *Chem. Eng. J.* 237 (2014) 70–80. doi:10.1016/j.cej.2013.09.081.
- [162] P. Lu, S. Liang, L. Qiu, Y. Gao, Q. Wang, Thin film nanocomposite forward osmosis membranes based on layered double hydroxide nanoparticles blended substrates, *J. Memb. Sci.* 504 (2016) 196–205. doi:10.1016/j.memsci.2015.12.066.



- [163] X. Song, Z. Liu, D.D. Sun, Nano gives the answer: Breaking the bottleneck of internal concentration polarization with a nanofiber composite forward osmosis membrane for a high water production rate, *Adv. Mater.* 23 (2011) 3256–3260. doi:10.1002/adma.201100510.
- [164] N.N. Bui, M.L. Lind, E.M. V Hoek, J.R. McCutcheon, Electrospun nanofiber supported thin film composite membranes for engineered osmosis, *J. Memb. Sci.* 385–386 (2011) 10–19. doi:10.1016/j.memsci.2011.08.002.
- [165] N.-N.N. Bui, J.R. McCutcheon, Hydrophilic nanofibers as new supports for thin film composite membranes for engineered osmosis., *Environ. Sci. Technol.* 47 (2013) 1761–9. doi:10.1021/es304215g.
- [166] M. Tian, C. Qiu, Y. Liao, S. Chou, R. Wang, Preparation of polyamide thin film composite forward osmosis membranes using electrospun polyvinylidene fluoride (PVDF) nanofibers as substrates, *Sep. Purif. Technol.* 118 (2013) 727–736. doi:10.1016/j.seppur.2013.08.021.
- [167] A. Tiraferri, Y. Kang, E.P. Giannelis, M. Elimelech, Highly hydrophilic thin-film composite forward osmosis membranes functionalized with surface-tailored nanoparticles., *ACS Appl. Mater. Interfaces.* 4 (2012) 5044–53. doi:10.1021/am301532g.
- [168] N. Ma, J. Wei, R. Liao, C.Y. Tang, Zeolite-polyamide thin film nanocomposite membranes: Towards enhanced performance for forward osmosis, *J. Memb. Sci.* 405–406 (2012) 149–157. doi:10.1016/j.memsci.2012.03.002.
- [169] M. Amini, M. Jahanshahi, A. Rahimpour, Synthesis of novel thin film nanocomposite (TFN) forward osmosis membranes using functionalized multi-walled carbon nanotubes, *J. Memb. Sci.* 435 (2013) 233–241. doi:10.1016/j.memsci.2013.01.041.
- [170] N. Niksefat, M. Jahanshahi, A. Rahimpour, The effect of SiO<sub>2</sub> nanoparticles on morphology and performance of thin film composite membranes for forward osmosis application, *Desalination.* 343 (2014) 140–146. doi:10.1016/j.desal.2014.03.031.
- [171] M.M. Pendergast, E.M.V. Hoek, A review of water treatment membrane nanotechnologies, *Energy Environ. Sci.* 4 (2011) 1946. doi:10.1039/c0ee00541j.
- [172] S. Yu, M. Liu, X. Liu, C. Gao, Performance enhancement in interfacially synthesized thin-film composite polyamide-urethane reverse osmosis membrane for seawater desalination, *J. Memb. Sci.* 342 (2009) 313–320. doi:10.1016/j.memsci.2009.07.003.

- [173] D.R. Lide, ed., CRC Handbook of Chemistry and Physics, 96th ed., CRC Press, n.d.
- [174] J.J. Jasper, The surface tension of pure liquid compounds, *J. Phys. Chem. Ref. Data.* 1 (1972) 841. doi:10.1063/1.3253106.
- [175] B.A. Grigoryev, B. V. Nemzer, D.S. Kurumov, J. V. Sengers, Surface tension of normal pentane, hexane, heptane, and octane, *Int. J. Thermophys.* 13 (1992) 453–464. doi:10.1007/BF00503882.
- [176] B.E. Poling, J.M. Prausnitz, J.P. O’Connell, *Properties of Gases and Liquids*, 5th ed., McGraw Hill Professional, Access Engineering, 2001.
- [177] M. Elimelech, A.E. Childress, Role of membrane surface morphology in colloidal fouling of cellulose acetate and composite aromatic polyamide reverse osmosis membranes, *J. Memb. Sci.* 127 (1997) 101–109. doi:10.1016/S0376-7388(96)00351-1.
- [178] S. Belfer, Surface characterization by FTIR-ATR spectroscopy of polyethersulfone membranes-unmodified, modified and protein fouled, *J. Memb. Sci.* 172 (2000) 113–124. doi:10.1016/S0376-7388(00)00316-1.
- [179] M. Oldani, G. Schock, Characterization of ultrafiltration membranes by infrared spectroscopy, esca, and contact angle measurements, *J. Memb. Sci.* 43 (1989) 243–258. doi:10.1016/S0376-7388(00)85101-7.
- [180] Y. Song, F. Liu, B. Sun, Preparation, characterization, and application of thin film composite nanofiltration membranes, *J. Appl. Polym. Sci.* 95 (2005) 1251–1261. doi:10.1002/app.21338.
- [181] P.S. Singh, A.P. Rao, P. Ray, A. Bhattacharya, K. Singh, N.K. Saha, et al., Techniques for characterization of polyamide thin film composite membranes, *Desalination.* 282 (2011) 78–86. doi:10.1016/j.desal.2011.04.039.
- [182] S. Mondal, S.R. Wickramasinghe, Produced water treatment by nanofiltration and reverse osmosis membranes, *J. Memb. Sci.* 322 (2008) 162–170. doi:10.1016/j.memsci.2008.05.039.
- [183] D. Briggs, G. Beamson, XPS studies of the Oxygen-1s and Oxygen-2s levels in a wide-range of functional polymers, *Anal. Chem.* 65 (1993) 1517–1523. doi:10.1021/ac00059a006.
- [184] G.P. Lopez, D.G. Castner, B.D. Ratner, XPS O 1s binding energies for polymers containing hydroxyl, ether, ketone and ester groups, *Surf. Interface Anal.* 17 (1991) 267–272. doi:10.1002/sia.740170508.
- [185] O. Agboola, J. Maree, R. Mbaya, Characterization and performance of nanofiltration membranes, *Environ. Chem. Lett.* 12 (2014) 241–255. doi:10.1007/s10311-014-0457-3.

- [186] D. Quéré, Wetting and roughness, *Annu. Rev. Mater. Res.* 38 (2008) 71–99. doi:10.1146/annurev.matsci.38.060407.132434.
- [187] C. Tsonopoulos, G.M. Wilson, High-temperature mutual solubilities of hydrocarbons and water. Part I: Benzene, cyclohexane and n-hexane, *AIChE J.* 29 (1983) 990–999. doi:10.1002/aic.690290618.
- [188] C.W. Haschets, A.D. Shine, R.M. Secor, Prediction of water solubilities in hydrocarbons and polyethylene at elevated temperatures and pressures, *Ind. Eng. Chem. Res.* 33 (1994) 1040–1046. doi:10.1021/ie00028a036.
- [189] IUPAC-NIST solubility database, 2007. <http://srdata.nist.gov/solubility/index.aspx>.
- [190] C.H. Tan, H.Y. Ng, Modified models to predict flux behavior in forward osmosis in consideration of external and internal concentration polarizations, *J. Memb. Sci.* 324 (2008) 209–219. doi:10.1016/j.memsci.2008.07.020.
- [191] N.T. Hancock, T.Y. Cath, Solute coupled diffusion in osmotically driven membrane processes, *Environ. Sci. Technol.* 43 (2009) 6769–6775. doi:10.1021/es901132x.
- [192] L. Huang, J.T. Arena, J.R. McCutcheon, Surface modified PVDF nanofiber supported thin film composite membranes for forward osmosis, *J. Memb. Sci.* 499 (2015) 352–360. doi:10.1016/j.memsci.2015.10.030.
- [193] L. Huang, J.R. McCutcheon, Impact of support layer pore size on performance of thin film composite Membranes for forward osmosis, *J. Memb. Sci.* (2015). doi:10.1016/j.memsci.2015.01.025.
- [194] A.K. Ghosh, E.M.V. Hoek, Impacts of support membrane structure and chemistry on polyamide–polysulfone interfacial composite membranes, *J. Memb. Sci.* 336 (2009) 140–148. doi:10.1016/j.memsci.2009.03.024.
- [195] P.S. Singh, S.V. Joshi, J.J. Trivedi, C.V. Devmurari, A.P. Rao, P.K. Ghosh, Probing the structural variations of thin film composite RO membranes obtained by coating polyamide over polysulfone membranes of different pore dimensions, *J. Memb. Sci.* 278 (2006) 19–25. doi:10.1016/j.memsci.2005.10.039.
- [196] G. Kang, Y. Cao, Development of antifouling reverse osmosis membranes for water treatment: A review., *Water Res.* 46 (2012) 584–600. doi:10.1016/j.watres.2011.11.041.
- [197] W. Guo, H.-H. Ngo, J. Li, A mini-review on membrane fouling., *Bioresour. Technol.* 122 (2012) 27–34. doi:10.1016/j.biortech.2012.04.089.
- [198] C.Y. Tang, T.H. Chong, A.G. Fane, Colloidal interactions and fouling of

- NF and RO membranes: A review, *Adv. Colloid Interface Sci.* 164 (2011) 126–43. doi:10.1016/j.cis.2010.10.007.
- [199] A.-S. Jönsson, G. Trägårdh, Fundamental principles of ultrafiltration, *Chem. Eng. Process. Process Intensif.* 27 (1990) 67–81. doi:10.1016/0255-2701(90)85011-R.
- [200] M.F.A. Goosen, S.S. Sablani, H. Al-Hinai, S. Al-Obeidani, R. Al-Belushi, D. Jackson, Fouling of reverse osmosis and ultrafiltration membranes: A critical review, *Sep. Sci. Technol.* 39 (2004) 2261–2298.
- [201] K. Katsoufidou, S.G. Yiantsios, A.J. Karabelas, Experimental study of ultrafiltration membrane fouling by sodium alginate and flux recovery by backwashing, *J. Memb. Sci.* 300 (2007) 137–146. doi:10.1016/j.memsci.2007.05.017.
- [202] A. Sofia, W.J. Ng, S.L. Ong, Engineering design approaches for minimum fouling in submerged MBR, *Desalination.* 160 (2004) 67–74. doi:10.1016/S0011-9164(04)90018-5.
- [203] N. Porcelli, S. Judd, Chemical cleaning of potable water membranes: A review, *Sep. Purif. Technol.* 71 (2010) 137–143. doi:10.1016/j.seppur.2009.12.007.
- [204] N. Hilal, O.O. Ogunbiyi, N.J. Miles, R. Nigmatullin, Methods employed for control of fouling in MF and UF membranes: A comprehensive review, *Sep. Sci. Technol.* 40 (2005) 1957–2005. doi:10.1081/SS-200068409.
- [205] D. Li, S.T. Hwang, Gas separation by silicon based inorganic membrane at high temperature, *J. Memb. Sci.* 66 (1992) 119–127. doi:10.1016/0376-7388(92)87002-F.
- [206] A.J. Burggraaf, Important characteristics of inorganic membranes, in: A.J. Burggraaf, L. Cot (Eds.), *Fundam. Inorg. Membr. Sci. Technol.*, Elsevier, 1996: pp. 21–34. doi:10.1016/S0927-5193(96)80005-2.
- [207] X. Jian, Y. Dai, G. He, G. Chen, Preparation of UF and NF poly (phthalazine ether sulfone ketone) membranes for high temperature application, *J. Memb. Sci.* 161 (1999) 185–191. doi:10.1016/S0376-7388(99)00112-X.
- [208] M.J.H. Snow, D. de Winter, R. Buckingham, J. Campbell, J. Wagner, New techniques for extreme conditions: high temperature reverse osmosis and nanofiltration, *Desalination.* 105 (1996) 57–61.
- [209] V. V Tarabara, Multifunctional Nanomaterial-Enabled Membranes for Water Treatment, in: *Nanotechnol. Appl. Clean Water*, 2nd ed., Oxford, 2014: pp. 155–171. doi:http://dx.doi.org/10.1016/B978-1-4557-3116-9.00010-

X.

- [210] Y. Liao, T.P. Farrell, G.R. Guillen, M. Li, J.A.T. Temple, X.-G. Li, et al., Highly dispersible polypyrrole nanospheres for advanced nanocomposite ultrafiltration membranes, *Mater. Horiz.* 1 (2014) 58–64. doi:10.1039/C3MH00049D.
- [211] E.M.V. Hoek, A.K. Ghosh, X. Huang, M. Liang, J.I. Zink, Physical–chemical properties, separation performance, and fouling resistance of mixed-matrix ultrafiltration membranes, *Desalination*. 283 (2011) 89–99. doi:10.1016/j.desal.2011.04.008.
- [212] N. Savage, M.S. Diallo, *Nanomaterials and Water Purification: Opportunities and Challenges*, *J. Nanoparticle Res.* 7 (2005) 331–342. doi:10.1007/s11051-005-7523-5.
- [213] S. Kumar, W. Ahlawat, G. Bhanjana, S. Heydarifard, M.M. Nazhad, N. Dilbaghi, Nanotechnology-based water treatment strategies., *J. Nanosci. Nanotechnol.* 14 (2014) 1838–58. <http://www.ncbi.nlm.nih.gov/pubmed/24749460> (accessed June 14, 2015).
- [214] T.-S. Chung, L.Y. Jiang, Y. Li, S. Kulprathipanja, Mixed matrix membranes (MMMs) comprising organic polymers with dispersed inorganic fillers for gas separation, *Prog. Polym. Sci.* 32 (2007) 483–507. doi:10.1016/j.progpolymsci.2007.01.008.
- [215] H. Cong, M. Radosz, B. Towler, Y. Shen, Polymer–inorganic nanocomposite membranes for gas separation, *Sep. Purif. Technol.* 55 (2007) 281–291. doi:10.1016/j.seppur.2006.12.017.
- [216] M.T.M. Pendergast, J.M. Nygaard, A.K. Ghosh, E.M.V. Hoek, Using nanocomposite materials technology to understand and control reverse osmosis membrane compaction, *Desalination*. 261 (2010) 255–263. doi:10.1016/j.desal.2010.06.008.
- [217] D. Li, H. Wang, Thin film nanocomposite membranes for water desalination, in: *Funct. Nanostructured Mater. Membr. Water Treat.*, 2013. doi:10.1002/9783527668502.ch7.
- [218] Y. Liao, D.-G. Yu, X. Wang, W. Chain, X.-G. Li, E.M. V Hoek, et al., Carbon nanotube-templated polyaniline nanofibers: synthesis, flash welding and ultrafiltration membranes., *Nanoscale*. 5 (2013) 3856–62. doi:10.1039/c3nr00441d.
- [219] Q. Li, S. Mahendra, D.Y. Lyon, L. Brunet, M. V. Liga, D. Li, et al., Antimicrobial nanomaterials for water disinfection and microbial control: Potential applications and implications, *Water Res.* 42 (2008) 4591–4602.

- doi:10.1016/j.watres.2008.08.015.
- [220] R.L. Davies, S.F. Etris, The development and functions of silver in water purification and disease control, *Catal. Today*. 36 (1997) 107–114. doi:10.1016/S0920-5861(96)00203-9.
- [221] K. Zodrow, L. Brunet, S. Mahendra, D. Li, A. Zhang, Q. Li, et al., Polysulfone ultrafiltration membranes impregnated with silver nanoparticles show improved biofouling resistance and virus removal., *Water Res.* 43 (2009) 715–23. doi:10.1016/j.watres.2008.11.014.
- [222] M. Gui, V. Smuleac, L.E. Ormsbee, D.L. Sedlak, D. Bhattacharyya, Iron oxide nanoparticle synthesis in aqueous and membrane systems for oxidative degradation of trichloroethylene from water, *J. Nanoparticle Res.* 14 (2012) 861. doi:10.1007/s11051-012-0861-1.
- [223] H. Wu, B. Tang, P. Wu, Development of novel SiO<sub>2</sub>–GO nanohybrid/polysulfone membrane with enhanced performance, *J. Memb. Sci.* 451 (2014) 94–102. doi:10.1016/j.memsci.2013.09.018.
- [224] R.D. Noble, Perspectives on mixed matrix membranes, *J. Memb. Sci.* 378 (2011) 393–397. doi:10.1016/j.memsci.2011.05.031.
- [225] Z. Xu, L. Yu, L. Han, Polymer-nanoinorganic particles composite membranes: a brief overview, *Front. Chem. Eng. China*. 3 (2009) 318–329. doi:10.1007/s11705-009-0199-0.
- [226] D. Wandera, S.R. Wickramasinghe, S.M. Husson, Stimuli-responsive membranes, *J. Memb. Sci.* 357 (2010) 6–35. doi:10.1016/j.memsci.2010.03.046.
- [227] S. Darvishmanesh, X. Qian, S.R. Wickramasinghe, Responsive membranes for advanced separations, *Curr. Opin. Chem. Eng.* 8 (2015) 98–104. doi:10.1016/j.coche.2015.04.002.
- [228] F. Liu, M.W. Urban, Recent advances and challenges in designing stimuli-responsive polymers, *Prog. Polym. Sci.* 35 (2010) 3–23. doi:10.1016/j.progpolymsci.2009.10.002.
- [229] D. Bhattacharyya, T. Schafer, S.R. Wickramasinghe, S. Daunert, *Responsive Membranes and Materials*, John Wiley & Sons, Inc., 2013.
- [230] J.-S. Park, H.-J. Lee, S.-J. Choi, K.E. Geckeler, J. Cho, S.-H. Moon, Fouling mitigation of anion exchange membrane by zeta potential control, *J. Colloid Interface Sci.* 259 (2003) 293–300. doi:10.1016/S0021-9797(02)00095-4.
- [231] A.E. Childress, M. Elimelech, Relating Nanofiltration Membrane Performance to Membrane Charge (Electrokinetic) Characteristics, *Environ.*

- Sci. Technol. 34 (2000) 3710–3716. doi:10.1021/es0008620.
- [232] C. Zhao, J. Xue, F. Ran, S. Sun, Modification of polyethersulfone membranes – A review of methods, *Prog. Mater. Sci.* 58 (2013) 76–150. doi:10.1016/j.pmatsci.2012.07.002.
- [233] G.R. Guillen, Y. Pan, M. Li, E.M. V. Hoek, Preparation and Characterization of Membranes Formed by Nonsolvent Induced Phase Separation: A Review, *Ind. Eng. Chem. Res.* 50 (2011) 3798–3817. doi:10.1021/ie101928r.
- [234] H.L. Richards, P.G.L. Baker, E. Iwuoha, Metal Nanoparticle Modified Polysulfone Membranes for Use in Wastewater Treatment: A Critical Review, *J. Surf. Eng. Mater. Adv. Technol.* 2 (2012) 183–193. doi:10.4236/jsemat.2012.223029.
- [235] S.P. Moulik, Physical aspects of electrofiltration, *Environ. Sci. Technol.* 5 (1971) 771–776. doi:10.1021/es60056a001.
- [236] H.M. Huotari, G. Trägårdh, I.H. Huisman, Crossflow Membrane Filtration Enhanced by an External DC Electric Field: A Review, *Chem. Eng. Res. Des.* 77 (1999) 461–468. doi:10.1205/026387699526304.
- [237] K. Weber, W. Stahl, Improvement of filtration kinetics by pressure electrofiltration, *Sep. Purif. Technol.* 26 (2002) 69–80. doi:10.1016/S1383-5866(01)00118-6.
- [238] S. Molla, S. Bhattacharjee, Prevention of colloidal membrane fouling employing dielectrophoretic forces on a parallel electrode array, *J. Memb. Sci.* 255 (2005) 187–199. doi:10.1016/j.memsci.2005.01.034.
- [239] A. V. Dudchenko, J. Rolf, K. Russell, W. Duan, D. Jassby, Organic fouling inhibition on electrically conducting carbon nanotube–polyvinyl alcohol composite ultrafiltration membranes, *J. Memb. Sci.* 468 (2014) 1–10. doi:10.1016/j.memsci.2014.05.041.
- [240] T. Weigert, J. Altmann, S. Ripperger, Crossflow electrofiltration in pilot scale, *J. Memb. Sci.* 159 (1999) 253–262. doi:10.1016/S0376-7388(99)00068-X.
- [241] R.G. Gordon, Criteria for Choosing Transparent Conductors, *MRS Bull.* 25 (2000) 52–57. doi:10.1557/mrs2000.151.
- [242] F. Lai, L. Lin, R. Gai, Y. Lin, Z. Huang, Determination of optical constants and thicknesses of In<sub>2</sub>O<sub>3</sub>:Sn films from transmittance data, *Thin Solid Films.* 515 (2007) 7387–7392. doi:10.1016/j.tsf.2007.03.037.
- [243] J. Lu, K. Minami, S. Takami, M. Shibata, Y. Kaneko, T. Adschiri, Supercritical hydrothermal synthesis and in situ organic modification of

- indium tin oxide nanoparticles using continuous-flow reaction system, *ACS Appl. Mater. Interfaces*. 4 (2012) 351–354. doi:10.1021/am2014234.
- [244] J.S. Lee, S.C. Choi, Solvent effect on synthesis of indium tin oxide nanoparticles by a solvothermal process, *J. Eur. Ceram. Soc.* 25 (2005) 3307–3314. doi:10.1016/j.jeurceramsoc.2004.08.022.
- [245] H. Shigetani, M. Senna, Preparation of high-density ITO ceramics by an *in situ* precipitation method, *J. Mater. Sci. Lett.* 14 (1995) 252–255.
- [246] H. Wang, X. Xu, J. Zhang, C. Li, A Cost-Effective Co-precipitation Method for Synthesizing Indium Tin Oxide Nanoparticles without Chlorine Contamination, *J. Mater. Sci. Technol.* 26 (2010) 1037–1040. doi:10.1016/S1005-0302(10)60171-5.
- [247] R. Abedini, M. Mousavi, R. Aminzadeh, Effect of sonochemical synthesized TiO<sub>2</sub> nanoparticles and coagulation bath temperature on morphology, thermal stability and pure water flux of asymmetric cellulose acetate membranes prepared via phase inversion method, *Chem. Ind. Chem. Eng. Q.* 18 (2012) 385–398. doi:10.2298/CICEQ111202014A.
- [248] Y. Treekamol, M. Schieda, L. Robitaille, S.M. MacKinnon, A. Mokrini, Z. Shi, et al., Nafion®/ODF-silica composite membranes for medium temperature proton exchange membrane fuel cells, *J. Power Sources*. 246 (2014) 950–959. doi:10.1016/j.jpowsour.2013.01.178.
- [249] H. Nagasawa, T. Minamizawa, M. Kanezashi, T. Yoshioka, T. Tsuru, High-temperature stability of PECVD-derived organosilica membranes deposited on TiO<sub>2</sub> and SiO<sub>2</sub>-ZrO<sub>2</sub> intermediate layers using HMDSO/Ar plasma, *Sep. Purif. Technol.* 121 (2014) 13–19. doi:10.1016/j.seppur.2013.10.042.
- [250] M. Sadrzadeh, J. Hajinasiri, S. Bhattacharjee, D. Pernitsky, Nanofiltration of oil sands boiler feed water: Effect of pH on water flux and organic and dissolved solid rejection, *Sep. Purif. Technol.* 141 (2015) 339–353. doi:10.1016/j.seppur.2014.12.011.
- [251] Y.-J. Zhao, K.-F. Wu, Z.-J. Wang, L. Zhao, S.-S. Li, Fouling and cleaning of membrane—a literature review, *J. Environ. Sci.* 12 (2000) 241–251. doi:1001-0742(2000)02\_0241-11.
- [252] A. Abdelrasoul, H. Doan, A. Lohi, Fouling in membrane filtration and remediation methods, in: H. Nakajima (Ed.), *Mass Transf. - Adv. Sustain. Energy Environ. Oriented Numer. Model.*, InTech, 2013. doi:10.5772/52370.
- [253] M. Hayatbakhsh, M. Sadrzadeh, D. Pernitsky, S. Bhattacharjee, J. Hajinasiri, Treatment of an *in situ* oil sands produced water by polymeric membranes, *Desalin. Water Treat.* (2015) 1–19.



doi:10.1080/19443994.2015.1069216.

- [254] C. Jucker, M.M. Clark, Adsorption of aquatic humic substances on hydrophobic ultrafiltration membranes, *J. Memb. Sci.* 97 (1994) 37–52.
- [255] K.L. Tu, A.R. Chivas, L.D. Nghiem, Effects of membrane fouling and scaling on boron rejection by nanofiltration and reverse osmosis membranes, *Desalination*. 279 (2011) 269–277. doi:10.1016/j.desal.2011.06.019.
- [256] Q. Li, Z. Xu, I. Pinnau, Fouling of reverse osmosis membranes by biopolymers in wastewater secondary effluent: role of membrane surface properties and initial permeate flux, *J. Memb. Sci.* 290 (2007) 173–181.
- [257] A.E. Childress, M. Elimelech, Effect of solution chemistry on the surface charge of polymeric reverse osmosis and nanofiltration membranes, *J. Memb. Sci.* 119 (1996) 253–268.
- [258] A. Maiti, M. Sadrezadeh, S. Guha Thakurta, D.J. Pernitsky, S. Bhattacharjee, M. Sadrzadeh, Characterization of boiler blowdown water from steam-assisted gravity drainage and silica–organic coprecipitation during acidification and ultrafiltration, *Energy & Fuels*. 26 (2012) 5604–5612. doi:10.1021/ef300865e.
- [259] J.H. Jhaveri, Z.V.P. Murthy, A comprehensive review on anti-fouling nanocomposite membranes for pressure driven membrane separation processes, *Desalination*. 379 (2016) 137–154. doi:10.1016/j.desal.2015.11.009.
- [260] S. Hernandez, A. Saad, L. Ormsbee, D. Bhattacharyya, Nanocomposite and Responsive Membranes for Water Treatment, in: *Emerg. Membr. Technol. Sustain. Water Treat.*, Elsevier, 2016: pp. 389–431.
- [261] D.R. Paul, D.R. Kemp, The diffusion time lag in polymer membranes containing adsorptive fillers, *J. Polym. Sci. Polym. Symp.* 41 (2007) 79–93. doi:10.1002/polc.5070410109.
- [262] B.-H. Jeong, E.M.V. Hoek, Y. Yan, A. Subramani, X. Huang, G. Hurwitz, et al., Interfacial polymerization of thin film nanocomposites: A new concept for reverse osmosis membranes, *J. Memb. Sci.* 294 (2007) 1–7. doi:10.1016/j.memsci.2007.02.025.
- [263] R. Das, S.B. Abd Hamid, M.E. Ali, A.F. Ismail, M.S.M. Annuar, S. Ramakrishna, Multifunctional carbon nanotubes in water treatment: The present, past and future, *Desalination*. 354 (2014) 160–179. doi:10.1016/j.desal.2014.09.032.
- [264] H.M. Hegab, L. Zou, Graphene oxide-assisted membranes: Fabrication and potential applications in desalination and water purification, *J. Memb. Sci.* 484 (2015) 95–106. doi:10.1016/j.memsci.2015.03.011.

- [265] A. Khataee, G.A. Mansoori, *Nanostructured Titanium Dioxide Materials*, WORLD SCIENTIFIC, 2011. doi:10.1142/8325.
- [266] S.-Y. Lee, S.-J. Park, TiO<sub>2</sub> photocatalyst for water treatment applications, *J. Ind. Eng. Chem.* 19 (2013) 1761–1769. doi:10.1016/j.jiec.2013.07.012.
- [267] C.S. Ong, P.S. Goh, W.J. Lau, N. Misdan, A.F. Ismail, Nanomaterials for biofouling and scaling mitigation of thin film composite membrane: A review, *Desalination*. 393 (2016) 2–15. doi:10.1016/j.desal.2016.01.007.
- [268] S.-Y.K. and, S.H. Kim, S.S. Kim, Hybrid organic/inorganic reverse osmosis (RO) membrane for bactericidal anti-fouling. 1. Preparation and characterization of TiO<sub>2</sub> nanoparticle self-assembled aromatic polyamide thin-film-composite (TFC) membrane, (2001). doi:10.1021/ES0017099.
- [269] S.S. Madaeni, N. Ghaemi, Characterization of self-cleaning RO membranes coated with TiO<sub>2</sub> particles under UV irradiation, *J. Memb. Sci.* 303 (2007) 221–233. doi:10.1016/j.memsci.2007.07.017.
- [270] J. Mo, S.-H. Son, J. Jegal, J. Kim, Y.H. Lee, Preparation and characterization of polyamide nanofiltration composite membranes with TiO<sub>2</sub> layers chemically connected to the membrane surface, *J. Appl. Polym. Sci.* 105 (2007) 1267–1274. doi:10.1002/app.25767.
- [271] B. Rajaeian, A. Rahimpour, M.O. Tade, S. Liu, Fabrication and characterization of polyamide thin film nanocomposite (TFN) nanofiltration membrane impregnated with TiO<sub>2</sub> nanoparticles, *Desalination*. 313 (2013) 176–188. doi:10.1016/j.desal.2012.12.012.
- [272] H.S. Lee, S.J. Im, J.H. Kim, H.J. Kim, J.P. Kim, B.R. Min, Polyamide thin-film nanofiltration membranes containing TiO<sub>2</sub> nanoparticles, *Desalination*. 219 (2008) 48–56. doi:10.1016/j.desal.2007.06.003.
- [273] D. Emadzadeh, M. Ghanbari, W.J. Lau, M. Rahbari-Sisakht, T. Matsuura, A.F. Ismail, et al., Solvothermal synthesis of nanoporous TiO<sub>2</sub>: the impact on thin-film composite membranes for engineered osmosis application, *Nanotechnology*. 27 (2016) 345702. doi:10.1088/0957-4484/27/34/345702.
- [274] J. Kim, B. Van der Bruggen, The use of nanoparticles in polymeric and ceramic membrane structures: Review of manufacturing procedures and performance improvement for water treatment, *Environ. Pollut.* 158 (2010) 2335–2349. doi:10.1016/j.envpol.2010.03.024.
- [275] R.-X. Zhang, L. Braeken, P. Luis, X.-L. Wang, B. Van der Bruggen, Novel binding procedure of TiO<sub>2</sub> nanoparticles to thin film composite membranes via self-polymerized polydopamine, *J. Memb. Sci.* 437 (2013) 179–188. doi:10.1016/j.memsci.2013.02.059.

- [276] S. Al Aani, C.J. Wright, M.A. Atieh, N. Hilal, Engineering nanocomposite membranes: Addressing current challenges and future opportunities, *Desalination*. 401 (n.d.) 1–15. doi:10.1016/j.desal.2016.08.001.
- [277] E.M. Hotze, T. Phenrat, G. V. Lowry, Nanoparticle aggregation: Challenges to understanding transport and reactivity in the environment, *J. Environ. Qual.* 39 (2010) 1909. doi:10.2134/jeq2009.0462.
- [278] W.J. Lau, S. Gray, T. Matsuura, D. Emadzadeh, J. Paul Chen, A.F. Ismail, A review on polyamide thin film nanocomposite (TFN) membranes: History, applications, challenges and approaches, *Water Res.* 80 (2015) 306–324. doi:10.1016/j.watres.2015.04.037.
- [279] R. Li, L. Zhang, P. Wang, R.P. Schwarzenbach, T. Egli, T.B. Hofstetter, et al., Rational design of nanomaterials for water treatment, *Nanoscale*. 7 (2015) 17167–17194. doi:10.1039/C5NR04870B.
- [280] G.-R. Xu, J.-N. Wang, C.-J. Li, Strategies for improving the performance of the polyamide thin film composite (PA-TFC) reverse osmosis (RO) membranes: Surface modifications and nanoparticles incorporations, *Desalination*. 328 (2013) 83–100. doi:10.1016/j.desal.2013.08.022.
- [281] T.A. Saleh, V.K. Gupta, T.A. Saleh, V.K. Gupta, Synthesis of Nanomaterial–Polymer Membranes by Polymerization Methods, in: *Nanomater. Polym. Membr.*, 2016: pp. 135–160. doi:10.1016/B978-0-12-804703-3.00005-X.
- [282] J. Yin, B. Deng, Polymer-matrix nanocomposite membranes for water treatment, *J. Memb. Sci.* 479 (2014) 256–275. doi:10.1016/j.memsci.2014.11.019.
- [283] J. Eastoe, R.F. Tabor, Surfactants and Nanoscience, in: *Colloid. Found. Nanosci.*, 2014: pp. 135–157. doi:10.1016/B978-0-444-59541-6.00006-0.
- [284] L.S. Wang, R.Y. Hong, Synthesis, surface modification and characterisation of nanoparticles, in: B. Reddy (Ed.), *Adv. Nanocomposites - Synth. Charact. Ind. Appl.*, InTech, Rijeka, Croatia, 2011: pp. 289–322.
- [285] U. Diebold, The surface science of titanium dioxide, *Surf. Sci. Rep.* 48 (2003) 53–229. doi:10.1016/S0167-5729(02)00100-0.
- [286] A. Fujishima, T.N. Rao, D.A. Tryk, Titanium dioxide photocatalysis, *J. Photochem. Photobiol. C Photochem. Rev.* 1 (2000) 1–21. doi:10.1016/S1389-5567(00)00002-2.
- [287] S. Leong, A. Razmjou, K. Wang, K. Hapgood, X. Zhang, H. Wang, TiO<sub>2</sub> based photocatalytic membranes: A review, *J. Memb. Sci.* 472 (2014) 167–184. doi:10.1016/j.memsci.2014.08.016.

- [288] A. Mills, S. Le Hunte, An overview of semiconductor photocatalysis, *J. Photochem. Photobiol. A Chem.* 108 (1997) 1–35. doi:10.1016/S1010-6030(97)00118-4.
- [289] J. Schneider, M. Matsuoka, M. Takeuchi, J. Zhang, Y. Horiuchi, M. Anpo, et al., Understanding TiO<sub>2</sub> photocatalysis: Mechanisms and materials, *Chem. Rev.* 114 (2014) 9919–9986. doi:10.1021/cr5001892.
- [290] U. Joost, K. Juganson, M. Visnapuu, M. Mortimer, A. Kahru, E. Nõmmiste, et al., Photocatalytic antibacterial activity of nano-TiO<sub>2</sub> (anatase)-based thin films: Effects on *Escherichia coli* cells and fatty acids, *J. Photochem. Photobiol. B Biol.* 142 (2015) 178–185. doi:10.1016/j.jphotobiol.2014.12.010.
- [291] M. Guo, H. Hu, J.R. Bolton, M.G. El-Din, Comparison of low- and medium-pressure ultraviolet lamps: Photoreactivation of *Escherichia coli* and total coliforms in secondary effluents of municipal wastewater treatment plants, *Water Res.* 43 (2009) 815–821. doi:10.1016/j.watres.2008.11.028.

# Appendix

## Copyrights and permissions

**ELSEVIER LICENSE  
TERMS AND CONDITIONS**

---

---

This Agreement between Behnam Khorshidi ("You") and Elsevier ("Elsevier") consists of your license details and the terms and conditions provided by Elsevier and Copyright Clearance Center.

License Number	4193260996136
License date	Sep 20, 2017
Licensed Content Publisher	Elsevier
Licensed Content Publication	Journal of Membrane Science
Licensed Content Title	Synthesis of thin film composite polyamide membranes: Effect of monohydric and polyhydric alcohol additives in aqueous solution
Licensed Content Author	Behnam Khorshidi,Babak Soltannia,Thomas Thundat,Mohtada Sadrzadeh
Licensed Content Date	Feb 1, 2017
Licensed Content Volume	523
Licensed Content Issue	n/a
Licensed Content Pages	10
Start Page	336
End Page	345
Type of Use	reuse in a thesis/dissertation
Intended publisher of new work	other
Portion	full article
Format	electronic
Are you the author of this Elsevier article?	Yes
Will you be translating?	No
Title of your thesis/dissertation	Advanced Thin Film Composite and Nanocomposite Polyamide Membrane for Water Treatment
Expected completion date	Sep 2017
Estimated size (number of pages)	190
Requestor Location	Behnam Khorshidi NINT 6-74, University of Alberta  Edmonton, AB T6G 2G8 Canada Attn: Behnam Khorshidi
Total	0.00 CAD

**ELSEVIER LICENSE  
TERMS AND CONDITIONS**

---

---

This Agreement between Behnam Khorshidi ("You") and Elsevier ("Elsevier") consists of your license details and the terms and conditions provided by Elsevier and Copyright Clearance Center.

License Number	4193260649392
License date	Sep 20, 2017
Licensed Content Publisher	Elsevier
Licensed Content Publication	Journal of Membrane Science
Licensed Content Title	A parametric study on the synergistic impacts of chemical additives on permeation properties of thin film composite polyamide membrane
Licensed Content Author	Behnam Khorshidi,Thomas Thundat,David Pernitsky,Mohtada Sadrzadeh
Licensed Content Date	Aug 1, 2017
Licensed Content Volume	535
Licensed Content Issue	n/a
Licensed Content Pages	10
Start Page	248
End Page	257
Type of Use	reuse in a thesis/dissertation
Portion	full article
Format	electronic
Are you the author of this Elsevier article?	Yes
Will you be translating?	No
Title of your thesis/dissertation	Advanced Thin Film Composite and Nanocomposite Polyamide Membrane for Water Treatment
Expected completion date	Sep 2017
Estimated size (number of pages)	190
Requestor Location	Behnam Khorshidi NINT 6-74, University of Alberta  Edmonton, AB T6G 2G8 Canada Attn: Behnam Khorshidi
Total	0.00 CAD

**ELSEVIER LICENSE  
TERMS AND CONDITIONS**

---

---

This Agreement between Behnam Khorshidi ("You") and Elsevier ("Elsevier") consists of your license details and the terms and conditions provided by Elsevier and Copyright Clearance Center.

License Number	4193261163268
License date	Sep 20, 2017
Licensed Content Publisher	Elsevier
Licensed Content Publication	Journal of Membrane Science
Licensed Content Title	Developing high throughput thin film composite polyamide membranes for forward osmosis treatment of SAGD produced water
Licensed Content Author	Behnam Khorshidi,Amrit Bhinder,Thomas Thundat,David Pernitsky,Mohtada Sadrzadeh
Licensed Content Date	Aug 1, 2016
Licensed Content Volume	511
Licensed Content Issue	n/a
Licensed Content Pages	11
Start Page	29
End Page	39
Type of Use	reuse in a thesis/dissertation
Intended publisher of new work	other
Portion	full article
Format	electronic
Are you the author of this Elsevier article?	Yes
Will you be translating?	No
Title of your thesis/dissertation	Advanced Thin Film Composite and Nanocomposite Polyamide Membrane for Water Treatment
Expected completion date	Sep 2017
Estimated size (number of pages)	190
Requestor Location	Behnam Khorshidi NINT 6-74, University of Alberta  Edmonton, AB T6G 2G8 Canada Attn: Behnam Khorshidi
Total	0.00 CAD



**ELSEVIER LICENSE  
TERMS AND CONDITIONS**

---

---

This Agreement between Behnam Khorshidi ("You") and Elsevier ("Elsevier") consists of your license details and the terms and conditions provided by Elsevier and Copyright Clearance Center.

License Number	4193261316775
License date	Sep 20, 2017
Licensed Content Publisher	Elsevier
Licensed Content Publication	Journal of Membrane Science
Licensed Content Title	Thermally resistant and electrically conductive PES/ITO nanocomposite membrane
Licensed Content Author	Behnam Khorshidi, Javad Hajinasiri, Guibin Ma, Subir Bhattacharjee, Mohtada Sadrzadeh
Licensed Content Date	Feb 15, 2016
Licensed Content Volume	500
Licensed Content Issue	n/a
Licensed Content Pages	10
Start Page	151
End Page	160
Type of Use	reuse in a thesis/dissertation
Intended publisher of new work	other
Portion	full article
Format	electronic
Are you the author of this Elsevier article?	Yes
Will you be translating?	No
Title of your thesis/dissertation	Advanced Thin Film Composite and Nanocomposite Polyamide Membrane for Water Treatment
Expected completion date	Sep 2017
Estimated size (number of pages)	190
Requestor Location	Behnam Khorshidi NINT 6-74, University of Alberta  Edmonton, AB T6G 2G8 Canada Attn: Behnam Khorshidi
Total	0.00 CAD

## ELSEVIER LICENSE TERMS AND CONDITIONS

---

This Agreement between Behnam Khorshidi ("You") and Elsevier ("Elsevier") consists of your license details and the terms and conditions provided by Elsevier and Copyright Clearance Center.

License Number	4194380590805
License date	Sep 22, 2017
Licensed Content Publisher	Elsevier
Licensed Content Publication	Ultrasonics Sonochemistry
Licensed Content Title	Parametric study on the stabilization of metal oxide nanoparticles in organic solvents: A case study with indium tin oxide (ITO) and heptane
Licensed Content Author	Zayed Almansoori, Behnam Khorshidi, Behnam Sadri, Mohtada Sadrzadeh
Licensed Content Date	Jan 1, 2018
Licensed Content Volume	40
Licensed Content Issue	n/a
Licensed Content Pages	11
Start Page	1003
End Page	1013
Type of Use	reuse in a thesis/dissertation
Portion	figures/tables/illustrations
Number of figures/tables/illustrations	1
Format	electronic
Are you the author of this Elsevier article?	Yes
Will you be translating?	No
Original figure numbers	Figure 1
Title of your thesis/dissertation	Advanced Thin Film Composite and Nanocomposite Polyamide Membrane for Water Treatment
Expected completion date	Sep 2017
Estimated size (number of pages)	190
Requestor Location	Behnam Khorshidi NINT 6-74, University of Alberta  Edmonton, AB T6G 2G8 Canada Attn: Behnam Khorshidi
Total	0.00 CAD